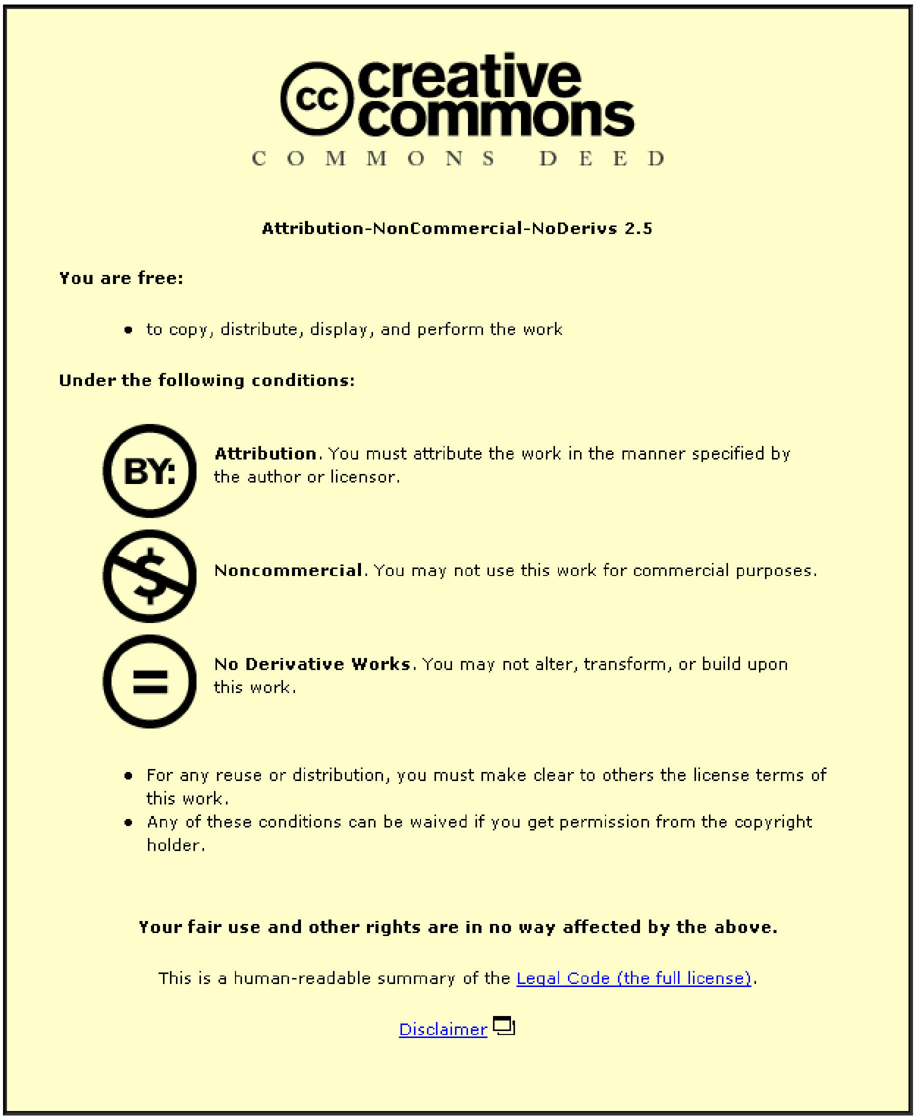

PICTURE CODING IN VIEWDATA SYSTEMS

by

K. N. NGAN

A Doctoral Thesis

Submitted in partial fulfilment of the requirements

for the award of

Doctor of Philosophy

of the Loughborough University of Technology

SYNOPSIS

Viewdata systems in commercial use at present offer the facility for transmitting alphanumeric text and graphic displays via the public switched telephone network. An enhancement to the system would be to transmit true video images instead of graphics. Such a system, under development in Britain at present uses Differential Pulse Code Modulation (DPCM) and a transmission rate of 1200 bits/sec. Error protection is achieved by the use of error protection codes, which increases the channel requirement.

In this thesis, error detection and correction of DPCM coded video signals without the use of channel error protection is studied. The scheme operates entirely at the receiver by examining the local statistics of the received data to determine the presence of errors. Error correction is then undertaken by interpolation from adjacent correct or previously corrected data.

DPCM coding of pictures has the inherent disadvantage of a slow build-up of the displayed picture at the receiver and difficulties with image size manipulation. In order to fit the pictorial information into a viewdata page, its size has to be reduced. Unitary transforms, typically the discrete Fourier transform (DFT), the discrete cosine transform (DCT) and the Hadamard transform (HT) enable lowpass filtering and decimation to be carried out in a single operation in the transform domain. Size reductions of different orders are considered and the merits of the DFT, DCT and HT are investigated.

With limited channel capacity, it is desirable to remove the redundancy present in the source picture in order to reduce the bit rate. Orthogonal transformation decorrelates the spatial sample distribution and packs most of the image energy in the low order coefficients. This property is exploited in bit-reduction schemes which are adaptive to the local statistics of the different source pictures used. In some cases, bit rates of less than 1.0 bit/pel are achieved with satisfactory received picture quality.

Unlike DPCM systems, transform coding has the advantage of being able to display rapidly a picture of low resolution by initial inverse transformation of the low order coefficients only. Picture resolution is then progressively built up as more coefficients are received and decoded. Different sequences of picture update are investigated to find that which achieves the best subjective quality with the fewest possible coefficients transmitted.

ERRATA

Page	Line	Correction
2	10	large amount → a large amount
17	8	well defined → easy to approximate
19	2	is the → is usually the
35	21	and are → and they are
87	1	by inserting → by first inserting
105	Equation (4.72)	$H\sqrt{x^2+y^2} \rightarrow H(\sqrt{f_x^2+f_y^2})$
116	4	enables lowpass → enables efficient lowpass
134	16	it set → it are set
152	12	delete "normalized"
160	9	delete "a measure of"
165	17	delete "normalized"
184	17	linearly → monotonically
196	16	redundancy exists → redundancy still exists

ACKNOWLEDGEMENTS

I wish to express my most sincere thanks to both my supervisors, Dr. R. Steele and Mr. R. J. Clarke for their constant guidance and encouragement throughout the course of this work. Thanks are also due to Mr. R. J. Clarke for his patience in reading the manuscript of this thesis. I also wish to express my thanks to Mr. P. Atkinson for preparing the photographic results in this thesis. Thanks to all my colleagues with whom I have had many interesting and useful discussions.

Special thanks to Dr. R. C. Nicol and Mr. B. A. Fenn of the British Telecom Research Laboratories, for many stimulating discussions and to BTRL itself for providing the financial support for this work. I am also grateful to the Department of Electronic and Electrical Engineering of Loughborough University of Technology for providing the facilities to carry out this work.

My deepest gratitude to my parents and Miss Nerissa Chin for their moral support throughout the course of this work. And lastly, I wish to thank Mrs. P. Higgs for typing the manuscript of this thesis.

LIST OF PRINCIPAL SYMBOLS AND ABBREVIATIONS

a_i	Predictor coefficients
{A}	Forward transformation matrix
AI	Activity index
ARF	Area reduction factor
{B}	Inverse tranformation matrix
$B_{m,n}$	(m,n)th block in the image
BER	Bit error rate
C	y-intercept of the linear equation in variance estimation
C_k	Numerical kth category value
C_X	Covariance matrix
d_i	Quantizer decision levels
D/A	Digital to analogue converter
DCT	Discrete cosine transform
DFT	Discrete Fourier transform
DPCM	Differential pulse code modulation
E[ ]	Expected value of variables in [ ]

$f(.)$	Spatial sample
$F(.)$	Transform coefficient
$\hat{F}(.)$	Quantized version of $F(.)$
FIR	Finite impulse response
$h(.)$	Filter impulse response
$H(.)$	Filter transfer function
$H(w)$	Transfer function of the eye
HT	Hadamard transform
HVS	Human visual system
IIR	Infinite impulse response
IP	Information provider
IRC	Information retrieval centre
J	Number of samples in variance estimation
k	Bit number
KLT	Karhunen-Loeve transform
$\ell n[\ ]$	Natural logarithm of variable in $[\ ]$
L	Number of quantizer levels
L_1	Error detector parameter

L_2	End-of-line error detector parameter
m	Slope of the linear equation in variance estimation
M	Reduced block size
M_b	Total number of bits in a block
MUX	Multiplexer
n_k	Number of images in the kth category
N	Original block size
N_c	Bit counter
NMSE	Normalised mean square error
p(.)	Probability density function
{P}	Decimated coefficient matrix
PCM	Pulse code modulation
pdf	Probability density function
$q_{i,j}$	PCM sample at the (i,j)th location
$Q_{i,j}$	Correct or corrected sample at the (i,j)th location
r	Correlation coefficient of the actual and estimated variances
r_i	Quantizer reconstruction levels

R(D)	Rate distortion function
RF	Sampling rate reduction factor
{S}	Selection matrix
S(w)	Power spectral density
SNR	Signal to noise ratio
SQNR	Signal to quantization noise ratio
t(.)	Impulse response of T(.)
T(.)	Truncating function
TQ	Tapered quantizer
U,V	Colour difference components
UDC	Update centre
UQ	Uniform quantizer
W	Baseband width
w_c	Cutoff frequency
w_s	Sampling frequency
$y_{i,j}$	DPCM sample at the (i,j)th location
Y	Luminance component
Δ_u	Uniform quantizer step size

Δ_T	Tapered quantizer step size
σ_d^2	Mean square difference of adjacent pels
σ_i^2	Variance of the ith coefficients
$\hat{\sigma}_i^2$	Estimated value of σ_i^2
ε^2	Mean square quantization error
ε_e^2	Mean square prediction error
η_i	Mean value of the ith coefficients
λ_i	Eigenvalue of C_x
α_m	Zero of the IIR filter
β_m	Pole of the IIR filter
ρ_V	Vertical correlation
ρ_H	Horizontal correlation
$[\ ]^T$	Transpose of $[\ ]$
$[\ ]^{-1}$	Inverse of $[\ ]$
$[\ ]^*$	Complex conjugate of $[\ ]$
$\otimes$	Direct product operator

CONTENTS

CHAPTER I - INTRODUCTION

CHAPTER II - ERROR DETECTION AND CORRECTION

CHAPTER III - IMAGE SIZE REDUCTION

CHAPTER IV - DATA COMPRESSION

CHAPTER V - IMAGE DISPLAY

CHAPTER VI - RECAPITULATION AND SUGGESTIONS FOR FUTURE WORK

CHAPTER I - INTRODUCTION

1.1 INTRODUCTION

This chapter provides the background knowledge for the material described in this thesis. First and foremost, an introduction to digital picture coding is given, followed by a description of different coding methods, in order to outline the different approaches employed to achieve data compression. A brief description of the psychophysical properties of human vision is included, with emphasis on the modelling of the human visual system which is commonly used in data compression applications. Methods for the assessment of picture quality are also discussed. A general description of the British Telecom viewdata system (Prestel) is given, in particular Picture Prestel, with which the work to be described in this theseis is associated. Finally, the organisation of the thesis is outlined.

1.2 DIGITAL PICTURE CODING - A REVIEW

Since the first demonstration of digital transmission of pictorial information in the 1920s, there has been considerable research into efficient image transmission techniques. Digital image processing finds applications in many fields, including broadcast and relay television, facsimile, remote image sensing, biomedical imaging, surveillance and viewdata systems. During the past decade, there has been much progress toward the design of more efficient image transmission systems, and this progress is mainly due to the discovery and refinement of new image coding techniques, and the advent of relatively inexpensive microprocessors, high-speed A/D and D/A converters and semiconductor memories.

The usual aim in the design of an efficient image transmission system is to achieve minimum transmission rate whilst maintaining acceptable image quality. Bandwidth, or in the case of digital systems, bit rate, reduction is possible because first, there is large amount of statistical redundancy or correlation in normal images and second, there is a large amount of psychovisual redundancy also. The redundancy may be removed without causing a loss in subjective quality of the image.

A general digital communication system is shown in Figure 1.1. It consists of an information source, encoder, channel, decoder and finally the information user. The information source generates a sequence of discrete symbols taken from a finite set, which means that images have to be sampled and quantized for transmission. The encoder is a device that transforms the source output into a form suitable for transmission over the channel (where errors occur during transmission). The decoder then converts the channel output into a form suitable for interpretation by the user. In the model shown in Figure 1.1, it is assumed that the source, channel and the user are given and cannot be altered, so the communication system designer must construct the

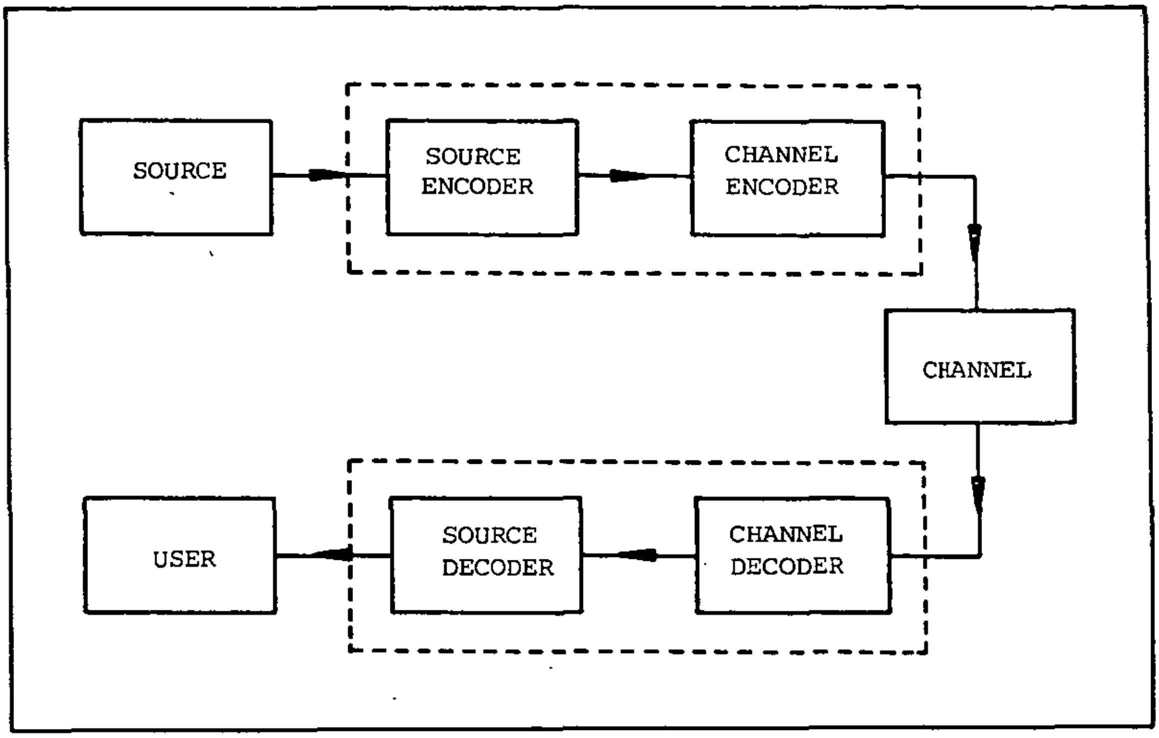

Figure 1.1 Digital communication system model

encoder and decoder to satisfy the rate and error criteria desired for the system.

The desire to reduce the channel requirement for digital image transmission systems has led to several approaches that reduce the redundancy in images. Two distinct approaches are considered : reversible and irreversible coding. For reversible coding, methods are sought that reproduce the sampled, quantized image information exactly. The noiseless coding theorem indicates that the amount of redundancy reduction that can be achieved is bounded by the source entropy. For irreversible coding, a certain amount of distortion is permissible in the design of the system. Statistical rate distortion theory(1-3) provides guidelines for transmitting images under these constraints. However, difficulties in the practical implementation of this theory are encountered, because no known objective distortion measure has been found that always agrees with human subjective judgement of picture quality. For example, noise may either increase or decrease the subjective quality of an image(4). Since the human observer is the end user of the received image, then the properties of the human visual system may be used to develop more efficient coding methods.

1.2.1 Pulse code modulation (PCM)

Pulse code modulation was invented by Reeves(5) in 1937 and has been extensively studied for image coding over the past two decades(6-9). In the basic PCM system shown in Figure 1.2, the analogue signal is bandlimited, sampled, quantized and encoded using a constant word-length code. If the base bandwidth of the input signal is W, then the sampling frequency must be greater than or equal to 2W to avoid aliasing and to allow perfect reconstruction of the original signal. The number of quantization levels must be large enough so that the quantization noise will not cause a grey scale contouring effect in the reconstructed image. The mean square quantization noise for a uniform quantizer with step size δ is given by

$$\varepsilon_q^2 = \frac{\delta^2}{12} \tag{1.1}$$

For a sinusoid $E_s \sin w_s t$ having a mean square value of $\frac{E_s^2}{2}$, then provided that the number of quantization levels is large and no peak

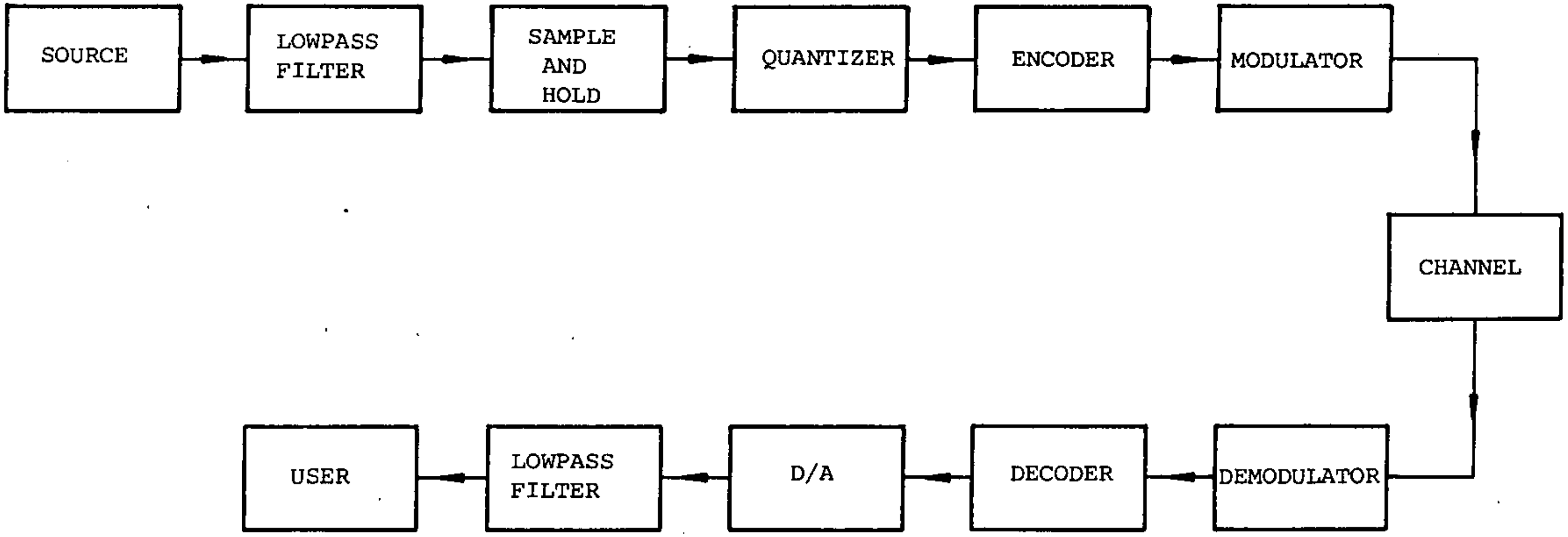

Figure 1.2 Pulse code modulation system

overload occurs, the peak signal to quantization noise ratio (SQNR) can be approximately represented by

$$\hat{SQNR} = 6.02n + 1.8 \text{ dB} \tag{1.2}$$

where n is the number of bits used to code a word.

For monochrome images, 50 or more quantization levels are required to prevent grey scale contouring. Consequently, in a PCM monochrome image coder, the image luminance is usually quantized at between 6 and 8 bits per picture element (pel). In terms of SQNR, a value from 38 dB to 50 dB is required to obtain satisfactory subjective quality.

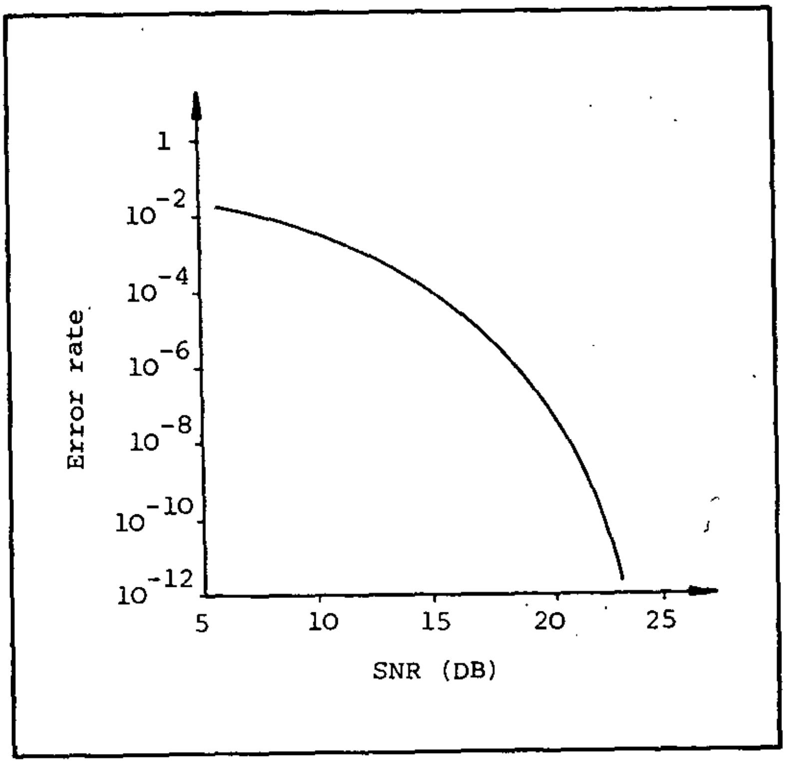

Figure 1.3 Channel error rate versus SNR for PCM system (after ref. 122)

Another important factor to consider in a digital imaging system is the channel error rate. As indicated in Figure 1.3, in which channel error rate is plotted against signal to noise ratio (SNR) for a PCM system, an SNR of 18 dB is sufficient (channel error rate 10^{-5}) to produce images of acceptable quality. Therefore the essential problem in digital image coding is to reduce the bandwidth at the expense of subjective quality.

1.2.2 Differential pulse code modulation (DPCM)

The general concept of linear predictive coding has developed from the invention by Cutler(10) of differential pulse code modulation. His original patent proposed that integrators be employed to predict the present sample based on the previous sample value along a line, and that the difference between the present sample and its estimate be quantized and coded for transmission. Since then numerous workers have improved the basic system and extended it to two- and three-dimensions(11-16).

Predictive coding techniques make use of the picture signal statistics and more recently, human visual characteristics(17,18) to reduce the bit rate. Television signals are highly correlated, both spatially and temporally. Correlation, or linear statistical dependence, indicates that a linear prediction of sample values based on the values of the neighbouring pels will result in prediction errors that have a smaller variance than the original pels. Owing to the smaller variance of the signal to be quantized, coded and transmitted, the amplitude range of the quantizer and thus the number of quantization levels can be reduced, resulting in fewer bits per pel than for the PCM system for the same SNR. By adapting non-uniform spacing of the quantization levels to the noise masking property of the human visual system, a further reduction in bit rate can be achieved.

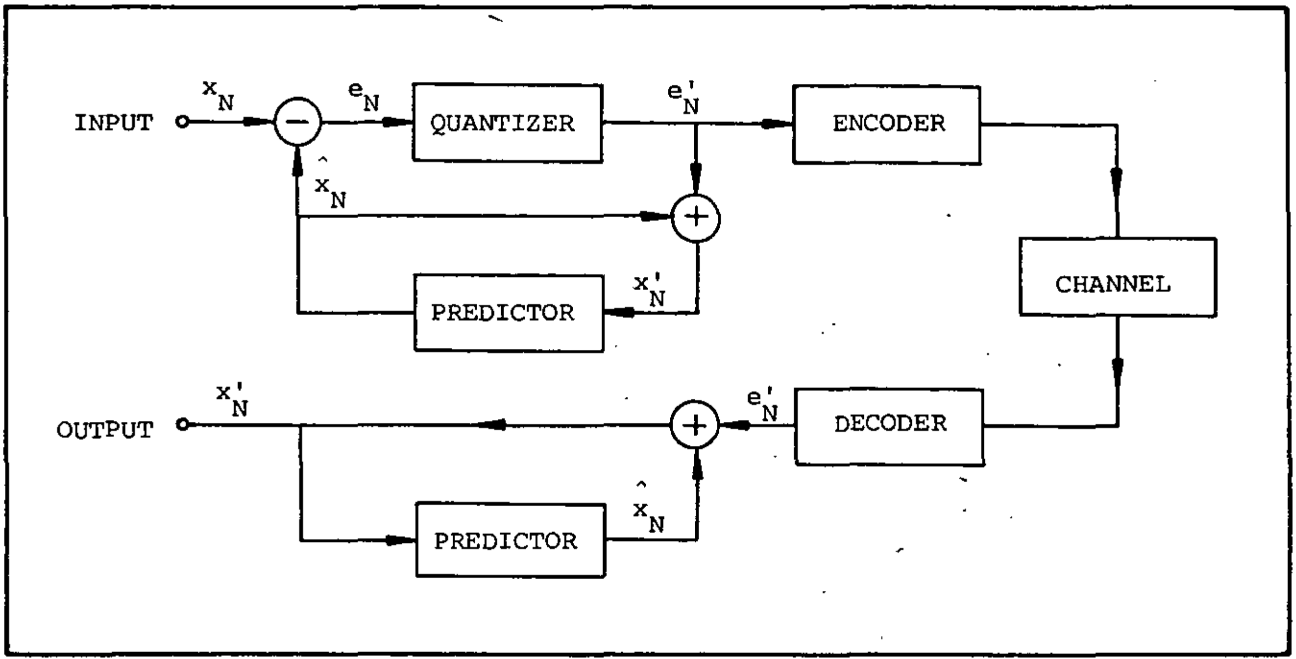

Figure 1.4 Block diagram of a DPCM system

A block diagram of a DPCM system is shown in Figure 1.4. The input signal x_N is a 8-bit PCM word. For every input sample x_N, the linear predictor generates a prediction value $\hat{x}_N$ which is calculated from (N-1) previous samples according to the relation

$$\hat{x}_N = \sum_{i=1}^{N-1} a_i \, x_{N-i} \tag{1.3}$$

Only previously transmitted samples are used for prediction, so that the receiver is also able to calculate $\hat{x}_N$. The predictor coefficients

a_i are optimised to yield a prediction error

$$e_N = x_N - \hat{x}_N \tag{1.4}$$

with minimum variance. The prediction error is then quantized with a non-uniform characteristic to produce e_N' and coded for transmission. At the receiver, the output x_N' is reconstructed, and can be shown to differ from the input signal x_N by the quantization error, q_N i.e.

$$x_N' = x_N + q_N \tag{1.5}$$

1.2.2.1 Optimization of the predictor

The values of a_i must be chosen such that the mean square value of the prediction error

$$\begin{aligned} \varepsilon_e^2 &= E\left[e_N^2\right] \\ &= E\left[(x_N - \hat{x}_N)^2\right] \\ &= E\left[(x_N - \sum_{i=1}^{N-1} a_i\, x_{N-i})^2\right] \end{aligned} \tag{1.6}$$

is a minimum. To find the predictor coefficients a_i that satisfy this condition, the partial derivatives of ε_e^2 with respect to each a_i are set to zero. Thus

$$\frac{\partial \varepsilon_e^2}{\partial a_i} = -\; 2E\left[(x_N - \sum_{i=1}^{N-1} a_i\, x_{N-i})\; x_{N-i}\right] = 0 \tag{1.7}$$

for i = 1,...., N-1. Expanding Equation (1.6) and using Equation (1.7),

$$\varepsilon_e^2 = E\left[x_N{}^2 - 2\, x_N \sum_{i=1}^{N-1} a_i\, x_{N-i} + \left(\sum_{i=1}^{N-1} a_i\, x_{N-i}\right)^2\right]$$

$$= E\left[x_N\ (x_N - \sum_{i=1}^{N-1} a_i\ x_{N-i})\right] + E\left[\sum_{i=1}^{N-1} a_i\ x_{N-i}(-x_N + \sum_{i=1}^{N-1} a_i\ x_{N-i})\right]$$

$$= E\left[x_N(x_N - \hat{x}_N)\right]$$

$$= E\left[x_N^2\right] - a_1\ E\ \left[x_{N-1}\ x_N\right] - \dots - a_{N-1}\ E\left[x_1\ x_N\right] \qquad (1.8)$$

Therefore knowing the autocovariances $E\left[x_N x_{N-i}\right]$ of the input signal, the optimum predictor coefficients a_i, based on a minimum mean square error criterion, can be calculated.

1.2.2.2 Quantizer optimization

In adaptive DPCM systems, optimization of the quantizer is carried out based on two criteria : mean square quantization error and the subjective visibility threshold of the quantization error. Since the mean square error criterion does not adequately take into account the human observer and hence the special properties of visual perception, its usefulness is restricted. The design of quantizers based on the visibility threshold of quantization errors has been developed by Sharma and Netravali(17). In their model, the visibility threshold, defined as the amount of quantization error at a picture element which is masked by the signal slope at the point (represented by the prediction error)

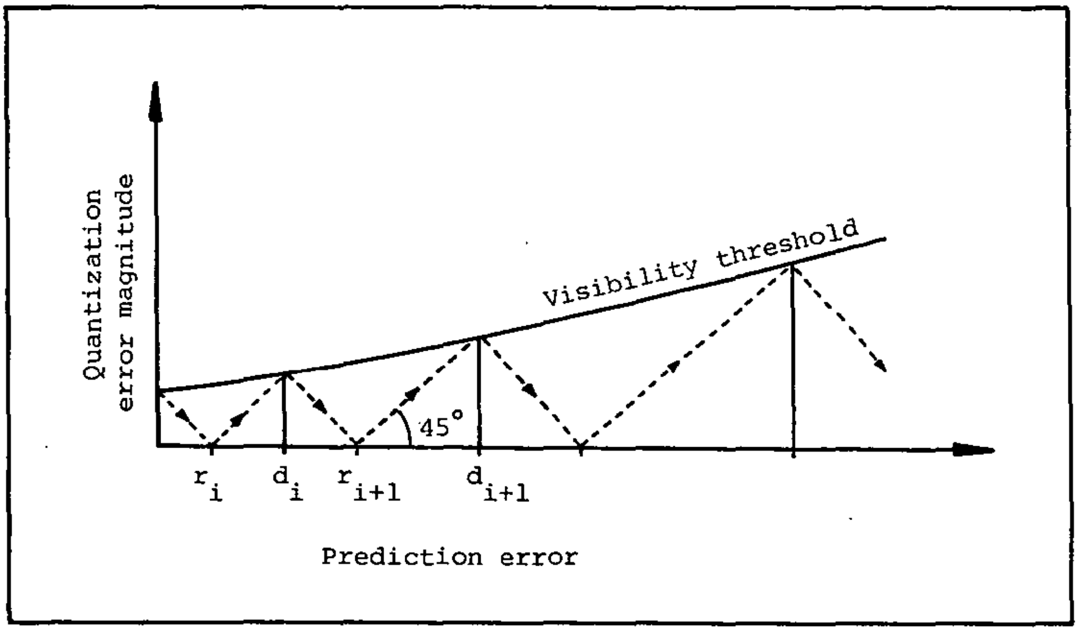

Figure 1.5 Symmetrical visibility threshold quantizer design procedure (after ref. 17)

is obtained by carrying out subjective tests. The method by which the decision and reconstruction levels are determined is illustrated in Figure 1.5. Here the reconstruction levels are given by the intersections of the dotted 45° lines and the abscissa. The decision levels can be obtained by dropping perpendiculars from the intersections of the dotted 45° lines and the visibility threshold curve to the abscissa. The procedure is continued until the last reconstruction level exceeds the amplitude range of the prediction error. This technique has been extended to quantize composite colour signals by Pearson(18), achieving a rate of 5.0 bits per pel with good picture quality.

1.2.3. Transform coding

Pictorial data contains redundancy which can be removed by efficient coding techniques. Correlation between the pels suggests that bit rate reduction can be achieved by transforming the spatial data into a set of independent coefficients, which can then be individually quantized according to some fidelity criterion. The transformations used are linear and unitary. For the purpose of transformation, the image is divided into subpictures, and this process means that redundancy existing between the subpictures is neglected. Therefore, purely on a statistical basis, it is advantageous to have large subpictures. However, for implementational simplicity, as well as to be able to exploit local changes in picture statistics and visual fidelity, a smaller subpicture is desirable. Also, since most of the compression results from dropping coefficients with small energy, an

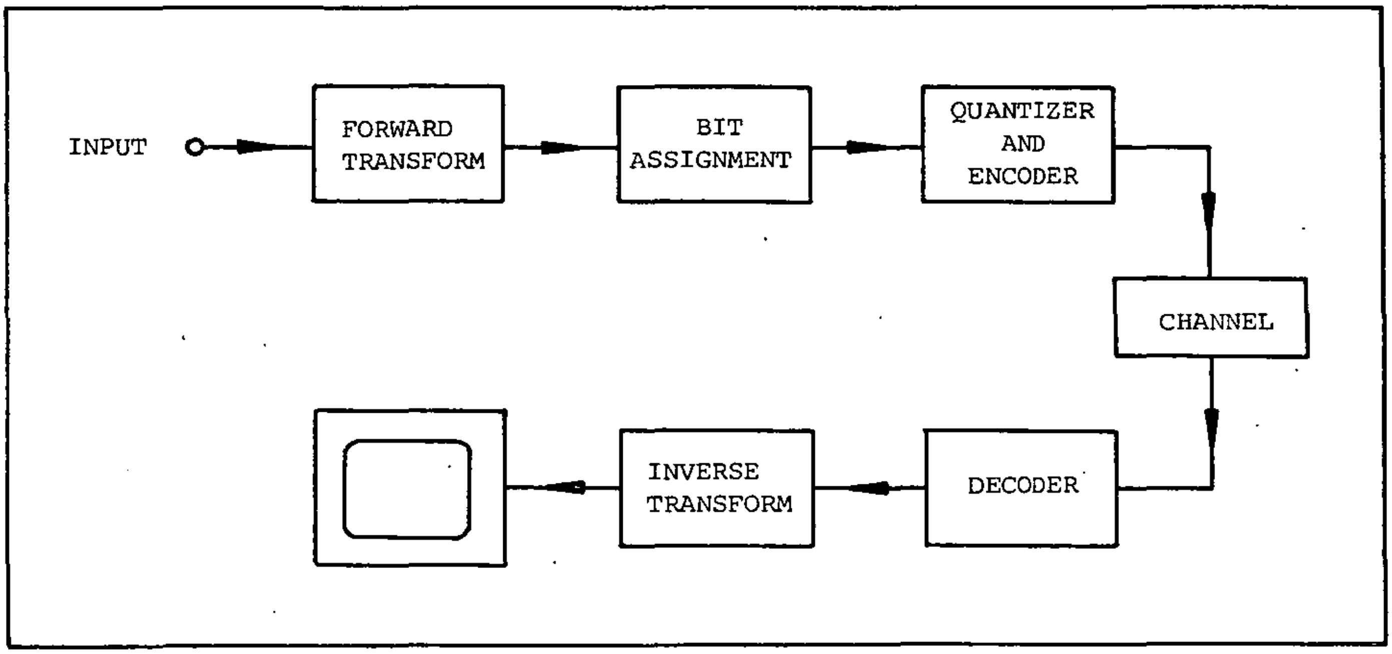

Figure 1.6 Block diagram of a transform coding system

important consideration for an efficient transform is the amount of energy compaction achievable.

Transform coding was first applied to coding of one-dimensional signals and then, many years later, to the coding of pictures by many independent workers(19-23). Figure 1.6 shows the block diagram of a transform coding system. Here, only the process of transformation and the probability density models of the transform coefficients are considered. The quantization and encoding aspects of transform coding will be described in Chapter IV.

1.2.3.1 Types of transform

The objective of transform coding is to reproduce images of good subjective quality using the least number of bits. Therefore, an optimum transform should produce coefficients that are statistically independent or at least uncorrelated. Since most of the bit reduction results from dropping some of the least significant coefficients, the mean square error produced in the reconstruction of the original image as a result of dropping those coefficients must be minimised. To achieve minimum mean square error, the image energy has to be compacted into as few coefficients as possible.

1.2.3.1.1 Optimum transform

The transform which satisfies the criteria mentioned in Section 1.2.3.1 is the Hotelling(24) (otherwise known as the Karhunen-Loeve) transform (KLT)(25-26). Let x be an N-component data vector and A the N x N transformation matrix. X is the coefficient vector containing the uncorrelated coefficients as a result of the transformation of x by A, i.e.

$$X = A \cdot x \tag{1.9}$$

The optimum transformation matrix A can be computed from the covariance matrix of the data vector x,

$$C_x = E\left[(x - E(x)) \cdot (x - E(x))^T\right] \tag{1.10}$$

where E is the statistical expectation and the superscript T denotes transpose. Rows of the optimum matrix A are normalized eigenvectors of the matrix C_x, i.e. they are solutions of the equation

$$C_x\, x = \lambda_i \cdot x \tag{1.11}$$

The coefficients of X that are obtained by such transformation have a covariance matrix given by

$$C_X = \begin{bmatrix} \lambda_1 & 0 & 0 & \cdots\cdots & 0 \\ 0 & \lambda_2 & 0 & \cdots\cdots & 0 \\ 0 & 0 & \lambda_3 & \cdots\cdots & 0 \\ \vdots & & & & \vdots \\ 0 & 0 & 0 & \cdots\cdots & \lambda_N \end{bmatrix} \tag{1.12}$$

where $\lambda_1, \ldots\ldots, \lambda_N$ are the eigenvalues of C_X. C_X, being a covariance matrix, has all its eigenvalues positive, and if they are ordered according to their magnitudes, maximum energy is compacted into the first M coefficients (M < N) corresponding to the eigenvectors of the M largest eigenvalues. If only the M coefficients corresponding to the largest eigenvalues are transmitted, then at the receiver the reconstruction error will have a mean square value given by

$$\varepsilon_r = \sum_{j=M+1}^{N} \lambda j \tag{1.13}$$

This is usually small, since only the smallest eigenvalues are included in the above summation.

Even though the KLT is the optimum transform, its practical application poses many problems. Firstly, the covariance function of an image is not stationary, and therefore one must either choose a different covariance matrix matched to different regions of the image or use an average, secondly, in practice, it is possible that some of the eigenvectors cannot be uniquely defined and finally, it does not possess a fast algorithm, even though Jain et al(27,28) have developed a fast KLT approximation. All the above problems render the hardware implementation of the KLT impractical, at least at the present.

1.2.3.1.2 Suboptimum transforms

Many other transforms have been devised which produce coefficients with less correlation than the image itself and which are easier to implement. Some of the more commonly used ones are the discrete Fourier transform(20), discrete cosine transform(29), Hadamard transform(30), Slant transform(31) and Haar transform(32). Unlike the KLT, these transforms are not dependent on image statistics. They are unitary i.e.

$$(A^T)^* = A^{-1} \tag{1.14}$$

where $(A^T)^*$ is the complex conjugate of A^T; and possess fast algorithms, and therefore are easier to implement. Table 1.1 shows the computational efficiency of the fast algorithms possessed by the transforms mentioned above.

Table 1.1 Computational requirement of image transforms

Transform	Computational requirement
Fourier	$(N \log_2 N)$ complex additions and multiplications
Hadamard	$(N \log_2 N)$ additions
Haar	$2(N-1)$ additions
Slant	$(N \log_2 N+2N-4)$ additions and multiplications
Cosine	$\frac{3N}{2}(\log_2 N-1)+2$ additions and $(N \log_2 N - \frac{3N}{2} + 4)$ multiplications.

1.2.3.2 Transform block size

If normalized mean square error is the criterion used to assess the quality of the decoded pictures, then performance should improve with increasing block size since the correlation between more pels is taken into account. However, the improvement is no longer significant as the block size is increased beyond 16 x 16, as shown in Figure 1.7(51) for different transforms, based on the assumption that the image is a two-dimensional Markov source with exponential horizontal and vertical correlation, ρ_H and ρ_V of 0.95 respectively. Also it is clear from the diagram that the cosine and sine transforms have performances very close to that of the KLT.

1.2.3.3 Probability density models for image transforms

Generally the probability density function (pdf) of the transform coefficients is difficult to obtain, since the short-term statistics of the image are not well defined. The first coefficient X(0,0) is the weighted sum of the original pels x(i,j) which are non-negative. As such X(0,0) itself is non-negative and its pdf is often modelled by a Rayleigh distribution given by

$$p(X(0,0)) = \frac{X(0,0)}{\sigma_X(0,0)} \exp\left[-\frac{X^2(0,0)}{2\,\sigma_X(0,0)}\right] \qquad (1.15)$$

where $\sigma_X(0,0)$ is the coefficient variance.

For other coefficients X(u,v) where $(u,v) \neq (0,0)$, Gaussian or Laplacian pdfs have been used. The Gaussian pdf is given by

$$p(X(u,v)) = \frac{1}{\sqrt{2\pi\sigma_X^2(u,v)}} \exp\left[-\frac{X^2(u,v)}{2\sigma_X(u,v)}\right] \qquad (1.16)$$

and the Laplacian pdf by

$$p(X(u,v)) = \frac{1}{\sqrt{2}\;\sigma_X(u,v)} \exp\left[\frac{2|X(u,v)|}{\sigma_X(u,v)}\right] \qquad (1.17)$$

The use of other models, such as the Gamma distribution$^{(33)}$, has been reported.

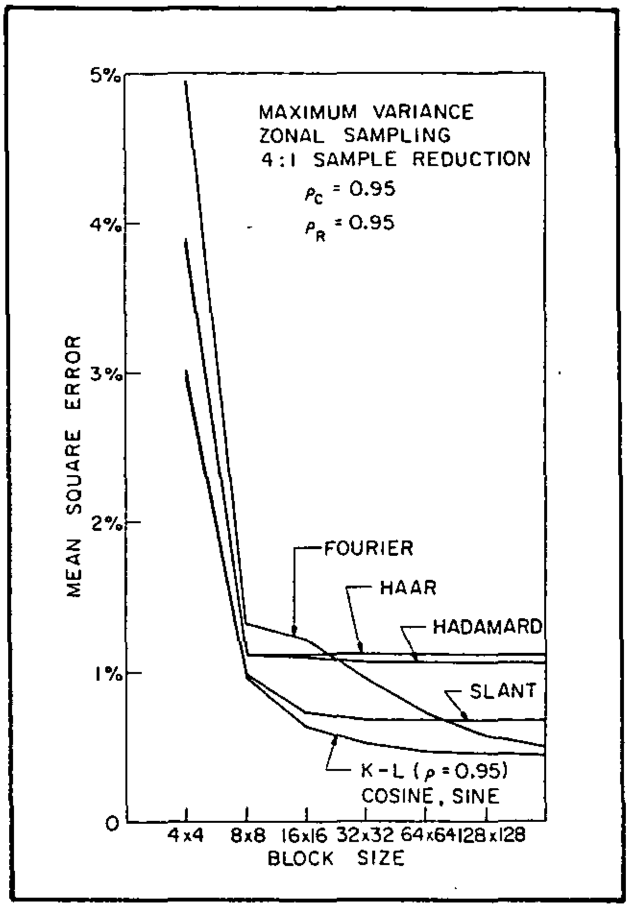

Figure 1.7 Normalised mean square error performance of image transforms as a function of block size (after ref. 51)

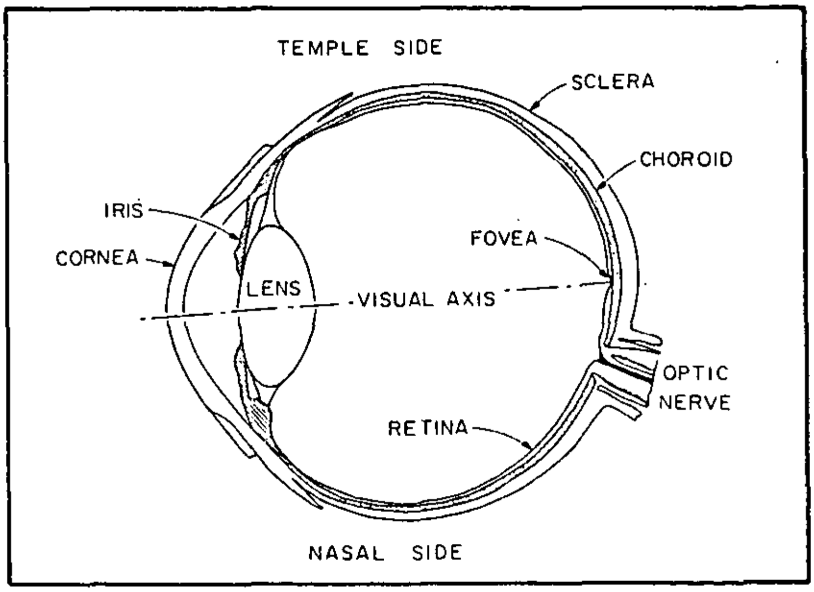

Figure 1.8 Cross section of the eye (after ref. 51)

1.2.4 Psychophysical properties of vision

Since the end user of any image processing system is the human observer, an understanding of the mechanism of human vision is clearly useful in the design of such systems. Such knowledge can be utilized to develop conceptual models of the human visual process. These models are not only useful in the design of image processing systems, but also in the construction of measures of image fidelity and intelligibility.

1.2.4.1 The eye

Figure 1.8 contains a sketch of the horizontal cross-section of a human eyeball. The front of the eye is covered by a transparent surface called the cornea. The remaining outer cover, called the sclera, is composed of a fibrous coat that surrounds the choroid, a layer containing blood capillaries. Inside the choroid is the retina, which is composed of two types of photoreceptors : rods and cones. Nerves connecting to the retina leave the eyeball through the optic nerve bundle. Light entering the cornea is focused to the retinal surface by a lens which changes shape under muscular control to perform proper focusing of near and distant objects. The iris acts as a diaphragm controlling the amount of light entering the eye.

The rods are more sensitive to light than the cones, and function at low intensities of illumination, whereas the cones function at high intensities and are responsible for colour vision(34). Figure 1.9 shows the relative sensitivities of rods and cones as a function of the illuminating wave length(35). The distribution of rods and cones over the surface of retina is uneven, as shown in Figure 1.10(36). At a point near the optic nerve, called the fovea, the density of the cones is the greatest. This is the region of maximum acuity (in terms of resolution). There are no rods or cones in the vicinity of the optic nerve, and this part of the retina is known as the blind spot.

There are three basic types of cones in the retina which have different absorption characteristics as a function of wavelength, with peak absorptions in the red, green and blue regions of the optical spectrum(35,37). This provides a physiological basis for the trichromatic theory of colour vision.

1.2.4.2 Contrast sensitivity

The ability of the eye to detect small changes of luminance or contrast plays an important role when considering visual display systems. A luminance difference which is below a certain threshold is impossible to detect and, in general, detection thresholds vary with the overall luminance of the background.

Against a uniform background of luminance L, the just noticeable difference in luminance ΔL increases proportionally with L. This is known as Weber's Law which states that

$$\frac{\Delta L}{L} = k \tag{1.18}$$

where k is a constant in the range 0.01 to 0.02. However, this result does not hold at very low and high values of L(38).

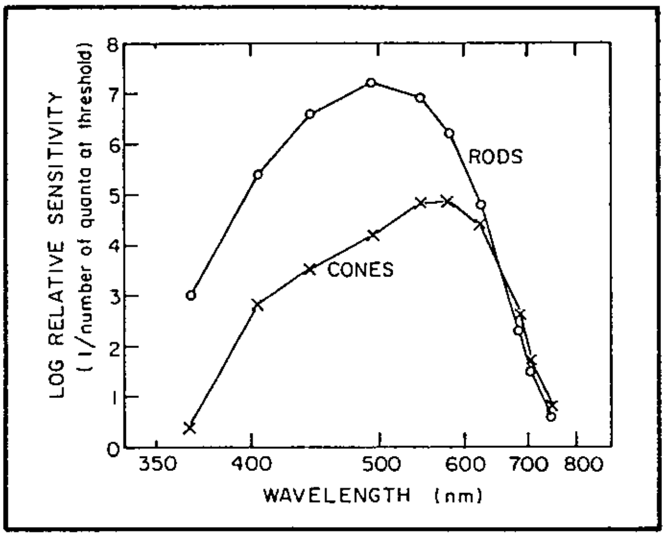

Figure 1.9 Sensitivity of rods and cones (after ref. 35)

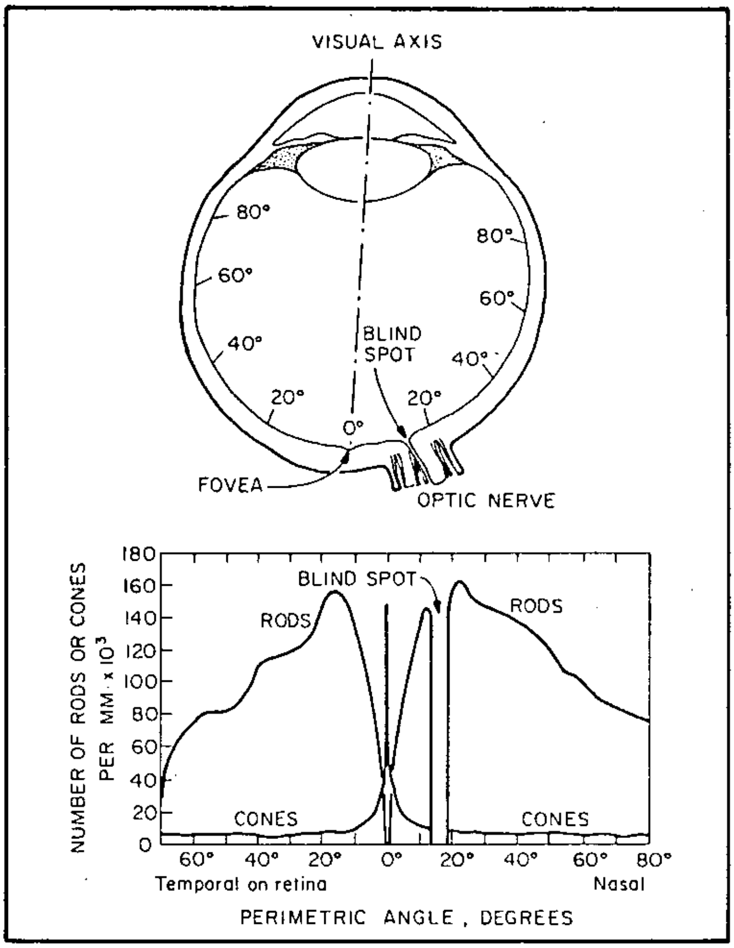

Figure 1.10 Distribution of rods and cones on retina

(after ref. 36)

Weber's Law assumes that the observer's vision is adapted to the background luminance L. Adaptation is an important mechanism which allows the observer a high contrast sensitivity over an enormous range of scene luminance. To allow for the viewing conditions, Stevens(39) introduced a power relationship of the form

$$B = c\, L^{\gamma} \tag{1.19}$$

where B is the absolute brightness, c is a constant and γ is an exponent which is adjusted to allow for viewing conditions. The value of γ varies between $\frac{1}{2}$ and $\frac{1}{3}$ for light and dark surround conditions respectively.

1.2.4.3 The modelling of the human visual system (HVS)

As image processing capabilities have grown in recent years, so has the complexity of human visual models which have been incorporated into image processing systems. Even though some recent models of human vision are quite elaborate, major differences still exist between the characteristics that these models can emulate and the actual properties of human vision. These differences are indicative of the current state of ignorance about the mechanisms of vision, and mark some of the present-day limitations on the accuracy with which visual behaviour can be simulated.

Hall and Hall(40) model the HVS as composed of a linear lowpass filter representing the formation of the retinal image by the eye's optics, a logarithmic non-linearity representing image sensing and a linear highpass filter representing neural image formation, as shown

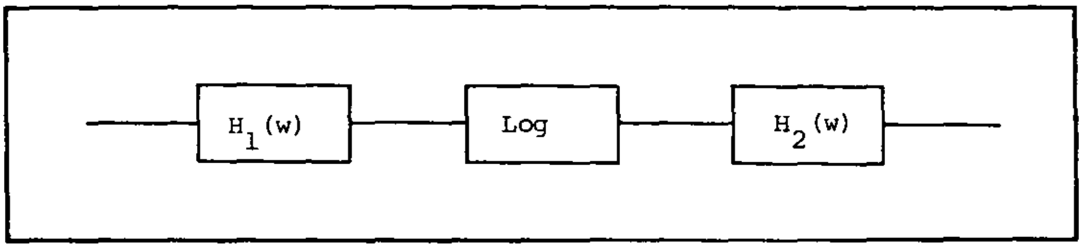

Figure 1.11 The Hall and Hall HVS model (after ref. 40)

in Figure 1.11. The transfer function $H_1(w)$ of the lowpass filter is found from the line spread function of the human eye with a pupil diameter of 3.0 mm$^{(41)}$ which is of the form

$$h_1(x) = \exp(-\alpha|x|) \tag{1.20}$$

where $\alpha = 0.7$. $H_1(w)$ is then given by the Fourier transform of Equation (1.20), i.e.

$$H_1(w) = \int_{-\infty}^{\infty} h_1(x) \exp(-jwx)\, dx$$

$$= \frac{2\alpha}{\alpha^2 + w^2} \tag{1.21}$$

For the highpass filter transfer function, there is assumed inhibitory feedback from neighbouring photoreceptors which decreases exponentially with distance. Thus

$$H_2(w) = \frac{a^2 + w^2}{2a_o a + (1 - a_o)(a^2 + w^2)} \tag{1.22}$$

By comparing their filter's response with actual data collected from psychophysical experiments, Hall and Hall arrived at the values $a = 0.01$, $a_o = 0.2$.

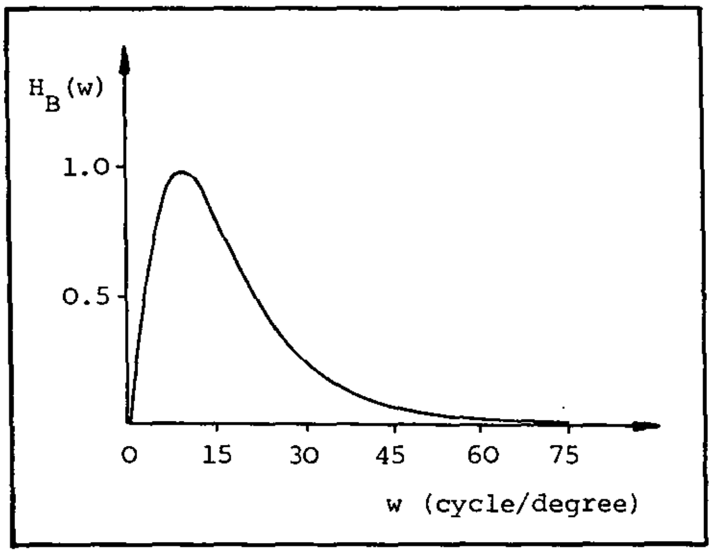

Figure 1.12 The Mannos and Sakrison HVS model (after ref. 42)

In another approach, Mannos and Sakrison(42) proposed a power law non-linearity and bandpass filter structure, where the non-linearity with power of 0.33 was proved to perform better than the logarithmic characteristic. The filter transfer function $H_B(w)$ is given by

$$H_B(w) = 2.6\left[0.0192 + 0.114w\right] \exp\left[-(0.114w)^{1.1}\right] \qquad (1.23)$$

and is illustrated in Figure 1.12. As can be seen from the figure, $H_B(w)$ has a peak value at $w = 8.0$ cycles per degree with a rapid decrease on either side of the peak.

1.2.5 Assessment of image quality

Two of the commonly used criteria of image quality are image fidelity and intelligibility. Image fidelity characterizes the departure of a processed image from some standard image, while image intelligibility denotes the ability of man or machine to extract relevant information from the image. It is clearly desirable to formulate quantitative measures of image fidelity and intelligibility as a basis for the design and evaluation of image processing systems. Much progress has been made in this direction but the measures that have been developed so far do not correlate well with the subjective rating of the images, and this is mainly due to our still poor understanding of the human visual system.

1.2.5.1 Image fidelity measures

The most common error measure in image processing is normalized mean square error (NMSE), given by

$$\mathrm{NMSE} = \frac{\sum_{m=0}^{M-1} \sum_{n=0}^{N-1} \left[x(m,n) - \hat{x}(m,n)\right]^2}{\sum_{m=0}^{M-1} \sum_{n=0}^{N-1} x(m,n)^2} \tag{1.24}$$

where $x(m,n)$ and $\hat{x}(m,n)$ are the original and processed image samples respectively, and MN is the total number of image samples. The NMSE is often expressed as an equivalent SNR

$$\mathrm{SNR} = -10 \log_{10}(\mathrm{NMSE}) \tag{1.25}$$

As mentioned earlier, the NMSE measure does not correlate well with the subjective evaluation of the image. However, it does provide an indication of the performance of an imaging system, and, coupled with informal subjective testing, it is a useful tool for the measurement of image fidelity.

1.2.5.2 Subjective rating of image quality

Experiments to judge image quality using human observers have been conducted by many workers(43-46). In some instances, untrained, 'non-expert' observers are used so that the judgement represents image quality as perceived by the average viewer. In others, tests are conducted with trained 'expert' observers experienced in image processing works and allegedly better able to provide a critical judgement of picture quality.

There are two common types of subjective evaluation : absolute and comparative. In the former, observers are shown an image and asked to judge its quality according to some predefined rating scale. The observer may be shown a set of reference images or may have to rely on his previous viewing experience. Comparative evaluation involves observer ranking of a set of images from 'best' to 'worst' for a particular group of images. Table 1.2 summarises the commonly used rating scales for subjective evaluation of images.

Table 1.2 Rating scales for subjective evaluation of images

I.	Quality scale
5	Excellent
4	Good
3	Fair
2	Poor
1	Bad
II.	Impairment scale
5	Imperceptible
4	Perceptible, but not annoying
3	Slightly annoying
2	Annoying
1	Very annoying
III.	Comparison scale
+3	Much better
+2	Better
+1	Slightly better
0	The same
-1	Slightly worse
-2	Worse
-3	Much worse

Subjective rating results are normally calculated as a mean opinion score defined as

$$C = \frac{\sum_{k=1}^{K} n_k c_k}{\sum_{k=1}^{K} n_k} \qquad (1.26)$$

where n_k is the number of images judged to be in the kth category and c_k is the numerical category value. At least twenty subjects are considered necessary to ensure statistical confidence in such subjective image quality experiments.

The results of the subjective testing are influenced by the types of images presented to the viewer and the viewing conditions. If the images are familiar to the observer, he is more likely to be more critical of impairments because of preconceived notions of the image structure. Further, test viewing conditions should be designed to match 'typical' viewing conditions as closely as possible. In the U.K., the viewing distance is specified as 6 times the picture height, the peak luminance as 50 cd/m^2, and the number of observers (who should be non-experts) around 20-25.

1.3 VIEWDATA SYSTEMS

Obtaining information about certain topics of interest can be a lengthy and costly process, and the alternative concept of bringing information into the home to be readily available at the touch of a button is not new. The BBC teletext service, Ceefax, and its ITV rival, Oracle have been in service for some time now. Teletext is basically a one way communication system in which the complete set of pages of text is transmitted at frequent intervals as part of the broadcast television programme using data signals carried within the blanking intervals. The only control available to the user is that he can select which particular page from the received set his decoder will accept, store and display, and the need continuously to repeat the whole set of pages tends to limit the total number of pages to one or two hundred.

Unlike teletext, the Viewdata system(47-49) does provide a two way communication link between the user and the viewdata computer via the telephone network. The desired page can be requested by sending a command signal directly to the computer at the local viewdata centre. This command is decoded by the computer and the selected page is then transmitted to the user and may be stored and displayed in much the same way as for teletext. Since there is no need to send whole sets of pages, the access time for a viewdata page is considerably shorter than that for a teletext page.

1.3.1 The Prestel system

1.3.1.1 System implementation

The world's first operational viewdata system is British Telecom's Prestel system. It essentially consists of a network of GEC 4082 computers interconnected by high-speed data links. There are two types of computer centre, the Information Retrieval Centres (IRCs) and the Update Centres(UDCs), as shown in Figure 1.13. Currently there is only one UDC, located in London. It is planned in future developments to have three interlinked UDCs, each with links to their own IRCs.

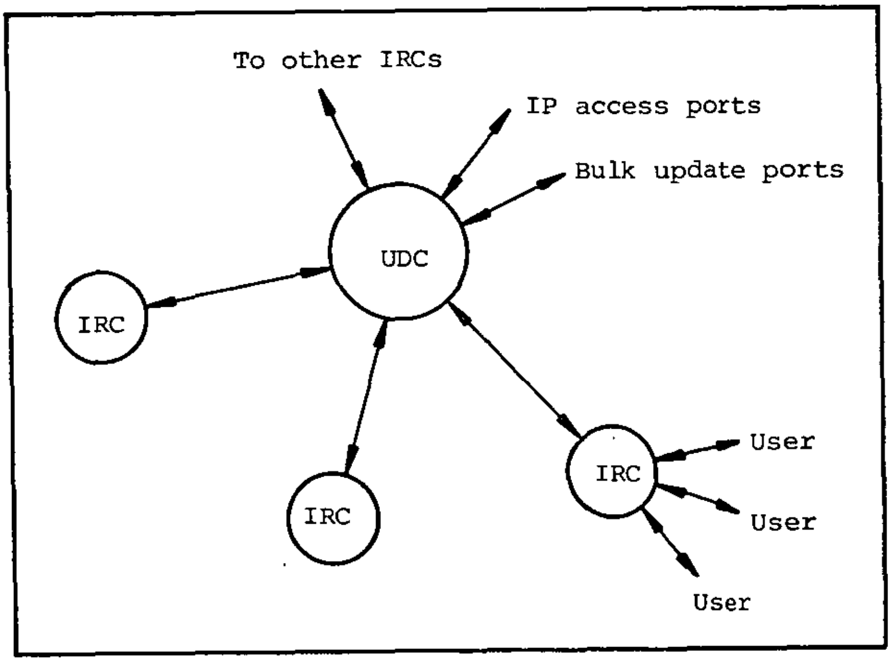

Figure 1.13 Current Prestel network topography

Each IRC has 'ports' available for access by users. These ports use a full duplex asynchronous interface which operates at 1200 bits/sec from the computer to the terminal and 75 bits/sec in the reverse direction. Each IRC computer has 384 kilobytes (Kb) of core storage and six 70 megabyte (Mb) disc drives. The database is held on the 70 Mb discs with a 'master' disc containing a 'userfile' for each authorised user, billing information and other system control data, a 'system' disc from which the software is loaded into core when the system is started, and four 'data' discs holding Prestel frames, each frame occupying 1 Kb. Dedicated lines connect each IRC to the local Regional Prestel Centre and to the National Prestel Centre to enable the operation staff to control and monitor the system.

Generally, the function of the UDC is to give access to the Information Providers (IPs) so that they can enter and amend Prestel frames on their part of the database. An IP is a person or organisation who places information on the database. The IP pays Prestel a yearly service charge and yearly rental for frames, and in return may charge a user for viewing the frames which he provides. Information is entered into the database by editing. Editing can either be done 'on-line' by the use of a simple editing terminal or by using bulk updating facilities.

1.3.1.2 The user

The Prestel user, on pressing a button on his keypad, will be routed through the Public Switched Telephone Network to the local IRC and charged as if making a local telephone call. Security of access by the user is controlled by the use of a unique terminal identifier in each Prestel set. This number is matched with a file of valid users held on each IRC computer. If desired, additional security can be provided by the user creating his own personal 'password'.

Having successfully obtained access to the system, the user follows a page selection procedure which uses a tree structure, where the user is gradually guided to the particular item of information he is seeking, as shown in Figure 1.14. Each Prestel frame contains 24 rows, each with 40 characters, both upper and lower case, and simple graphics, which can be displayed in seven colours in any of the eight backgrounds. The complete Prestel code table is shown in Table 1.3.

1.3.1.3 The terminal

A Prestel terminal is an ordinary colour television receiver with a Prestel decoder built into it. The block diagram of a Prestel decoder is shown in Figure 1.15. The line termination unit interfaces the decoder to the telephone line, and also contains barrier circuitry to prevent the possibility of dangerous voltages within the television set from being connected to the telephone line. The modem converts the Frequency Shift Keyed data from the computer at 1200 bits/sec into low voltage logic levels and transmits data at 75 bits/sec to the computer from the keypad. The viewdata electronics accepts data in serial form and converts this to parallel form for storage in the memory. In addition, it also detects errors, controls the line termination unit and monitors the keypad for new commands from the user. The memory, as the name implies, stores the frame of information being displayed, so allowing constant 'refreshing' of the display, following the receipt of the frame from the computer, even if the terminal has subsequently been disconnected from the telephone line. The character generator converts the data stored in the memory to a form suitable for display as recognisable characters and shapes on the screen. The timing circuits are used to synchronise the display of

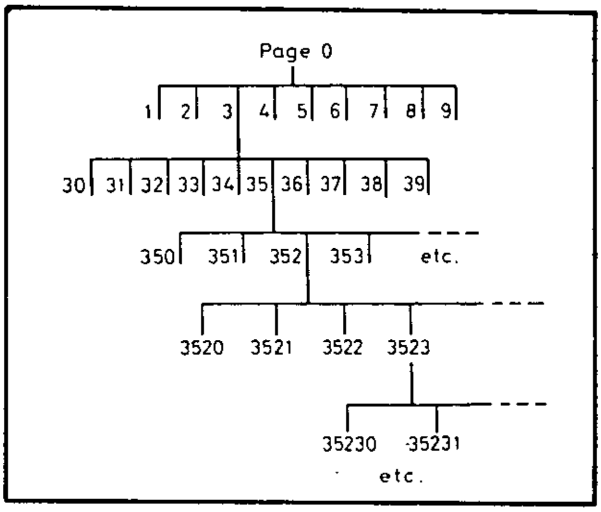

Figure 1.14 Tree structure for page selection in Prestel (after ref. 47)

Table 1.3 Prestel code table (after ref. 47)

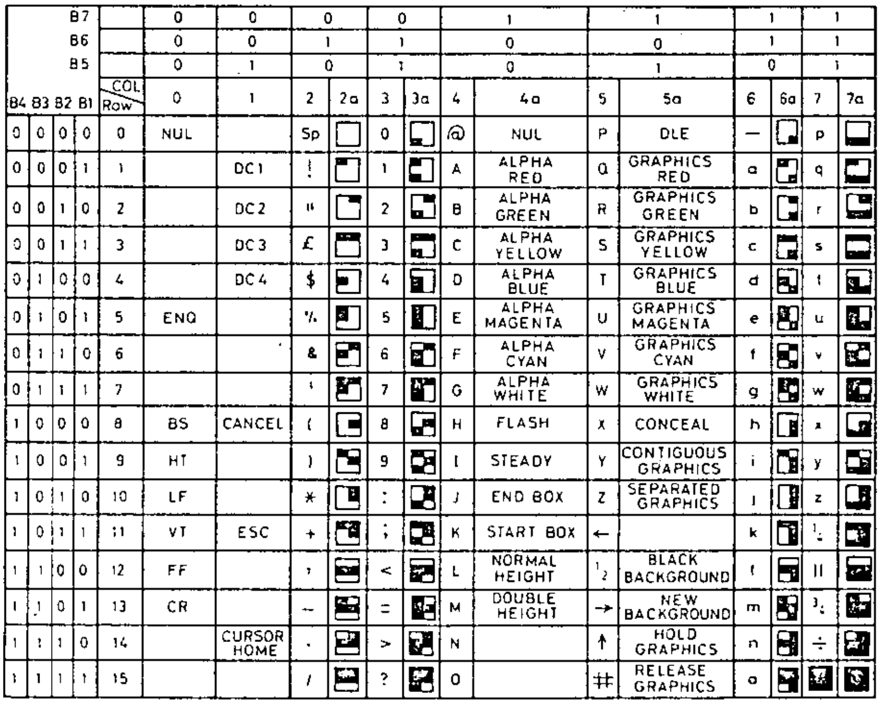

			B7		0	0	0		0		1		1		1		1	
			B6		0	0	1		1		0		0		1		1	
			B5		0	1	0		1		0		1		0		1	
B4	B3	B2	B1	COL Row	0	1	2	2a	3	3a	4	4a	5	5a	6	6a	7	7a
0	0	0	0	0	NUL		Sp		0		@	NUL	P	DLE	—		p	
0	0	0	1	1		DC1	!		1		A	ALPHA RED	Q	GRAPHICS RED	a		q	
0	0	1	0	2		DC2	"		2		B	ALPHA GREEN	R	GRAPHICS GREEN	b		r	
0	0	1	1	3		DC3	£		3		C	ALPHA YELLOW	S	GRAPHICS YELLOW	c		s	
0	1	0	0	4		DC4	$		4		D	ALPHA BLUE	T	GRAPHICS BLUE	d		t	
0	1	0	1	5	ENQ		%		5		E	ALPHA MAGENTA	U	GRAPHICS MAGENTA	e		u	
0	1	1	0	6			&		6		F	ALPHA CYAN	V	GRAPHICS CYAN	f		v	
0	1	1	1	7			'		7		G	ALPHA WHITE	W	GRAPHICS WHITE	g		w	
1	0	0	0	8	BS	CANCEL	(		8		H	FLASH	X	CONCEAL	h		x	
1	0	0	1	9	HT		)		9		I	STEADY	Y	CONTIGUOUS GRAPHICS	i		y	
1	0	1	0	10	LF		*		:		J	END BOX	Z	SEPARATED GRAPHICS	j		z	
1	0	1	1	11	VT	ESC	+		;		K	START BOX	←		k		¼	
1	1	0	0	12	FF		,		<		L	NORMAL HEIGHT	½	BLACK BACKGROUND	l		||	
1	1	0	1	13	CR		-		=		M	DOUBLE HEIGHT	→	NEW BACKGROUND	m		¾	
1	1	1	0	14		CURSOR HOME	.		>		N		↑	HOLD GRAPHICS	n		÷	
1	1	1	1	15			/		?		O		#	RELEASE GRAPHICS	o			

COLUMNS 2a, 3a, 6a, 7a produced after Graphics select code
COLUMNS 4a, 5a produced after ESC code

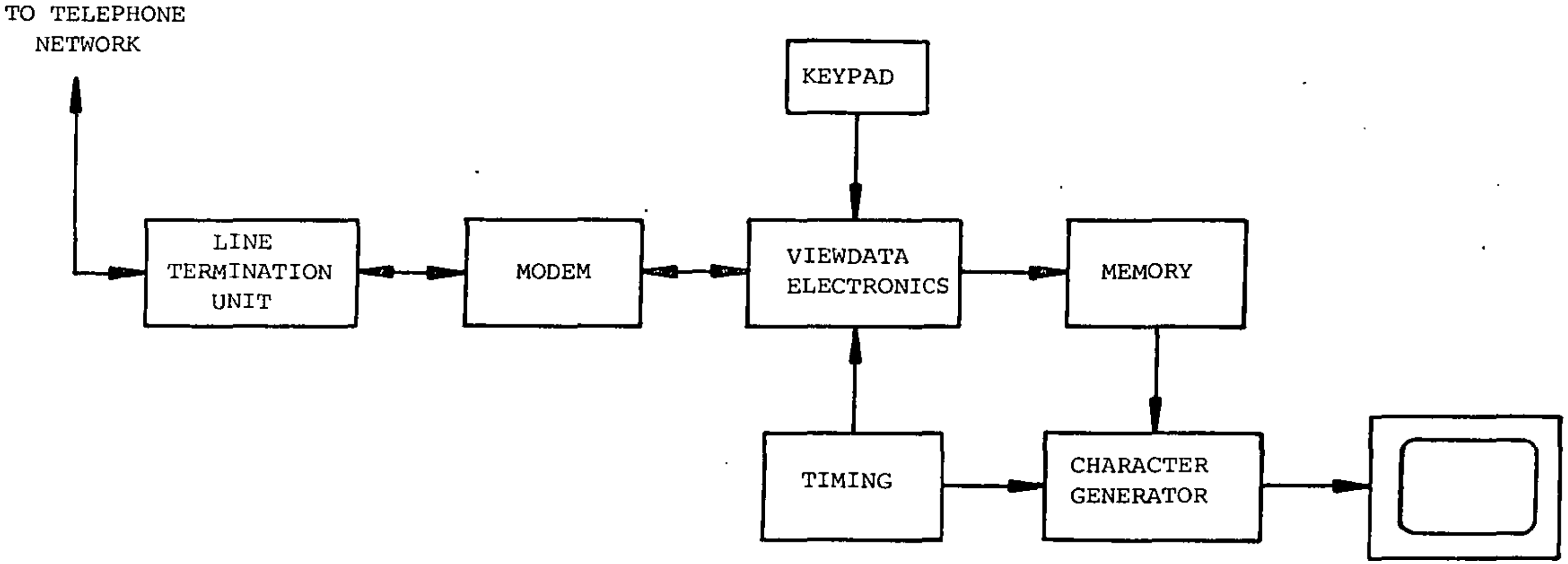

Figure 1.15 Block diagram of a Prestel terminal

characters from the generator with the line and field scans of the display section.

An important enhancement of the system is the insertion of a still picture of television quality into an information frame. This concept and the proposed system is called Picture Prestel.

1.3.2 Picture Prestel

The new Picture Prestel service is able to transmit not only alphanumerics and graphics, but also still colour picture inserts in a single frame. To reduce the storage requirement and the transmission time, the picture area has to be limited to a fraction of the Prestel frame. In addition, a further reduction in the data to be stored and transmitted can be achieved by the use of data compression techniques.

The overall system is shown in Figure 1.16(50). The original picture is converted by a television camera into its luminance (Y) and two colour difference components (U and V). The Y component is sampled at 8 MHz and the U and V components at 2 MHz. The size of the picture is then reduced to a fraction of that of the picture frame, either optically or by a combination of digital lowpass filtering and a decimation process. DPCM is then employed to code the Y, U and V components at 4 bits per pel, and are then multiplexed for storage at the Prestel Centre and transmission to the customer's receiver.

At the receiver, once a picture is requested and a 'start picture' command received, the incoming picture data is decoded by a

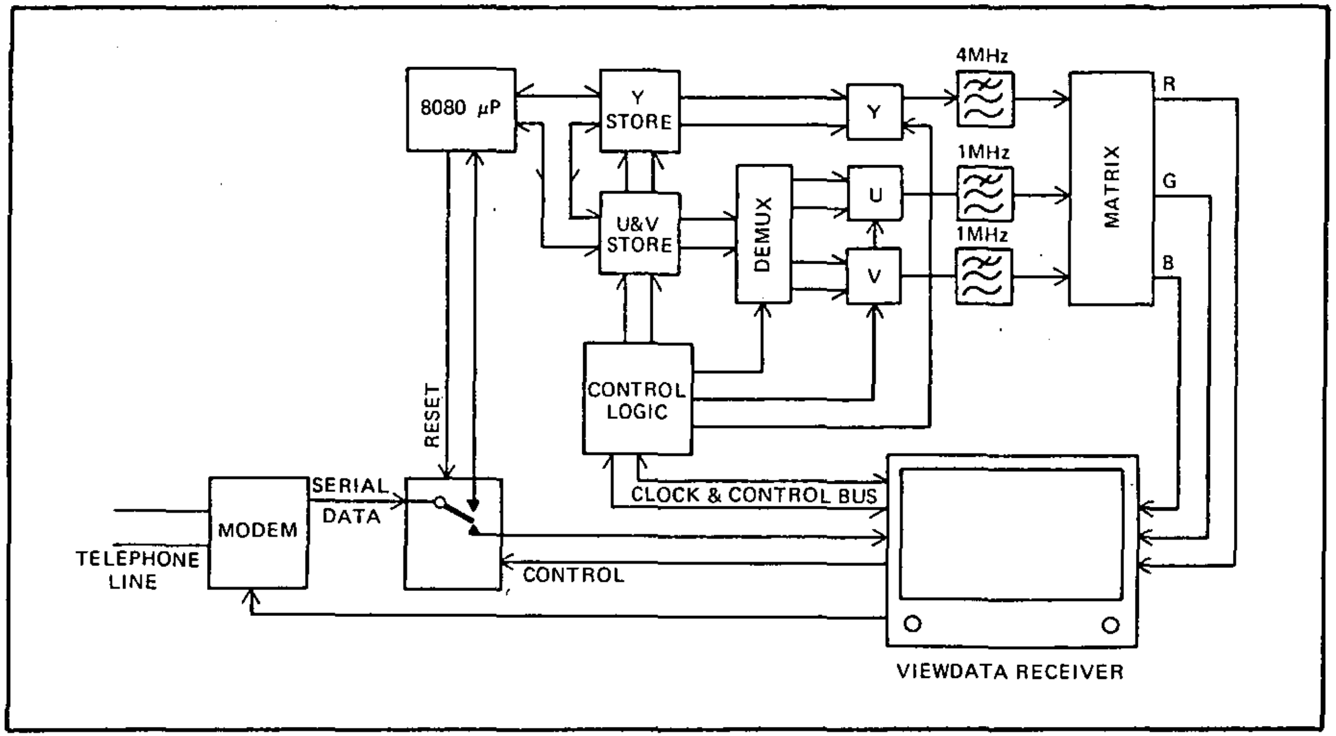

Figure 1.16 Block diagram of a Picture Prestel terminal (after ref. 50)

microprocessor into 8 bit PCM words and stored in a separate picture insert memory. 16 Kb of memory are provided for the luminance and 4 Kb for each of the chrominance signals. The displayed picture bandwidth is about 4 MHz for luminance and 1 MHz for each of the chrominance signals.

The normal Prestel character store holds the page of alphanumerics associated with the picture. A start insert code on this page switches the display to the picture store via appropriate digital-to-analogue converters. The display is switched back to the character store at the end of each line of the picture by a special codeword in the picture data. Error detection is by means of 2 parity check bits at the end of each picture line and correction is performed by repeating the previous line.

Line repetition as a means of error concealment works well at low error rates. At high error rates, it produces an unpleasant mosaic structure due to the frequent repetition of adjacent lines. Also, at the present transmission rate of 1200 bits/sec, it would take about 1 minute to transmit a picture insert of 128 x 128 pels. To improve the quality of the received picture in the event of errors occuring in the channel, a statistical error detection and correction procedure is examined which detects and corrects only the erroneous pel without tampering with other 'correct' pels. Further, to reduce the update time, transform coding techniques are investigated. Another advantage of using transform coding is its ability to produce a progressive build-up of the picture.

1.4 ORGANISATION OF THE THESIS

Following this introductory chapter, Chapter II deals with an error detection and correction scheme based on the statistics of the signal. Implementation of the scheme using both PCM and DPCM systems is described, with an account of the formulation of the detection algorithm in case of PCM, and how it is then extended to detect errors in DPCM systems.

Chapter III describes the various techniques developed for the reduction of picture size to form such a picture insert as that to be used in the viewdata system. Conventional methods of digital lowpass filtering and decimation using different source pictures are outlined in the first part of the chapter. The latter parts of the chapter are devoted to investigations of the feasibility of carrying out lowpass filtering and decimation in the transform domain using different unitary transforms.

Having achieved picture size reduction, which itself produces a substantial amount of data compression, the picture insert is coded, further to reduce the bit rate. Chapter IV contains details of the various transform coding schemes investigated and the results obtained using different source pictures, taking into consideration the bit rate reduction achievable and the subjective quality of the picture obtained. This chapter also contains a short review of adaptive transform coding techniques that have been developed recently.

Chapter V deals with the display of the received image data. One of the advantages of transform coding is the ability progressively to update the pictorial information as more coefficients are decoded. Inverse transformation of a different coefficient or a combination of coefficients produces markedly different visual effects. Hierarchical transmission of coefficients is investigated and the results compared to find the best sequence for coefficient transmission.

The thesis concludes with Chapter VI which collates the ideas and work that has been performed during the course of the research programme and suggests new ideas for future work.

CHAPTER II - ERROR DETECTION AND CORRECTION

2.1 INTRODUCTION

The viewdata system currently on trial in the U.K. employs DPCM encoding to transmit the video information. To protect the transmitted codewords, error protection coding is used, which involves extra bits for each transmitted DPCM word. To reduce transmission rate further, error detection and correction without employing protection codes is investigated here. First the detection and correction algorithm is investigated using a PCM system and then further extended to a DPCM system.

Transmitted PCM and DPCM video images are composed of binary words which represent, at each sampling instant, the amplitude of the luminance level, and the difference between the luminance level and a locally reconstructed level, respectively. Binary errors are said to occur at the receiver if bits are regenerated that have the opposite level to those transmitted, i.e. a logical 1 is regenerated as a logical 0 or vice versa. The inaccuracy of the decoded sample depends on which bit in the received word is erroneous. If the most significant bit is in error the decoded sample may be in error by one half, or even the total luminance range of the quantizer, whereas a bit-error in the least significant position in the binary word produces the smallest luminance error.

The effect of a transmission error in PCM or DPCM video images is radically different. In the former the erroneous pel is perceived as a spot on the image, whereas in DPCM using previous pel prediction, the solitary error results in a streak whose origin is the erroneous pel and which may extend to the end of the scan line. Thus transmission errors in DPCM are more serious than in PCM. However, in the absence of transmission errors, DPCM requires fewer bits per pel than PCM for a given picture quality, and its greater vulnerability to channel errors has thus prompted numerous proposals for combatting errors.

Channel coding is an obvious way to protect the DPCM bit stream, and BCH-codes have been investigated for this purpose(52,53). The employment of error detecting and correcting codes results in an increase in transmitted bit-rate and system complexity. Another approach(54-56) is to reduce marginally the performance of the source codec in order to improve its robustness to transmission errors, and thereby avoid channel coding. However, the enhancement of badly corrupted pictures is often inadequate.

The length of the erroneous luminous streaks can be reduced by transmitting PCM codewords after a block of DPCM codewords(57-59) or by a leaky prediction. It is found that replacement of an erroneous line by an average of adjacent lines results in a marked improvement in picture quality and that two-dimensional prediction results in less visible error patterns than previous element (1-D) prediction and these observations are confirmed by the theoretical analysis of the error pattern of Jung and Lippmann(55). For reducing the error streaks of one-dimensional prediction, a combination of DPCM and PCM coding called hybrid D-PCM has been introduced(61).

Other approaches rely on exploiting the redundancy inherent in most images. For example(62), blocks of DPCM words can be Walsh Hadamard transformed into a format such that when the receiver recovers the transformed coefficients the presence of an isolated error in the block will be detected and its magnitude known. Correlation techniques are then used to locate the sequency in error, inverse transformation applied, and the DPCM signal recovered. This method can be viewed as an unusual form of channel coding that relies on signal statistics. The detection and correction procedures can be made at the receiver without recourse to any channel coding, the corrections being made exclusively on the received data(63). The decision as to whether a pel is in error can be made by comparing its value with pels on the previous and subsequent lines, and if these differences are above certain threshold values the pel is considered to be in error. To aid the detection process, bit assignment of DPCM codewords is arranged such that if a bit-error occurs the recovered pel has error either of a small or large magnitude. Correction is performed by replacing the erroneous pel by the corresponding pel in the previous line.

PCM and DPCM are widely used to encode speech, and significant improvements in the perceptual quality of speech have been achieved by exploiting the statistical properties of the speech signal(64-70). In the treatment to follow some of the concepts used in combatting errors in PCM and DPCM speech are borrowed and adapted to the strategies employed in enhancing PCM and DPCM pictures degraded by transmission errors. For example, in Section 2.2, an enhancement scheme that was conceived for PCM speech$^{(65)}$ is extended to allow for the two-dimensional properties of PCM images. Section 2.3 is concerned with DPCM enhancement in which PCM updates are used. Error detection is performed adaptively by acknowledging simple statistical properties of the image, correction is achieved by interpolation, and failure to detect a known error is partially overcome by line replacement. Also, the way in which enhanced picture quality can be traded against system complexity is discussed. Discussion of the results is presented in Section 2.4 and conclusions in Section 2.5.

2.2 PCM ENHANCEMENT

The PCM enhancement system is illustrated in Figure 2.1. The received PCM image consisting of $(MN)^2$ binary words, each word representing the n-bit uniform quantization of a pel, is decoded N lines at a time. The system operates on blocks of N^2 pels, commencing with $B_{1,1}$, composed of the first N lines and the first N pels on each line. The block arrangement for the image is shown in Figure 2.2. It is emphasized that the square block structure is used for convenience rather than for necessity.

2.2.1 Error detection

The error detection system searches for a pel having an

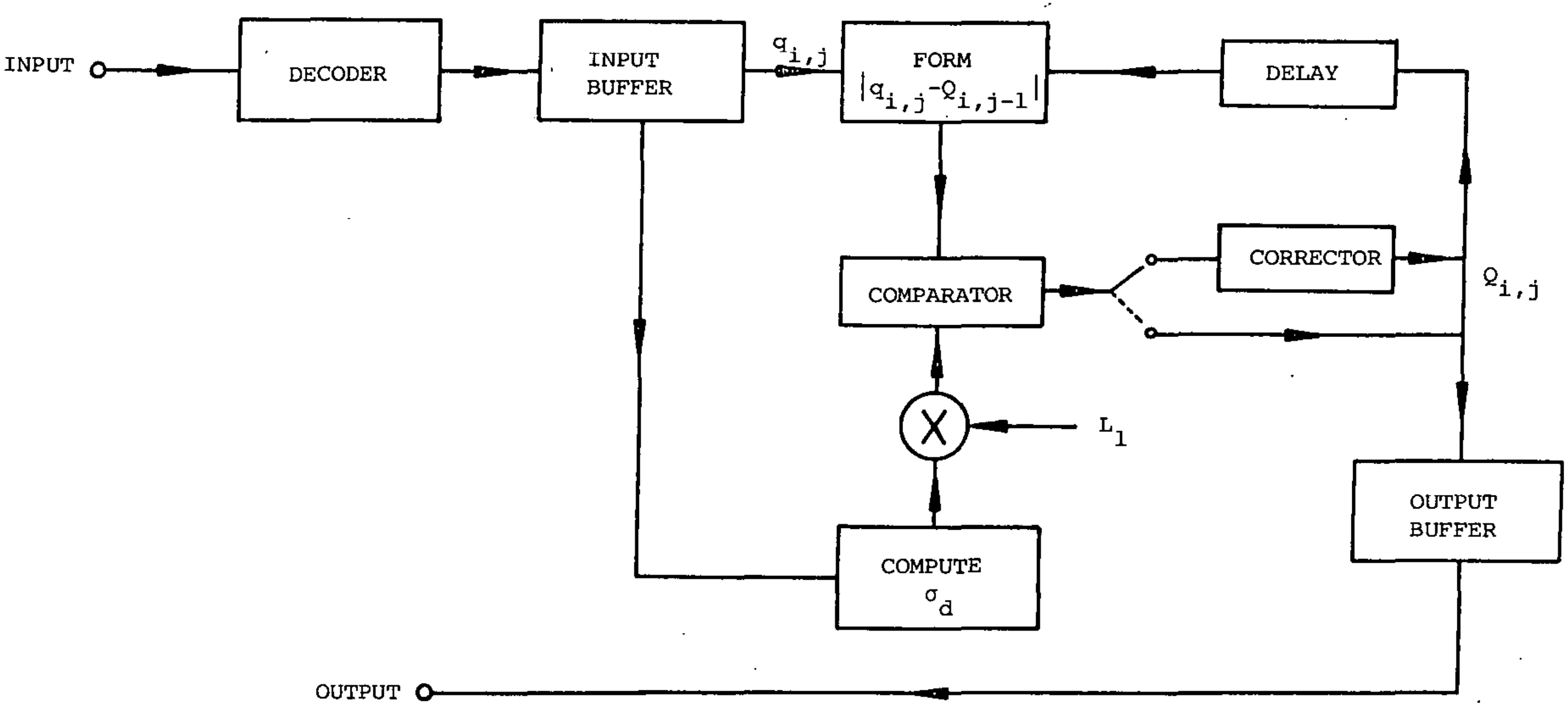

Figure 2.1 PCM enhancement system

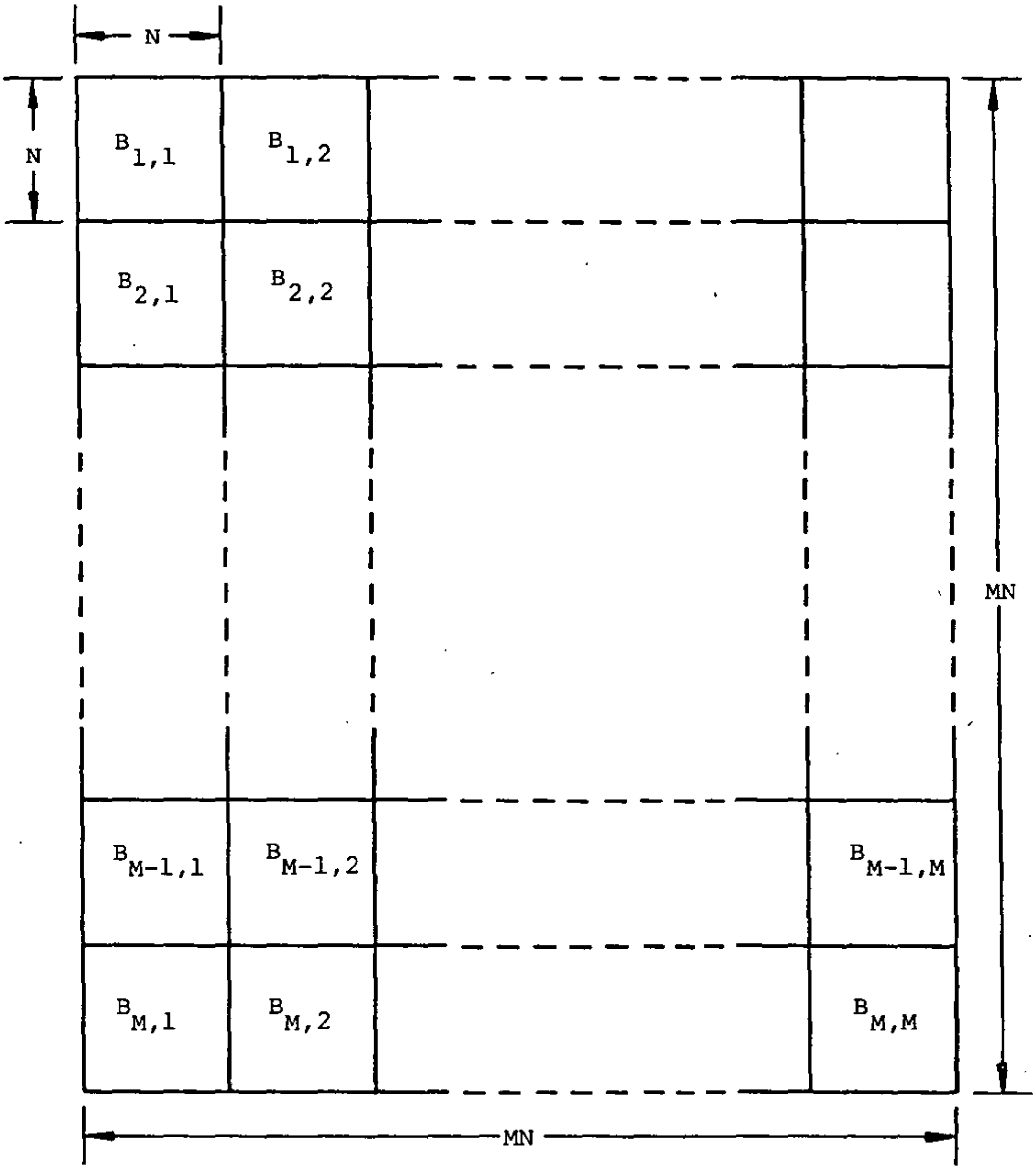

Figure 2.2 Block arrangement for enhancing received image

unexpected amplitude. Due to the high correlation in the picture, errors cause local decorrelation. Although changes in local correlation have been used in PCM speech to detect erroneous samples(64), the technique has the weakness of not being able to identify the erroneous sample with precision. The correction process therefore has to modify the samples, i.e., to undertake partial correction, of a number of samples in the vicinity of the erroneous sample. Tampering with samples other than the corrupted one is clearly undesirable. To avoid this situation a pel is considered to be in error if there is an unexpected change in the luminance level between the pel under examination and the previous pel along on the scan line (already tested and deemed correct) relative to an adaptive threshold. This threshold depends on the rms value of the differences between adjacent samples measured over a local area of the image. Specifically, a decoded PCM pel $q_{i,j}$ on the ith row of the jth column of a block is considered to be in error if

$$|q_{i,j} - Q_{i,j-1}| > L_1\sigma_d \tag{2.1}$$

where $Q_{i,j-1}$ is the previous accepted or 'corrected' pel, σ_d is the rms difference between adjacent pels on adjacent rows and columns, and L_1 is a system parameter whose value is a function of σ_d. q and Q are the decoded pels prior and subsequent to the detection and correction process, respectively. σ_d is given by

$$\sigma_d^2 = \frac{1}{4(N-1)^2} \sum_{i=2}^{N} \sum_{j=2}^{N} \{(q_{i,j}-q_{i,j-1})^2 + (q_{i,j}-q_{i,j+1})^2$$

$$+ (q_{i,j}-q_{i-1,j})^2 + (q_{i,j}-q_{i+1,j})^2\} \tag{2.2}$$

2.2.2 Error correction

If Inequality (2.1) is satisfied, the erroneous pel $q_{i,j}$ is replaced by the simple interpolation,

$$Q_{i,j} = \frac{1}{4} (Q_{i,j-1} + Q_{i-1,j} + q_{i,j+1} + q_{i+1,j}). \qquad (2.3)$$

If no error is detected,

$$Q_{i,j} = q_{i,j}. \qquad (2.4)$$

The image enhancement system processes blocks $B_{1,1}, B_{1,2}, \ldots, B_{1,M}$, when the next N lines are decoded and blocks $B_{2,1}, B_{2,2}, \ldots, B_{2,M}$ are examined, and so on to block $B_{M,M}$. The enhanced image experiences a delay of N lines duration.

2.2.3 Experimental procedure

The evaluation of the enhancement methods was made using computer simulation. The 'GIRL' image shown in Figure 2.3(a) was digitally encoded, and the bit stream subjected to random errors. Original, corrupted and enhanced images were displayed on a video monitor from which photographs were made. In addition to these subjective results, signal-to-noise ratio (SNR) measurements were made, where SNR is the ratio between the signal power in the original image to the power in the difference between the original and displayed image, the measurement being over the entire image of 256 lines, 256 pels per line.

2.2.4 Results

For the PCM image, each of the 65,536 pels was uniformly quantized with n=8 bits such that 256 Δ_u equalled the range of the video signal. In the enhancement process the block size N=64, and the number of blocks $M^2 = 16$. The detection parameter L_1 of Inequality (2.1) was found by experiment to be:

$$L_1 = \begin{cases} 6.0 , & 0<\sigma_d<8.5 \\ -1.04\sigma_d+14.9 , & 8.5\leqslant\sigma_d<11.0 \\ -0.31\sigma_d+6.86 , & 11.0\leqslant\sigma_d<12.0 \\ 1.0 , & 12.0\leqslant\sigma_d \end{cases} \tag{2.5}$$

Figure 2.3(a) shows the original image. The photograph in Figure 2.3 (b) is the corrupted image when the percentage bit error rate (BER) is 0.6, and it is characterized by a random distribution of dots where pels have had their luminance levels altered by the transmission errors. Figure 2.3(c) shows how the enhancement system removes most of the effects of the transmission errors with negligible introduction of false errors. The variation of SNR as a function of BER for the corrupted and enhanced images is displayed in Figure 2.4. The SNR improvement is ≈10 dB for 0.1%< BER < 2.0%. Negligible degradation of the image occurs at BER < 0.05 percent.

2.3 DPCM ENHANCEMENT

Consider the DPCM encoder shown in Figure 2.5 having a first order predictor and a 16 level tapered quantizer (TQ). The predictor

(a) Original

(b) Corrupted

(c) Corrected

Figure 2.3 PCM enhancement, BER = 0.6%

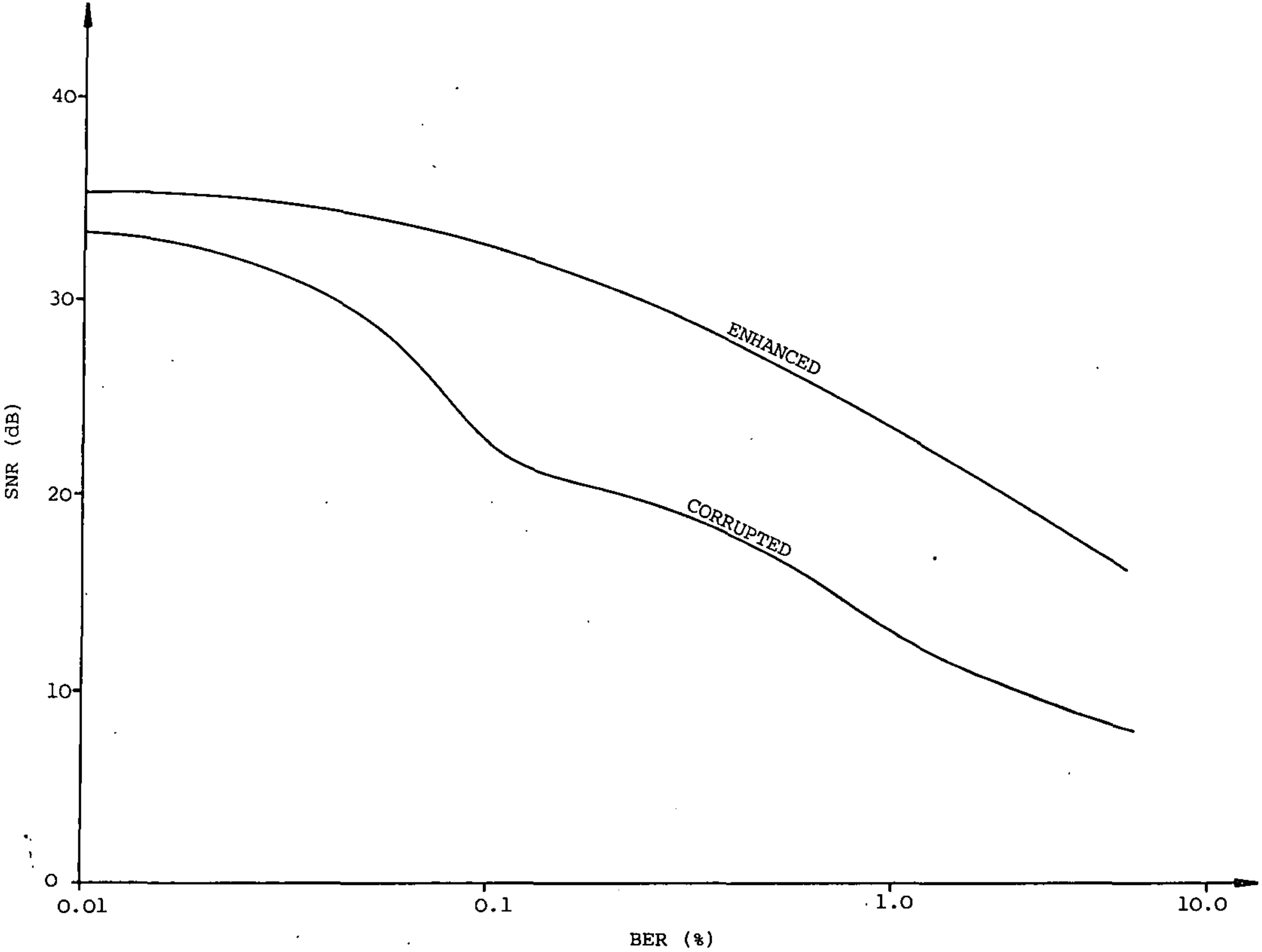

Figure 2.4 Variation of SNR as a function of BER for corrupted and enhanced PCM picture

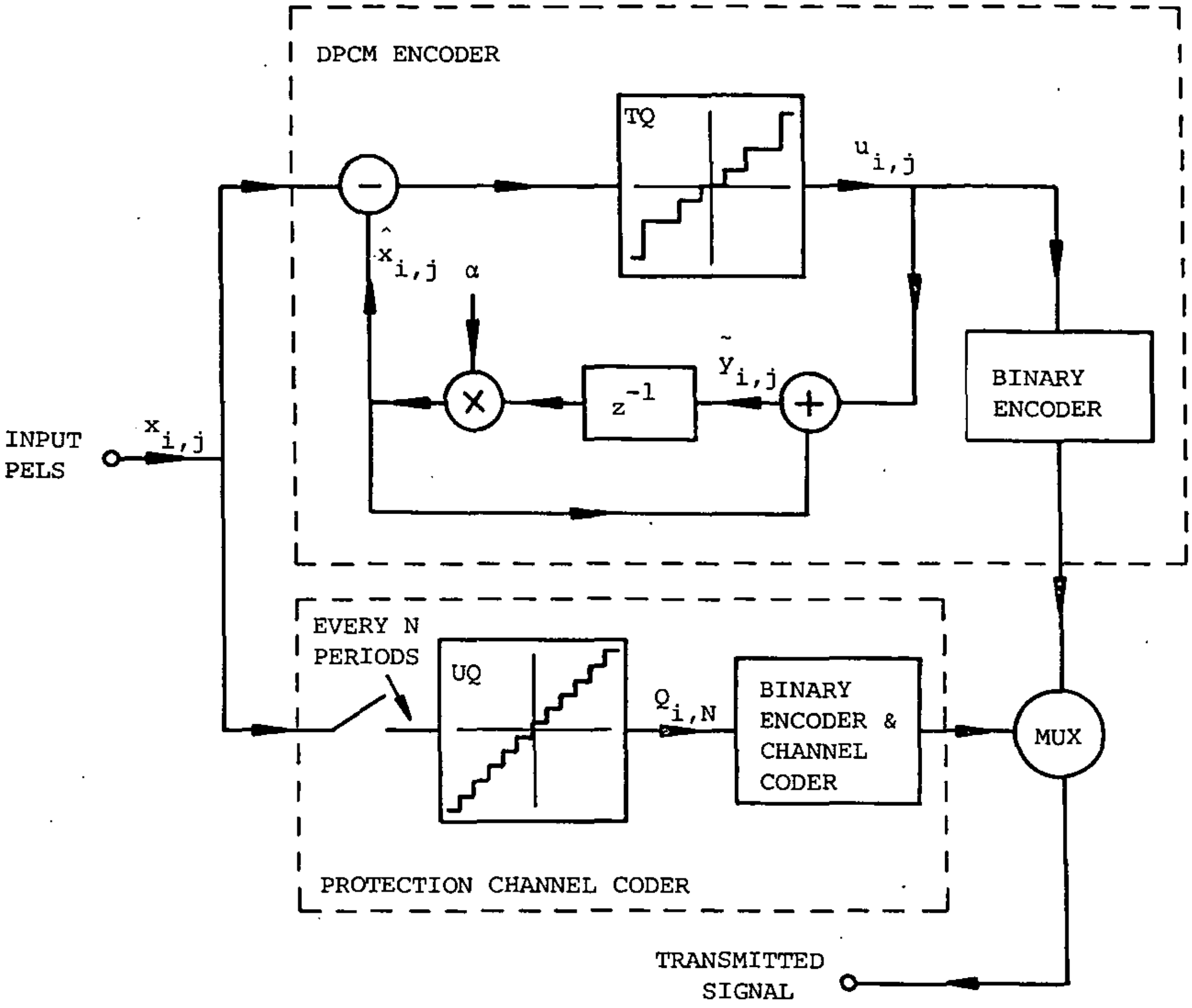

Figure 2.5 DPCM encoder and protection channel coder

coefficient is α, and z^{-1} represents a delay of one sampling period. The predicted pel in the jth position on the ith scan line is therefore

$$x_{i,j} = (x_{i,j-1} + n_{i,j-1})\alpha \qquad (2.6)$$

where $x_{i,j-1}$ is the previous pel along the scan line and $n_{i,j-1}$ is the quantization noise generated in encoding $x_{i,j-1}$. The locally decoded pel $\tilde{y}_{i,j}$ is equal to the input pel $x_{i,j}$ plus the noise component $n_{i,j}$ generated in the quantization process. The tapered quantizer characteristic used in the DPCM encoder is specified in Table 2.1. The quantizer is a symmetrical odd function that spans the input range -128 to +128 units of Δ_T. The most significant bit b_o of the binary code word specifies the polarity (0 for positive, 1 for negative) while the remaining bits relate to the magnitude of the quantized level number. The quantized output level $u_{i,j}$ is obtained from the code word by removing b_o, decoding the remaining bits to give the magnitude of the level number $|v_{i,j}|$, and calculating b_o times 2 to the power of $|v_{i,j}|$. For example, if the transmitted code word is 1101, $b_o = 1$, $|v_{i,j}| = 5$, and the decoded pel is $(-1)2^5 = -32$.

To increase the speed and quality of the enhancement process at the receiver a protection channel coder is employed (see Figure 2.5) whose function is to transmit periodic PCM updates(57,58,68). Its uniform quantizer (UQ) spans the range of the luminance signal, has 256 levels, a constant step-size of Δ_u, and quantizes every Nth pel. This constancy of step-size is in contrast to that of TQ whose minimum step-size Δ_T is equal to Δ_u. The quantized samples from TQ and UQ are binary encoded and multiplexed to give blocks of N DPCM words and one

PCM protection word.

The multiplexed binary signal is transmitted, impaired by the channel, regenerated at the receiver, demultiplexed, binary decoded and the first N lines of samples stored. The picture enhancement procedure divides the N lines of samples into blocks $B_{1,1}, B_{1,2}, \ldots, B_{1,M}$, as shown in Figure 2.2. The DPCM samples are decoded for block $B_{1,1}$ and at the end of each row there is a protection sample (generated by the protection channel coder) whose value is known to an accuracy of $\pm\Delta_u/2$. The decoded DPCM sample $y_{i,N}$ at the end of the ith row is compared with the protection sample $Q_{i,N}$, and an error is considered to exist along the ith row if

$$|Q_{i,N} - y_{i,N}| > L_2\Delta_u \qquad (2.7)$$

where L_2 is a system parameter, typically 5. Note that $y = \tilde{y}$ in Figure 2.5, only in the absence of transmission errors.

If the end-of-row test is positive, i.e., Inequality (2.7) applies, we examine each pel using Inequality (2.1) with $q_{i,j}$ and $Q_{i,j-1}$ replaced by $y_{i,j}$ and $Y_{i,j-1}$, respectively. The procedure is to start with the second pel (the pels in the first column of the image are assumed to be correct as they are transmitted using the protection channel coder) in the row, namely $y_{i,2}$, and continue to test each pel in sequence until the last pel $y_{i,N}$ is tested. Suppose pel $y_{i,j}$ is considered to be in error. The 'corrected' value of $y_{i,j}$ is found by adding the average of the step changes before and after the erroneously detected sample, to the previously corrected pel $Y_{i,j-1}$, viz:-

$$Y_{i,j} = 0.5\{(Y_{i,j-1} - Y_{i,j-2}) + (y_{i,j+1} - y_{i,j})\} + Y_{i,j-1} \qquad (2.8)$$

$\{Y\}$ and $\{y\}$ are the enhanced and original sequence of luminance pels, respectively.

The error $\approx(y_{i,j}-Y_{i,j})$ in the pel at the ith row, jth column is propagated to subsequent y values along the row (scan line) and if these pels are not adjusted to allow for propagation effects before they are subjected to error detection many errors will be erroneously detected. Figure 2.6 shows an arbitrary group of pels along the ith scan line, an error at the jth position, and how subsequent pels $y_{i,j+k}$, $k \geq 1$, are in error due to the effect of propagation. The reason for error propagation is innate in the DPCM decoder, whose output given by

$$y_{i,j} = u_{i,j} + y_{i,j-1}\alpha \ , \quad i,j = 1,2,\ldots,N \qquad (2.9)$$

is the sum of the received quantized sample $u_{i,j}$ and the weighted previous decoded sample. It is the dependence of the current output on the previous outputs that results in error propagation, perceived as a streak of incorrect luminance along the scan line.

Thus before pel $y_{i,j+1}$ is subjected to error detection, this pel and subsequent pels along the scan line in block $B_{1,1}$ are modified to:

$$y^{*}_{i,j+k} = y_{i,j+k} - \alpha^{k}(y_{i,j} - Y_{i,j}); \quad k = 1,2,\ldots,N-k \qquad (2.10)$$

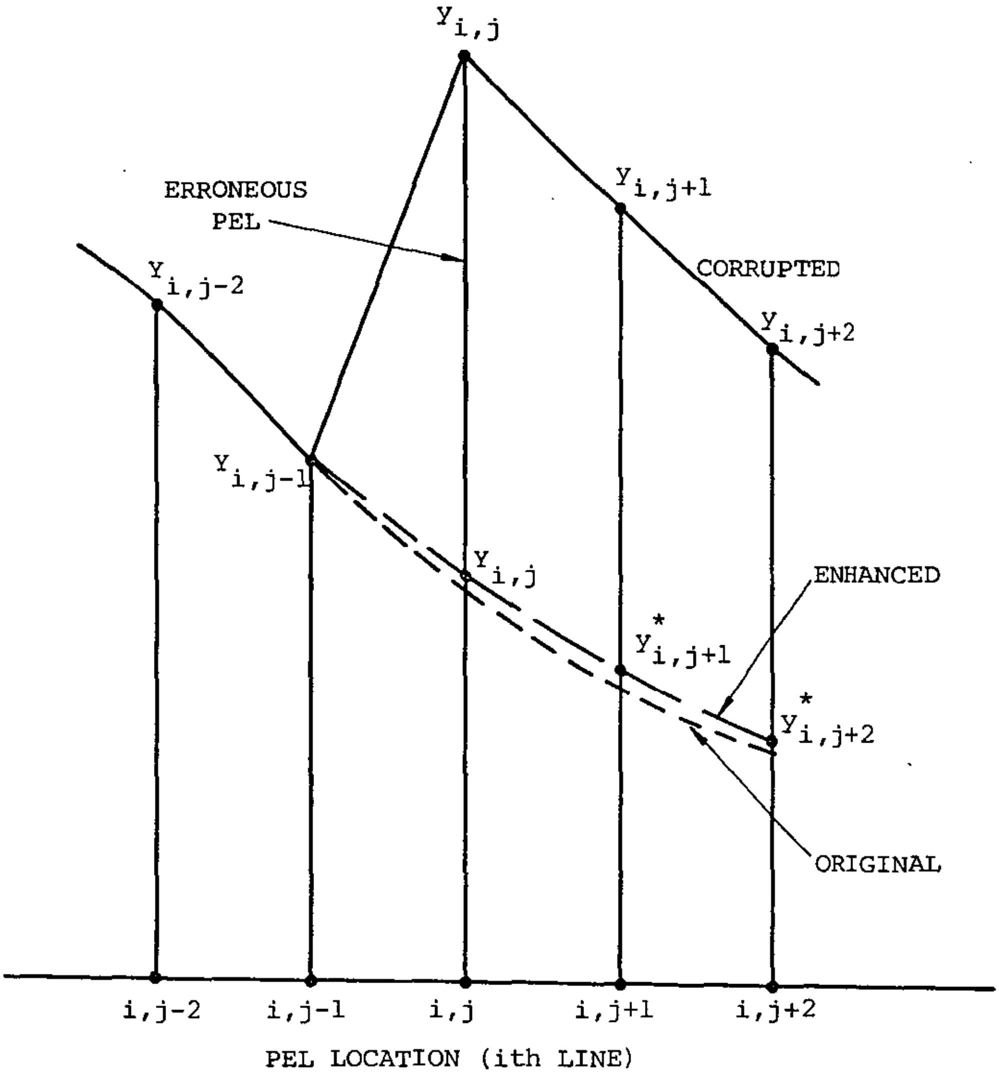

Figure 2.6 Effect of transmission error at the (i,j)th location

After error detection and correction of $y_{i,j}$, adjustment of all subsequent pels for propagation effects to the end of the block (j=N), the end-of-row test of Inequality (2.7) is again performed. If this again proves positive, the above procedure is repeated starting with pel $y_{i,j+1}$, and is continued until the end-of-row test reveals that no more errors are present along the row, or having reached $y_{i,N}$, that an error still exists. In the latter case errors have not been detected and/or properly corrected. To prevent the error propagating into block $B_{1,2}$,$y_{i,N}$ is forced to the value $Q_{i,N}$. Further, to prevent the uncorrected row being perceived as an erroneous luminous streak of N pels, all pels in this row, except $y_{i,N}$, are replaced by the presumed correct pels in the previous line, i.e., the erroneous row is replaced by the row above it in the picture. The (i+1)th line is processed next using the same procedure and so on until all the pels in block $B_{1,1}$ have been examined and modified where appropriate.

Blocks $B_{1,2}$,$B_{1,3}$ to $B_{1,M}$ are then enhanced, followed by $B_{2,1}$ to $B_{2,M}$, $B_{3,1}$ to $B_{3,M}$, and this sequential processing of the blocks is continued until $B_{M,M}$ is reached.

In this enhancement system the pels along the first scan line and along the first column in the picture (not the picture block) are sent via the protection channel coder of Figure 2.5, in addition to the protection samples sent every N pels. Thus in processing block $B_{1,1}$ the enhancement system starts by examining the second row, and if the end-of-row test indicates the presence of a transmission error, pel $y_{2,2}$ is the first pel to be scrutinized. If an error is detected,

$y_{2,2}$ is replaced by $y_{1,2}$ as the correction procedure of Equation (2.8) cannot be used for the second pel along a line. Generally if pels $y_{i,2}$, $i=2,3,\ldots,N$, are deemed to be in error they are replaced by $y_{i-1,2}$, $i=2,3,\ldots,N$, no matter which block is being processed. The number of pels used in the columns and rows of each block are 32 and 32 for $B_{1,1}$; 33 and 32 for $B_{1,m}$; $m=2,3,\ldots,M$; 32 and 33 for $B_{n,1}$; $n=2,3,\ldots,M$; and 33 and 33 for $B_{n,m}$; $n,m=2,3,\ldots,M$; respectively. Thus by overlapping the blocks (by one column and one row in the case of $B_{m,n}$; $m,n=2,3,\ldots,M$) and using the replacement procedure for $y_{i,2}$; $i=2,3,\ldots,N$ when necessary, the correction procedure of Equation (2.8) can be used with confidence for $i=3,4,\ldots,N$.

2.3.1 Results

The same experimental procedure was used as in the case of PCM described in Section 2.2.3. The DPCM encoder used the tapered quantizer (TQ) having the characteristic of Table 2.1, and a predictor coefficient α of 0.99. The received image was divided into 64 equal size square blocks as shown in Figure 2.2, where N=32. A smaller block size is used here (N=64 in the PCM case) to minimize the storage requirement, since the block size does not affect the performance of the system significantly. The detection parameter L_1 for the DPCM image enhancement system is given by

$$L_1 = \begin{cases} 3.0 , & 0<\sigma_d<11.0 \\ -0.19\sigma_d+5.1 , & 11.0\leq\sigma_d<22.0 \\ -0.024\sigma_d+1.43 , & 22.0\leq\sigma_d \end{cases} \qquad (2.11)$$

Table 2.1 4-bit DPCM tapered quantizer characteristic

(The decimal numbers in the table are to be scaled by Δ_T)

INPUT SIGNAL RANGE	QUANTIZED OUTPUT LEVEL NUMBER	BINARY CODE	QUANTIZED OUTPUT LEVEL
>96	7	0111	128
48 → 96	6	0110	64
24 → 48	5	0101	32
12 → 24	4	0100	16
6 → 12	3	0011	8
3 → 6	2	0010	4
1.5 → 3	1	0001	2
-1.5 → 1.5	0	0000	0
-3 → -1.5	-1	1001	-2
-6 → -3	-2	1010	-4
-12 → -6	-3	1011	-8
-24 → -12	-4	1100	-16
-48 → -24	-5	1101	-32
-96 → -48	-6	1110	-64
<-96	-7	1111	-128

The variation of SNR as a function of BER for the enhanced and corrupted DPCM 'GIRL' image is shown in Figure 2.7 by curves (e) and (a), respectively. Their shapes are similar to those obtained for the PCM image (Figure 2.4) although the SNR gains for DPCM are more substantial due to the greater noise in DPCM resulting from error-streaking. We observe in Figure 2.7 that the enhancement in SNR is approximately 18 dB over a range of BER from 0.1 to 1.0%, representing a pronounced enhancement in picture quality. For BER < 0.1%, the image enhancement procedure virtually restores the image to its original quality.

The corrupted image due to a BER of 0.1% is shown in Figure 2.8(a). When the DPCM enhancement system was applied the image was virtually restored, except for a few short luminance streaks, as shown by the photograph of Figure 2.8(e). When the BER was increased to 1.0% the corruption to the image was extensive, see Figure 2.9(a), and although a few small streaks remained after enhancement as shown in Figure 2.9(e), the improvement in picture quality was dramatic. It is apparent that the quality of the enhanced image in Figure 2.9(e) where BER = 1.0%, is significantly more acceptable than the corrupted image of Figure 2.8(a) when the BER is only 0.1%. Thus Figure 2.7 is a guide to subjective performance, implying that the quality of the corrupted image when the BER ≃ 0.02% is similar to that of the enhanced system when BER is 1.0%. Of course care must be exercised in making these comparisons because of the differing lengths of the streaks in the corrupted and enhanced pictures. However, the shorter streaks are probably less annoying than the longer streaks, for the same error power.

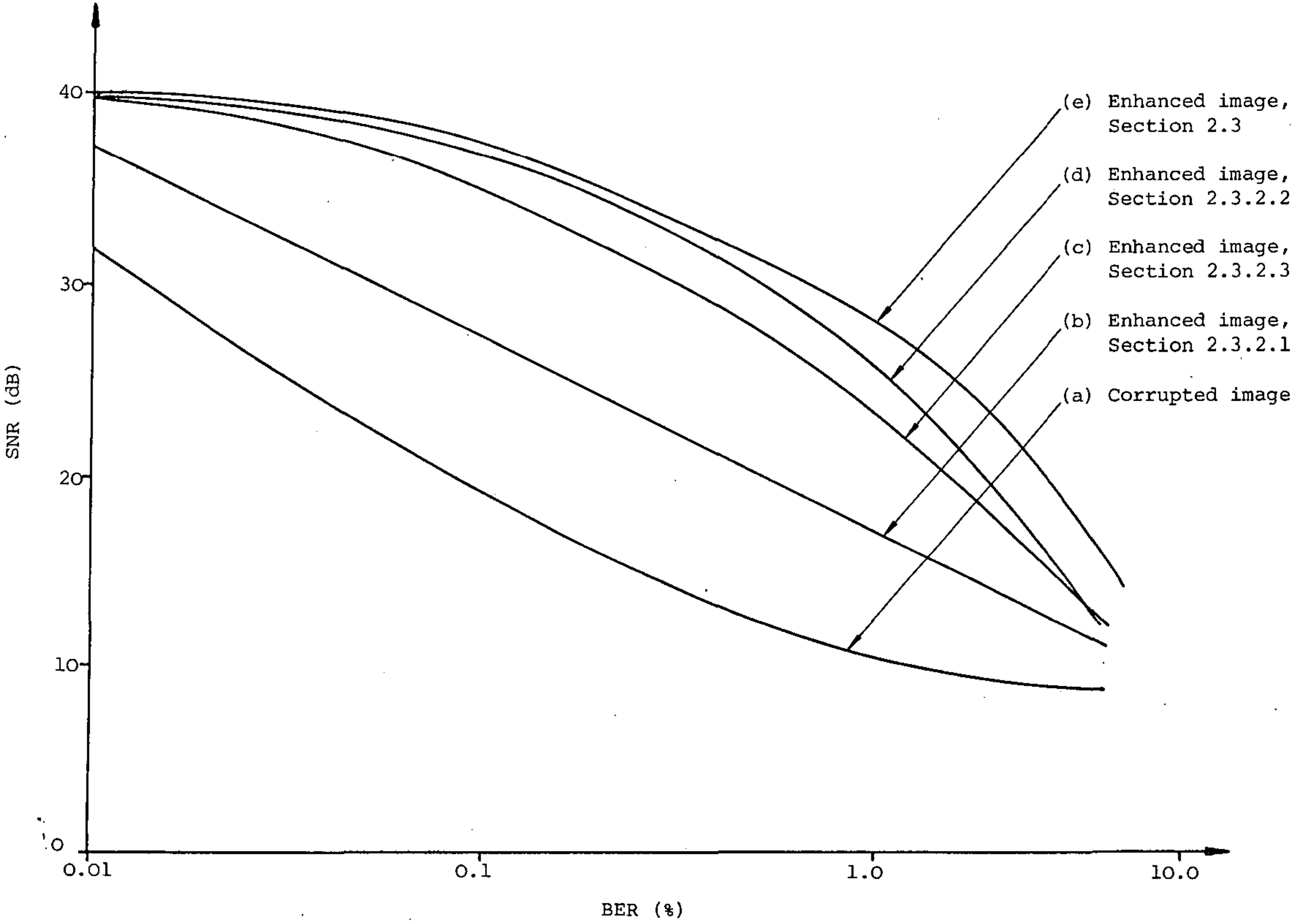

Figure 2.7 Variation of SNR as a function of BER for corrupted and enhanced DPCM picture

(a) Corrupted

(b) Section 2.3.2.1

(c) Section 2.3.2.3

(d) Section 2.3.2.2

(e) Section 2.3

Figure 2.8 DPCM enhancement, BER = 0.1%

(a) Corrupted

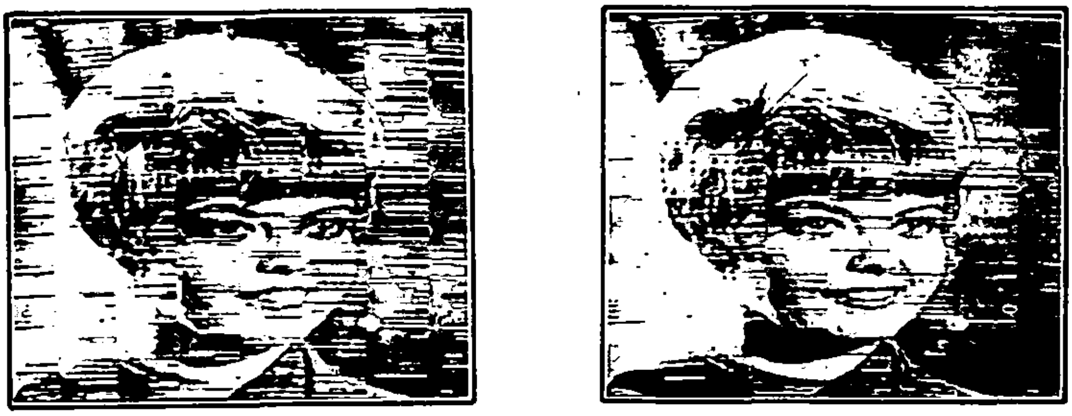

(b) Section 2.3.2.1

(c) Section 2.3.2.3

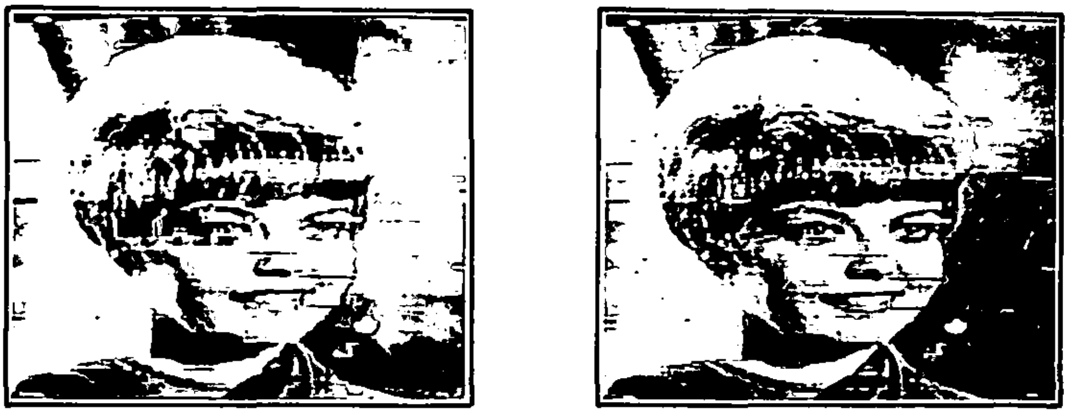

(d) Section 2.3.2.2

(e) Section 2.3

Figure 2.9 DPCM enhancement, BER = 1.0%

2.3.2 Balancing enhanced picture quality against system complexity

By reducing the complexity of the DPCM enhancement method described in Section 2.3, the quality of the recovered image is reduced. However, the trade-off may be acceptable depending on the application. Three simpler derivatives of the system are now presented.

2.3.2.1 Restricting the propagation error

In this method, whenever the end-of-row-test (see Equation (2.7)) indicates the presence of an error in the row of length N, no search is made for the location of the error, instead $y_{i,N}$ is forced to $Q_{i,N}$. Thus the effect of one or more errors in a row of length N is to cause a luminance streak whose length is $<(N-1)$. This is essentially the method of forced PCM-updates(57,58).

The SNR performance of this system is indicated by curve (b) in Figure 2.7, where the improvement in SNR compared to the corrupted picture is typically 8 dB over a wide range of BER. The images using this simple enhancement method for BER of 0.1 and 1.0% are shown in Figures 2.8(b) and 2.9(b), respectively.

2.3.2.2 Previous row replacement

Whenever Inequality (2.7) is satisfied all the pels in the ith row, say, of length N are replaced by the pels that have been previously processed in the (i-1)th row. No attempt is made to carry out statistical detection and correction of pels within the erroneous row as described in Section 2.3. Because of the high correlation in the

'GIRL' picture, this method is very successful as curve (d) in Figure 2.7 demonstrates, and is compatible with the findings of reference (71). The SNR is within 3 dB of that of the system using individual pel enhancement over the range of BER considered. The enhanced image for BER = 0.1% is very similar to the enhanced image using the technique described in Section 2.3 (compare Figures 2.8(d) and (e)). However, at BER = 1.0%, the advantage of using statistical detection and correction methods is apparent when Figures 2.9(d) and (e) are examined.

A variant of the previous row replacement method was investigated. In this scheme, when the end-of-row test indicated the presence of one or more errors in the row, all the pels in the row were replaced as previously described. However, when two consecutive rows were in error the first erroneous row, the ith say, was replaced with pels in the (i-1)th line, while the erroneous (i+1)th row was replaced with the pels in the (i+2)th row. If the i, (i+1) and (i+2)th rows were all in error, the i and (i+2)th rows were replaced with pels in the (i-1) and (i+3)th rows, and the pels in the (i+1)th row were replaced with pels whose values were found by interpolation between pels in rows (i-1) and (i+3). The technique increased the processing complexity, while the enhancement obtained was not significantly different from that of the previous line enhancement method, the experiments being performed using the 'GIRL' image.

2.3.2.3 Statistical detection and correction

This arrangement is essentially that described in Section 2.3, except that pels in the uncorrected row are not replaced by the corresponding pels in the previous row as in Section 2.3.2.2. The number of streaks is greater, but the mosiac structure typified by Figure 2.9(d) is avoided, as erroneous pels are corrected rather than replaced. The SNR as a function of BER is shown in Figure 2.7(c), and the photographs of the enhanced image are displayed in Figures 2.8(c) and 2.9(c). Although the SNR is lower than for the previous row replacement technique, the subjective effect is different and perhaps preferable at high values of BER.

2.4 DISCUSSION

The enhancement techniques for PCM and DPCM pictures described here are relatively simple and offer significant improvements in picture quality as shown by the photographs. The techniques have the virtue of introducing negligible errors at zero or low error rates; are capable of removing nearly all picture distortion at percentage bit error rates (BER) < 0.6 and 0.1 for PCM and DPCM encoded images, respectively; and offer substantial improvements in picture quality at high values of BER.

The percentage increase in the bit-rate due to transmitting protection pels in DPCM images is 3.9 percent, but as each protection pel must itself be protected by channel coding this value of 3.9 percent will be increased. If majority voting is used and each protection PCM word is tripled the side-information increases to 11.7 percent. The receiver reproduces the protection word, one bit at a time, by accepting the logic value which is the majority of the three transmitted values.

As an example, consider the relatively high BER of 1 percent. The probability of a protection pel (specified by an 8 bit PCM word) being in error is 2.38×10^{-3}. Thus we anticipate that on the average one protection pel will be in error for every 420 pels transmitted, i.e., 6 erroneous protection pels in the image. This corresponds to one erroneous protection pel every 10,700 pels or 43 Kbits of data. However, if the first line and column of pels in the image are not sent in protected form, thereby reducing the number of protected pels by approximately 25%, the effect on recovered picture quality is not serious.

At low values of BER (< 0.1%), the real improvement in corrupted DPCM images derives from applying the simple end-of-row test and, on detecting errors, replacing the erroneous pels with those in the previous row. Simple row replacement of pels at high bit error rates (≳1%) produces a mosaic structure in highly detailed areas of the picture, as can be seen in Figure 2.9(d). Although there are fewer streaks in Figure 2.9(d) than in 2.9(c), some of the fine picture detail has been obscured by the row replacement of pels. The forced PCM update with statistical detection and correction strategy may be preferred because it offers partial pel correction rather than pel replacement from the preceding row. The combination of error correction when possible, and error replacement on other occasions, as depicted by Figure 2.9(e), provides the best enhanced picture quality of those pictures displayed in Figure 2.9.

Although streaks remain in Figure 2.9, some of them can be removed by more complex processing. For example, if the gradients $(y_{i-1,N/2} - y_{i,N/2})$ and $(y_{i,N/2} - y_{i+1,N/2})$ for the (i-1), i, (i+1)th rows, and the $\frac{N}{2}$ column exceed $L_2\Delta_u$ (defined by Inequality (2.7)) and are of opposing signs, then an error streak $< N$ but $> \frac{N}{2}$ is assumed to be present. All the pels in the row containing the erroneous streak are replaced by pels in the preceding row. For some blocks this enhancement procedure is effective, while in others the distortion increased. Thus if further improvements in picture quality are to be achieved different algorithms must be tried for each block in the picture, and the algorithm selected should be the one providing the least perceptual degradation. This implies non-real time processing, and probably human intervention. The enhancement techniques described give good results with simple techniques, yet they do enable an improvement in detail and feature recognition, as exemplified by the transformation of Figure 2.9(a) to Figure 2.9(e).

2.5 CONCLUSIONS

Error detection and correction of PCM and DPCM encoded images for viewdata system was investigated. For PCM images, the improvement in SNR is ≃ 10dB for BER between 0.1 and 2.0%. All the errors were virtually being removed when BER < 0.6%. In the case of DPCM images, the improvement in SNR is 18 dB over a range of BER from 0.1 to 1.0% representing a substantial enhancement in picture quality. Simpler methods can be employed at the expense of system performance depending on the application. Sending a PCM-update at the end of a DPCM block stops the error propagating into the next block. Previous row replacement technique is effective at low error rates but tends to produce a mosaic structure in the enhanced image at high error rates. The simple statistical detection and correction method even though it gives a lower SNR curve than the previous row replacement technique has subjective effect that is different and may be preferred at high values of BER.

2.6 NOTE ON PUBLICATIONS

Three papers, based on the work described in Chapter II, were produced. The first, entitled "Adaptive partial correction scheme for PCM encoded monochrome pictures" was presented in the 1979 Picture Coding Symposium held in Ipswich, England. The second, entitled "Enhancement by simple statistical methods of PCM and DPCM images corrupted by transmission errors" (invited paper) was presented in the 1980 National Telecommunication Conference held in Houston, Texas, USA and published in the conference proceedings. The third, "Enhancement of PCM and DPCM images corrupted by transmission errors" was published in the IEEE Transactions on Communications, January issue, 1982. All the above papers are in joint authorship with Dr R Steele.

CHAPTER III - IMAGE SIZE REDUCTION

3.1 INTRODUCTION

The viewdata system(47) currently in service in the U.K. offers a mosaic type of graphics for the display of pictorial information. An improvement to the system would be the transmission of still video pictures of high definition. To fit the video information into a viewdata page which already contains alphanumeric text, the picture size has to be reduced. Also, since the current transmission rate of the viewdata system is only 1.2 kbits/sec, transmission of a smaller picture will reduce the picture update time at the receiver.

Image size modification is essentially a two-dimensional sampling rate conversion which in the present case is a sampling rate reduction, or decimation. The process of sampling rate conversion has been examined from different viewpoints(72-79). Crooke et al(72) have shown that for bandlimiting applications, computational efficiencies can be gained by sampling rate reduction. Schafer and Rabiner(73) have shown that both sampling rate increase and reduction are basically interpolation processes and can be efficiently implemented using finite impulse response (FIR) digital filters. Furthermore, they show that sampling rate conversion for any rational ratio of sampling frequencies can be efficiently implemented by a two-stage process consisting of an integral sampling rate increase followed by an integral sampling rate decrease. Bellanger et al(74) found that efficient implementations of lowpass FIR filters could be obtained by a process of first reducing the sampling rate, filtering, and then increasing the sampling rate back to the original frequency. Shively(75) proposed a procedure for optimally choosing the reduction ratios at each stage such that the amount of computation in the overall sampling rate reduction process was minimised and Crochiere and Rabiner(76) presented a general theory of multistage decimators and interpolators for sampling rate reduction and increase.

In this chapter, different approaches to image reduction are examined. In Section 3.2, the general properties of the unitary transforms used are outlined. In Section 3.3, lowpass filtering and decimation in the spatial domain is described. However, instead of performing the lowpass filtering in the spatial domain, one can perform the operation in the frequency or transform domain by virtue of the multiplication-convolution property of the orthogonal transformation. This is particularly useful if the source coder of the image processing system is a transform coder. In Section 3.4, the source signal is lowpass filtered in the cosine domain and then decimation carried out in the spatial domain. In Section 3.5, the feasibility of both lowpass filtering and decimation in the transform domain is investigated. In this case, Fourier, cosine and Hadamard transforms are considered.

3.2 UNITARY TRANSFORMS

3.2.1 Fourier transform

The discrete Fourier transform (DFT) has long been used for signal analysis(80,81) and was the first transform used in the early development of transform coding(82-84). The discrete two-dimensional Fourier transform of an image array is defined in series form as

$$F(u,v) = \frac{1}{N} \sum_{k=0}^{N-1} \sum_{\ell=0}^{N-1} f(k,\ell) \exp\{\frac{-j2\pi}{N} (uk + v\ell)\} \tag{3.1}$$

where $j = \sqrt{-1}$, and the discrete inverse transform is given by

$$f(k,\ell) = \frac{1}{N} \sum_{u=0}^{N-1} \sum_{v=0}^{N-1} F(u,v) \exp\{\frac{j2\pi}{N}(uk + v\ell)\} \tag{3.2}$$

The basis functions of the transform are complex exponentials and may be decomposed into sine and cosine components i.e.

$$\begin{aligned} A(k,\ell;u,v) &= \exp\{\frac{-j2\pi}{N}(uk + v\ell)\} \\ &= \cos\{\frac{2\pi}{N}(uk + v\ell)\} - j \sin\{\frac{2\pi}{N}(uk + v\ell)\} \end{aligned} \tag{3.3}$$

$$\begin{aligned} B(k,\ell;u,v) &= \exp\{\frac{j2\pi}{N}(uk + v\ell)\} \\ &= \cos\{\frac{2\pi}{N}(uk + v\ell)\} + j \sin\{\frac{2\pi}{N}(uk + v\ell)\} \end{aligned} \tag{3.4}$$

Figure 3.1 contains the plots of the sine and cosine components of the one dimensional Fourier basis functions for N=16.

The spectral component at the origin of the Fourier domain

$$F(0,0) = \frac{1}{N} \sum_{k=0}^{N-1} \sum_{\ell=0}^{N-1} f(k,\ell) \qquad (3.5)$$

is equal to N times the spatial average of the image plane intensity. If $f(k,\ell)$ represents a luminance field, then $F(0,0)$ is the average brightness in the spatial domain.

The two-dimensional Fourier transform of an image is essentially a Fourier series representation of a two-dimensional field. For the Fourier series representation to be valid, the field must be periodic. For a real positive function, $f(k,\ell)$, its Fourier transform will, in general, be complex containing $2N^2$ components. However, $F(u,v)$ exhibits the property of conjugate symmetry, and therefore one-half of the transform domain samples are redundant, that is, they can be generated from the other transform samples.

The transformation matrix A can be written in direct product form as

$$A = A_C \otimes A_R \qquad (3.6)$$

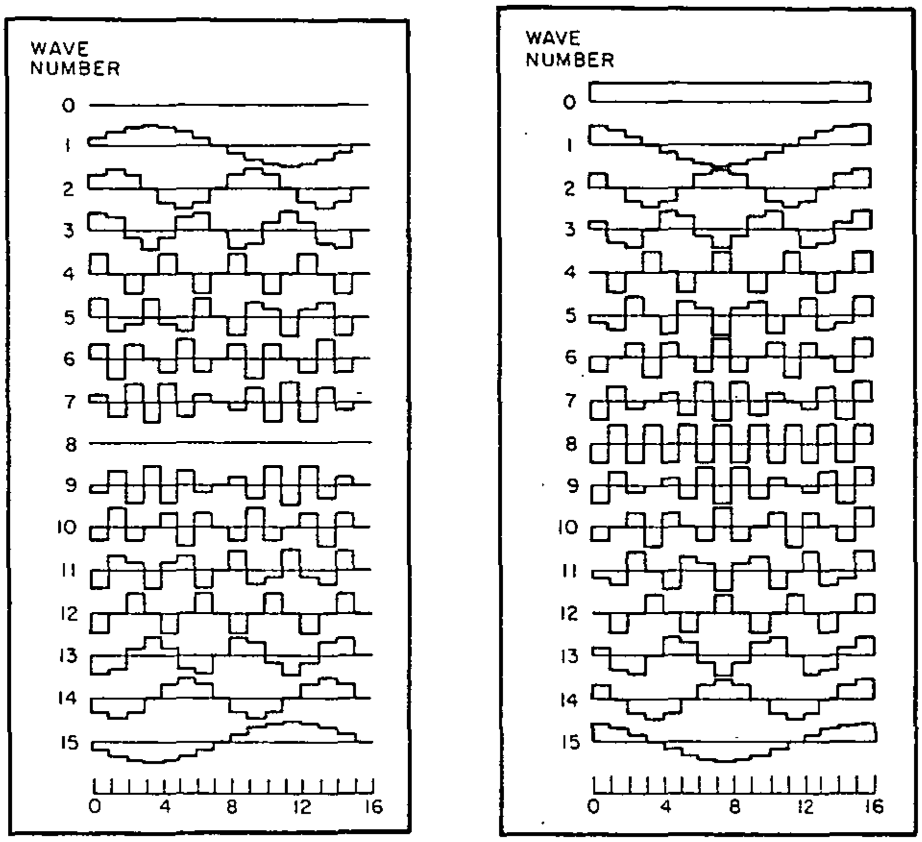

(a) Sine component

(b) Cosine component

Figure 3.1 Fourier basis functions (after ref. 51) where

$$A_R = A_C = \frac{1}{\sqrt{N}} \begin{bmatrix} w^0 & w^0 & w^0 & \cdots & w^0 \\ w^0 & w^1 & w^2 & \cdots & w^{N-1} \\ w^0 & w^2 & w^4 & \cdots & w^{2(N-1)} \\ \vdots & & & & \vdots \\ w^0 & \cdots & & \cdots & w^{(N-1)^2} \end{bmatrix} \qquad (3.7)$$

with $w = \exp\{-2\pi j/N\}$.

3.2.2 Cosine transform

The performance of the discrete cosine transform (DCT) has been shown to compare closely to that of the Karhunen-Loeve (K-L) transform(29) which is known to be optimal with respect to the following performance criteria : variance distribution(85), estimation using the mean square error criterion(86,87) , and the rate distortion function(88) . Since there is no fast algorithm for the K-L transform, and fast algorithms have been developed for the DCT(89,90) , the latter has been used increasingly for transform coding.

The discrete two-dimensional cosine transform is defined as

$$F(u,v) = \frac{2}{N} C(u)\ C(v) \sum_{k=0}^{N-1} \sum_{\ell=0}^{N-1} f(k,\ell) \cos\{\frac{\pi}{N}\left[u(k+\frac{1}{2})\right]\} \cos\{\frac{\pi}{N}\left[v(\ell+\frac{1}{2})\right]\} \qquad (3.8)$$

and its inverse is defined as


NATIONAL MOTOR MUSEUM BEAULI

F4·57

3 stage MSMSVQ
|| Adap.
64 entry

~~16~~ 32 entry Chroma

2-stage

Y ~ 1·25 b/p

U,V ~ 1·38/16 b/p

$$f(k,\ell) = \frac{2}{N} \sum_{u=0}^{N-1} \sum_{v=0}^{N-1} C(u)C(v)\ F(u,v)\ \cos\left\{\frac{\pi}{N}\left[u(k+\frac{1}{2})\right]\right\} \cos\left\{\frac{\pi}{N}\left[v(\ell+\frac{1}{2})\right]\right\} \quad (3.9)$$

where $C(0) = \frac{1}{\sqrt{2}}$ and $C(m) = 1$ for $m = 1, 2, \ldots. N-1$.
Figure 3.2 contains plots of the cosine transform basis functions for $N = 16$.

3.2.3 Hadamard transform

The Hadamard transform(30) is based upon the Hadamard matrix, which is a square array of plus and minus ones whose rows and columns are orthogonal. A normalised N x N Hadamard matrix satisfied the relation

$$H\, H^T = I \qquad (3.10)$$

where I is an identity matrix.

If a Hadamard matrix of order N exists $(N > 2)$, then $N = 0 \bmod 4$. The existence of a Hadamard matrix for every value of N satisfying this requirement has not been shown, but constructions are available for all permissible values of N up to 200. The simplest construction is for a Hadamard matrix of order $N = 2^n$ where n is an integer. In this case, if H_N is a Hadamard matrix of order N, the matrix

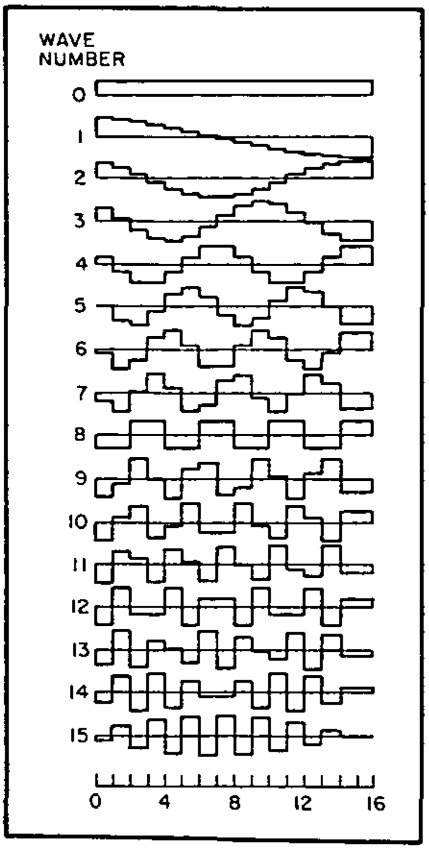

Figure 3.2 Cosine basis functions (after ref. 51)

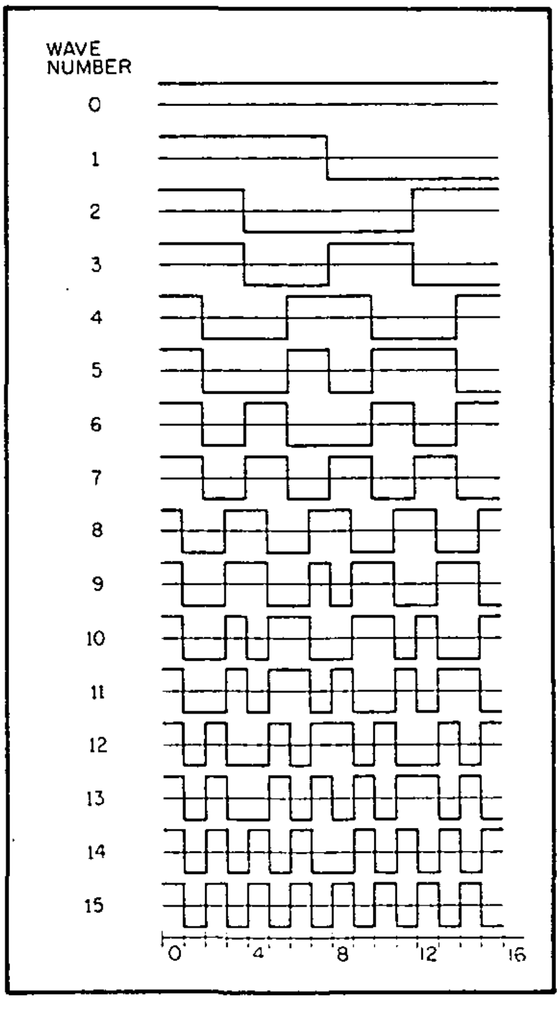

Figure 3.3 Hadamard basis functions (after ref. 51)

$$H_{2N} = \frac{1}{\sqrt{2}} \begin{bmatrix} H_N & H_N \\ H_N & -H_N \end{bmatrix} \tag{3.11}$$

is a Hadamard matrix of order 2N.

The rows of the Hadamard matrix can be considered to be samples of rectangular waves with a subperiod of $\frac{1}{N}$ units. These continuous functions called Walsh functions are further related to the Rademacher block pulse functions. The number of sign changes along each row of the Hadamard matrix divided by two is called the sequency of the row.

For symmetric Hadamard matrices of order $N=2^n$, the two dimensional Hadamard transform may be written in series form as

$$F(u,v) = \frac{1}{N} \sum_{k=0}^{N-1} \sum_{\ell=0}^{N-1} f(k,\ell) \ (-1)^{p(k,\ell;u,v)} \tag{3.12}$$

where $$p(k,\ell;u,v) = \sum_{i=0}^{n-1} (u_i k_i + v_i \ell_i) \tag{3.13}$$

The terms u_i, v_i, k_i, ℓ_i are the bit states of the binary representations of u, v, k, ℓ respectively. Another series representation exists for a Hadamard matrix in 'ordered' form in which the sequency of each row is higher than the preceding row. By this representation,

$$F(u,v) = \frac{1}{N} \sum_{k=0}^{N-1} \sum_{\ell=0}^{N-1} f(k,\ell)\ (-1)^{q(k,\ell;u,v)} \tag{3.14}$$

where $$q(k,\ell;u,v) = \sum_{i=0}^{n-1} \left[g_i(u)\ k_i + g_i(v)\ \ell_i \right] \tag{3.15}$$

and

$$\begin{aligned} g_0(u) &\equiv u_{n-1} \\ g_1(u) &\equiv u_{n-1} + u_{n-2} \\ g_2(u) &\equiv u_{n-2} + u_{n-3} \\ &\vdots \\ g_{n-1}(u) &\equiv u_1 + u_0 \end{aligned} \tag{3.16}$$

Hadamard transform basis functions for the ordered transform with N = 16 are shown in Figure 3.3.

3.2.4 Implementation of two-dimensional unitary transforms

The forward unitary transformation of a N x N image array f(j,k) results in an N x N transformed image array as defined by

$$F(u,v) = \sum_{k=0}^{N-1} \sum_{\ell=0}^{N-1} f(k,\ell)\ A(k,\ell;u,v) \tag{3.17}$$

where $A(k,\ell;u,v)$ represents the forward transform kernel. An inverse transformation provides a mapping from the transform domain to the image space as given by

$$f(k,\ell) = \sum_{u=0}^{N-1} \sum_{v=0}^{N-1} F(u,v)\ B(k,\ell;u,v) \qquad (3.18)$$

where $B(k,\ell;u,v)$ denotes the inverse transform kernel.

It is obvious that

$$B(k,\ell;u,v) = A^{-1}(k,\ell;u,v) \qquad (3.19)$$

For a real unitary transformation the matrix inverse is given by

$$A^{-1}(k,\ell;u,v) = A^{T}(k,\ell;u,v) \qquad (3.20)$$

and A is said to be orthogonal.

Image transformation can be considered as a multidimensional rotation of coordinates. One of the major properties of a unitary transformation is that measure is preserved. For example, a mean-square difference between two images is equal to the mean-square difference between the transforms of the image. Another approach to the visualisation of image transformation is to consider Equation (3.17) as a means of synthesizing an image with a set of two-dimensional mathematical functions $A(k,\ell;u,v)$ for each transform coordinate (u,v). In this interpretation the kernel $A(k,\ell;u,v)$ is the two-dimensional basis function and the transform coeffient $F(u,v)$ is the amplitude of the basis function required in the synthesis of the image.

3.3 LOWPASS FILTERING AND DECIMATION IN THE SPATIAL DOMAIN

A general illustration of a sampling rate conversion system is shown in Figure 3.4(91). Given the signal x(n), sampled at the rate $F = \frac{1}{T}$, y(m) is to be computed with a new sampling rate $F' = \frac{1}{T'}$. Only cases where the ratio of sampling periods of y(m) and x(n) can be expressed as a rational fraction are considered, i.e.

$$\frac{T'}{T} = \frac{F}{F'} = \frac{M}{L} \tag{3.21}$$

where M and L are integers.

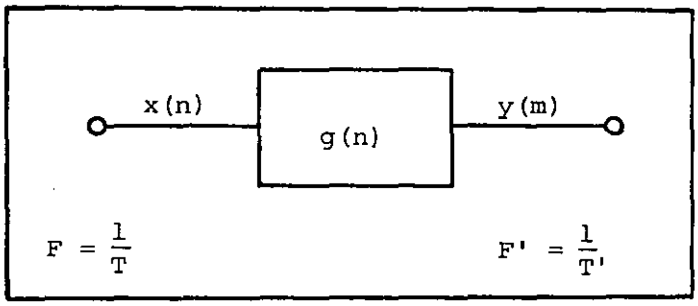

Figure 3.4 Generalised sampling rate reduction system

The system shown in Figure 3.4 is an inherently linear time-varying system with response g(n). Since the system is linear, each output sample y(m) can be expressed as a linear combination of input samples:

$$y(m) = \sum_{n=-\infty}^{\infty} g(n)x(m-n) \tag{3.22}$$

3.3.1 Theoretical background

3.3.1.1 Sampling rate reduction-decimation by an integral factor M

Consider the process of reducing the sampling rate of x(n) by an integral factor M, i.e.

$$\frac{T'}{T} = M \tag{3.23}$$

Then the new sampling rate is $F' = \frac{F}{M}$. Assume that x(n) represents a full bandwidth signal, i.e. its spectrum is non-zero for all frequencies f in the range $-\frac{F}{2} \leq f \leq \frac{F}{2}$, with $w = 2\pi fT$, i.e.

$$|X(e^{jw})| \neq 0, \quad |w| \leq \pi \tag{3.24}$$

except possibly at an isolated set of points. In order to reduce the sampling rate and to avoid aliasing at this lower rate, it is necessary to filter the signal x(n) with a digital lowpass filter which approximates the ideal characteristic

$$H(e^{jw}) = \begin{cases} 1, & |w| \leq \frac{\pi}{M} \\ 0, & \text{otherwise} \end{cases} \tag{3.25}$$

The sampling rate reduction is then achieved by forming the sequence y(m) by extracting every Mth sample of the filtered output. This process is illustrated in Figure 3.5. If we denote the lowpass filter unit impulse response as h(n), then we have

$$q(n) = \sum_{k=-\infty}^{\infty} h(k)\, x(n-k) \tag{3.26}$$

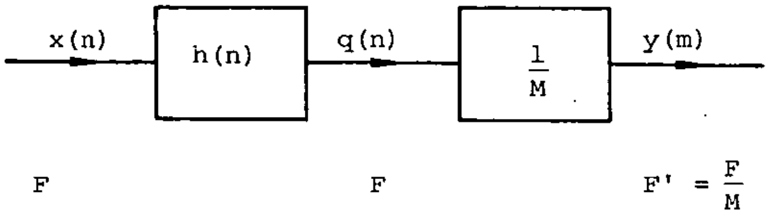

Figure 3.5 Block diagram for sampling rate reduction by a factor of M

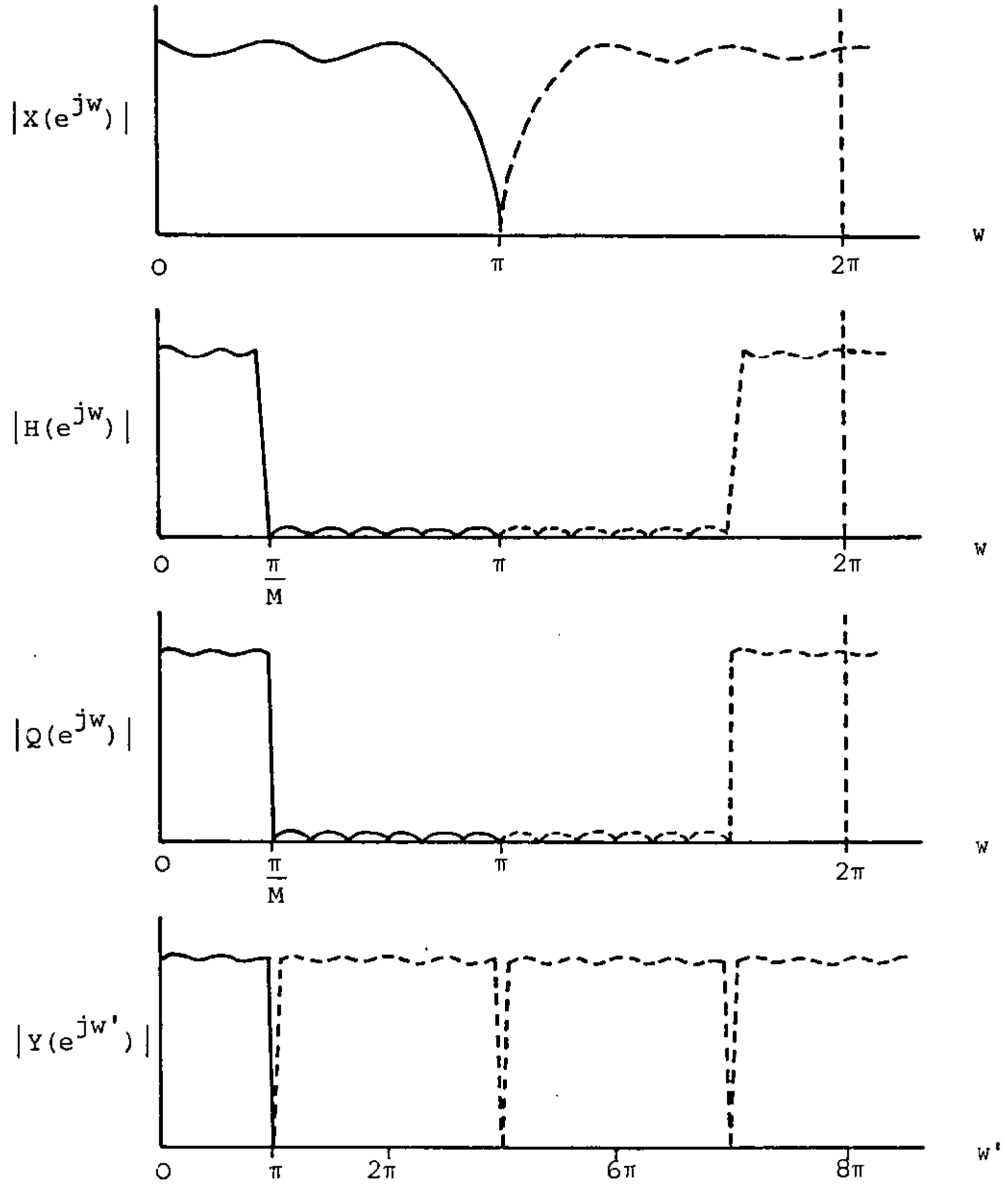

Figure 3.6 Typical spectra for sampling rate reduction by a factor of M (after ref. 91)

where q(n) is the filtered output. The final output y(m) is then obtained as

$$y(m) = q(Mm) \tag{3.27}$$

Figure 3.6 shows the typical amplitude spectra of the signals x(n), h(n), q(n) and y(m) for an M to 1 sampling rate reduction.

By substituting Equation (3.26) into Equation (3.27), the relationship between y(m) and x(n) is obtained, i.e.

$$y(m) = \sum_{k=-\infty}^{\infty} h(k)\, x(Mm-k) \tag{3.28}$$

To derive the relationship between the z-transforms of y(m) and x(n) we define the signal

$$q'(n) = \begin{cases} q(n), & n = 0, \underline{+}M, \underline{+}2M, \ldots\ldots \\ 0, & \text{otherwise} \end{cases} \tag{3.29}$$

A convenient and useful representation of q'(n) is then

$$q'(n) = q(n) \left[\frac{1}{M} \sum_{\ell=0}^{M-1} e^{\frac{j2\pi\ell n}{M}} \right] , \quad -\infty < n < \infty \tag{3.30}$$

where the term in brackets corresponds to a discrete Fourier series representation of a periodic impulse train with a period of M samples. Thus we have

$$y(m) = q'(Mm) = q(Mm) \tag{3.31}$$

The z-transform of y(m) is

$$Y(z) = \sum_{m=-\infty}^{\infty} y(m)\, z^{-m}$$

$$= \sum_{m=-\infty}^{\infty} q'(Mm)\, z^{-m} \qquad (3.32)$$

and since q'(m) is zero except at integral multiples of M, Equation (3.32) becomes

$$Y(z) = \sum_{m=-\infty}^{\infty} q'(m)\, z^{\frac{-m}{M}}$$

$$= \sum_{m=-\infty}^{\infty} q(m) \left[\frac{1}{M} \sum_{\ell=0}^{M-1} e^{\frac{j2\pi\ell m}{M}} z^{\frac{-m}{M}} \right]$$

$$= \frac{1}{M} \sum_{\ell=0}^{M-1} \left[\sum_{m=-\infty}^{\infty} q(m)\, e^{\frac{j2\pi\ell m}{M}} z^{\frac{-m}{M}} \right]$$

$$= \frac{1}{M} \sum_{\ell=0}^{M-1} Q\left(e^{\frac{-j2\pi\ell}{M}} z^{\frac{1}{M}}\right) \qquad (3.33)$$

Since

$$Q(z) = H(z).\, X(z) \qquad (3.34)$$

We can express Y(z) as

$$Y(z) = \frac{1}{M} \sum_{\ell=0}^{M-1} \left[H\left(e^{\frac{-j2\pi\ell}{M}} z^{\frac{1}{M}}\right) .\, X\left(e^{\frac{-j2\pi\ell}{M}} z^{\frac{1}{M}}\right) \right] \qquad (3.35)$$

Evaluating Y(z) on the unit circle, $z = e^{jw'}$, leads to the result

$$Y(e^{jw'}) = \frac{1}{M} \sum_{\ell=0}^{M-1} \left[H(e^{\frac{j(w'-2\pi\ell)}{M}}) \, . \, X(e^{\frac{j(w'-2\pi\ell)}{M}}) \right] \qquad (3.36)$$

where

$$w' = 2\pi f T' \qquad (3.37)$$

Equation (3.36) expresses the Fourier transform of the output signal y(m) in terms of the transforms of the aliased components of the filtered input signal x(n). By expanding Equation (3.36) we see that

$$Y(e^{jw'}) = \frac{1}{M} \left[H(e^{\frac{jw'}{M}}) \, . \, X(e^{\frac{jw'}{M}}) \right.$$

$$\left. + H(e^{\frac{j(w'-2\pi)}{M}}) \, . \, X(e^{\frac{j(w'-2\pi)}{M}}) + \ldots \right] \qquad (3.38)$$

Since $H(e^{jw})$ is negligible for $|w| \leqslant \frac{\pi}{M}$, Equation (3.38) then becomes

$$Y(e^{jw'}) \cong \frac{1}{M} \left[X(e^{\frac{jw'}{M}}) \right] \quad \text{for } |w| \leqslant \pi \qquad (3.39)$$

3.3.1.2 Sampling rate reduction by a rational factor $\frac{M}{L}$

In the previous section, sampling rate reduction by an integral factor M was demonstrated. Now the general case of conversion by the ratio

$$\frac{T'}{T} = \frac{M}{L} \qquad (3.40)$$

or

$$F' = \frac{L}{M} F \qquad (3.41)$$

where L < M will be considered.

This conversion is achieved by first increasing the sampling rate by L and then decreasing it by M as in Figure 3.7(a). It is important to note that interpolation by L must precede decimation by M so that the width of the baseband of the intermediate signal s(k) is greater than or equal to the baseband of x(n) or y(m).

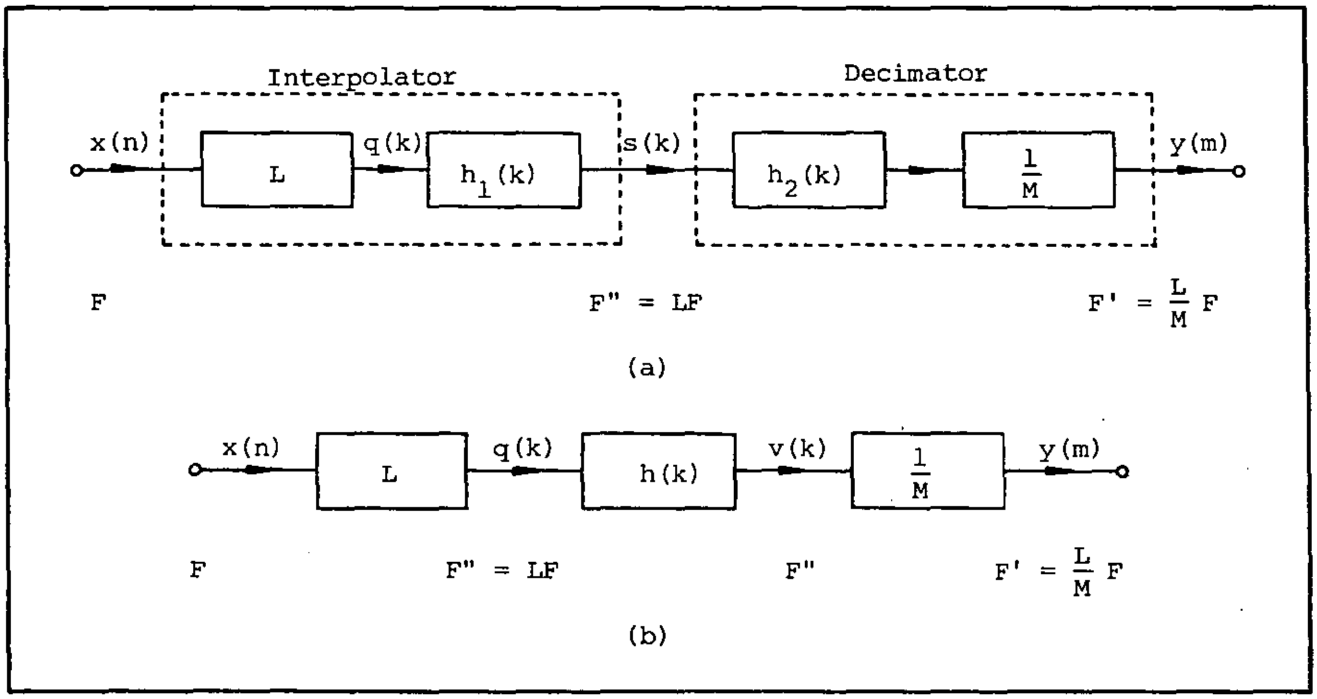

Figure 3.7 (a) Cascade of integral interpolator and decimator for achieving sampling rate conversion by rational fractions

(b) A more efficient implementation of this process

Interpolation is carried out by inserting L-1 zero-value samples between each pair of samples of x(n), giving the signal

$$q(k) = \begin{cases} x(\frac{k}{L}) , & k = 0, \pm L, \pm 2L \\ 0 , & \text{otherwise} \end{cases} \tag{3.42}$$

as illustrated in Figure 3.8.

It is clear that from Figure 3.8, the spectrum of q(k) contains not only the baseband frequencies of interest (i.e. $-\frac{\pi}{L}$ to $\frac{\pi}{L}$) but also images of the baseband centered at harmonics of the original sampling frequency. To recover the baseband signal, the signal q(k) is filtered with a lowpass filter which approximates the ideal characteristic.

$$H_1(e^{jw'}) = \begin{cases} G , & |w'| \leq \frac{\pi}{L} \\ 0 , & \text{otherwise} \end{cases} \tag{3.43}$$

where G = L to ensure that the amplitude of s(k) is correct.

To show that G = L; we make use of the convolution theorem,

$$\begin{aligned} S(e^{jw'}) &= H_1(e^{jw'}) \, . \, Q(e^{jw'}) \\ &= H_1(e^{jw'}) \, . \, X(e^{jw'L}) \end{aligned} \tag{3.44}$$

and within the range $|w'| \leq \frac{\pi}{L}$, we have

$$S(e^{jw'}) = G \, . \, X(e^{jw'L}) \tag{3.45}$$

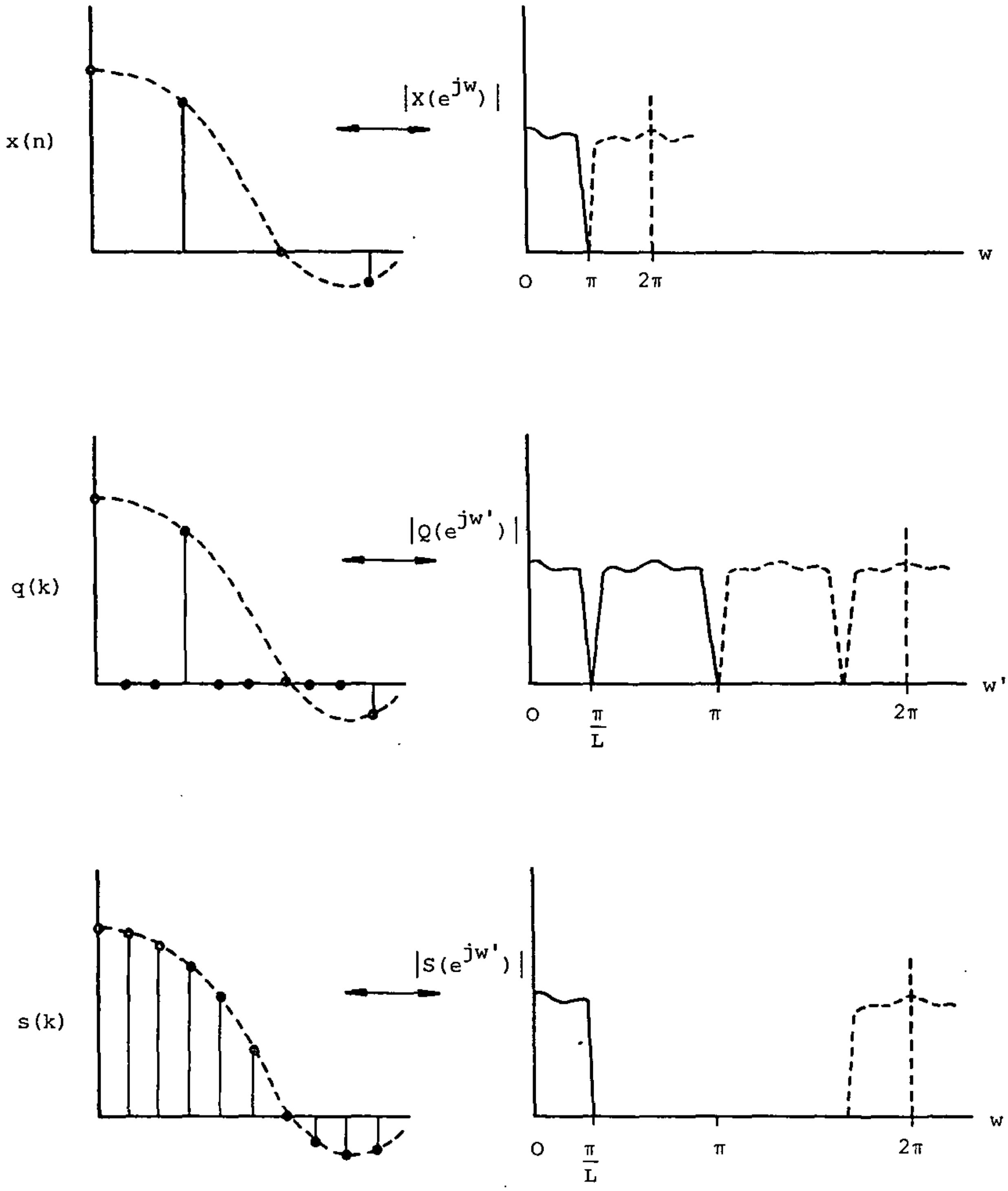

Figure 3.8 Typical waveforms and spectra for sampling rate increase by L = 3 (after ref. 91)

Taking the d.c. component of the inverse Fourier transform of $S(e^{jw'})$,

$$s(0) = \int_{-\pi}^{\pi} S(e^{jw'})\, dw'$$

$$= G \int_{-\pi}^{\pi} X(e^{jw'L})\, dw'$$

$$= \frac{G}{L} \int_{-\pi}^{\pi} X(e^{jw})\, dw \tag{3.46}$$

Therefore a gain $G = L$ is required to match the amplitudes of the envelopes of $s(k)$ and $x(n)$.

Decimation by M is then carried out on $s(k)$ to obtain $y(m)$ as described in Section 3.3.1.1.

A more efficient way of implementing the overall process can be achieved if the filters $h_1(k)$ and $h_2(k)$ are combined to form a composite lowpass filter $h(k)$ as shown in Figure 3.7(b). This filter must approximate the ideal lowpass filter characteristic

$$H(e^{jw''}) = \begin{cases} L & , \quad |w''| \leqslant \min \left|\frac{\pi}{L}, \frac{\pi}{M}\right| \\ 0 & , \quad \text{otherwise} \end{cases} \tag{3.47}$$

where $w'' = \frac{2\pi fT}{L}$ and the sampling rate of the filter is $F'' = LF$.

To derive the time domain relationship between $x(n)$ and $y(m)$ in Figure 3.7 (b), we express $y(m)$ in terms of $v(k)$, i.e.

$$y(m) = v(Mm) \tag{3.48}$$

where

$$v(k) = \sum_{n=-\infty}^{\infty} h(k-n)\ q(n)$$

$$= \sum_{n=-\infty}^{\infty} h(k-n)\ x(\tfrac{n}{L})$$

$$= \sum_{r=-\infty}^{\infty} h(k-rL)\ x(r) \qquad (3.49)$$

Combining Equations (3.48) and (3.49) gives,

$$y(m) = \sum_{r=-\infty}^{\infty} h(Mm-rL)\ x(r) \qquad (3.50)$$

3.3.2 Realization of digital lowpass filters

The decimation process as described in Section 3.3.1 was implemented with two different type of digital lowpass filters :

(i) the Infinite Impulse Response Filter

(ii) the Finite Impulse Response Filter.

Realizations of the filters are given below.

3.3.2.1 Infinite Impulse Response (IIR) Filter

The transfer function H(z) of an IIR filter of order N is given as a ratio of two polynomials in z^{-1} :

$$H(z) = \frac{a_0 + a_1 z^{-1} + - - - - + a_M z^{-M}}{1 + b_1 z^{-1} + - - - - + b_N z^{-N}} \tag{3.51}$$

If the poles and zeroes are known, Equation (3.51) can then be expressed in factored form as

$$H(z) = \frac{a_0(1 - \alpha_1 z^{-1})(1-\alpha_2 z^{-1}) - - -(1-\alpha_M z^{-1})}{(1-\beta_1 z^{-1})(1-\beta_2 z^{-1}) - - - - (1-\beta_N z^{-1})} \tag{3.52}$$

H(z) can be implemented by cascading several second order sections in serial form as in Equation (3.53)

$$H(z) = H_1(z) H_2(z) - - - H_K(z) \tag{3.53}$$

where $H_1(z)$, $H_2(z)$, - - -, $H_K(z)$ are second order sections. Figure 3.9 shows a block diagram of an IIR filter constructed in this way.

An Nth order Butterworth lowpass filter designed using the above technique has a squared magnitude function(92)

$$|H(e^{jw})|^2 = \frac{1}{1 + \left[\dfrac{\tan(\pi \frac{w}{w_s})}{\tan(\pi \frac{w_c}{w_s})}\right]^{2N}} \tag{3.54}$$

where w_s = sampling frequency

w_c = cutoff frequency

The poles are given by the values of β_m which fall within

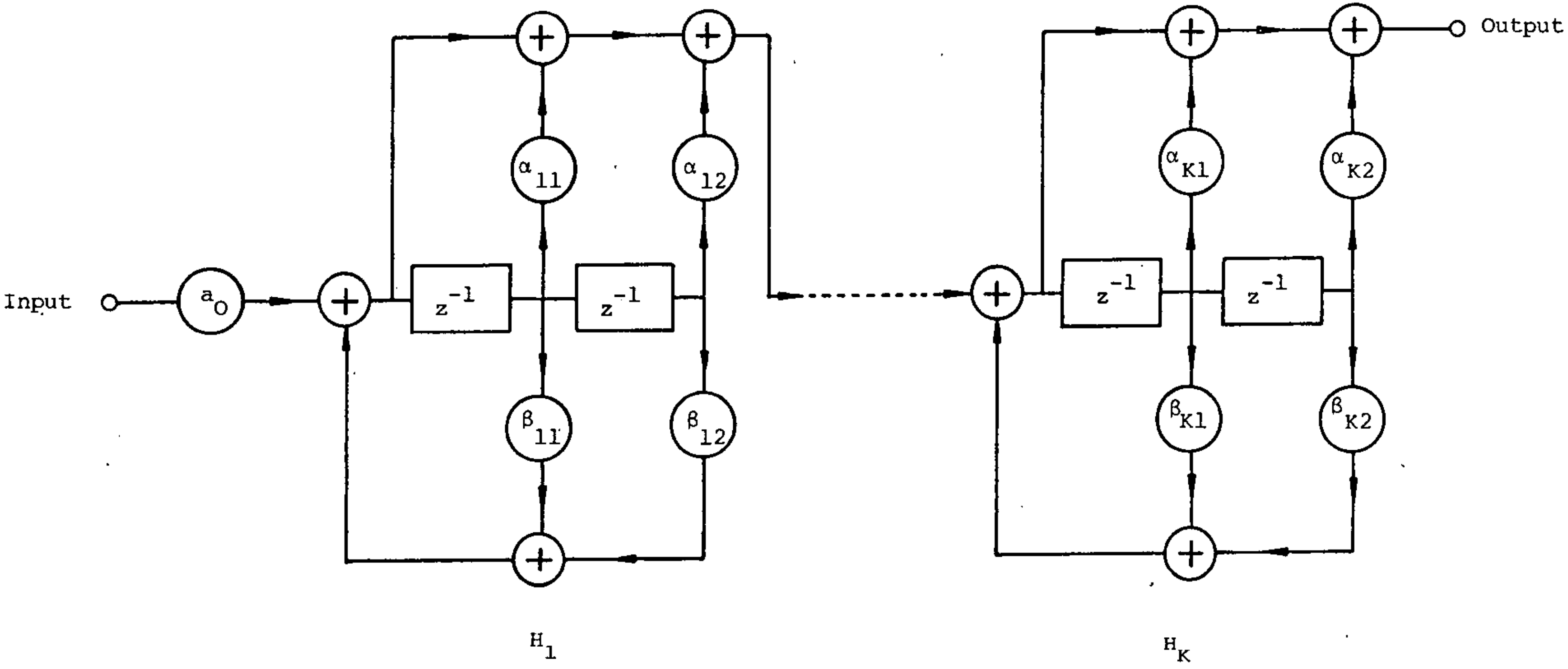

Figure 3.9 Realization of an Nth order IIR filter by serial form (N = 2K)

the unit circle in the z-plane. The real and imaginary parts X_m and Y_m of β_m can be calculated from the following expressions:

$$X_m = \frac{1 - \tan^2(\pi \frac{w_c}{w_s})}{d} \tag{3.55}$$

$$Y_m = \frac{2 \tan(\pi \frac{w_c}{w_s}) \sin(\frac{m\pi}{N})}{d} \tag{3.56}$$

where

$$d = 1 - 2 \tan(\pi \frac{w_c}{w_s}) \cos(\frac{m\pi}{N}) + \tan^2(\pi \frac{w_c}{w_s}) \tag{3.57}$$

$$m = 0, 1, - - - -, 2N-1$$

If N is even, $\frac{m\pi}{N}$ should be replaced by $\frac{\pi(2m+1)}{2N}$ in the above equations. All the zeroes of the filter are situated at $z = -1$.

Figure 3.10 shows the magnitude and phase responses of Butterworth filters with N = 2 to N = 10. From the magnitude responses, it is obvious that the higher the order of the filter, the sharper is the magnitude response. Unfortunately, the corresponding phase response becomes increasingly nonlinear. A sharp cutoff in the magnitude response reduces aliasing; however, it produces 'ringing' and has an associated nonlinear phase response. On the other hand, as the order of the filter decreases, the phase nonlinearity lessens and the overshoots in the output signal are reduced but the smoother cut-off introduces aliasing which is visible in the picture.

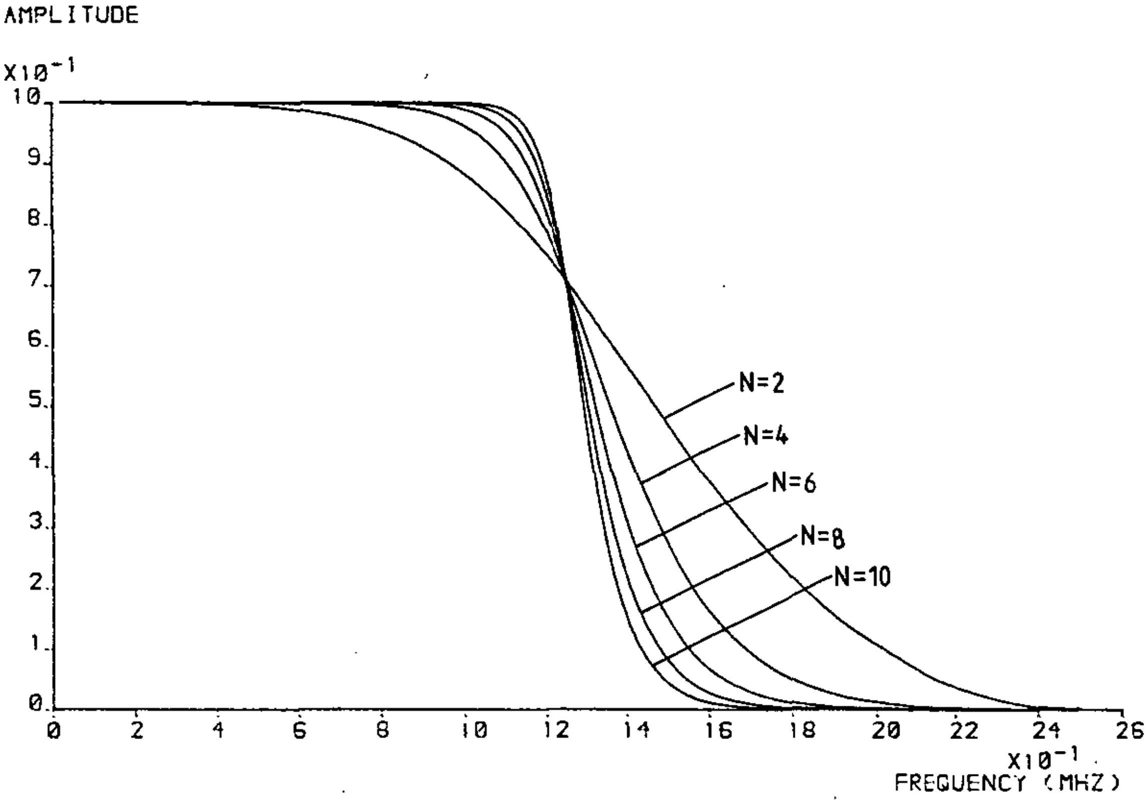

(i) Amplitude responses

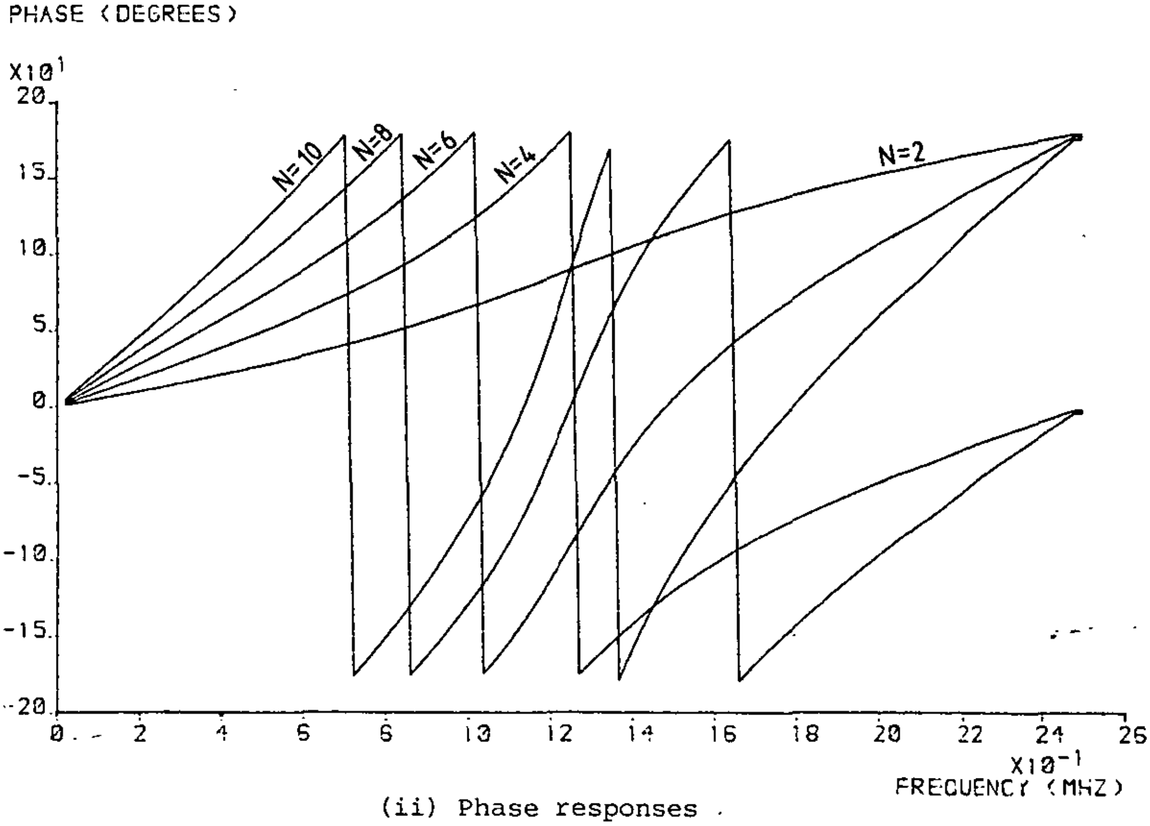

(ii) Phase responses

Figure 3.10 Frequency responses of Butterworth filters (N=2 to N=10)

Figures 3.11 (i) to (iv) show the filtered and decimated versions of part of the BBC Testcard F using, respectively, Butterworth filters of 2nd, 4th, 6th, and 8th orders with the same cutoff frequency and sampling rate reduction. It is obvious from the figures that the 2nd order filter has too smooth a response whereas that of the 8th order filter is too sharp. A good compromise appears to be the 4th order Butterworth filter.

3.3.2.2 Finite Impulse Response (FIR) Filter

Given a finite-duration filter impulse response h(0), h(1), - - - -, h(N-1) the z-transform of this filter is

$$H(z) = \sum_{n=0}^{N-1} h(n) z^{-n} \tag{3.58}$$

Since h(n) is of finite duration, it can be represented in terms of its discrete Fourier transform (DFT) H(k), k = 0, 1, - - - -, N-1, as follows:

$$h(n) = \frac{1}{N} \sum_{k=0}^{N-1} H(k)\, e^{\frac{j2\pi kn}{N}} \tag{3.59}$$

where

$$H(k) = H(z)\Big|_{z = e^{\frac{j2\pi k}{N}}} \tag{3.60}$$

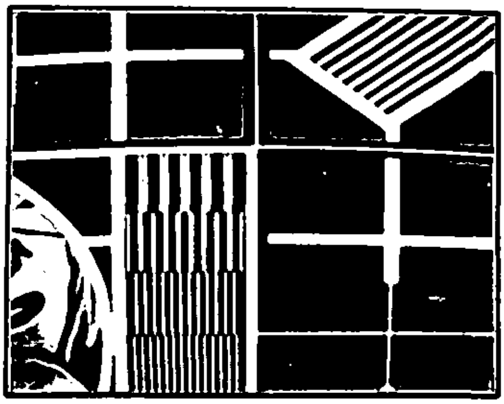

Figure 3.13 'TESTCARD' image

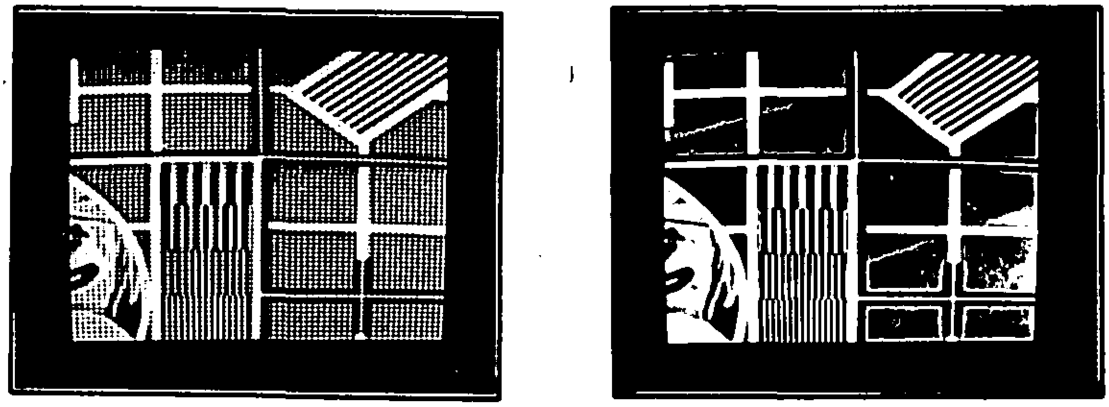

(i) 2nd order

(ii) 4th order

(iii) 6th order

(iv) 8th order

Figure 3.11 Filtered images using the Butterworth filters, ARF = $(\frac{1}{4})^2$

Substituting Equation (3.59) in Equation (3.58) and interchanging sums, we observe that the sum over the n index can be evaluated in closed form so that

$$H(z) = \frac{1-z^{-N}}{N} \sum_{k=0}^{N-1} \frac{H(k)}{\left[1 - z^{-1} e^{\frac{j2\pi k}{N}}\right]} \qquad (3.61)$$

Evaluating Equation (3.61) on the unit circle where $z = e^{jw}$ leads to the interpolated frequency response (see Appendix I)

$$H(e^{jw}) = \frac{\exp\left[-jw\left(\frac{N-1}{2}\right)\right]}{N} \sum_{k=0}^{N-1} \frac{\left[H(k)\; e^{\frac{-j\pi k}{N}} \sin\left(\frac{wN}{2}\right)\right]}{\sin\left(\frac{w}{2} - \frac{\pi k}{N}\right)} \qquad (3.62)$$

The phase is taken to be linear with delay equal to $(\frac{N-1}{2})$ samples.

Given the set of N values of H(k), the impulse response h(n) can be computed using the inverse DFT, as in

$$h(n) = \begin{cases} \frac{1}{N} \sum_{k=0}^{N-1} H(k)\; e^{\frac{j2\pi kn}{N}} \;, & n = 0, 1, - - - - , N-1 \\ 0 \;, & \text{otherwise} \end{cases} \qquad (3.63)$$

In the design of a lowpass filter one would choose the frequency coefficients H(k) in the passband to be 1.0 and those in the stopband to be 0.0. The values of the coefficients which occur in the transition band are chosen to maximise sidelobe ripple cancellation.

It can be seen from Equation (3.62) that $H(e^{jw})$ is a linear function of the frequency coefficients H(k). Thus linear programming techniques can be used to find the optimum values of the transition coefficients. This approach, first proposed by Gold and Jordon(93) and developed by Rabiner et al(94) has been used to design a variety of filters. Figure 3.12 shows a typical specification of a FIR lowpass filter. In this example, there are (2B-1) coefficients in the passband, 2M transition coefficients and the remaining coefficients in the stopband.

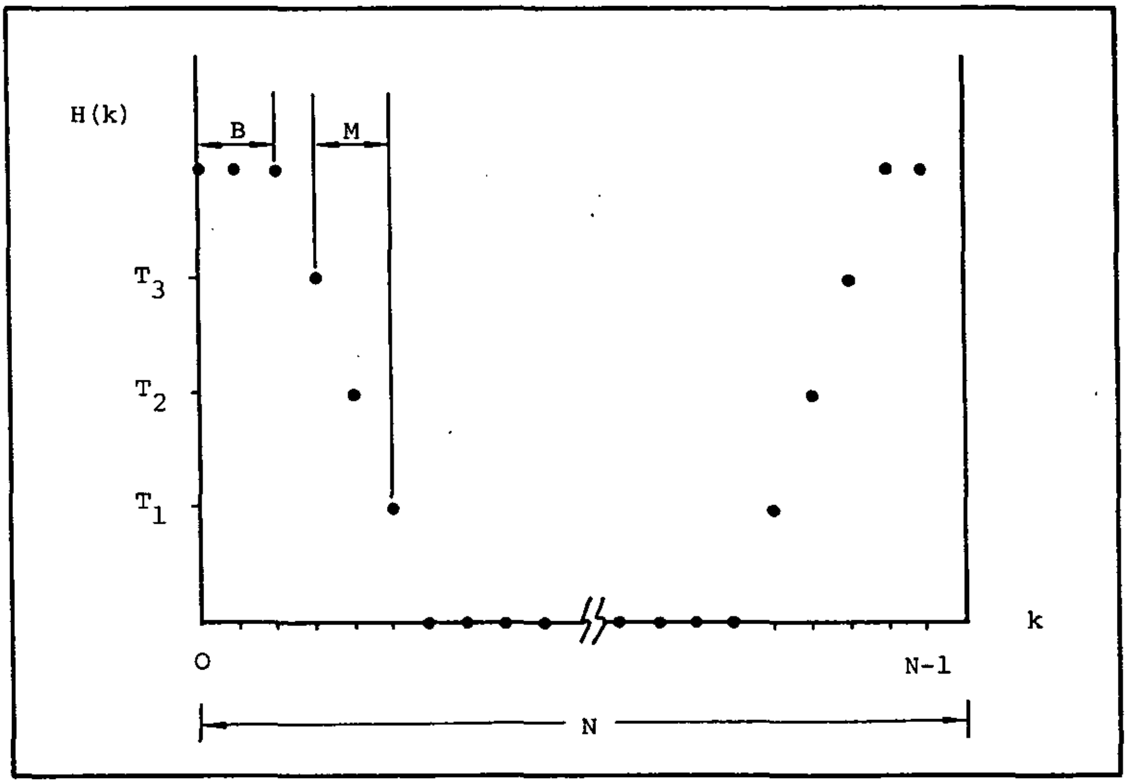

Figure 3.12 Typical specification of a FIR lowpass filter

3.3.3 Experimental results

Experiments were carried out on two test images :

(i) the 'GIRL' image (ii) the 'TESTCARD' image as shown in Figures 2.3(a) and 3.13 respectively. The latter was used to provide the severest test for the algorithms as it contains frequencies far in excess of those to be found in the typical scenes. The sources images, sampled at 5.0 MHz and containing 256 x 256 pels, were lowpass filtered and decimated by factors of ¾, ½, ⅜, and ¼ in each dimension. Two dimensional filtering and decimation were achieved by carrying out the processes separately, first horizontally and then vertically.

Figures 3.14 (i) to (iv) contain the decimated images of 'TESTCARD' with area reduction factors (ARF) of $(\frac{3}{4})^2$, $(\frac{1}{2})^2$, $(\frac{3}{8})^2$ and $(\frac{1}{4})^2$ respectively using a 4th order Butterworth lowpass filter. Figure 3.15 shows the same results for the 'GIRL' image. Similarly Figures 3.16 and 3.17 show the decimated images for 'TESTCARD' and 'GIRL' images respectively using the FIR filter with $N = 256$, $M = 3$.

3.3.4 Discussion

Judging from the results obtained, it is apparent that both filters produced decimated images of good quality even at the large ARF of $(\frac{1}{4})^2$. However if the images are critically examined, the degradations introduced by each filter can be identified and so their performances compared.

The obvious visible impairments in the images are the vertical and horizontal lines present at the right-hand and bottom edges of Figure 3.16 and 3.17. This is due to 'ringing' resulting from the

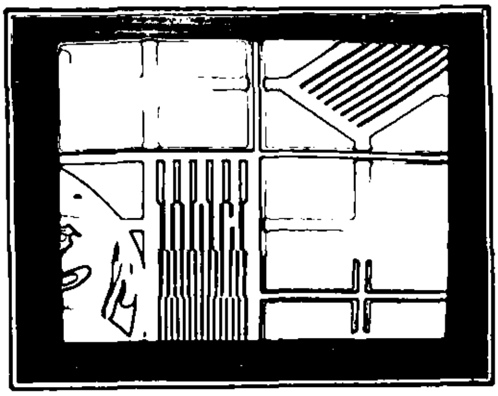

(i) ARF = $(\frac{3}{4})^2$

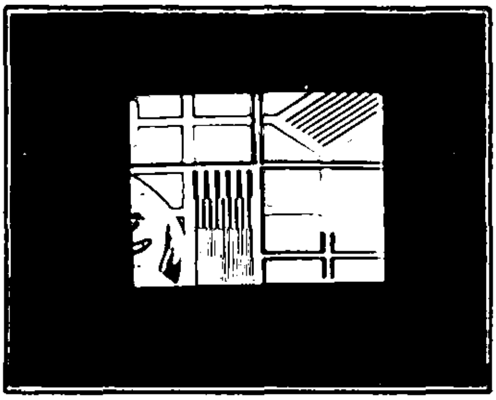

(ii) ARF = $(\frac{1}{2})^2$

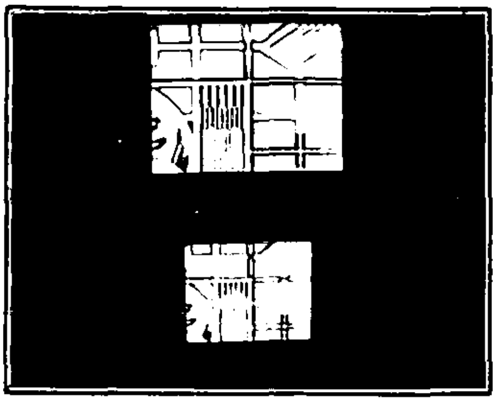

(iii) ARF = $(\frac{3}{8})^2$

(iv) ARF = $(\frac{1}{4})^2$

Figure 3.14

(i) ARF = $(\frac{3}{4})^2$

(ii) ARF = $(\frac{1}{2})^2$

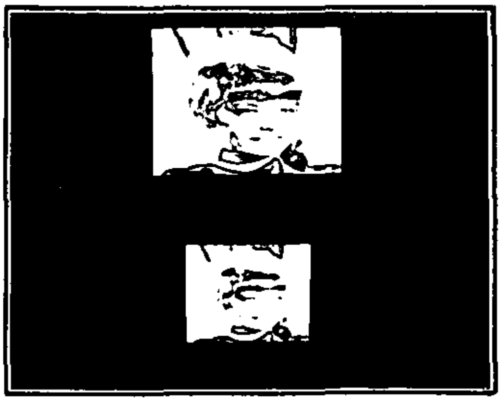

(iii) ARF = $(\frac{3}{8})^2$

(iv) ARF = $(\frac{1}{4})^2$

Figure 3.15

Decimated images using the 4th order Butterworth filter

(i) ARF = $(\frac{3}{4})^2$

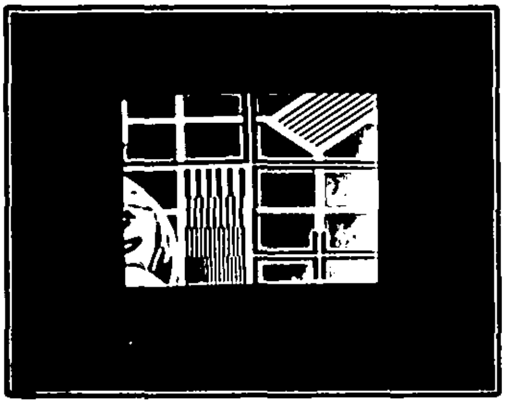

(ii) ARF = $(\frac{1}{2})^2$

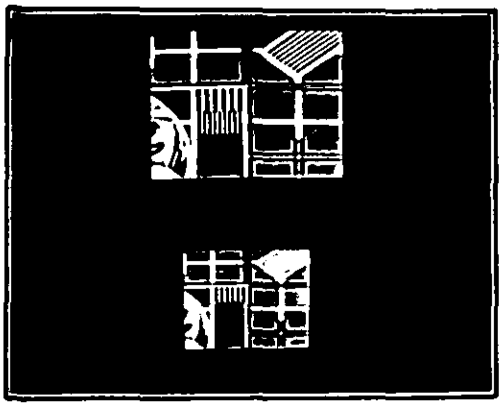

(iii) ARF = $(\frac{3}{8})^2$

(iv) ARF = $(\frac{1}{4})^2$

Figure 3.16

(i) ARF = $(\frac{3}{4})^2$

(ii) ARF = $(\frac{1}{2})^2$

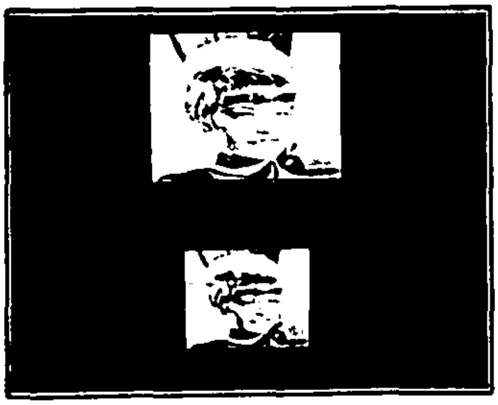

(iii) ARF = $(\frac{3}{8})^2$

(iv) ARF = $(\frac{1}{4})^2$

Figure 3.17

Decimated images using the FIR filter

approximation of the infinite filter impulse response by truncation or windowing. To eliminate ringing, it is necessary to choose a filter with enough coefficients in its bandwidth such that the magnitudes of the out-of-band coefficients are negligible.

Comparing Figures 3.14 and 3.16, it is noticed that more high frequency components are retained in the former case than the latter. This arises because the 4th order Butterworth filter response has a smoother roll-off than that of the FIR filter resulting in the retention of more high frequency components. However, this can work to its own disadvantage as is evident in Figures 3.14 (iii) and (iv) where large reduction factors require sharp cutoffs to avoid aliasing. Since the 4th order Butterworth filter does not have as sharp a cutoff as the FIR filter, the folding-back of the high frequency components can be observed near the vertical edges of the images. One solution to the problem might be to use filters of higher orders but as pointed out earlier, the sharp roll-off of the higher order filters will introduce ringing at the edges of the filtered images.

It is therefore a question of trade-offs. Since in natural scenes, like the 'GIRL' image, the occurrence of straight edges in succession (as in the 'TESTCARD' image) is rare, the effect of aliasing is usually hardly noticeable, as in Fig 3.15. On the other hand, ringing occurs at the end of image block and would be most annoying if the image is segmented and processed block by block. Then the degradation will appear as vertical and horizontal lines across the filtered image.

3.4 LOWPASS FILTERING IN THE TRANSFORM DOMAIN AND DECIMATION IN THE SPATIAL DOMAIN

In Section 3.3, lowpass filtering and decimation in the spatial domain was described. Instead of carrying out the filtering process in the spatial domain, it can be achieved in the transform domain. This is particularly advantageous in a transform coding system where signal processing is carried out in the transform domain. In this section, lowpass filtering in the cosine transform domain and decimation in the spatial domain to achieve image size reduction is described.

3.4.1 The convolution-multiplication property of the DCT

If $X_c(k)$ is the DCT of $x(n)$, it can be shown$^{(95)}$ that $X_c(k)$ may be derived from the DFT of a sequence $\hat{x}(n)$ where

$$\hat{x}(n) = \begin{cases} x(n) & , \quad n = 0, 1, ---, N-1 \\ & \\ x(2N-n-1) & , \quad n = N, N+1, ---, 2N-1 \end{cases} \tag{3.64}$$

and

$$X_c(k) = 2C(k)e^{\frac{-j\pi k}{N}} \hat{X}_F(k) \tag{3.65}$$

where $\hat{X}_F(k)$ is the DFT of $\hat{x}(n)$, defined as

$$\hat{X}_F(k) = \frac{1}{2N} \sum_{n=0}^{2N-1} \hat{x}(n)\, e^{\frac{-j2\pi nk}{2N}} \tag{3.66}$$

$$k = 0, 1, -----, 2N-1$$

and
$$C(k) = \begin{cases} \frac{1}{\sqrt{2}} & , \; k = 0 \\ 1 & , \; k = 1, 2, ----, N-1 \\ 0 & , \; \text{otherwise} \end{cases} \qquad (3.67)$$

Let h(n) be the impulse response of the filter. The filtered sequence is given by

$$w(n) = x(n) * h(n) \qquad (3.68)$$

which in the frequency domain is equivalent to

$$W_F(k) = X_F(k) \; H_F(k) \qquad (3.69)$$

where $W_F(k)$ and $H_F(k)$ are the DFTs of w(n) and h(n) respectively.

Chen and Fralick$^{(95)}$ have shown that the DCT possesses a circular convolution-multiplication property similar to that of the DFT. Hence, if

$$W_c(k) = X_c(k) \; H_c(k) \qquad (3.70)$$

where $W_c(k)$ and $H_c(k)$ are the DCTs of w(n) and h(n) respectively, then

$$w(n) = \hat{x}(n) * \hat{h}(n) * 4 \left\{ \left(\frac{1}{2\sqrt{2}} - 1\right) + \cos\left[\frac{\pi}{4N} (2n-1)(N-1)\right] \frac{\sin\left[\frac{\pi}{4}(2n-1)\right]}{\sin\left[\frac{\pi}{4n}(2n-1)\right]} \right\} \qquad (3.71)$$

(see Appendix II)

From Equation (3.71), the approximate convolution of $\hat{x}(n)$ with $\hat{h}(n)$ in the cosine transform domain can be carried out by multiplying $X_c(k)$ with $H_c(k)$. Inverse transformation of $W_c(k)$ gives w(n), the filtered sequence, which has only N distinct values.

3.4.2 Experimental procedure

Experiments were carried out on the 'GIRL' image sampled at 5.0 MHz and lowpass filtered at 1.0 MHz. The image is sub-divided into one-dimensional (1-D) or two-dimensional (2-D) blocks and the blocks are overlapped to reduce the block edge effects inherent in such a method of signal processing. For the 1-D case, the filter characteristic H(f) used is the 2nd order Butterworth filter illustrated in Figure 3.18 (i), whereas in the 2-D case, a circular symmetric filter characteristic is used which is generated from a rotation of H(f) in the form

$$H(f_x, f_y) = H\sqrt{x^2+y^2} \qquad (4.72)$$

where f_x and f_y are the spatial frequencies in the x and y directions respectively. Figure 3.18 (ii) shows a plot of $H(f_x, f_y)$.

Four schemes were investigated as illustrated in Figure 3.19. In scheme 1, the image is scanned line by line first horizontally and then vertically. Each line is divided into blocks of N pels and processed using H(f) as shown in Figure 3.18 (i). In scheme 2, the same procedure is adopted except that there is a 50% overlap in forming

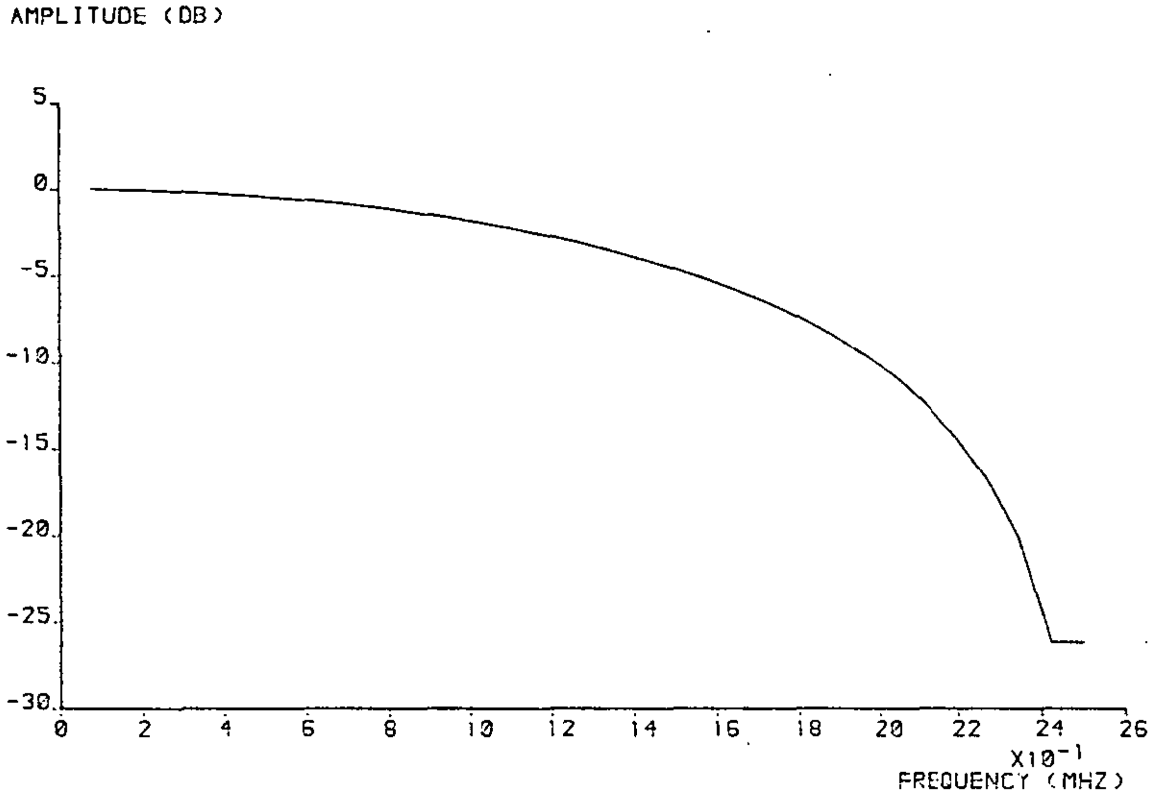

(i) 1-D amplitude response

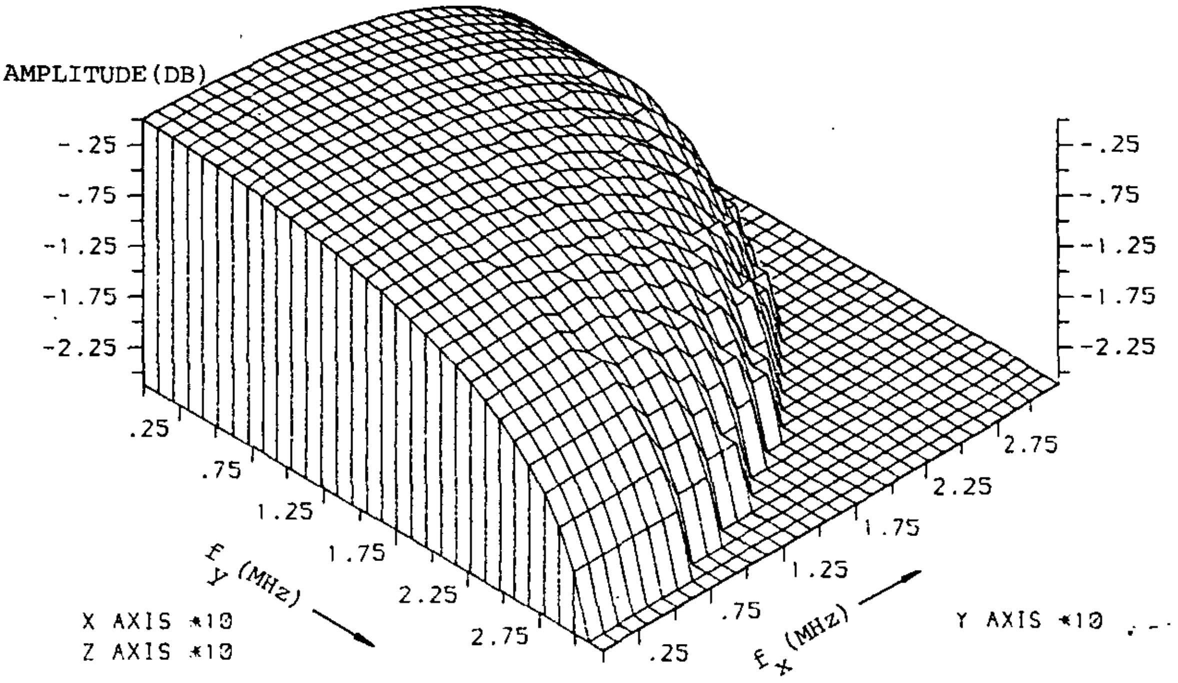

(ii) 2-D amplitude response

Figure 3.18 Second order Butterworth lowpass filter

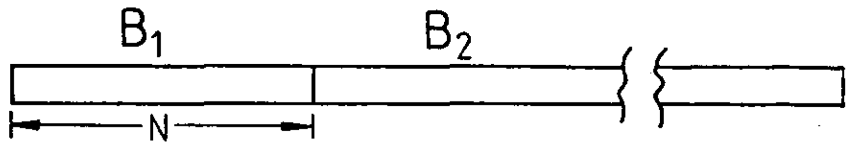

(a) Scheme 1

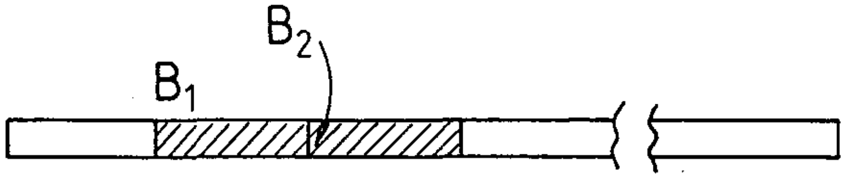

(b) Scheme 2

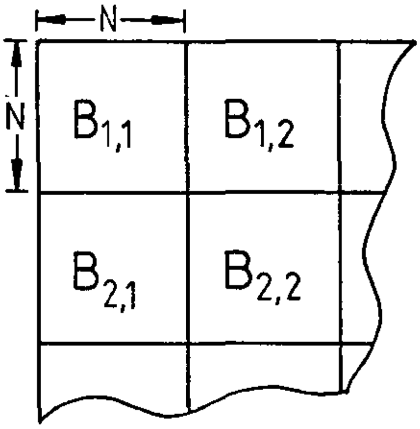

(c) Scheme 3

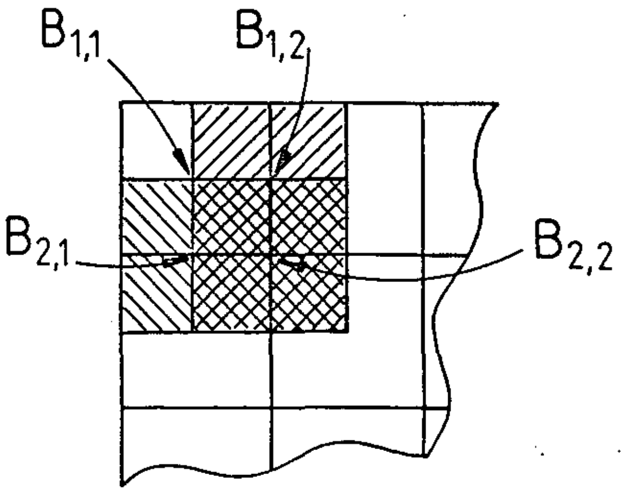

(d) Scheme 4

Figure 3.19

the blocks. In scheme 3, the image is divided into blocks of N x N pels and processed using $H(f_x, f_y)$ as shown in Figure 3.18 (ii). In scheme 4, the same procedure is followed except that each new block is formed by the overlapping of the previous blocks.

To further reduce block edge effects, two linear processes were carried out. The first, termed 'compensation', involves the computation of the mean error ε of the filtered samples in each block defined by

$$\varepsilon = \frac{\sum_{n=0}^{N} \left| q(n) - x(n) \right|}{N} \tag{3.73}$$

where $x(n)$ and $q(n)$ are the original and filtered sequences respectively. ε is then added to the filtered samples, $q(n)$, in order to smooth out the abrupt changes in amplitude at the edges of the blocks. The second process is a linear interpolation over L samples on either side of the edges using a ramp function where L=1 for N=4 and N=8.

3.4.3 Results

The four schemes were implemented as shown in Figure 3.20 with N=4 and N=8 and decimation was then carried out as described in Section 3.3.1.1 on the filtered image with N=4 to reduce the sampling rate by ½ to 2.5 MHz. Figures 3.21 (i) and (ii) contain the results for scheme 1 with N=8 and N=4 respectively whereas Figure 3.21 (iii) contains the decimated version of Figure 3.21 (ii). Similarly

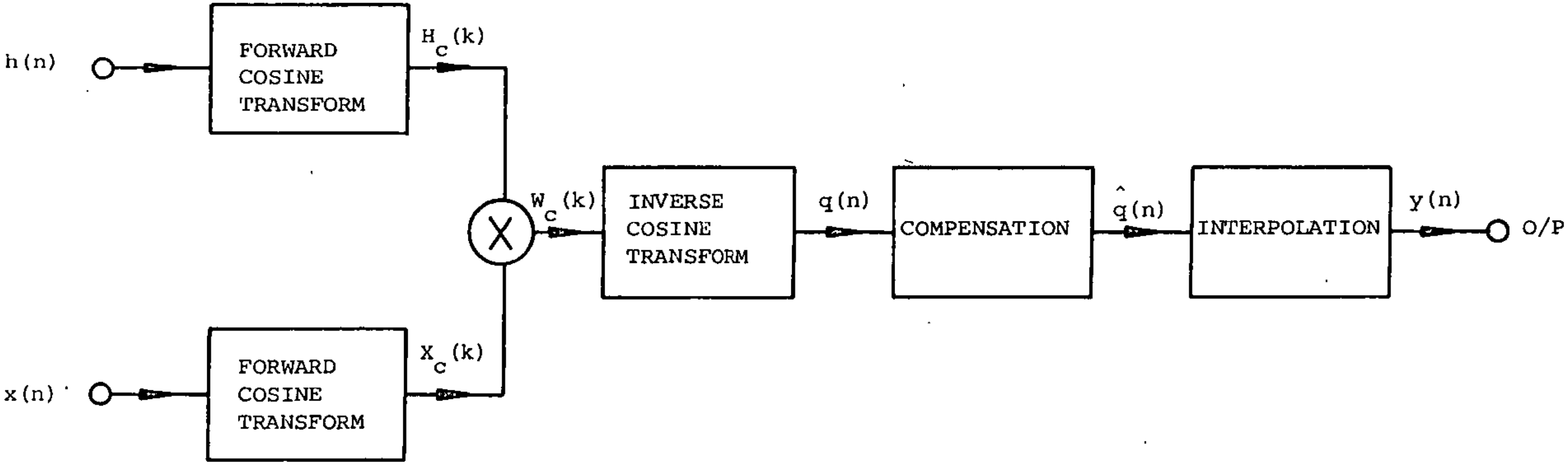

Figure 3.20 Block diagram of cosine transform filter

Figures 3.22, 3.23 and 3.24 show the results for schemes 2, 3 and 4 respectively.

3.4.4 Discussion

Figures 3.21 to 3.24 clearly show that for lowpass filtering in cosine transform domain to work, overlapping of the transform blocks is essential. Block edge effects are clearly noticeable in Figures 3.21 and 3.23, even with as small a block size as 4 x 4. On the other hand, they are hardly noticeable in Figures 3.22 and 3.24. The decimated images give the same results, indicating that schemes 2 and 4 achieved adequate lowpass filtering such that the high frequency components are mostly removed.

It is also evident that small block size improves the subjective quality of the filtered images since it effectively localises the mean energy of small areas, rendering the energy difference between adjacent sub-blocks small. Hence, on inverse transformation, the average amplitudes in adjacent sub-blocks differ little.

Even though second order Butterworth filter was used in the simulations, filters of different orders can also be used. However, considerations must be given to the effects of ringing that filters of high orders (>4) may introduce into the processed pictures. The same considerations apply when using filters other than Butterworth filters e.g. FIR filters.

(i) N = 8

(ii) N = 4

(iii) ARF = $(\frac{1}{2})^2$

Figure 3.21 Scheme 1

(i) N = 8

(ii) N = 4

(iii) ARF = $(\frac{1}{2})^2$

Figure 3.22 Scheme 2

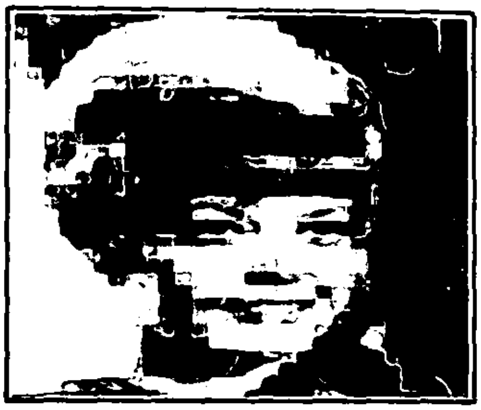

(i) N = 8

(ii) N = 4

(iii) ARF = $(\frac{1}{2})^2$

Figure 3.23 Scheme 3

(i) N = 8

(ii) N = 4

(iii) ARF = $(\frac{1}{2})^2$

Figure 3.24 Scheme 4

3.5 LOWPASS FILTERING AND DECIMATION IN THE TRANSFORM DOMAIN

In the previous section, an image reduction system was described in which lowpass filtering was carried out in the transform domain and decimation in the spatial domain. However, it would be advantageous to be able to effect both operations in the transform domain and so dispense with the use of the band limiting lowpass filter.

It has been demonstrated that simply truncating the high order coefficients in the transform domain (setting them to zero) achieves a lowpass filtering effect. If, instead of setting the truncated coefficients to zero, they are discarded so that only the number of coefficients predetermined by the sampling rate reduction factor (RF) are retained, then inverse transformation of the reduced coefficient matrix with an inverse transformation matrix of order M where M is the reduced block size results in the decimated image. To equalise the total energy of the reduced block size, according to Parseval's theorem, the retained coefficients are normalized by $\frac{M}{N}$.

3.5.1 Theoretical development

To describe the theoretical basis of the operation carried out to achieve lowpass filtering and decimation in the transform domain, the DFT is employed, though the same principle applies to other transforms which obey the convolution-multiplication property.

Let f(k) be the image vector and F(n) its spectrum. F(n) and f(k) form the discrete Fourier transform pair and are defined as

$$F(n) = \frac{1}{\sqrt{N}} \sum_{k=0}^{N-1} f(k) \exp\{-\frac{2\pi j}{N}(nk)\} \tag{3.74}$$

and

$$f(k) = \frac{1}{\sqrt{N}} \sum_{n=0}^{N-1} F(n) \exp\{\frac{2\pi j}{N}(nk)\} \tag{3.75}$$

where $j = \sqrt{-1}$.

A truncating function T(n), n=0, 1, - - - -, N-1 defined as

$$T(n) = \begin{cases} 1 , & 0 \leqslant n \leqslant M-1 \\ 0 , & \text{elsewhere} \end{cases} \tag{3.76}$$

is illustrated in Figure 3.25.

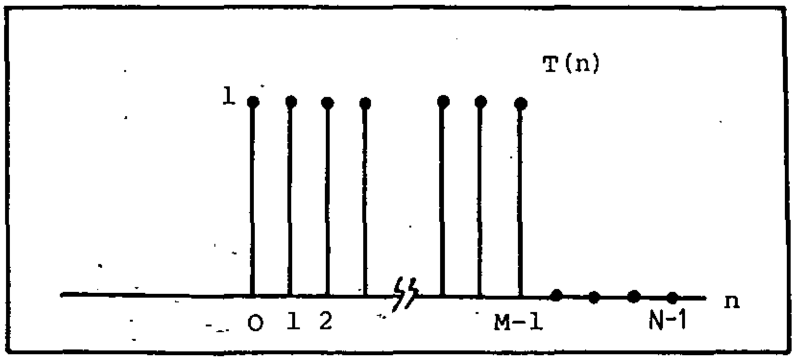

Figure 3.25 Truncating function, T(n)

To find the impulse response of T(n), the IDFT of Equation (3.76) is taken i.e.

$$t(k) = \frac{1}{\sqrt{N}} \sum_{n=0}^{N-1} T(n) \exp\{\frac{2\pi j}{N}(nk)\}$$

$$= \frac{1}{\sqrt{N}} \sum_{n=0}^{M-1} \exp\{\frac{2\pi j}{N}(nk)\} \quad (3.77)$$

From Equation (3.77),

$$\sum_{n=0}^{M-1} \exp\{\frac{2\pi j}{N}(nk)\} = \frac{1 - \exp(2\pi jkM/N)}{1 - \exp(\frac{2\pi j}{N}k)} \quad (3.78)$$

The numerator of Equation (3.78) can be expressed in terms of sine and exponential functions. Thus

$$1 - \exp(2\pi jk\frac{M}{N}) = -2j\exp(\pi jk\frac{M}{N})\sin(\pi k\frac{M}{N}) \quad (3.79)$$

Similarly

$$1 - \exp(\frac{2\pi j}{N}k) = -2j\exp(\frac{\pi jk}{N}) \sin(\frac{\pi}{N}k) \quad (3.80)$$

Therefore Equation (3.77) becomes

$$t(k) = \frac{1}{\sqrt{N}} \exp\{\frac{\pi jk}{N}(M-1)\} \frac{\sin(\pi kM/N)}{\sin(\frac{\pi}{N}k)} \quad (3.81)$$

To decimate an image in the transform domain, we compute Y(n), n = 0, 1, - - -, M-1 given by

$$Y(n) = F(n)\ T(n) \quad (3.82)$$

which in the spatial domain gives

$$y(k) = \frac{1}{N} \sum_{m=0}^{N-1} f(m)\ t(k-m) \qquad (3.83)$$

$$k = 0, ----, M-1.$$

the decimated image.

The important property of superior energy compaction of some unitary transforms enables lowpass filtering and decimation to be carried out in the transform domain. Each spectral component in the transform domain corresponds to the amount of energy of the spectral function within the image. Through transformation, most of the energy in the spatial domain is concentrated in the few coefficients of the lower 'frequency' spectrum as shown in Figure 3.26 for the 'GIRL' image using the DCT with a transform block size of 32 x 32 pels.

Note that for the Hadamard transform* (HT), the properties pertaining to convolution are somewhat different. In the case of the DFT, the convolution is cyclic as defined in Equation (3.83) whereas the HT obeys the dyadic convolution property, i.e.

$$y(k) = \frac{1}{N} \sum_{m=0}^{N-1} f(m)\ t(k \theta m) \qquad (3.84)$$

where θ denotes modulo 2 subtraction.

However, it has been shown(96) that the HT power spectrum, like the DFT power spectrum, is invariant to positional shift of the data sequence, which in the case of the DFT is cyclic and for the HT

---

* The HT used in this work is the Walsh - ordered Hadamard transform.

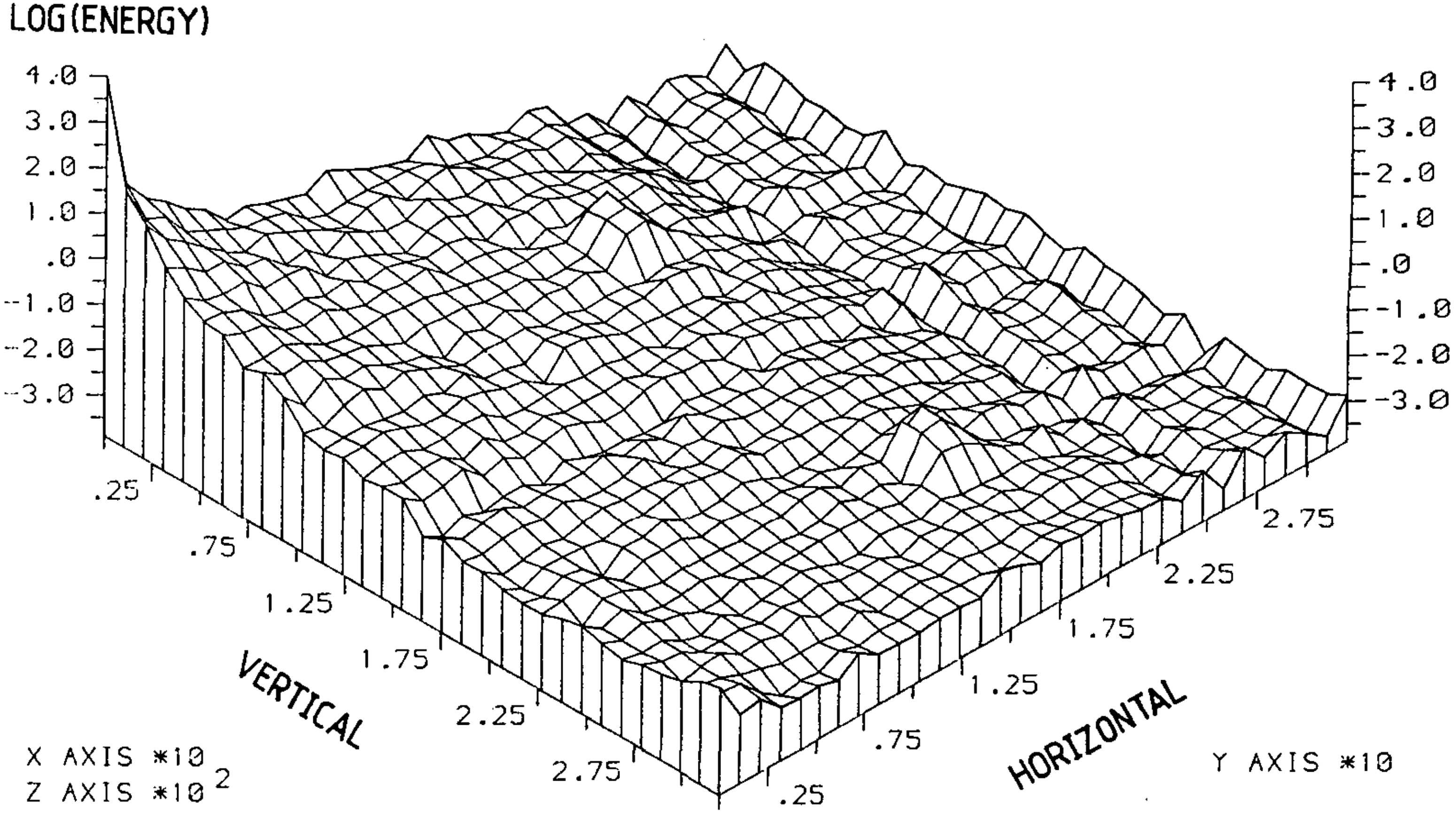

Figure 3.26 Energy distribution of the 'GIRL' image

is dyadic. It is this unique property which makes possible lowpass filtering and decimation in the Hadamard transform domain.

3.5.2 Experimental procedure

Figure 3.27 contains the block diagram of the transform image reduction system. N lines of input data are read into the input buffer and are then segmented into blocks of N x N pels. For each of these blocks, a forward transformation is performed. If we denote the image matrix, the forward transformation matrix and the resultant coefficient matrix as {f}, {A} and {F} respectively, we have

$$\{F\} = \{A\}\,\{f\}\,\{A\}^T \tag{3.85}$$

A selection matrix {S} is formed having dimensions of M by N where M is determined by the sampling rate reduction factor, RF and N, i.e.

$$M = RF \,.\, N \tag{3.86}$$

{S} is shown in Figure 3.28 for M = 4, N = 8.

$$\{S\} = \begin{bmatrix} 1 & 0 & 0 & 0 & 0 & 0 & 0 & 0 \\ 0 & 1 & 0 & 0 & 0 & 0 & 0 & 0 \\ 0 & 0 & 1 & 0 & 0 & 0 & 0 & 0 \\ 0 & 0 & 0 & 1 & 0 & 0 & 0 & 0 \end{bmatrix}$$

Figure 3.28 Selection matrix, {S} for M = 4, N = 8.

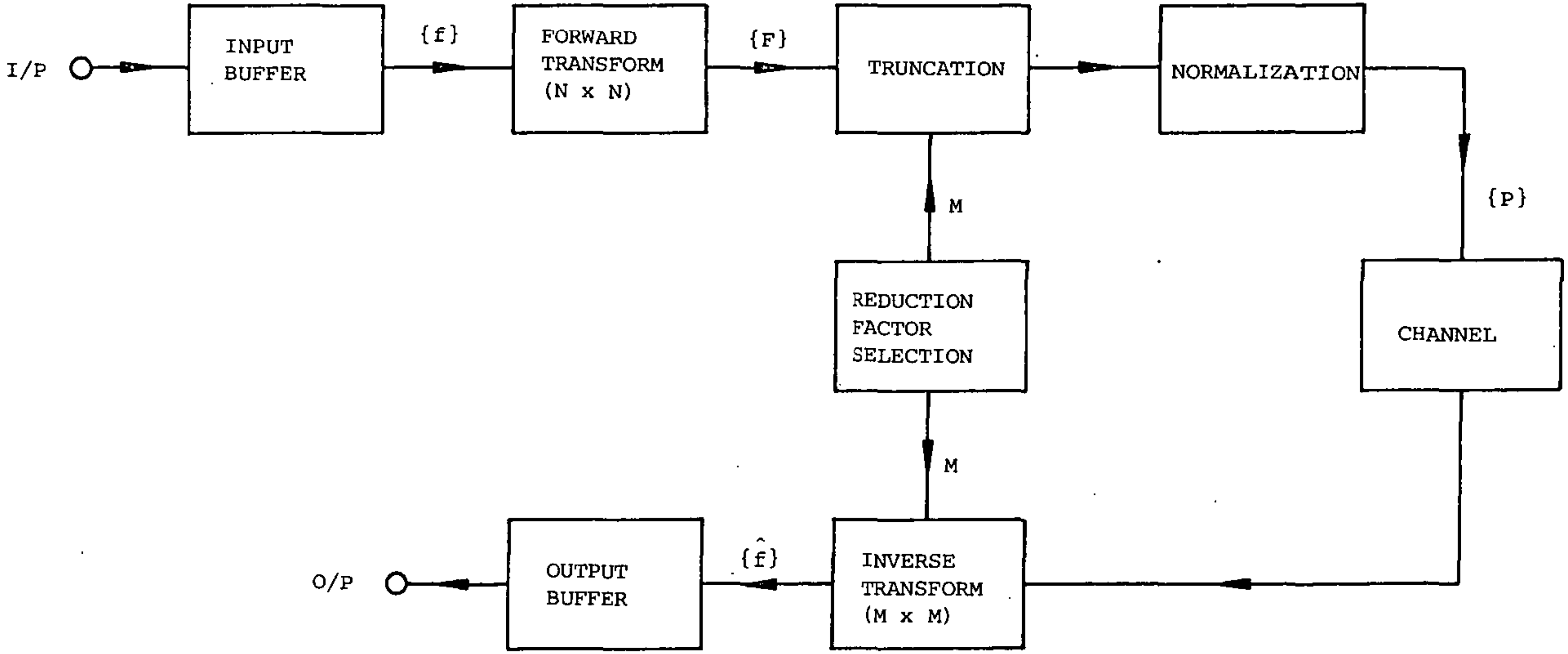

Figure 3.27 Block diagram of transform image reduction system

The decimated coefficient matrix, {P} of dimension M by M is then obtained by the matrix multiplication

$$\{P\} = \{S\}\,\{F\}\,\{S\}^T \tag{3.87}$$

where $\{S\}^T$ is the transpose of {S}. Equalization of the total energy in both the spatial and transform domains is carried out by normalizing the coefficients by $\frac{M}{N}$.

Inverse transformation of {P} with an inverse transformation matrix, {B} of dimension M by M gives the decimated spatial matrix, $\{\hat{f}\}$. Thus we have

$$\{\hat{f}\} = \frac{M}{N}\,\{B\}\,\{P\}\,\{B\}^T \tag{3.88}$$

The process described above is generally true for all transform image reduction systems, but the DFT has a double-sided spectrum and an imaginary part even though only half of the samples are distinct. Therefore, to decimate a data block {f} of N x N pels, we form an array {f'} of 2N x 2N pels by folding over {f} as shown in Figure 3.29 where the arrow indicates the orientation of the block. The imaginary parts are set to zero. Forward transformation of {f'} results in {F'} with the (N+1)th row and column containing zeroes. Truncation is then carried out on each quadrant separately as described above by discarding all the coefficients outside the shaded regions. This is done for both real and imaginary parts of {F'}. The shaded regions are then concatenated to form {P'}, of size 2M x 2M. To preserve the conjugate

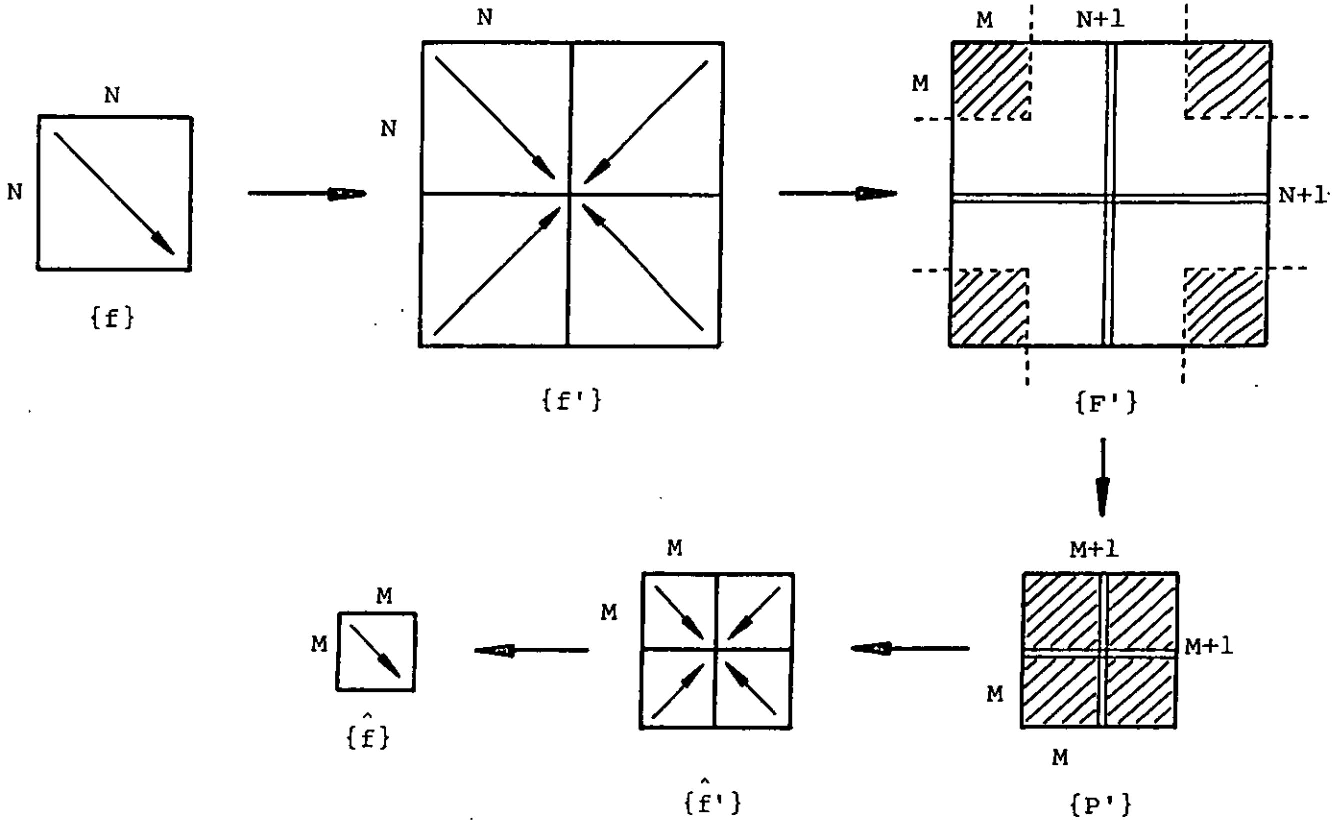

Figure 3.29 Decimation in the DFT domain

symmetry property of the DFT, the (M+1)th row and column are set to zero. The decimated block of M x M pels is finally obtained from the second quadrant of the real part of $\{\hat{f}'\}$ upon inverse transformation of $\{P'\}$.

3.5.3 Results

Simulations were carried out on the 'GIRL' and 'TESTCARD' images shown in Figure 2.3(a) and Figure 3.13 respectively. The images were transformed using the DFT, DCT and HT with an original block size of 32 x 32 pels and sampling rate reduction factors of ½ and ¼ i.e. area reduction factors (ARF) of $(\frac{1}{2})^2$ and $(\frac{1}{4})^2$ were achieved. Furthermore, intermediate ARFs of $(\frac{3}{8})^2$ and $(\frac{3}{4})^2$ were investigated by using the DFT and the DCT.

Figures 3.30 (i) to (iv) show the results for the 'TESTCARD' employing the DFT with ARFs of $(\frac{3}{4})^2$, $(\frac{1}{2})^2$, $(\frac{3}{8})^2$ and $(\frac{1}{4})^2$ respectively. Figure 3.31 shows the same for the 'GIRL' image. In Figure 3.32, the results for the 'TESTCARD' image employing the DCT with ARFs of $(\frac{3}{4})^2$, $(\frac{1}{2})^2$, $(\frac{3}{8})^2$ and $(\frac{1}{4})^2$ respectively are shown. The same results for the 'GIRL' image are shown in Figure 3.33. However for the HT, only results for ARFs of $(\frac{1}{2})^2$ and $(\frac{1}{4})^2$ are obtainable and are shown in Figures 3.34 and 3.35 for the 'TESTCARD' and 'GIRL' images respectively Also, the frequency responses of three truncating functions for DFT, DCT and HT are plotted in Figures 3.36 (a) to (c) respectively.

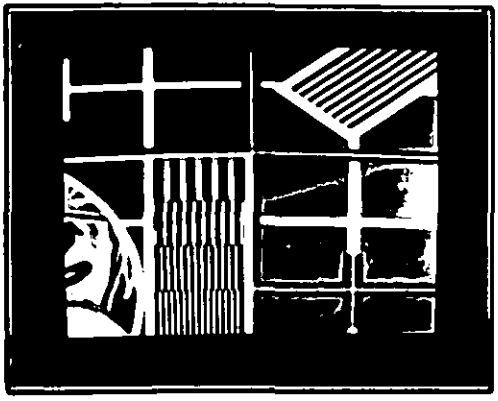

(i) ARF = $(\frac{3}{4})^2$

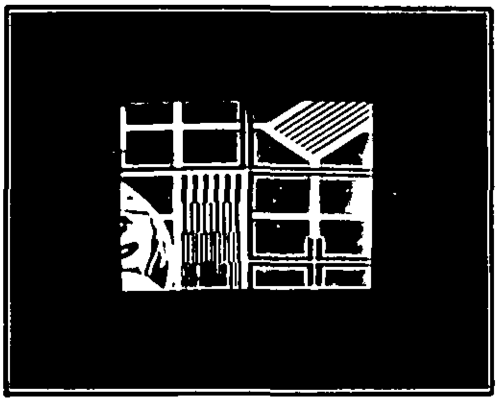

(ii) ARF = $(\frac{1}{2})^2$

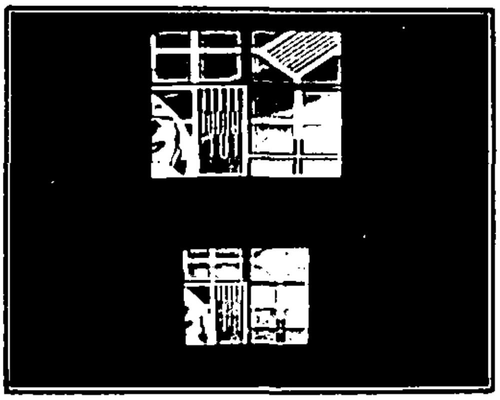

(iii) ARF = $(\frac{3}{8})^2$

(iv) ARF = $(\frac{1}{4})^2$

Figure 3.30

(i) ARF = $(\frac{3}{4})^2$

(ii) ARF = $(\frac{1}{2})^2$

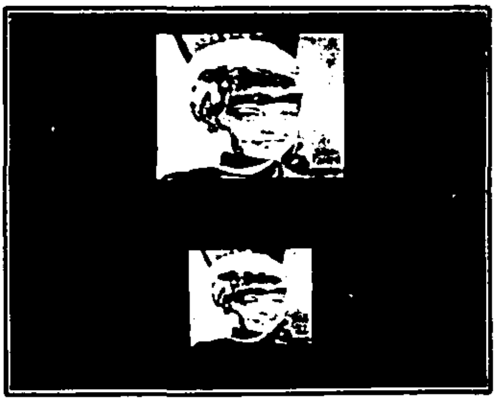

(iii) ARF = $(\frac{3}{8})^2$

(iv) ARF = $(\frac{1}{4})^2$

Figure 3.31

Decimated images in the DFT domain

(i) ARF = $(\frac{3}{4})^2$

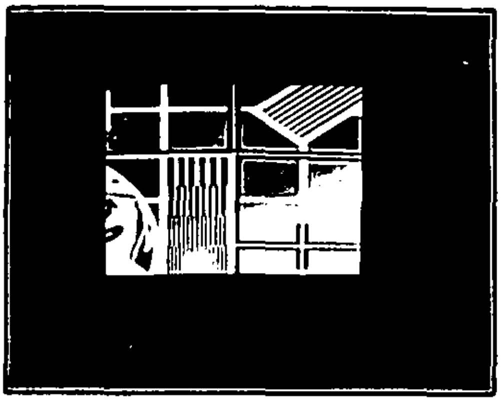

(ii) ARF = $(\frac{1}{2})^2$

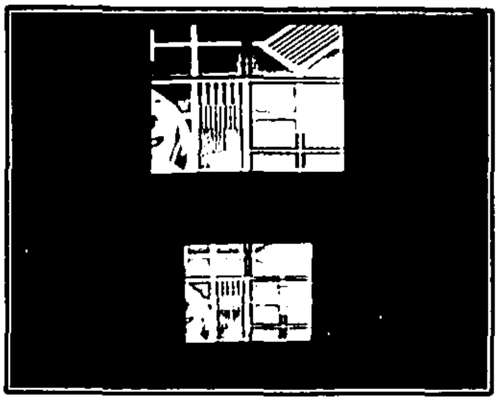

(iii) ARF = $(\frac{3}{8})^2$

(iv) ARF = $(\frac{1}{4})^2$

Figure 3.32

(i) ARF = $(\frac{3}{4})^2$

(ii) ARF = $(\frac{1}{2})^2$

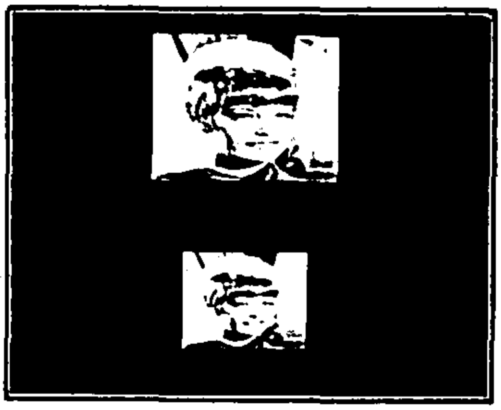

(iii) ARF = $(\frac{3}{8})^2$

(iv) ARF = $(\frac{1}{4})^2$

Figure 3.33

Decimated images in the DCT domain

(i) ARF = $(\frac{1}{2})^2$

(ii) ARF = $(\frac{1}{4})^2$

Figure 3.34

(i) ARF = $(\frac{1}{2})^2$

(ii) ARF = $(\frac{1}{4})^2$

Figure 3.35

Decimated images in the HT domain

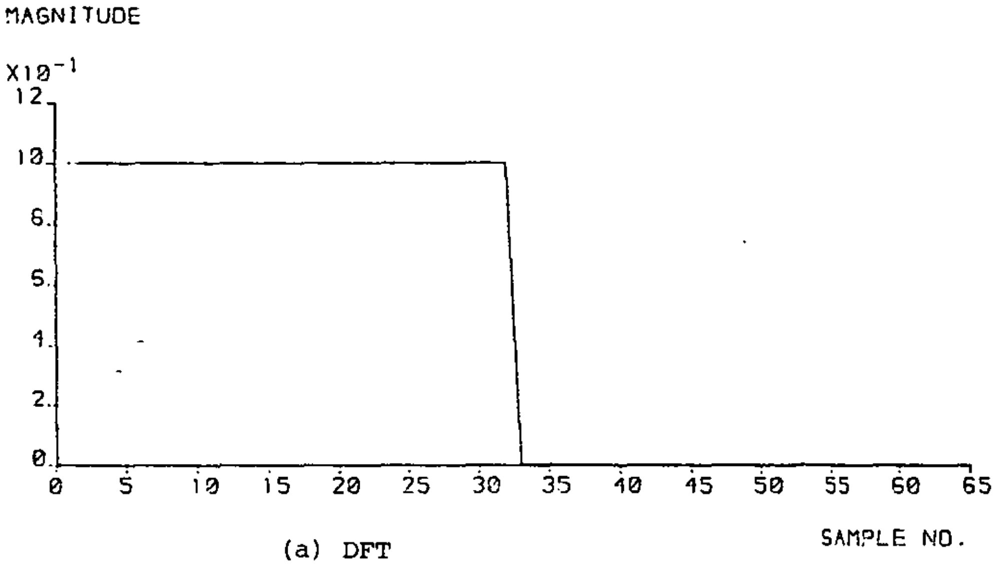

(a) DFT

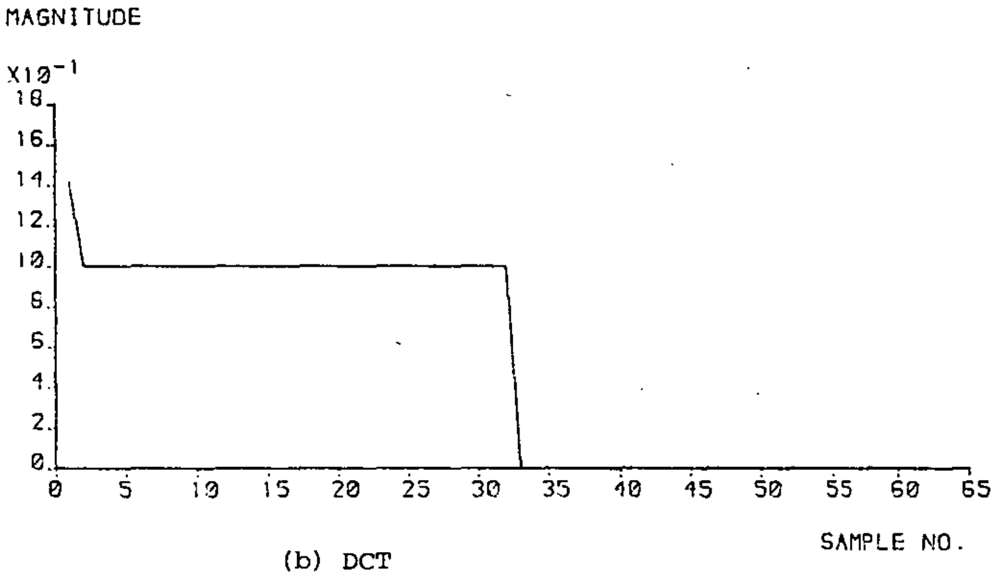

(b) DCT

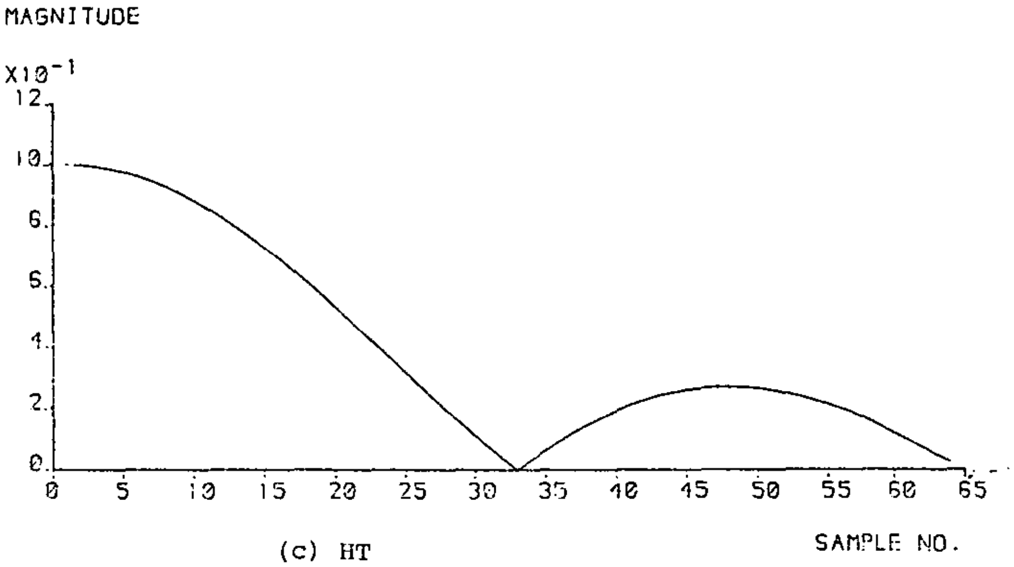

(c) HT

Figure 3.36 Frequency responses of the truncating function

3.5.4 Discussion

The decimated images obtained using the three unitary transforms, when viewed by observers at the standard viewing distance of six times the picture height, were judged to be subjectively acceptable. However, on closer examination, faint streaks were found around the vertical and horizontal edges in the DFT and DCT processed images. This is due to ringing as shown in Figure 3.37. Figure 3.37(a) shows a time waveform consisting of several vertical edges while Figures 3.37 (b) and (c) show the results after decimation by ½ in the DCT and HT domains respectively.

The frequency responses of the DFT and DCT truncating functions are quite similar (see Figure 3.36), which is not at all surprising since one can derive the DCT from the DFT and vice versa. However, the HT response shows a more gradual roll-off which means that the out-of-band frequencies will not be attentuated as much as those for the DFT and DCT. Figures 3.34 (i) and (ii) illustrate this point.

Even though the DFT and DCT truncating function responses are quite similar, their performances especially at large ARFs e.g. $(\frac{1}{4})^2$ are markedly different. The performance in the DCT domain is superior than that in the DFT domain as evident in Figures 3.30(iv) and 3.32(iv) mainly attributed to the superior energy compaction of the DCT which means that more information is retained in the DCT coefficients than in the same number of the DFT coefficients.

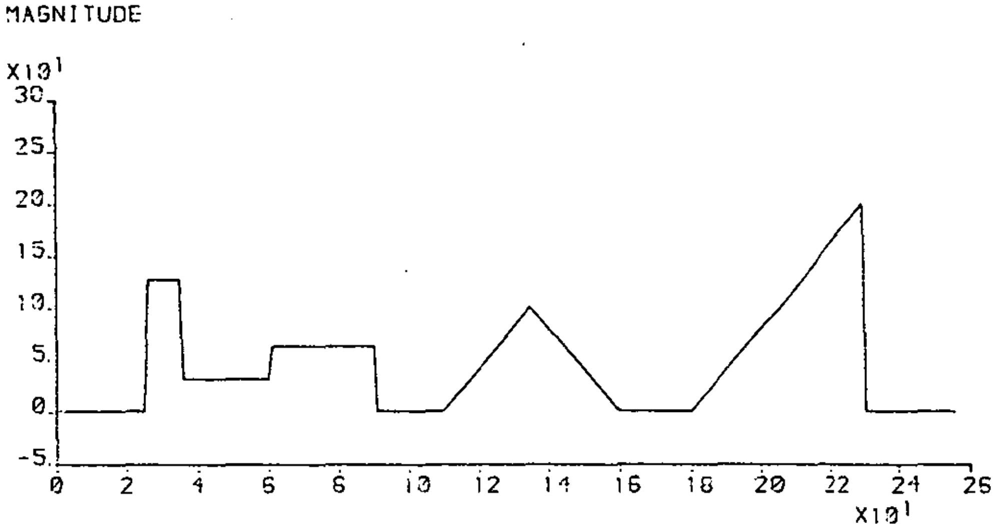

(a) Original waveform

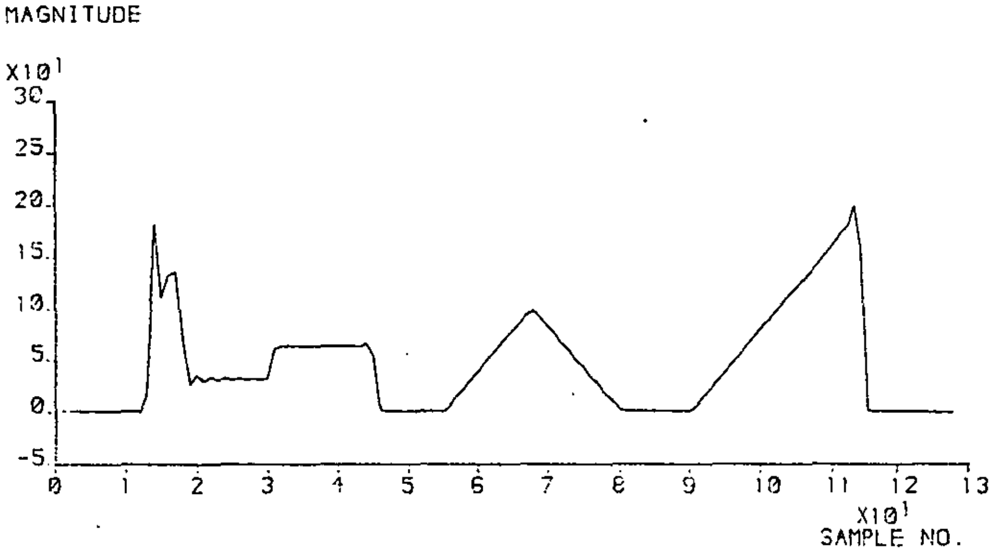

(b) DCT decimated waveform, RF = ½

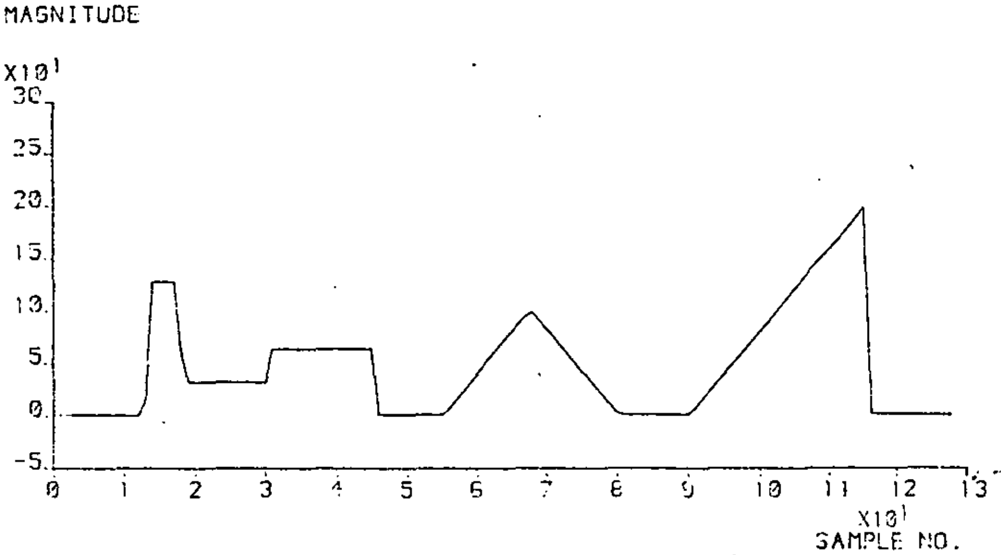

(c) HT decimated waveform, RF = ½

Figure 3.37 Waveforms showing the effects of 'ringing'

In considering the merits of the three transforms in the context of image reduction, one has to take into account of (i) the ease of implementation of the transform, (ii) the ability of the transform to achieve reduction of different sizes and (iii) the performance of the transform in terms of subjective picture quality. All three transforms investigated are shown to produce decimated images of acceptable picture quality. However, as was noted earlier on, the DFT requires four times as much memory space as the DCT and HT since it possesses an additional imaginary component. Therefore, the computation time goes up proportionately. For a two-dimensional transformation of N x N pels, the DCT requires $2N^3$ multiplications and additions whereas the DFT would need $2(2N)^3$ i.e. 8 times more than the DCT. Moreover, with an inferior degree of energy compaction compared with the DCT, the DFT is unlikely to be used in transform image reduction systems.

On the other hand, the HT basis functions contain only ±1s, and therefore transformation only involves additions and subtractions. It is true that the HT basis functions of order N exist for N = 0 modulo 4 but construction of the basis functions often follows different mathematical theorems(97,98). Hence there exist HT basis functions of different types and unless the same type of basis function is used consistently throughout, one would obtain unpredicted and sometimes disastrous results. This means that the use of the HT for image reduction is limited to factors of powers of two only. Even though there is a fast algorithm(96) to implement the HT which requires only $N \log_2 N$ additions, the limitation in image size selection is a severe one.

The DCT offers the advantage of having basis functions of multiples of two, if the even version of the transform is used(51). Despite the degradations around the vertical and horizontal edges which in any case are less noticeable in natural scenes, it is clearly the best transform to use considering the three criteria set out above.

3.6 CONCLUSIONS

The design of an image reduction system for viewdata systems was investigated using a systematic and methodical approach. Conventional systems in which lowpass filtering and decimation are both carried out in the spatial domain were simulated using (i) an IIR filter (the 4th order Butterworth filter) and (ii) a FIR filter with 256 coefficients and 3 transition coefficients. From the results obtained, it was shown that the implementation of the 4th order Butterworth filter achieved a better subjective performance than the FIR filter. It is also worth noting that the implementation of the Butterworth filter in serial form is more efficient than that of the FIR filter.

In the following section, lowpass filtering in the cosine transform domain was investigated. The results indicate the importance of overlapping of blocks in reducing the block edge effects inherent in the processing of sub-blocks in the image. Furthermore, it is found that the use of smaller block sizes improves the subjective quality of the filtered and decimated images.

Finally, a transform image reduction system was implemented in which both lowpass filtering and decimation were carried out in the transform domain. Different unitary transforms were used and the subjective results compared. The choice of the transforms was decided taking into consideration the ease of implementation of the transforms and the availability of a wide range of image sizes, in addition to subjective performance. Based on the above criteria, it is found that the DCT is the best transform to use.

The ability to alter the image size in the transform domain is significant in that all the operations such as lowpass filtering, data compression, decimation and encoding can be carried out in the transform domain without going back to the spatial domain. This will not only reduce the complexity and thus the cost of the transform coding system but also save the computation time.

3.7 NOTE ON PUBLICATIONS

The work described in Section 3.4 has appeared in a paper entitled "Lowpass filtering in the cosine transform domain". It was presented in the 1980 International Communication Conference held in Seattle, Washington, USA and published in the conference proceedings. A second paper based on the work described in Section 3.5 and entitled "Filtering and subsampling using transform coding techniques" has been accepted for presentation in the International Conference on Electronic Image Processing to be held in University of York, England on

26-28 July, 1982 and will be published in the conference proceedings. The above two papers are in co-authorship with Mr R J Clarke.

Also, a U.K. patent application (No. 8122640) entitled "Method of transmitting an image and apparatus for carrying out the method", in co-authorship with Dr R C Nicol, Mr B A Fenn and Mr R J Clarke, has been made to claim originality of invention on techniques developed in Section 3.5.

CHAPTER IV - DATA COMPRESSION

4.1 INTRODUCTION

Any source signal, analogue or digital, contains redundancy, which increases the channel requirement for transmission in its original form. Therefore, it is advantageous if some form of bandwidth reduction or data compression technique is employed to reduce the redundancy and hence improve coding efficiency.

Numerous techniques have been advanced by various researchers in search of the above goal. Of these, DPCM(10,102) and transform coding(23) are prominent in the field of digital image processing. Even though DPCM is easier and cheaper to implement, the data compression ratio achievable is lower than that of transform coding. Furthermore, with the rapid advancement of semiconductor electronics, coupled with the decrease in price brought about by the mass production of silicon chips employing very large scale integration (VSI), the cost of an image transform coding system is falling rapidly indeed.

Orthogonal transformation maps the highly correlated spatial data into a set of weakly correlated transform coefficients, thus minimising the statistical redundancy and improving coding efficiency. Each transform coefficient is a weighted sum of spatial elements and therefore its statistical variation due to scene changes is less than that of the original image. Further, since each successive group of coefficients is independently processed, error propagation is restricted to that transform block.

The efficiency of transform coding can be greatly improved if the coding algorithm is adapted to the local statistics of the picture block being coded, since the local statistics may be highly non-stationary. Two types of adaptation are possible, namely, one in which the adaptation is based upon previously transmitted data, and the other in which future data is used to compute the changes in parameters. In the latter case, there is some 'overhead' due to the transmission of the adaptation information.

4.2 ADAPTIVE TRANSFORM CODING - A REVIEW

The simplest form of adaptive transform coding is perhaps threshold coding(51) of the transform coefficients. In this scheme, a threshold is determined based on some criterion, and only those coefficients whose amplitudes are larger than the threshold are selected, quantized and transmitted, whilst those below it set to zero. The addressing information and the locations of the transmitted coefficients are sent as overhead information. The adaptivity of the system derives from the fact that the image changes from one block to the next, and thus the number of coefficients larger than the threshold varies from block to block. Dillard(103) used threshold coding for a 4 x 4 Hadamard transform in which the DC coefficient and the largest AC coefficients are sent along with their addressing information. The same technique was used by Anderson and Huang(104) for a 16 x 16 DFT in which the threshold level was selected according to the standard deviation of the block. Good results at a rate of 1.25 bits per pel were reported.

Another adaptive system developed by Huang and Schultheiss(105) is that of a zonal coding, in which a set of zones is established in each transform block. The zones may be derived from an optimum block quantization algorithm where the number of quantization levels for each transform coefficient is set proportional to its expected variance, such that the quantization error for each transform coefficient is the same. Therefore, the number of bits b_k used to code coefficient a_k should be proportional to $\log_2 \sigma_k$, where σ_k is the standard deviation of a_k. Wintz and Kurtenbach(106) developed the following rule which was successfully used by Habibi and Wintz(107), for image coding with several linear transformations. The bit assignment for a block of N coefficients is given by

$$b_k = \mathrm{INT}\left[\frac{M}{N} + 2 \log_2 \sigma_k^2 - \frac{2}{N} \sum_{i=1}^{N} \log_2 \sigma_i^2\right] \tag{4.1}$$

where $$M = \sum_{i=1}^{N} b_i \tag{4.2}$$

A lower mean squared error for a given channel rate can be achieved by employing Huffman, rather than constant word length coding, at the expense of system complexity.

Another approach to adaptation is to measure the activity of the transform block and sort them into a number of classes, and then adaptively quantize and select the coefficients to be transmitted. Claire(108) and Gimlett(109) have proposed a definition of 'activity index' using a weighted sum of the absolute values of the transform coefficients, and assign more bits for coding to those transform blocks with a higher activity index. Netravali et al[110] eliminated the adaptation overhead information by first selecting coefficients for transmission (zonal sampling) and then choosing a certain order for coefficient transmission. Quantization scales and the threshold for adaptation were obtained by subjective measurements to optimise the picture quality. They demonstrated this technique on a 2 x 2 x 2 Hadamard transform, in which quantization of the first coefficient was made coarse if the weighted sum of the magnitudes of all the other coefficients was above a certain threshold. Chen and Smith[111] computed the AC energy of the coefficients in each block and then assigned it to one of four classes, each with equal numbers of transform blocks. Adaptivity results from the assignment of more bits to higher energy blocks. In another classification technique, Tasto and Wintz[112] studied an adaptive transform coding system in which image blocks are classified into three categories according to the luminance activity.

In a different approach, Tescher et al[113-115] estimated the variances of the coefficients of the DFT in the transform domain and used the estimated variances for adaptive bit assignment. The variance of the amplitude of individual coefficients is estimated using a predictor that combines the variances of a number of adjacent quantized elements to predict the variance of a given coefficient. This system requires knowledge of the variances of at least some initial values to start the process. Bits are allocated in proportion to the logarithm of the estimated coefficient variance, with the phase component having twice the number of quantization levels of the amplitude component. The algorithm has also been extended to the Hadamard transform.

In another approach, Tescher and Cox (116) use a diagonal scanning pattern to convert the two-dimensional data into a one-dimensional format in the transform domain, in an effort to smooth the decay of the variances of the transform coefficients. Estimation of the variance of the one-dimensional data sequence and bit assignment in proportion to its logarithm are then carried out. The estimate of the variance for the ith transform coefficient $\hat{\sigma}_i^2$ is

$$\sigma_i^2 = A_1 \hat{\sigma}_{i-1}^2 + (1 - A_1) \hat{x}_{i-1}^2 \tag{4.3}$$

where $\hat{x}_{i-1}$ is the quantized form of the (i-1)th transformed coefficient (in the one-dimensional sequence) and A_1 is a weighting factor which is chosen to be 0.75. Good results have been reported using cosine and slant transforms for monochrome images.

Wong and Steele (117,118) developed the idea of variance estimation further by employing a simple linear relationship

$$\ell n\left[\hat{E}(m,n)\right] = C_1 \ell n\left[Q(m,n)\right] + C_2 \tag{4.4}$$

where $\hat{E}(m,n)$ is the estimated variance; $Q(m,n)$ is a distance factor and C_1 and C_2 represent the slope and intercept of the log-log relationship respectively. Bit assignment is then carried out proportional to the logarithm of the estimated variance. Furthermore, transform coefficients are selected adaptively such that only those with an estimated energy $E'(m,n)$ greater than a predetermined threshold are transmitted. $E'(m,n)$ is computed from the average energy of three local coefficients, $\hat{a}(.)$, given by

$$E'(m,n) = \frac{1}{3}\left[\hat{a}^2(m,n-1) + \hat{a}^2(m-1,n) + \hat{a}^2(m-1,n-1)\right] \qquad (4.5)$$

Good results of an average of 0.55 bit per pel have been achieved with acceptable picture quality.

In other block classification techniques, Ohira et al (119,120) used three kinds of bit assignment, the optimum one being adaptively selected according to the detail in the input signal, and Mauersberger (121) considered the use of a two-dimensional variable which relates to the mean squared difference between adjacent pels.

The adaptive schemes described so far all have adaptation parameters dependent upon local image statistics. Very little effort has been made, however, to adapt parameters according to psychovisual criteria, mainly because these criteria are not well understood, especially in the transform domain. The modelling of the human visual system (HVS) has been described in Section 1.2.4.3. However, the incorporation of the HVS model into the design of a transform coding system has not been satisfactorily achieved.

The basic structure of a subjective image data compression scheme is illustrated in Figure 4.1. The original image is transformed with a visual model; a coding algorithm is applied to the transformed data and then after transmission, a decoding algorithm is applied and the image inverted from the perceptual domain back into the intensity domain.

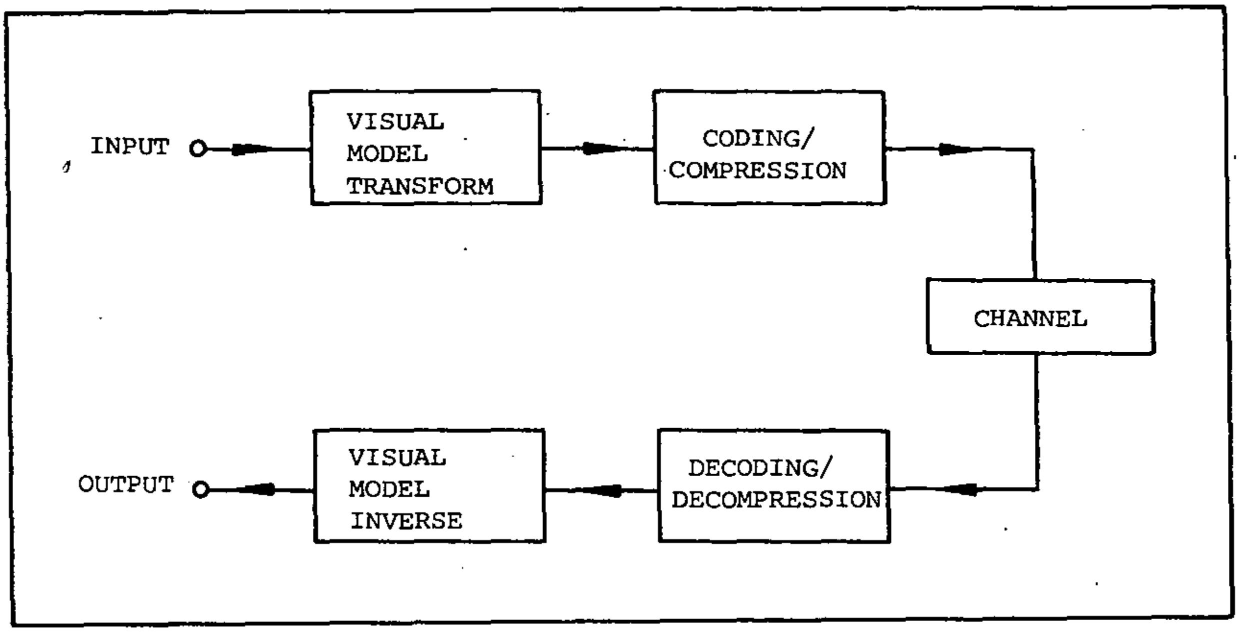

Figure 4.1 Block diagram of a subjective image data compression system

Subjective image coding results are quite good down to an average rate of 1.0 bit per pel and are acceptable, depending upon coding schemes and applications, down to 0.1 bit per pel. The simplest subjective image coder is a logarithmic transformation of the pel amplitude to 6.0 bits per pel (from an original of 8.0 bits per pel) without any noticeable loss of picture quality. By using a model which includes the spatial and chromatic response characteristics of the retina, much better results can be achieved. Hall(122) has demonstrated that an achromatic visual model can improve the compression of still pictures by a factor of almost 10 when used in conjunction with Fourier transform coding systems. The same techniques were extended to code colour signals with good results at 1.0 bit per pel, and acceptable quality even down to 0.25 bit per pel.

A practical problem in adaptive transform coding systems is the resulting variable data rate. Since the communication channel operates at a fixed rate, the source coder rate fluctuation must be absorbed. This can be achieved by the use of a rate-equalizing buffer between the source coder and the channel$^{(123,124)}$. One possible arrangement of a variable-rate transform coding system is shown in Figure 4.2$^{(124)}$. The rate at which the buffer is filled is controlled by parameters derived from image statistics. An identical buffer and controller are employed at the receiver to ensure synchronisation of the system.

4.3 ADAPTIVE TRANSFORM CODING OF VIDEO SIGNALS

From the review in Section 4.2, it can be established that an efficient adaptive transform coding system will satisfy the following criteria:

1) it achieves a high data compression ratio
2) it does not require excessive overhead information
3) it produces pictures of good subjective quality

The criteria above may be self-contradictory since the adaptivity of the system (and hence the compression ratio), in general, increases in proportion to the overhead information. However, a compromise is sought such that a good compression ratio is achieved while keeping the overhead information as low as possible but still with acceptable subjective quality.

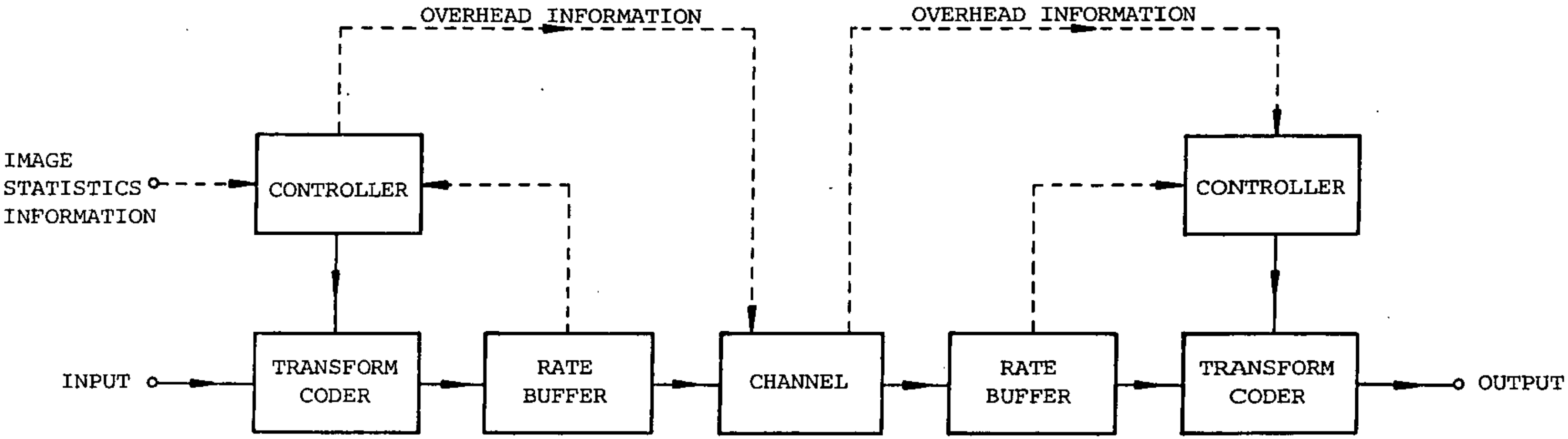

Figure 4.2 Variable-rate transform coding system (after ref. 124)

The objective of the work described in this section is to find a system which satisfies the above-mentioned criteria. Several different techniques were investigated in an effort to compare the merits of each in consideration of the three criteria above. Source images were taken from the output of the DCT image reduction system described in Section 3.5. Three source images, each consisting of 128 lines with 128 pels per line*, encoded with 8-bit PCM were selected to provide a wide range of source statistics for the adaptive algorithms.

In its simplest form, an adaptive transform coding system may be as represented in Figure 4.3. The original image is divided into smaller subpictures and transformed into a set of transform coefficients. Bits are adaptively assigned to each of these coefficients according to some criterion. The coefficients are then adaptively quantized and coded for transmission, and at the receiver, decoded and inverse transformed to reconstruct the picture elements.

4.3.1 Transformation

A detailed account of the process of image transformation is given in Section 1.2.3 and therefore will not be repeated here.

4.3.2 Quantization

Quantization is the process of mapping a set of discrete input levels {x} into a set of discrete output levels {y} according to a chosen quantizer characteristic. It takes place by assigning the value r_i to y_i if x_i lies between d_i and d_{i+1} where {d} and {r} are

---

* This represents a reduced picture with ARF of $(\frac{1}{2})^2$ from an original picture of 256 x 256 pels.

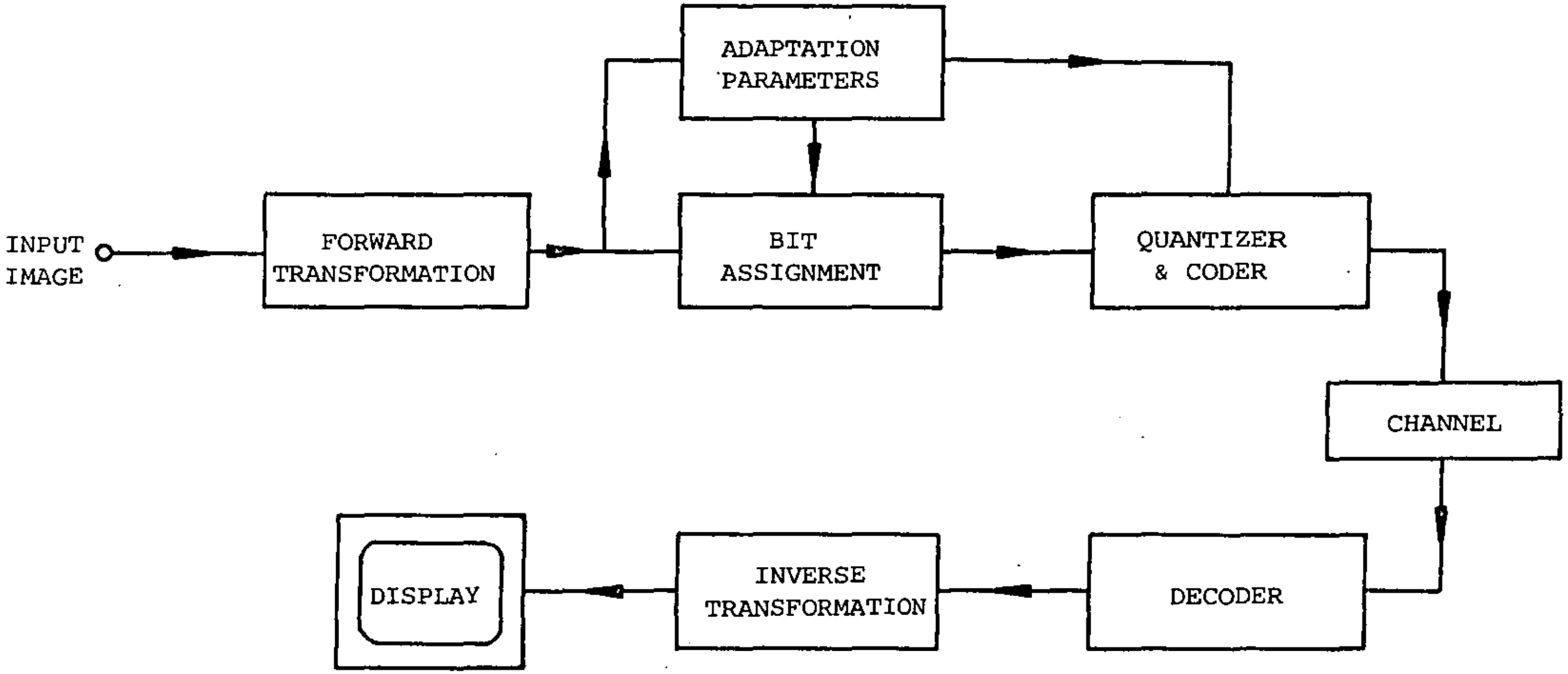

Figure 4.3 Adaptive transform coding system

decision and reconstruction levels respectively. The quantizer design problem is to determine the optimum decision and reconstruction levels, given the probability density function p(x) and an optimization criterion. Since the quantization process is irreversible, the quantizer introduces distortion, which any good quantizer design must attempt to minimise. There are several quantizer designs available (which will be discussed below) that offer various tradeoffs between simplicity and performance.

4.3.2.1 The Max quantizer[(126)]

The optimization criterion of the Max quantizer is to minimise the mean squared quantization error for a fixed number of quantization levels. This error is defined as

$$\varepsilon^2 = \sum_{i=1}^{L} \int_{d_i}^{d_{i+1}} (x-y_i)^2 \, p(x)\,dx \qquad (4.6)$$

The decision and reconstruction levels, d_i and r_i respectively, are given by

$$d_i = \frac{r_i + r_{i-1}}{2} \qquad (4.7)$$

and

$$r_i = \frac{\int_{d_i}^{d_{i+1}} x\, p(x)\,dx}{\int_{d_i}^{d_{i+1}} p(x)\,dx} \qquad (4.8)$$

The procedure for computation of d_i and r_i is as follows: starting with an initial value r_1, successive values of d_i and r_i are calculated by recursive use of Equations (4.7) and (4.8). If for a fixed number of quantization levels L, r_L is the centroid of the curve between d_L and d_∞, then the initial choice r_1 is correct, otherwise the whole process is repeated with a new value of r_1.

The probability density function (pdf) of the transform coefficients has been modelled as a Rayleigh density for the DC coefficients and a Gaussian or Laplacian density for the remainder. Ghanbari and Pearson(33) found that the Hadamard AC coefficients approximate to a Gamma pdf. However, from a study of the histograms of the DCT coefficients of the 'GIRL' image as shown in Figures 4.4(i) to (viii), it can be seen that the pdf of the AC coefficients approximates more to a Laplacian than a Gaussian distribution. Optimum quantization can thus be computed and tabulated as shown in Table 4.1 for the Laplacian density distribution (L = 2 to L = 128).

By minimising ε in Equation (4.6) by the method of Lagrange multipliers, the decision levels can be computed to a good approximation from the integral equation(127)

$$d_i = (a_L - a_0)\frac{\int_{a_0}^{a_i} p(x)^{-\frac{1}{3}}\,dx}{\int_{a_0}^{a_L} p(x)^{-\frac{1}{3}}\,dx} + a_0 \qquad (4.9)$$

where

$$a_i = \frac{i(a_L - a_0)}{L} + a_0 \qquad (4.10)$$

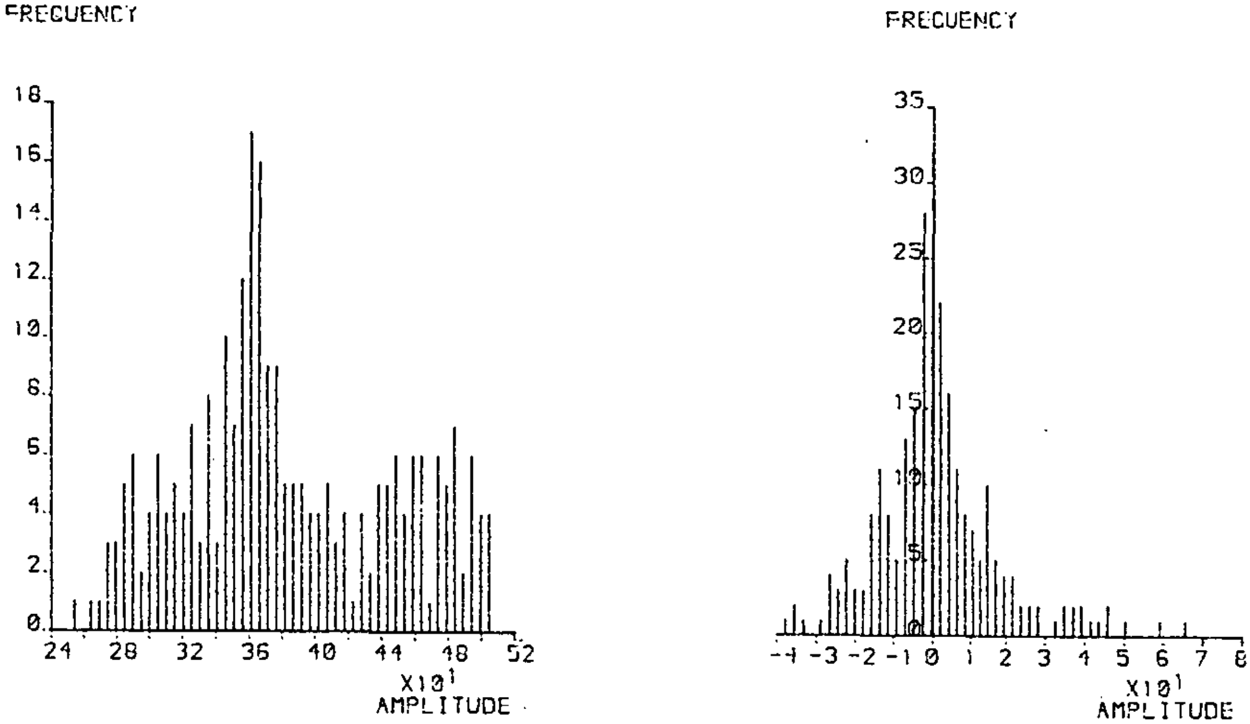

(i) F(0,0)

(ii) F(0,1)

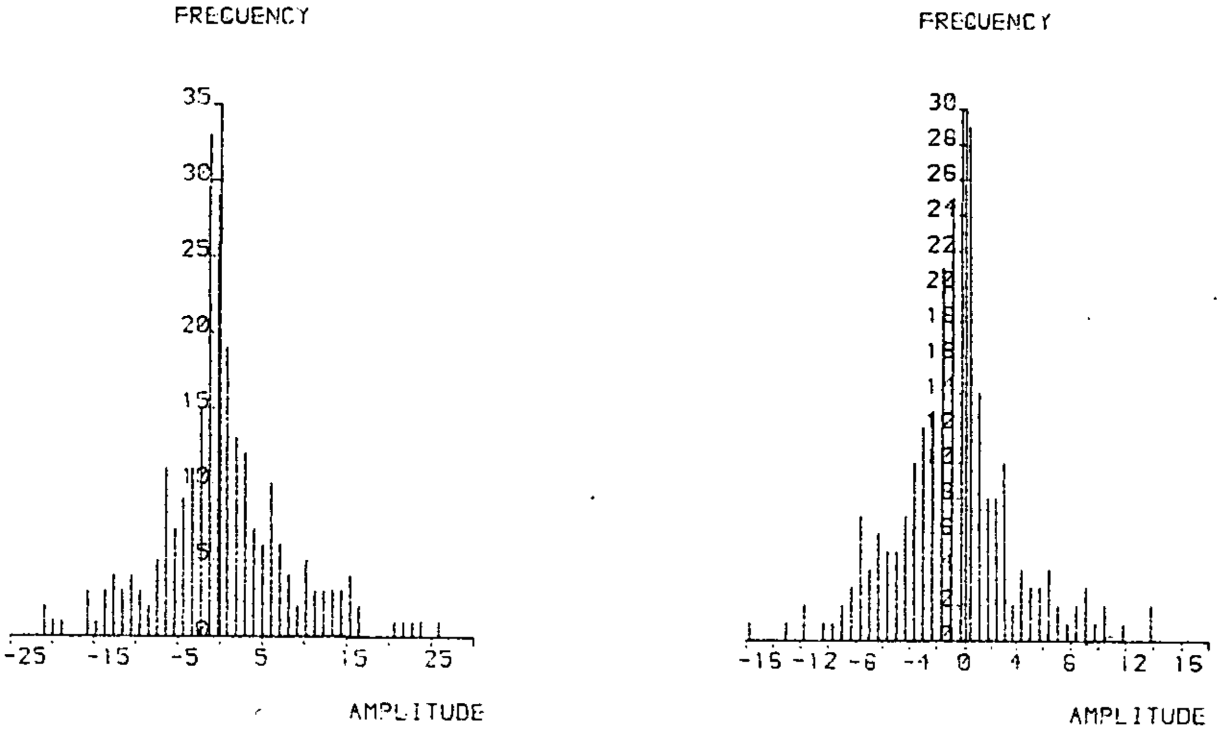

(iii) F(0,2)

(iv) F(0,3)

Figure 4.4 Histograms of the DCT coefficients of the 'GIRL' picture

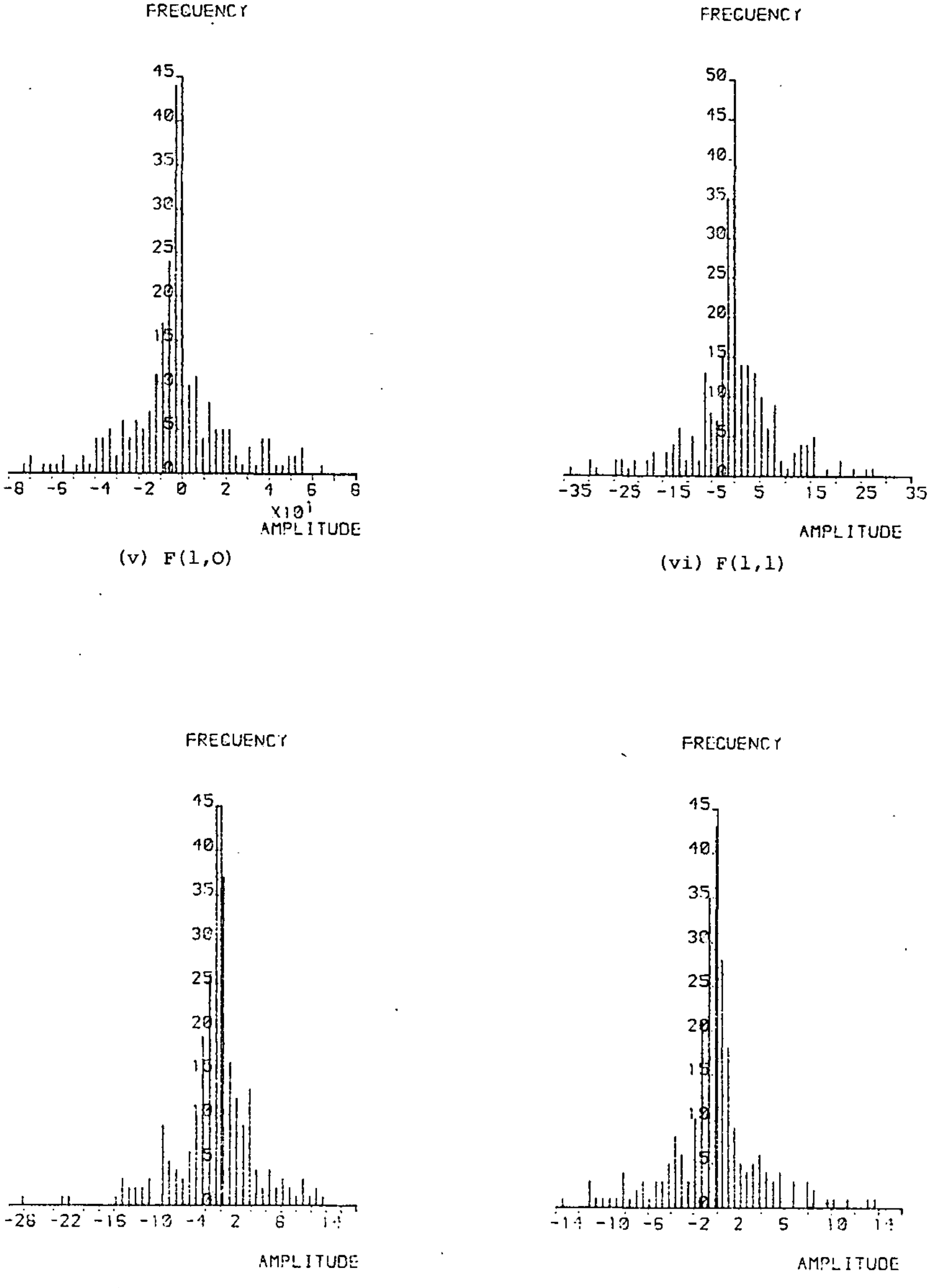

(v) F(1,0)

(vi) F(1,1)

(vii) F(1,2)

(viii) F(1,3)

Figure 4.4 Histograms of the DCT coefficients of the 'GIRL' picture

Table 4.1 Placement of decision and reconstruction levels of Laplacian quantizers

Bits	X_i	Y_i
1	0.00000	0.70711
2	0.00000	0.41976
	1.12686	1.83397
3	0.00000	0.23340
	0.53318	0.83296
	1.25274	1.67251
	2.37965	3.08680
4	0.00000	0.12399
	0.26442	0.40484
	0.56675	0.72866
	0.91984	1.11102
	1.34443	1.57784
	1.87764	2.17743
	2.59722	3.01701
	3.72421	4.43142
5	0.00000	0.06404
	0.13220	0.20035
	0.27320	0.34605
	0.42428	0.50251
	0.58697	0.67144
	0.76322	0.85500
	0.95548	1.05596
	1.16697	1.27798
	1.40199	1.52601
	1.66648	1.80695
	1.96891	2.13088
	2.32214	2.51340
	2.74694	2.98048
	3.28050	3.58051
	4.00074	4.42098
	5.12949	5.83800
6	0.00000	0.03258
	0.06619	0.09979
	0.13449	0.16919
	0.20507	0.24094
	0.27806	0.31519
	0.35366	0.39213
	0.43206	0.47199
	0.51348	0.55498
	0.59816	0.64135
	0.68637	0.73139
	0.77841	0.82542
	0.87462	0.92381
	0.97541	1.02701
	1.08125	1.13550
	1.19267	1.24984
	1.31026	1.37069
	1.43478	1.49887
	1.56709	1.63530
	1.70820	1.78110
	1.85938	1.93766
	2.02216	2.10667
	2.19851	2.29034
	2.39090	2.49146
	2.60256	2.71366
	2.83777	2.96188
	3.10245	3.24303
	3.40514	3.56725
	3.75870	3.95015
	4.18397	4.41780
	4.71828	5.01876
	5.43991	5.86106
	6.57225	7.28344
7	0.00000	0.01639
	0.03304	0.04969
	0.06660	0.08351
	0.10070	0.11788
	0.13535	0.15282
	0.17059	0.18836
	0.20643	0.22451
	0.24290	0.26128
	0.28000	0.29872
	0.31778	0.33684
	0.35625	0.37567
	0.39545	0.41524
	0.43540	0.45556
	0.47611	0.49666
	0.51762	0.53858
	0.55996	0.58133
	0.60315	0.62498
	0.64726	0.66954
	0.69231	0.71508
	0.73836	0.76164
	0.78543	0.80923
	0.83357	0.85792
	0.88282	0.90772
	0.93323	0.95873
	0.98486	1.01099
	1.03778	1.06458
	1.09208	1.11957
	1.14780	1.17603
	1.20502	1.23402
	1.26384	1.29366
	1.32434	1.35502
	1.38661	1.41821
	1.45077	1.48334
	1.51694	1.55054
	1.58524	1.61995
	1.65582	1.69170
	1.72884	1.76598
	1.80447	1.84296
	1.88290	1.92284
	1.96435	2.00587
	2.04907	2.09227
	2.13731	2.18235
	2.22938	2.27641
	2.32563	2.37485
	2.42646	2.47808
	2.53234	2.58659
	2.64376	2.70094
	2.76138	2.82182
	2.88592	2.95002
	3.01824	3.08647
	3.15938	3.23230
	3.31059	3.38888
	3.47341	3.55794
	3.64979	3.74164
	3.84220	3.94276
	4.05388	4.16499
	4.28913	4.41326
	4.55388	4.69449
	4.85665	5.01881
	5.21034	5.40187
	5.63580	5.86973
	6.17040	6.47107
	6.89260	7.31412
	8.02641	8.73870

F4·55

S2

32entry Chroma.

3stage MSMSVQ 1Adap

1 Adap

Y ~ 1·25 b/p

U,V ~ 0·81/16 b/p

for i = 0,1,.....,L and $a_0 - a_L$ is the input amplitude range. The reconstruction levels are then given by

$$r_i = \frac{d_{i+1} + d_i}{2} \qquad (4.11)$$

However if the number of quantization levels is not large, the approximation of Equation (4.9) becomes inaccurate, and exact solutions given by Equations (4.7) and (4.8) must be used.

4.3.2.2 The compander

It is also possible to perform non-linear quantization with a compander (compressor-expander) where a uniform quantizer is preceded and succeeded by non-linear transformations as shown in Figure 4.5(128,129). The input signal x is first passed through a non-linear memoryless transformation f(.) to yield $\hat{x}$. $\hat{x}$ is uniformly quantized to give $\hat{y}$, which is non-linearly transformed by g(.) to yield the output y. The overall transformation from x to y is that of a non-linear quantizer. The functions f(.) and g(.) are determined so that the overall system approximates the Max quantizer. Table 4.2(51) contains the functions f(.) and g(.) for the Gaussian, Rayleigh and Laplacian probability density functions.

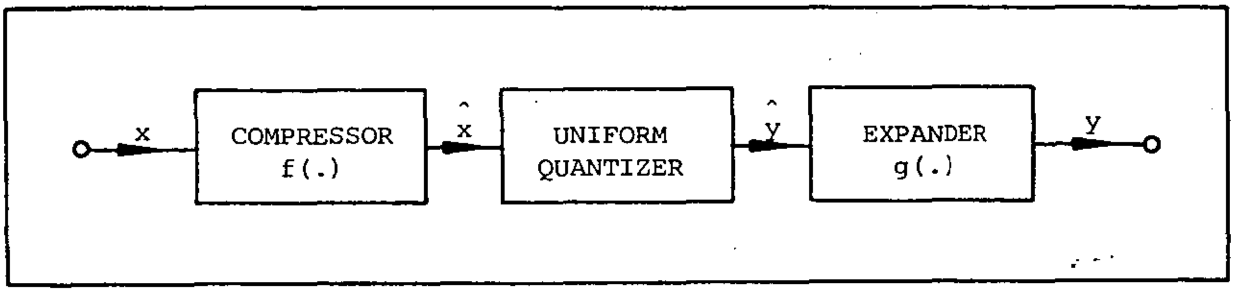

Figure 4.5 The compander

Table 4.2 Companding quantization transformation (after ref. 51)

	Probability Density	Forward Transformation	Inverse Transformation
Gaussian	$p(f) = (2\pi\sigma^2)^{-1/2} \exp - \left\{\frac{f^2}{2\sigma^2}\right\}$	$g = \frac{1}{2} \operatorname{erf}\left\{\frac{f}{\sqrt{2}\sigma}\right\}$	$\hat{f} = \sqrt{2}\sigma \operatorname{erf}^{-1}\{2\hat{g}\}$
Rayleigh	$p(f) = \frac{f}{\sigma^2} \exp\left\{-\frac{f^2}{2\sigma^2}\right\}$	$g = \frac{1}{2} - \exp\left\{-\frac{f^2}{2\sigma^2}\right\}$	$\hat{f} = [\sqrt{2}\sigma^2 \ln\{1/(\frac{1}{2} - \hat{g})\}]^{1/2}$
Laplacian	$p(f) = \frac{\alpha}{2} \exp\{-\alpha \lvert f \rvert\}$	$g = \frac{1}{2}[1 - \exp\{-\alpha f\}] \quad f \geq 0$	$\hat{f} = -\frac{1}{\alpha} \ln[1 - 2\hat{g}] \quad \hat{g} \geq 0$
	$\alpha = \frac{\sqrt{2}}{\sigma}$	$g = -\frac{1}{2}[1 - \exp\{\alpha f\}] \quad f < 0$	$\hat{f} = \frac{1}{\alpha} \ln[1 + 2\hat{g}] \quad \hat{g} < 0$

4.3.3 Bit assignment

Rate distortion theory$^{(1-3)}$ states that the minimum distortion free transmission rate is bounded by the source entropy. It also states that for a given distortion D, the minimum transmission rate is given by the rate distortion function, R(D). Hence, a communication channel with capacity equal to or greater than R(D) is required to transmit the information with distortion less than or equal to D. For a source with Gaussian pdf and mean squared distortion measure, it has been shown$^{(1-3)}$ that

$$R(D) = \begin{cases} \frac{1}{2} \log_2 \frac{\sigma^2}{D}, & 0 \leq D \leq \sigma^2 \\ 0, & D > \sigma^2 \end{cases} \tag{4.12}$$

where σ^2 is the coefficient variance. The variance can either be calculated in the transform domain or from a knowledge of the power spectral density, or equivalently, the autocorrelation function, of the image.

The rate R(D) is the number of bits per pel needed for transmission. Therefore, the number of quantization levels L is given by

$$L = 2^{R(D)} \qquad (4.13)$$

The optimum placement of levels within the coefficient amplitude range to provide minimum distortion D is given by the Max quantizer described in Section 4.3.2.1. Even though Equation (4.12) above is only applicable to Gaussian data, it does provide an upper bound on achievable performance for any non-Gaussian source.

Another approach to bit assignment is to equalise the weighted quantization distortion from the individual transform coefficients(130). The weighted quantization distortion $\hat{\varepsilon}^2_{i,j}(k)$ is given by

$$\hat{\varepsilon}^2_{i,j}(k) = \varepsilon^2(k) . \sigma_{i,j}^{2} \; ; \quad k = \text{bit number} \qquad (4.14)$$

where $\sigma_{i,j}^{2}$ is the coefficient variance at (i,j)th location and $\varepsilon^2(k)$ is the mean squared quantization distortion given by Equation (4.6).

In this approach, the total number of bits in a block, M_b, is distributed among the coefficients such that the resulting weighted quantization distortion from each coefficient is equal. The procedure is as follows:

(i) the weighted quantization distortions of the AC coefficients for different numbers of bits are determined. The bit counter N_c is set to zero.

(ii) one bit is assigned to the coefficient with the largest weighted quantization distortion. N_c is incremented by 1.

(iii) if $N_c \geqslant M_b$, the process is terminated; otherwise it returns to step (ii).

4.3.3.1 Bit assignment based on human visual system (HVS) response

The human visual system responds differently to the different spatial frequencies conveyed by the transform coefficients, and thus the quantization distortion for different coefficients will have varying visibility. In order that the quantization distortion should subjectively correspond to the criteria of the eye, the distortion is weighted with the transfer function of the eye given by(42)

$$H(w_{i,j}) = 2.6(0.0192 + 0.114\, w_{i,j}) \exp\left[-(-0.114 w_{i,j})^{1.1}\right] \qquad (4.15)$$

where $w_{i,j}$ is the normalized spatial frequency in cycles per degree. The normalizing factor is 22.5 cycles per degree since the highest resolvable spatial frequency for system I television pictures when viewed at a distance of six times the picture weight is 45 samples per degree(43). Hence the weighted mean squared quantization distortion based on HVS becomes(130)

$$\overline{\varepsilon}^2_{i,j}(k) = \varepsilon^2(k) \;.\; H(w_{i,j}) \;.\; \sigma^2_{i,j} \;; \quad k = \text{bit number} \qquad (4.16)$$

Tables of values of $\overline{\varepsilon}^2_{i,j}(k)$ for different bit numbers k can then be computed. The bit assignment map is derived by sequential search through the tables as described in Section 4.3.3. A typical bit

7	6	4	4	3	3	3	3	2	2	2	1	1	1	0	0
6	4	4	4	3	3	3	2	2	2	1	1	1	0	0	0
5	4	4	3	3	3	2	2	2	2	1	1	1	0	0	0
4	4	3	3	3	2	2	2	2	1	1	1	0	0	0	0
4	3	3	3	2	2	2	2	1	1	1	1	0	0	0	0
3	3	3	2	2	2	2	1	1	1	1	0	0	0	0	0
3	2	2	2	2	2	1	1	1	1	0	0	0	0	0	0
2	2	2	2	2	1	1	1	1	0	0	0	0	0	0	0
2	2	2	1	1	1	1	1	0	0	0	0	0	0	0	0
2	2	1	1	1	1	1	0	0	0	0	0	0	0	0	0
2	1	1	1	1	1	0	0	0	0	0	0	0	0	0	0
1	1	1	1	1	0	0	0	0	0	0	0	0	0	0	0
1	1	1	1	0	0	0	0	0	0	0	0	0	0	0	0
1	1	1	0	0	0	0	0	0	0	0	0	0	0	0	0
1	0	0	0	0	0	0	0	0	0	0	0	0	0	0	0
0	0	0	0	0	0	0	0	0	0	0	0	0	0	0	0

Figure 4.6 Bit assignment map

assignment map derived by the above technique with an average bit rate of 1.0 bit per pel for a block size of 16 x 16 DCT coefficients is shown in Figure 4.6.

4.4 EXPERIMENTAL PROCEDURE

Experiments were carried out by computer simulation on three video images with different statistics namely the 'GIRL', 'FLAT' and 'SCENE' images which are shown in Figures 4.12, 4.13 and 4.14 respectively. Each image consists of 128 lines with 128 pels per line, encoded with 8 bits i.e. a dynamic range of 256 intensity levels. To reduce the computer memory requirement, each image is divided into subpictures of 16 x 16 pels. Five adaptive schemes were investigated, adaptation being based on different parameters of the source data. In designing the schemes, consideration is given to the amount of overhead information required to implement the schemes and in cases where excessive overhead information is required, interpolation or estimation techniques were used to overcome the problem.

The evaluation of the processed picture quality is the measurement of its normalised mean square error (NMSE) expressed as a percentage and defined as

$$\mathrm{NMSE} = \frac{\sum_{j=0}^{N-1} \sum_{k=0}^{N-1} \left[f(j,k) - \hat{f}(j,k)\right]^2}{\sum_{j=0}^{N-1} \sum_{k=0}^{N-1} f(j,k)^2} \times 100\ \% \qquad (4.17)$$

where $f(.)$ and $\hat{f}(.)$ are original and processed pels respectively and $N = 128$.

Informal subjective tests were also carried out, in which viewers were asked to assess the quality of the processed pictures according to the five-grade quality scale (see Table 1.2-I) at a viewing distance of six times picture height.

All five adaptive schemes to be described can be represented by Figure 4.3, with different adaptive strategies employed in bit assignment and coefficient selection for transmission. The quantizer used is the optimum Max quantizer with Laplacian density distribution. The following sections describe each scheme in detail.

4.4.1 Scheme I

In this scheme, bits are assigned to the coefficients according to the logarithms of their variances as in Equation (4.12). The variance of the coefficients at the (a,b)th location is defined as

$$\sigma_{a,b}^2 = \frac{1}{PQ} \sum_{j=0}^{P-1} \sum_{k=0}^{Q-1} \left[F_{a,b}(j,k) - \eta_{a,b}\right]^2 \qquad (4.18)$$

where $F_{a,b}(.)$ is the amplitude of the coefficient at (a,b)th location and

$$\eta_{a,b} = \frac{1}{PQ} \sum_{j=0}^{P-1} \sum_{k=0}^{Q-1} F_{a,b}(j,k) \qquad (4.19)$$

where PQ is the total number of subpictures.

Before quantization, the coefficients are normalised by their respective standard deviations, $\sigma_{a,b}$, to yield coefficients with unity variance. Hence in order that the coefficients can be regenerated at the receiver, the variance map has to be transmitted. Also it is required to generate the identical bit allocation map at the receiver. Depending on the block size of the subpictures, this can prove to be excessively large.

It has been shown(116) that the logarithms of the variances of the transform coefficients are highly correlated with the coefficient numbers in the zig-zag scan path as shown in Figure 4.7. A plot of the variance against the coefficient number along the scan path is contained in Figure 4.8. Thus given a set of variance values, a linear regression technique can be employed to fit a straight line to the given points. This line can then be used to estimate the variances at the receiver.

Let x_i be the logarithm of the coefficient number along the diagonal scan path, y_i, be the logarithm of the variance and J the number of samples. It can be shown that (see Appendix III) the slope m, and the y-intercept c, of the linear equation

$$y_i = mx_i + c \tag{4.20}$$

are determined as follows:

$$m = \frac{\frac{1}{J}\sum_{i=1}^{J} x_i y_i - \overline{x}\,\overline{y}}{\sigma_x^{\,2}} \tag{4.21}$$

$$c = \overline{y} - m\overline{x} \tag{4.22}$$

where

$$\overline{x} = \frac{1}{J}\sum_{i=1}^{J} x_i \tag{4.23}$$

$$\overline{y} = \frac{1}{J}\sum_{i=1}^{J} y_i \tag{4.24}$$

$$\sigma_x^{\,2} = \frac{1}{J}\sum_{i=1}^{J} x_i^2 - (\overline{x})^2 \tag{4.25}$$

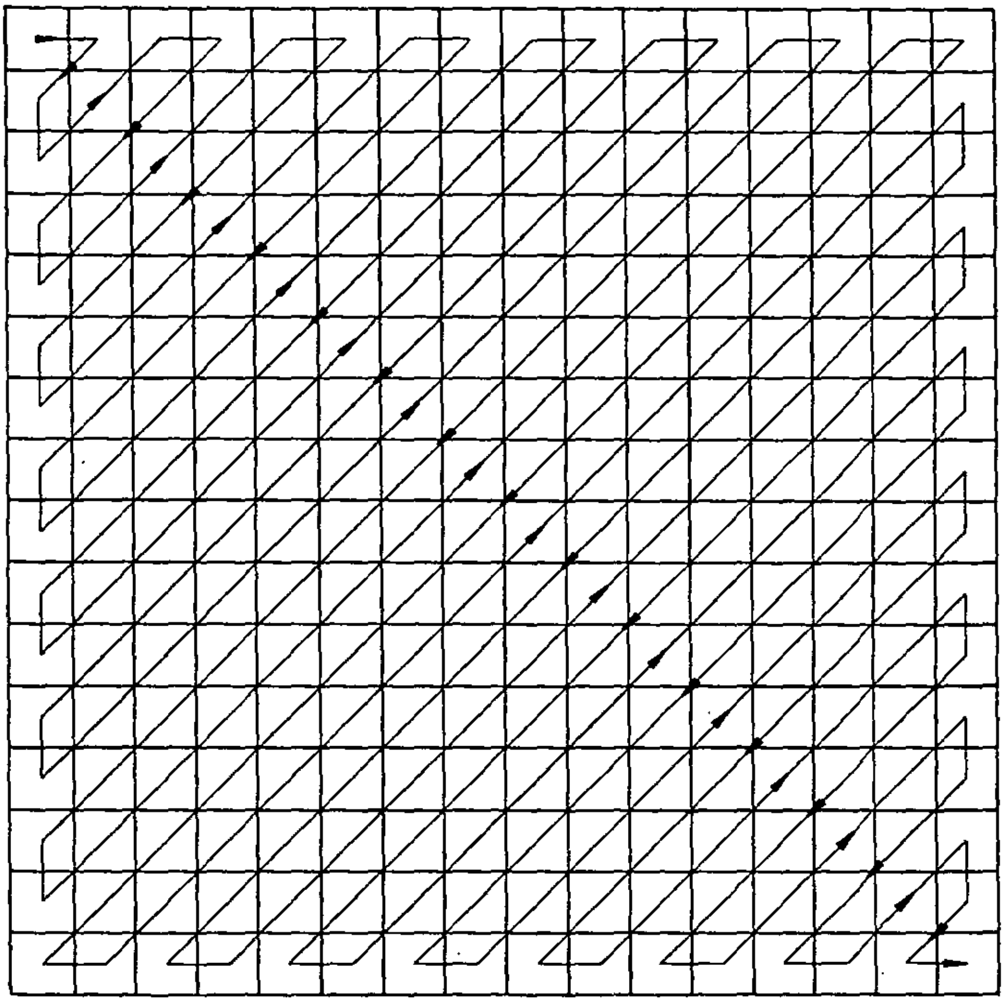

Figure 4.7 Scan path used in variance estimation

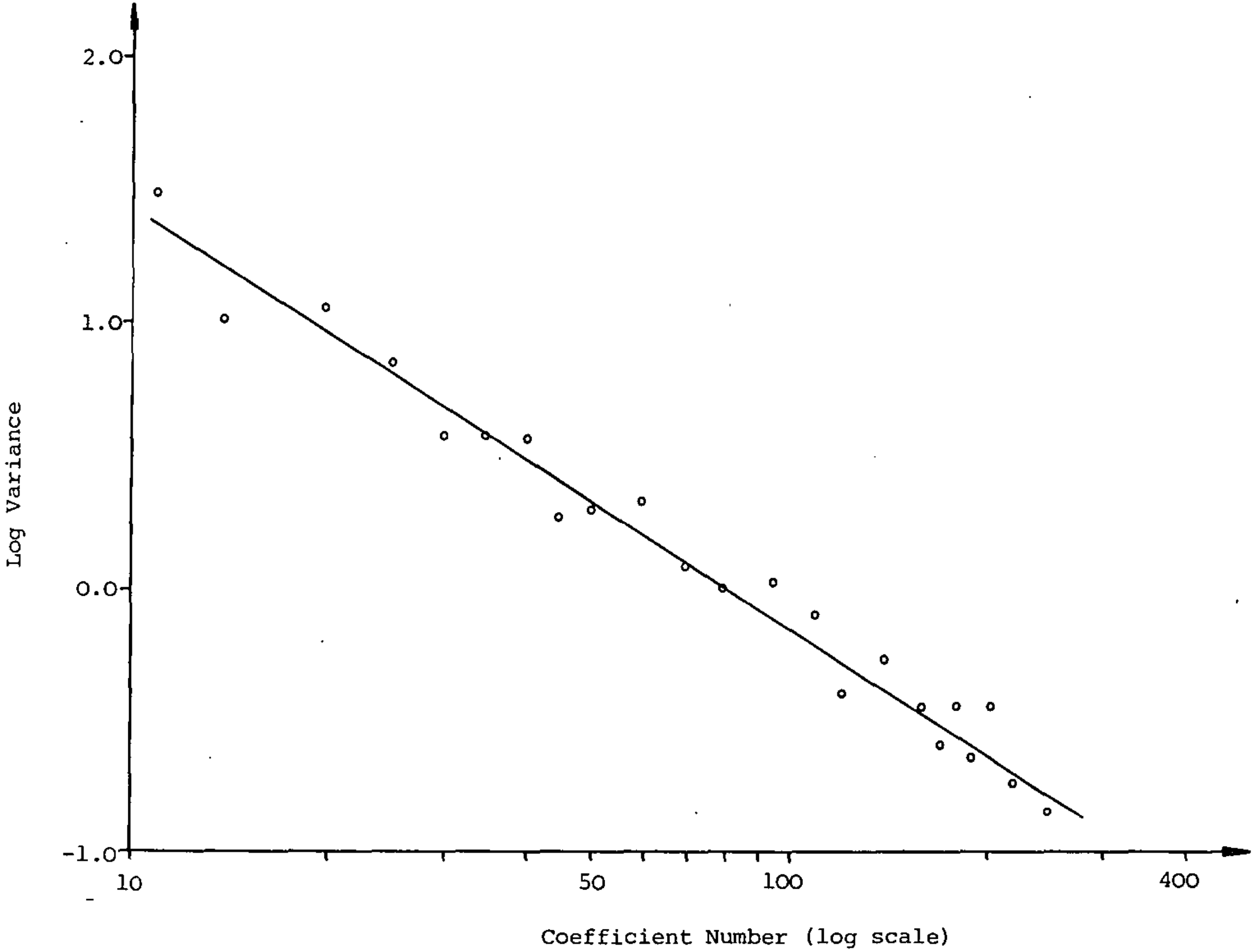

Figure 4.8 Plot of variance versus coefficient number

Also the correlation coefficient r between the actual and the estimated variances is given by

$$r = \frac{m\,\sigma_x}{\sigma_y} \qquad (4.26)$$

where

$$\sigma_y^2 = \frac{1}{J}\sum_{i=1}^{J} y_i^2 - (\overline{y})^2 \qquad (4.27)$$

Table 4.3 contains the correlation coefficients for the 'GIRL', 'FLAT', 'SCENE' images respectively, employing the DCT and the HT.

Having determined m and c, the estimated variance is then given by

$$\hat{\sigma}_i^2 = 10^{\hat{y}_i} \qquad (4.28)$$

where

$$\hat{y}_i = m x_i + c \qquad (4.29)$$

and the bit assignment according to Equation (4.12) (except that σ^2 is now replaced by $\hat{\sigma}_i^2$) is carried out to generate the bit allocation map.

Table 4.3 Correlations between the estimated and actual variances

PICTURE	TRANSFORM	CORRELATION
GIRL	DCT	0.972
	HT	0.940
FLAT	DCT	0.903
	HT	0.888
SCENE	DCT	0.909
	HT	0.905

4.4.2 Scheme II

Unlike Scheme I, where each transform block is assigned the same bit allocation map, this scheme exploits the changes in local statistics within the transform block. To detect such changes, the activity within each block of M x M pels is measured and represented by the activity index (AI) which is defined as

$$AI_1 = \{\sum_{j=0}^{M-1} \sum_{k=0}^{M-1} F(j,k)^2\} - F(0,0)^2 \tag{4.30}$$

where F(.) is the amplitude of the transform coefficient and $M = 16$.

Even though the above expression gives an indication of the activity in the block, it is also a measure of the AC energy. An alternative criterion which measures the energy attributed to the changes in amplitude of adjacent pels in the spatial domain is given by

$$AI_2 = \frac{1}{4(M-1)^2} \sum_{j=1}^{M-1} \sum_{k=1}^{M-1} \Big[\{f(j,k) - f(j,k-1)\}^2 + \{f(j,k) - f(j,k+1)\}^2 + \{f(j,k) - f(j-1,k)\}^2 + \{f(j,k)-f(j+1,k)\}^2\Big] \tag{4.31}$$

Having computed the activity index of each transform block, it is then assigned to one of the four classes, such that each class contains the same number of blocks. Bit rates are allocated such that the blocks in the lowest activity class are coded with the lowest bit rate while those in the highest activity class are coded with the highest bit rate. The difference in bit rates between the classes which gives the best performance was found experimentally to be 0.2 bit per pel. However to reconstruct the lowest activity blocks in the image without any noticeable degradation, a minimum of 0.4 bit per pel is required.

The overhead information that has to be transmitted to the receiver so that the correct bit allocation map is used is the classification map for the image. This is shown in Figure 4.9 for the 'GIRL' image using the DCT. One method for alleviating the necessity of transmitting this is somehow to extract the classification map from the received coefficients in the receiver. If the first two AC coefficients are transmitted using a fixed number of bits (say 6), since these two coefficients contain most of the AC energy, their mean squared value will give an indication of the activity in the block. Thus the estimated AI is

$$\tilde{AI} = \frac{1}{2}\{\hat{F}(0,1)^2 + \hat{F}(1,0)^2\} \tag{4.32}$$

where $\hat{F}(.)$ is the received quantized version of $F(.)$. To decide the class for a particular block, the receiver only has to know the AI values that define the classes, thus effecting a saving of overhead information.

2	3	3	4	2	4	4	4
2	4	1	3	3	2	3	3
2	1	3	4	1	4	4	1
1	4	3	2	2	1	1	1
1	1	3	1	1	1	2	2
1	4	1	4	3	1	3	2
4	4	1	4	3	1	3	2
4	3	2	3	2	4	3	2

Figure 4.9 Classification map

Comparison was made between the two schemes, one with the classification map transmitted, and the other estimated at the receiver, as described above. Figure 4.10 shows the results on the 'GIRL' image using the DCT. It shows that the estimated activity index model performed unsatisfactorily. Hence it is apparent that the estimation of AI is not accurate enough in the present case and in order to attain a good performance, the classification map has to be transmitted with an increase in overhead information of only 0.008 bit per pel.

To determine the merits of the two measures of image activity as given by Equations (4.30) and (4.31), NMSE against bit rate curves for two adaptive schemes employing the two activity measures for classification purpose are plotted in Figure 4.11. From the results, it can be seen that AI_2 gives a better indication of the activity within the block than AI_1.

4.4.3 Scheme III

This is basically similar to Scheme II except that the bit allocation described in Section 4.3.3.1 is used. This scheme is complicated and therefore time consuming but it takes into account the human visual system in computing the quantization distortion.

4.4.4 Scheme IV

In the earlier schemes, the variances of the coefficients are estimated. The variance map is then used for all the blocks. In this

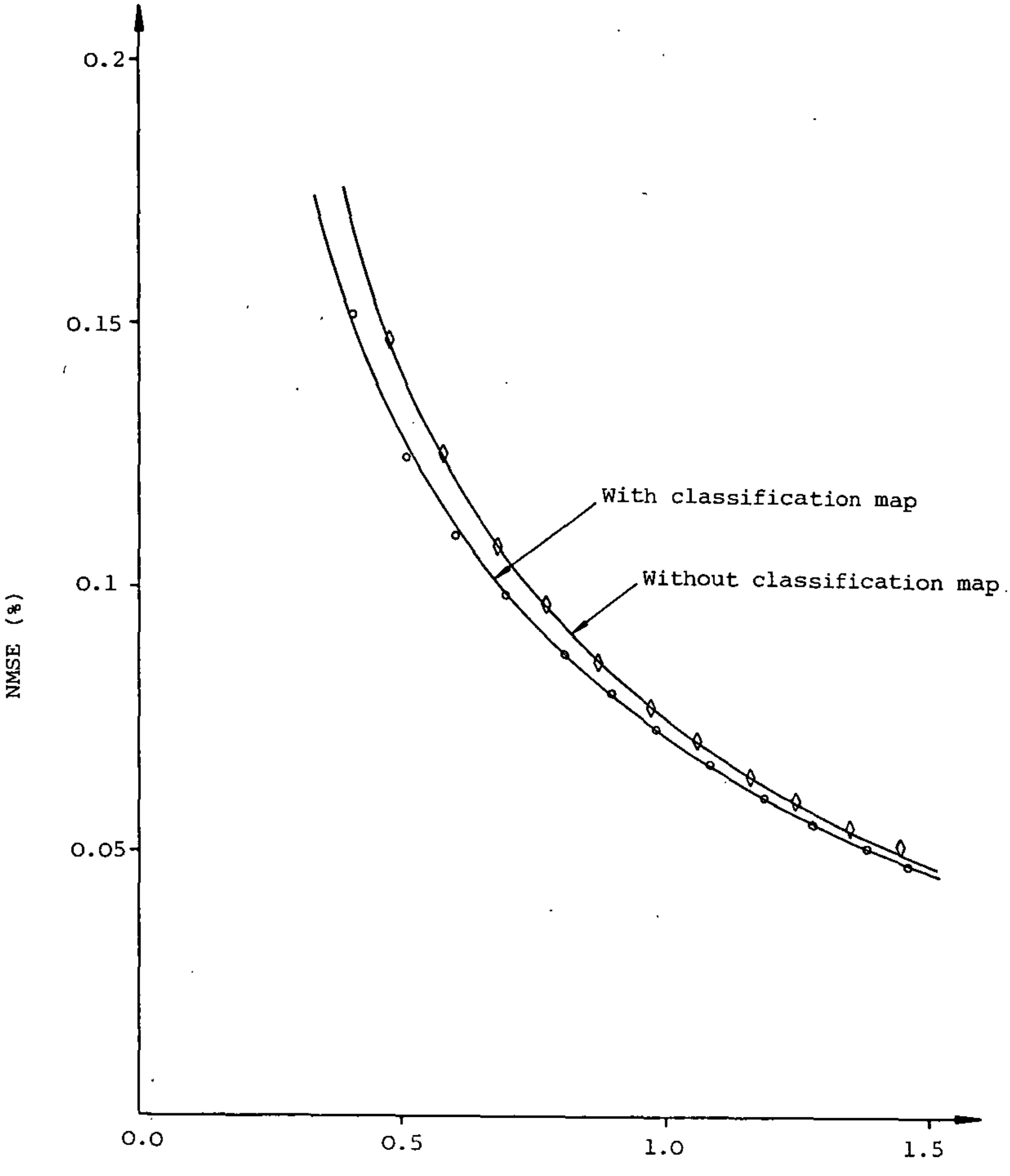
0.2
0.15
0.1
0.05
NMSE (%)
0.0
0.5
1.0
1.5
Bit Rate (bits/pel)
With classification map
Without classification map

Figure 4.10

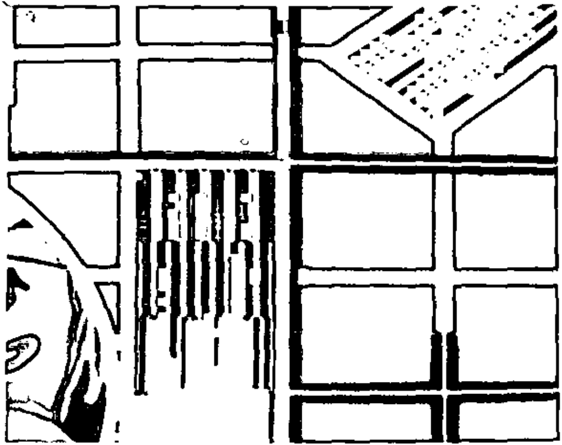

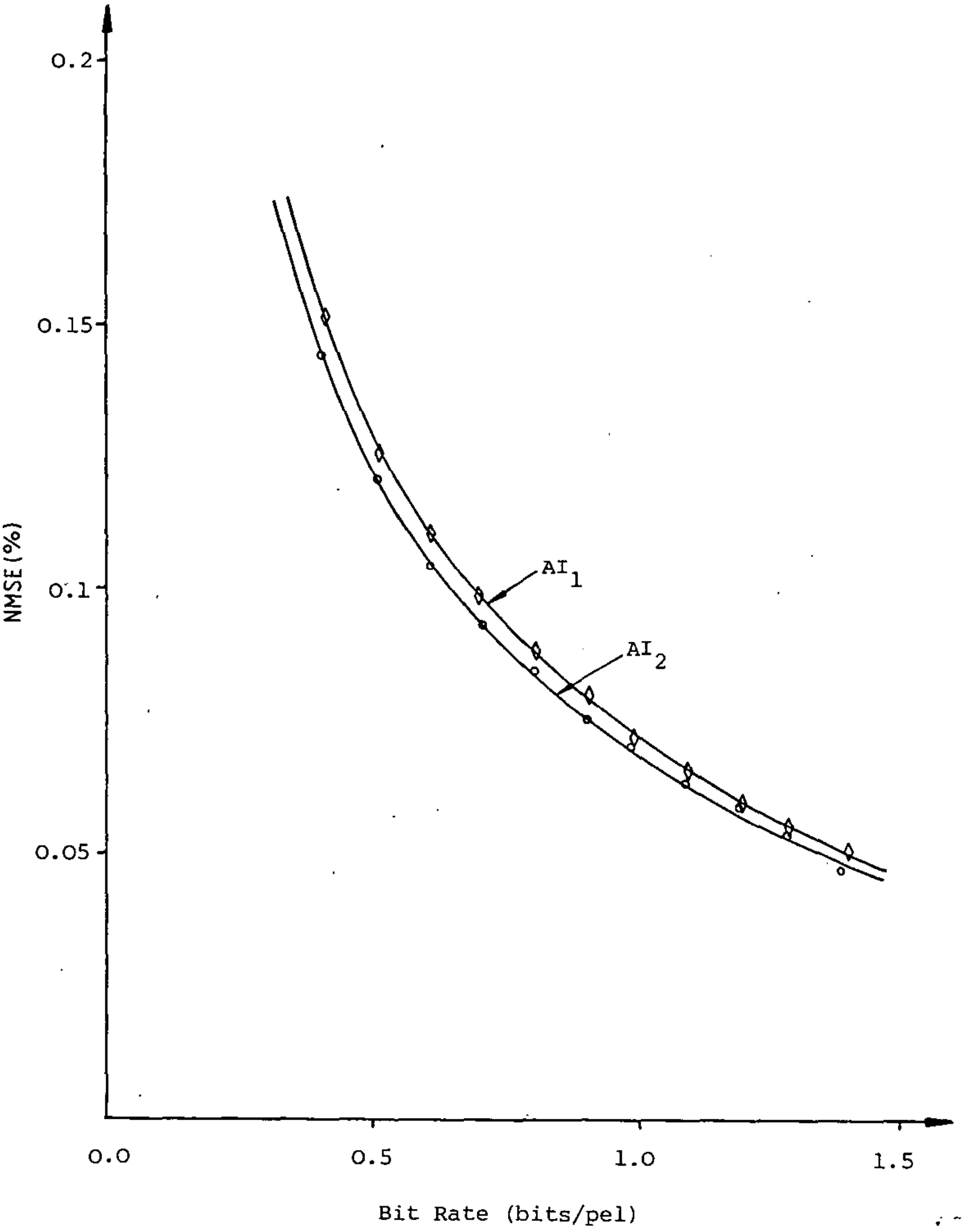

Figure 4.11

scheme the variances in each block are dynamically estimated along the same scan path as shown in Figure 4.7.

Let the reordered one dimensional sequence be $\{X_i\}$ where X_i is the ith coefficient and the corresponding decoded sequence is $\{\hat{X}_i\}$. The dynamically estimated variance represented by $\{\sigma_i^2\}$ is then given by

$$\hat{\sigma}_i^2 = A_1 \hat{\sigma}_{i-1}^2 + (1-A_1) \hat{X}_{i-1}^2 \qquad (4.33)$$

where $A_1 = 0.75$ was chosen experimentally to give the best estimation. The initial value $\hat{\sigma}_1^2$ is interpolated from adjacent values of $\{\hat{X}_i\}$

$$\hat{\sigma}_1^2 = \frac{1}{2} (\hat{X}_1 + \hat{X}_2) \qquad (4.34)$$

The bit assignment procedure is similar to Scheme II. In order to initialize the variance estimation procedure at the receiver, X_1 and X_2 are always transmitted with a fixed number of bits. This scheme does not require any overhead information.

4.4.5 Scheme V

A new bit allocation procedure based on a variance map calculated from the power spectral density in the perceptual domain is used in this scheme. The power spectrum equation as derived by Hall(40) is

$$S(w_{i,j}) = \frac{\alpha\, \sigma_x^2}{\alpha^2 + w_{i,j}^2} \left|H(w_{i,j})\right|^2 \qquad (4.35)$$

where $w_{i,j}$ is the normalized spatial frequency in cycles per degree and $H(w_{i,j})$ is given by Equation (4.15). σ_x^2 is the variance of the input image whose correlation is assumed to be of first order Markov form

$$\rho_x(\tau) = \exp(-\alpha|\tau|) \tag{4.36}$$

and α is a constant.

Let the variance of the (i,j)th coefficient be $\sigma_{i,j}^2$. Then

$$\sigma_{i,j}^2 = S(w_{i,j}) \tag{4.37}$$

and the bit allocation map may then be generated by Equation (4.12).

4.5 RESULTS

Simulation results for the 'GIRL', 'FLAT' and 'SCENE' images as shown in Figures 4.12, 4.13 and 4.14 respectively, employing the five schemes described in Section 4.4 are shown in Figures 4.15 to 4.20. The DCT and HT were used to transform the spatial samples.

Figures 4.15, 4.16 and 4.17 show the results on the 'GIRL', 'FLAT' and 'SCENE' images respectively using the DCT, whereas Figures 4.18, 4.19 and 4.20 show the same using the HT. Due to the different statistics of the source images, the NMSE value at which the subjective quality of the processed images is considered accaptable differs. Therefore, in order to derive meaningful comparison of the results, the NMSE value for acceptable picture quality for each source image must be defined. They are found to be 0.1%, 1.1% and 0.4% for the 'GIRL'

Figure 4.12

Figure 4.13

Figure 4.14

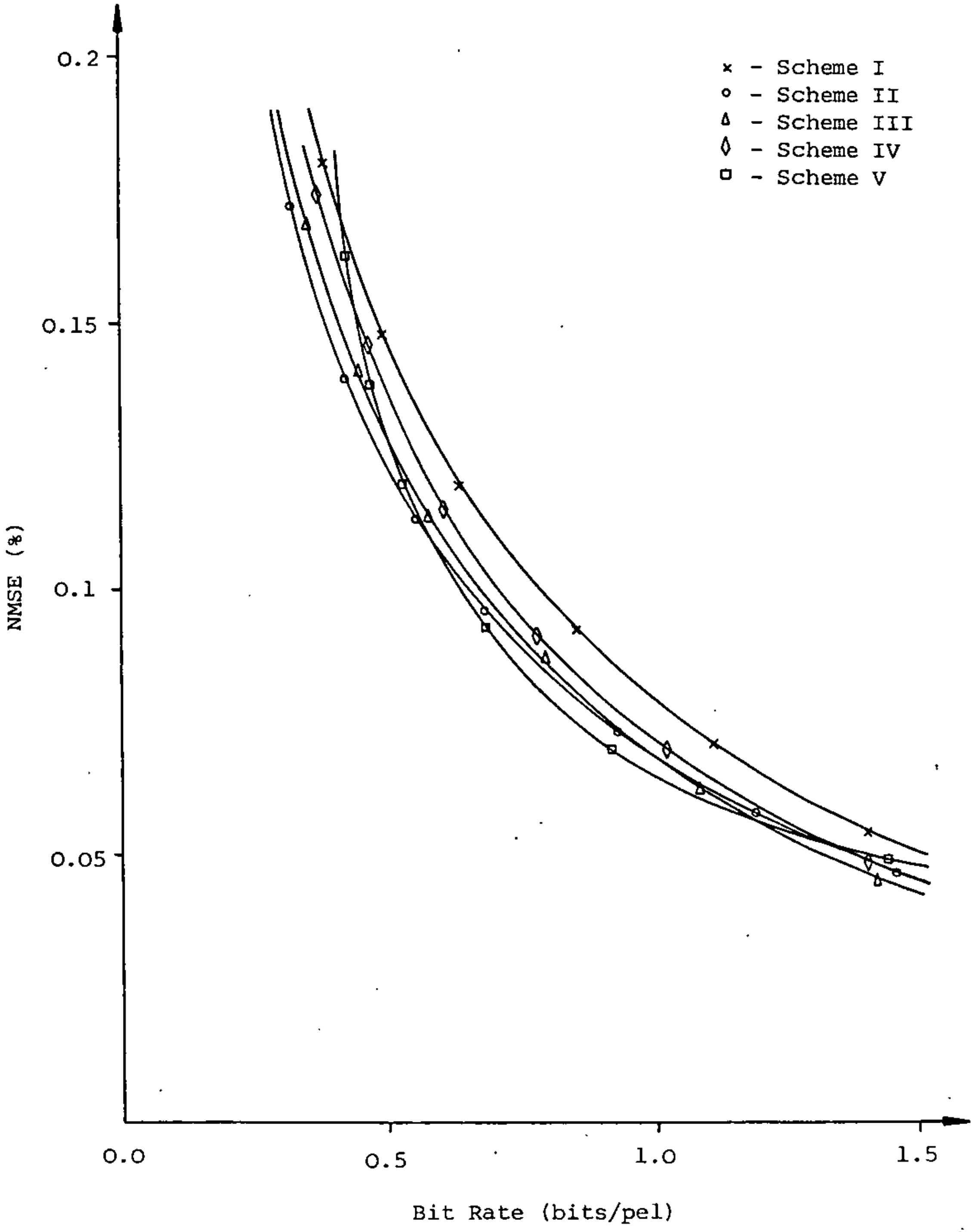

Figure 4.15 Results of Schemes I-V using the DCT on the 'GIRL' picture

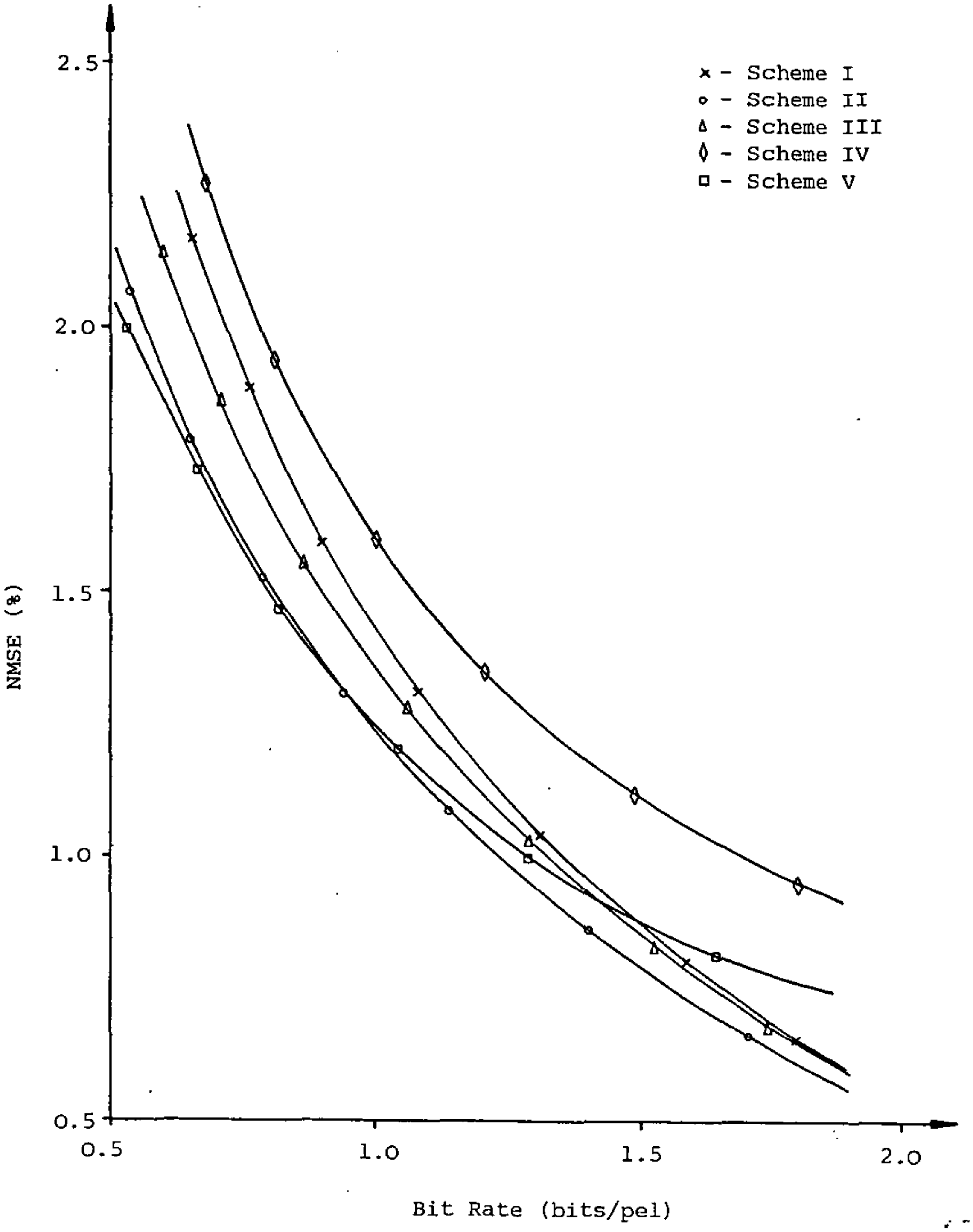

Figure 4.16 Results of Schemes I-V using the DCT on the 'FLAT' picture

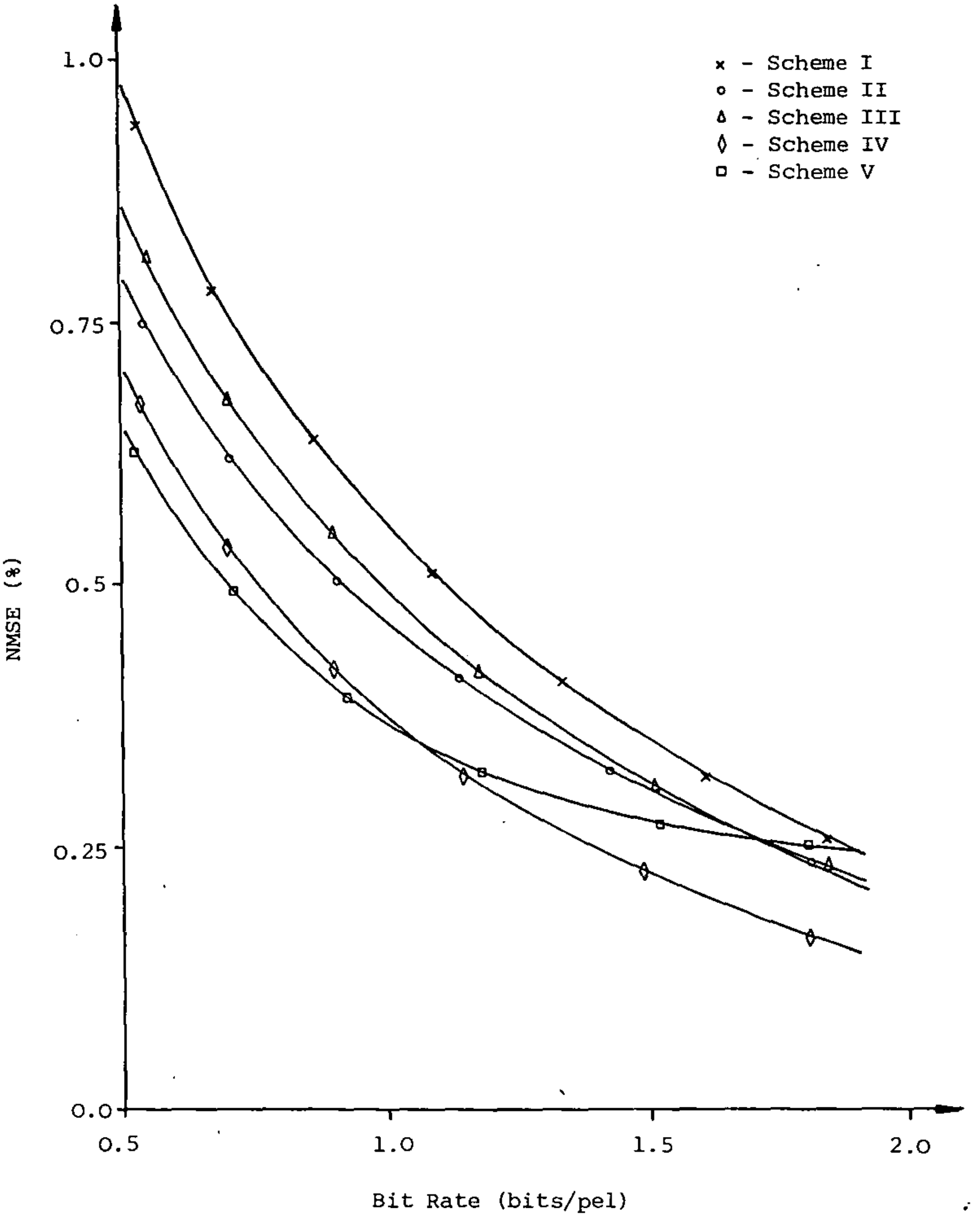

Figure 4.17 Results of Schemes I-V using the DCT on the 'SCENE' picture

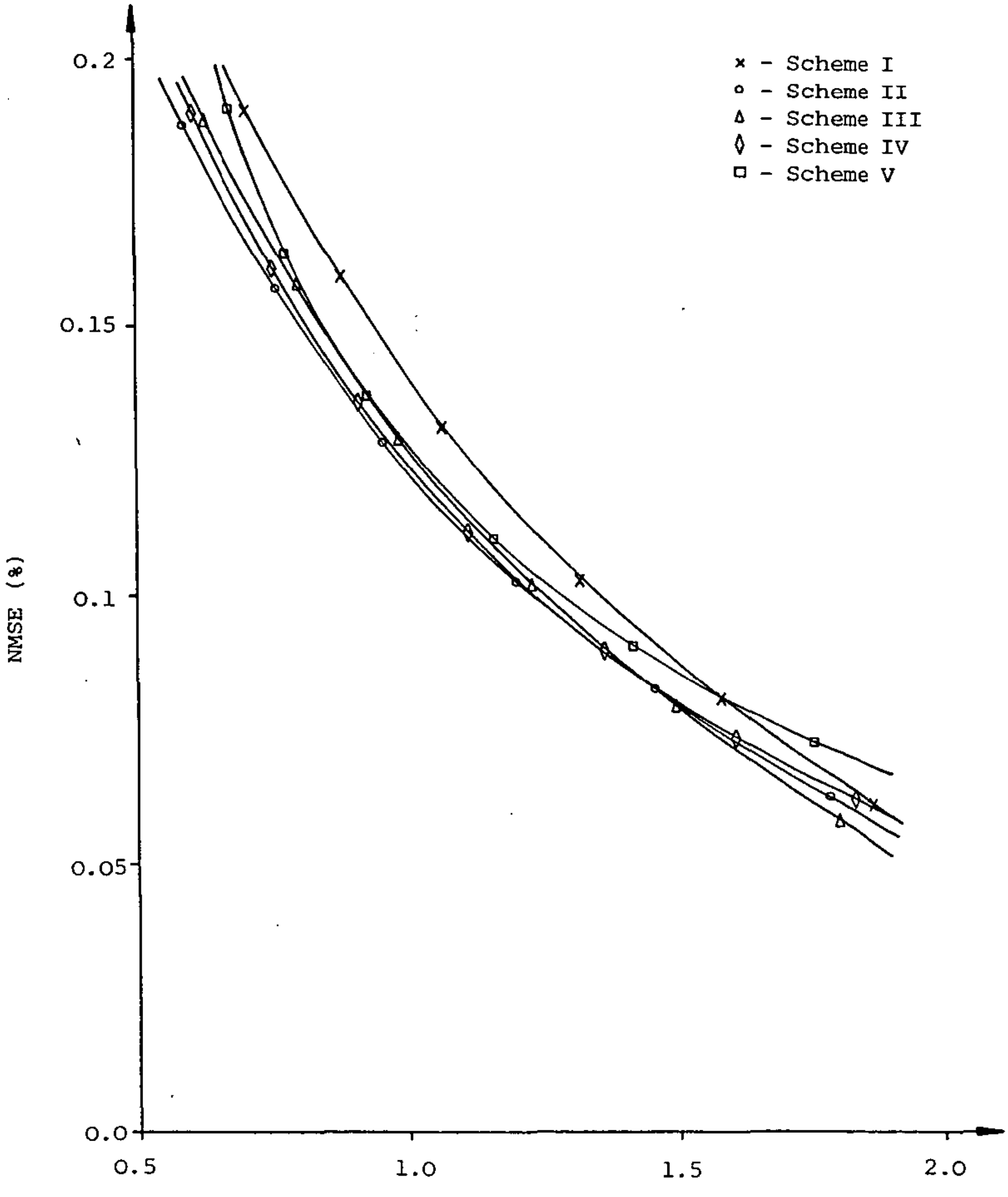

Figure 4.18 Results of Schemes I-V using the HT on the 'GIRL' picture

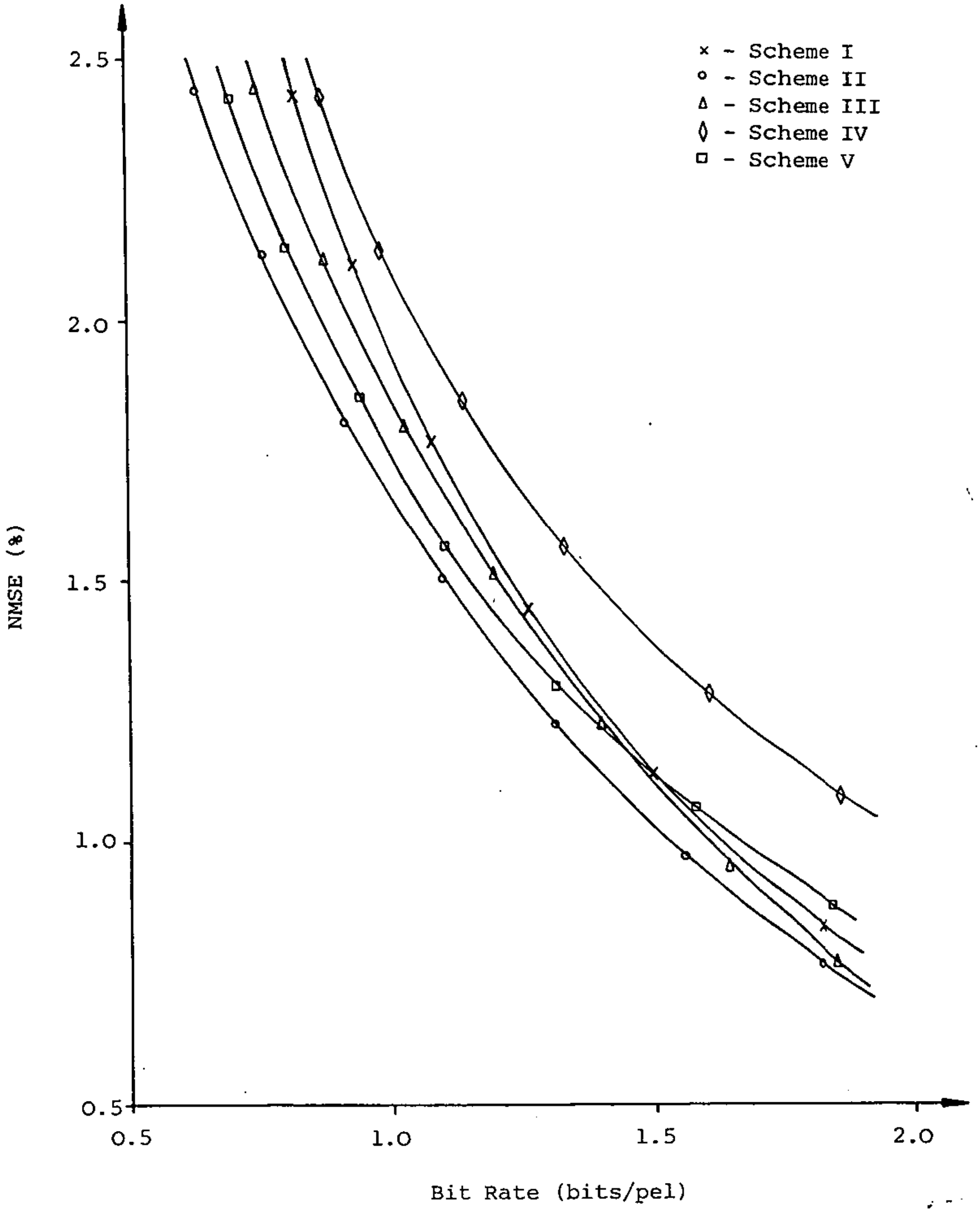

Figure 4.19 Results of Schemes I-V using the HT on the 'FLAT' picture

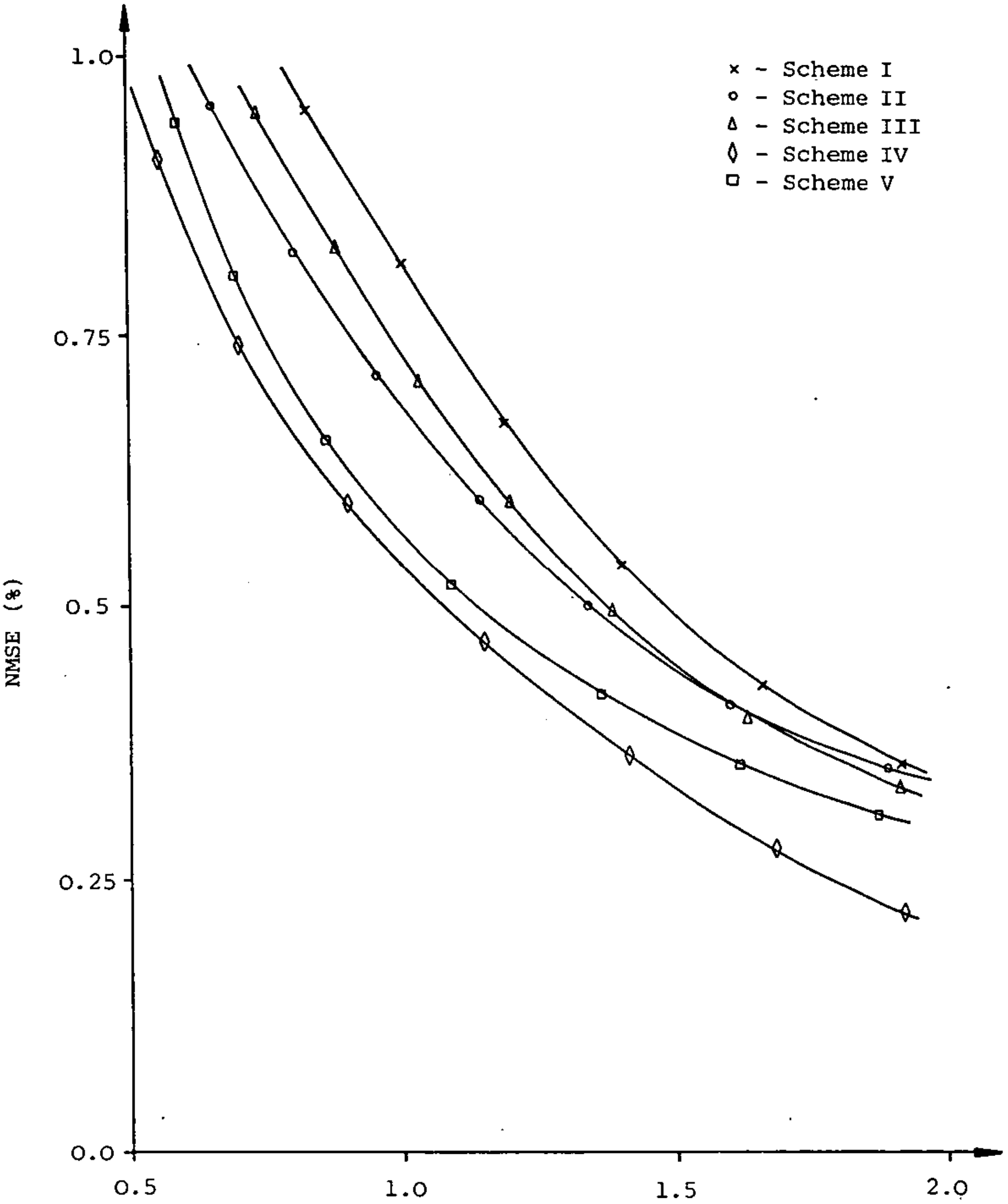

Figure 4.20 Results of Schemes I-V using the HT on the 'SCENE' picture

'FLAT' and 'SCENE' images respectively. These values are then used as basis of comparison for the results obtained for each source image. Based on these criteria, and from Figures 4.15 to 4.20, the bit rates required for each scheme with different transforms and source images are tabulated in Table 4.4.

Photographs corresponding to the results in Table 4.4 are also presented. Figures 4.21 (i) to (v) show the results for the 'GIRL' image using the DCT employing Schemes I to V respectively. The same results using the HT are shown in Figures 4.22 (i) to (v). Similarly, for the 'FLAT' image, the results are contained in Figures 4.23 and 4.24 and for the 'SCENE' image, in Figures 4.25 and 4.26.

4.6 DISCUSSION

From the results obtained, it is clear that the performance of different schemes depends on two important factors : (i) the source image (ii) the type of transform used. Different transforms introduce different degradations. The DCT, being a gradually varying function, introduces distortions which look subjectively like granular noise (see Figure 4.21). On the other hand, the HT introduces distortions which are step-like in shape (see Figure 4.26). Depending on where the distortion occurs, it could, on the one hand, be quite objectionable to the viewer but, on the other hand, it could be masked by the surrounding picture details. For example, distortions introduced by the DCT can be quite annoying if they appear on the plain part of the image but

Table 4.4 Bit rate (bits/pel) required for acceptable picture quality

TYPE OF TRANSFORM	SOURCE PICTURE	SCHEME				
		I	II	III	IV	V
DCT	GIRL	0.78	0.65	0.67	0.70	0.63
	FLAT	1.26	1.12	1.23	1.51	1.15
	SCENE	1.23	1.03	1.10	0.92	0.89
HT	GIRL	1.36	1.23	1.25	1.22	1.27
	FLAT	1.53	1.41	1.51	1.86	1.55
	SCENE	1.75	1.65	1.64	1.32	1.45

Table 4.5 Best scheme for the 'GIRL', 'FLAT' and 'SCENE' pictures using the DCT and HT

PICTURE	TRANSFORM	SCHEME
GIRL	DCT	V
	HT	IV
FLAT	DCT	II
	HT	II
SCENE	DCT	V
	HT	IV

(i) Scheme I

(ii) Scheme II

(iii) Scheme III

(iv) Scheme IV

(v) Scheme V

Figure 4.21

(i) Scheme I

(ii) Scheme II

(iii) Scheme III

(iv) Scheme IV

(v) Scheme V

Figure 4.22

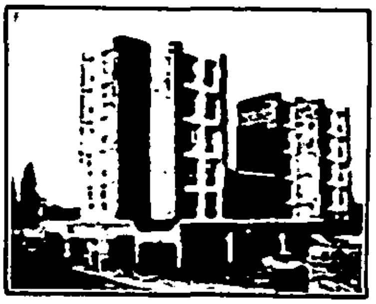

(i) Scheme I

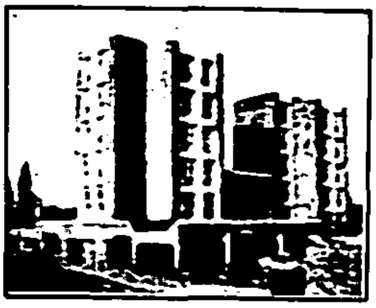

(ii) Scheme II

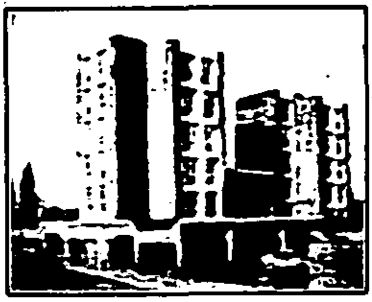

(iii) Scheme III

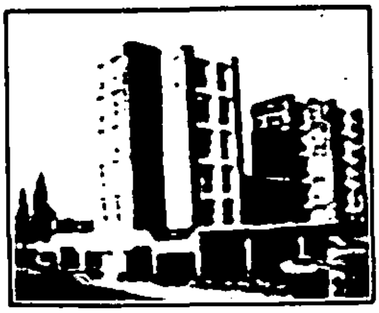

(iv) Scheme IV

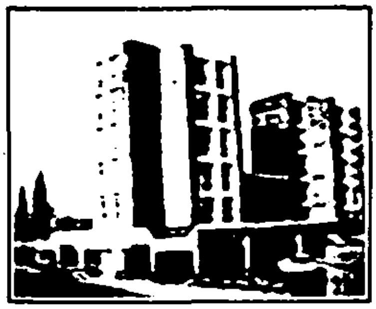

(v) Scheme V

Figure 4.23

(i) Scheme I

(ii) Scheme II

(iii) Scheme III

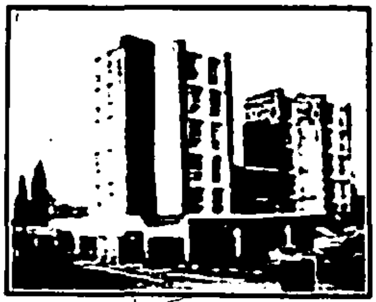

(iv) Scheme IV

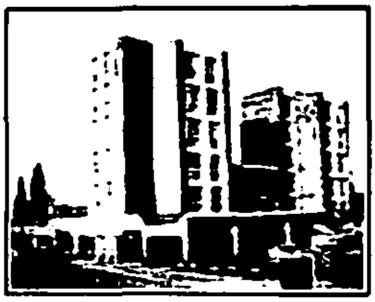

(v) Scheme V

Figure 4.24

(i) Scheme I

(ii) Scheme II

(iii) Scheme III

(iv) Scheme IV

(v) Scheme V

Figure 4.25

(i) Scheme I

(ii) Scheme II

(iii) Scheme III

(iv) Scheme IV

(v) Scheme V

Figure 4.26

are hardly noticeable in the busier part, whereas those introduced by the HT will be disturbing if they occur at an edge in the image.

In general, the DCT is clearly superior to the HT in terms of data compression, achieving a lower bit rate for the same picture quality for all schemes. Also the 'GIRL' image seems to be the best of the three images to code since it has the highest data compression figures for all schemes no matter what transform is used. This is mainly due to the smoothness of the image i.e. it does not contain many high frequency components, which makes the adaptation algorithm more efficient. From Table 4.4, the best schemes for each image with different transforms are summarised as shown in Table 4.5.

It is noticed that with the DCT, Scheme V gives the best results for the 'GIRL' and 'SCENE' images, but is second to Scheme II for the 'FLAT' image. However, with the HT, the best scheme for the 'GIRL' and 'SCENE' images is Scheme IV but for the 'FLAT' image, it is Scheme II. The results are encouraging because Schemes IV and V use less overhead information than the other schemes and hence are able to achieve better data compression.

From the photographs shown in Figures 4.21 to 4.26, Scheme V gives the best performance. It introduces the least distortion into the plain part of the processed image and retains the details most faithfully. Images processed with the DCT give better overall subjective quality than the corresponding ones using the HT at the same NMSE for the 'GIRL' image. However for the 'FLAT' image, it is the other way round, mainly because that image contains many horizontal and vertical edges which are more amenable to Hadamard transformation.

The better performance of Scheme V compared with Scheme I, II and IV demonstrates the importance of incorporating the human visual characteristic in the design of an adaptive transform coding system. Weighting the power spectral density of the image with the human visual characteristic as in Equation (4.35) suppresses low frequency noise which, if appearing in the plain areas of the image, is most objectionable to the eye. The performance of Scheme III is not as good as that of Scheme V, probably because the computation of the weighted quantization distortion makes use of the estimated variances of the transform coefficients, which in the short-term may not be independent. Similarly the use of the estimated variances based on the transform coefficients in Schemes I, II and IV may be the reason why they have an inferior performance compared with that of Scheme V.

4.7 CONCLUSIONS

From the studies above, it can be concluded that the performance of an adaptive transform coding system depends on (i) the adaptive algorithm (ii) the source image and (iii) the transform used. Given the same adaptive algorithm, different source images are amenable to coding using different unitary transforms. The human visual system also plays an important role in the design of an efficient adaptive transform coding system. Of the two transforms investigated, the DCT performs better than the HT for all schemes and source images. In general, Scheme V is preferred to the other schemes because it gives the best picture quality for the processed images, but the amount of data compression achievable overall is dependent on the source statistics of the images and the transform used.

4.8 NOTE ON PUBLICATION

A paper entitled "Adaptive transform coding of video images" has been accepted for publication in the IEE Proceedings, Part F. It is an abridged version of Chapter IV.

CHAPTER V - IMAGE DISPLAY

5.1 INTRODUCTION

In a low bit rate image coding system, the time taken for an image to fill the screen can be considerable. Therefore, the way in which the image is progressively built up from the moment the first pel is received until the last pel is transmitted is important. DPCM processes the image a line or a few lines at a time depending on whether one-dimensional or two-dimensional prediction is used. Therefore, at the receiver, the image is decoded and displayed line by line from top to bottom. The viewer will have no idea about the full content of the image until nearly all the lines are received and displayed.

Transform coding, apart from achieving a greater bit rate compression ratio than the DPCM, possesses the ability to produce a blurred but recognisable image upon transmitting and inverse transforming at the receiver the first few coefficients of highest magnitude. Since the viewer is being given a 'preview' of what he is going to see if the full set of coefficients is received and converted into the pel domain, he will have the option of terminating the transmission of further coefficients if the image is of little use to him, thus effecting savings in time and cost.

In this chapter, different sequences of transmitting the transform coefficients for image display are investigated. Different source images are used in order to ascertain how the source statistics affect the selection of the transmission sequence. In the next section, details of different sequences of coefficient transmission are described. Results of the simulations are presented in Section 5.3 while the following section contains a discussion of the results. Finally, conclusions are included in Section 5.5.

5.2 IMAGE DISPLAY TECHNIQUES

An image transformation can be viewed as a decomposition of the image data into a generalised two-dimensional spectrum. Each spectral component in the transform domain corresponds to the amount of energy of the spectral function within the image. Typically, the first (DC) coefficient defines the average brightness of the picture block and is therefore positive and the next few (AC) coefficients are large since in most images, low frequency components predominate. The AC coefficients give an indication of the amount of detail in the picture block. For example, the presence of large amount of vertical detail will manifest itself in large AC coefficients along the vertical edge of the transform block. Transmission of different coefficients gives visual effects of different kinds. The objective of this investigation is to find a transmission sequence that not only give the best subjective effect but needs only the minimum number of coefficients.

5.2.1 Scheme I

In this scheme, the order in which the coefficients are transmitted is based on the hierarchy of the coefficients used in reconstructing the image. The position in the hierarchy occupied by a coefficient is found by ranking it among the rest of the coefficients according to the NMSE of its reconstructed image when only that coefficient together with the DC coefficient are transmitted. Examples of the hierarchy of the DCT coefficients are given in Figure 5.1 for the 'GIRL', 'FLAT' and 'SCENE' images shown in Figures 4.12 to 4.14 respectively, with a block size of 8 x 8 pels.

Having established the hierarchy of the coefficients within the block, the coefficients are then transmitted according to the hierarchy in ascending order until an image of acceptable quality is obtained.

5.2.2 Scheme II

It has been shown that(116) the logarithm of variance of the transform coefficients decreases linearly along the zig-zag path as shown in Figure 4.7. In this scheme, the same zig-zag path is followed in transmitting the coefficients until an image of acceptable quality is obtained.

5.2.3 Scheme III

Unlike the two previous schemes, Scheme III is directional in nature. The transmission sequence starts with the DC coefficient and

1	3	6	10	16	23	22	30
2	4	9	13	19	21	29	37
5	8	11	17	24	35	34	44
7	12	18	25	32	31	42	53
14	15	20	33	40	46	54	49
28	26	38	39	52	47	56	59
27	36	41	48	55	57	60	63
45	43	51	61	50	64	58	62

(i) 'GIRL' image

1	2	3	5	7	8	14	20
4	9	10	18	21	26	31	40
6	13	16	25	29	33	44	46
11	15	27	28	35	41	47	54
12	17	23	34	36	50	63	57
19	24	32	38	45	51	53	60
22	30	42	43	48	58	59	64
37	39	49	55	52	56	61	62

(ii) 'FLAT' image

1	3	9	17	23	28	41	50
2	5	10	19	29	36	48	56
4	6	13	16	30	35	46	52
7	8	14	22	40	44	51	53
11	12	15	25	34	55	60	59
18	20	26	31	39	49	61	63
21	24	33	37	42	54	58	62
32	27	38	45	47	43	57	64

(iii) 'SCENE' image

Figure 5.1 Hierarchy maps of the cosine transform coefficients follows the vertical column until it reaches the end of the first column. It then continues with the next column and so on until an image of acceptable quality is obtained.

5.2.4 Scheme IV

This scheme is basically the same as Scheme III except that the transmission sequence now follows the rows instead of the columns.

5.2.5 Scheme V

This scheme follows the sequence as depicted in Figure 5.2, taking into account both the horizontal and vertical correlation in the image.

1	2	4	6	8	10	12	14
3	16	17	19	21	23	25	38
5	18	27	28	30	34	40	45
7	20	29	32	36	42	47	51
9	22	31	35	43	49	53	56
11	24	33	41	48	54	58	60
13	26	39	46	52	57	61	63
15	37	44	50	55	59	62	64

Figure 5.2 Scheme V

5.3 RESULTS

Simulations were carried out employing the five schemes described in the last section on three source images, namely the 'GIRL', 'FLAT' and 'SCENE' images shown respectively in Figures 4.12 to 4.14. Throughout the investigation, the DCT was used. Graphs of NMSE versus the number of coefficients transmitted are plotted for the five schemes with different source images. Figures 5.3 to 5.5 show the results for the 'GIRL', 'FLAT' and 'SCENE' images respectively.

Furthermore, to demonstrate the visual effect of the transmission sequences, six frames each from the sequences in Scheme I and II are presented as photographs for the 'GIRL' and 'SCENE' images as shown in Figures 5.6 and 5.8 respectively. For the 'FLAT' image, the sequences in Scheme I and V are presented as shown in Figure 5.7. Each frame contains four coefficients more than its preceding frame and the minimum number of coefficients is 4.

5.4 DISCUSSION

As evident from Figures 5.3 to 5.5, Scheme I gives the best performance in terms of NMSE for any given number of coefficients transmitted for all three images. This is the case because the order in which the coefficients are transmitted is the optimum one for image reconstruction. However the drawback of the scheme is the need to compute the hierarchy map for each different image. Fortunately the problem can be overcome by selecting the transmission sequence used in

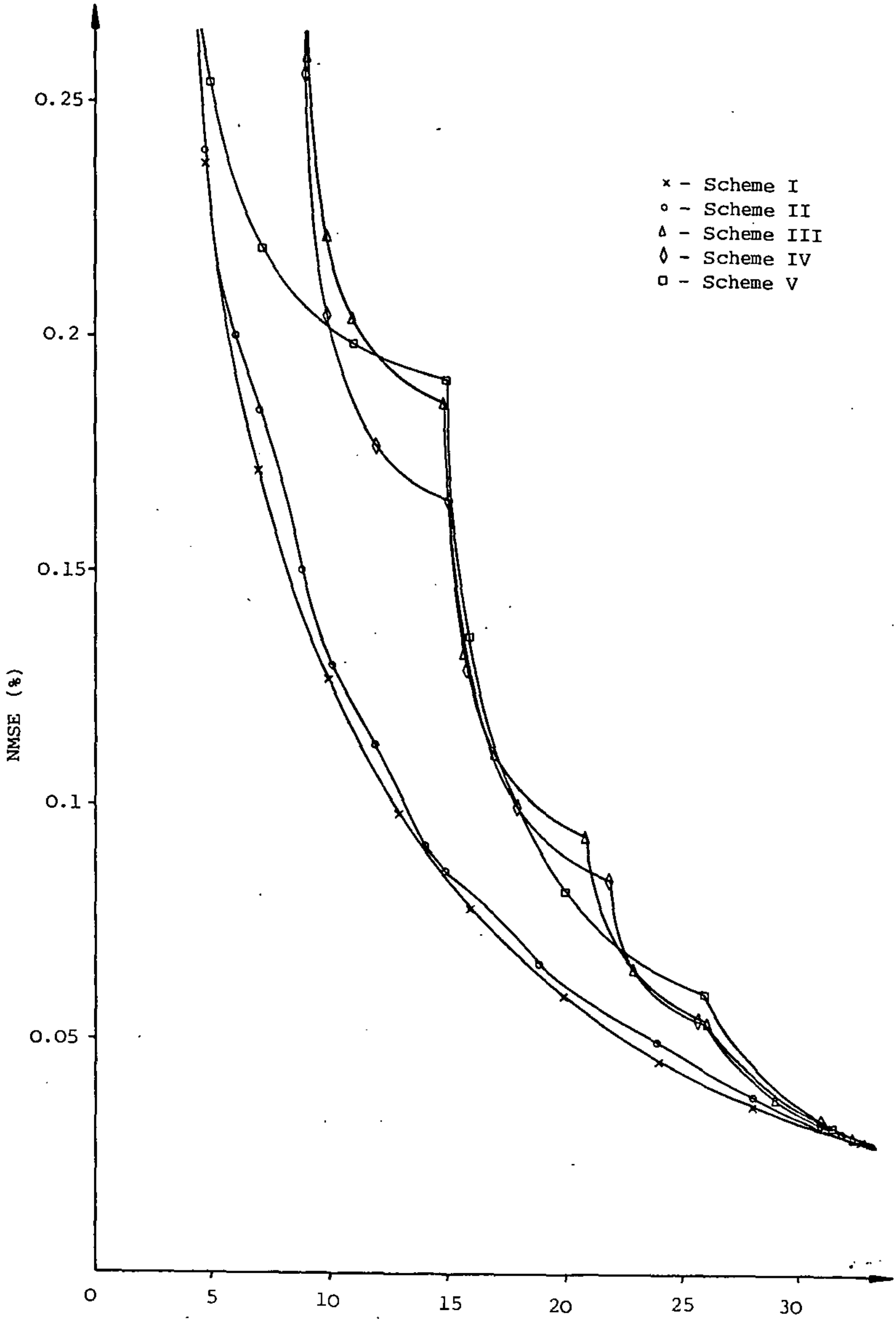

Figure 5.3 Results for the 'GIRL' picture

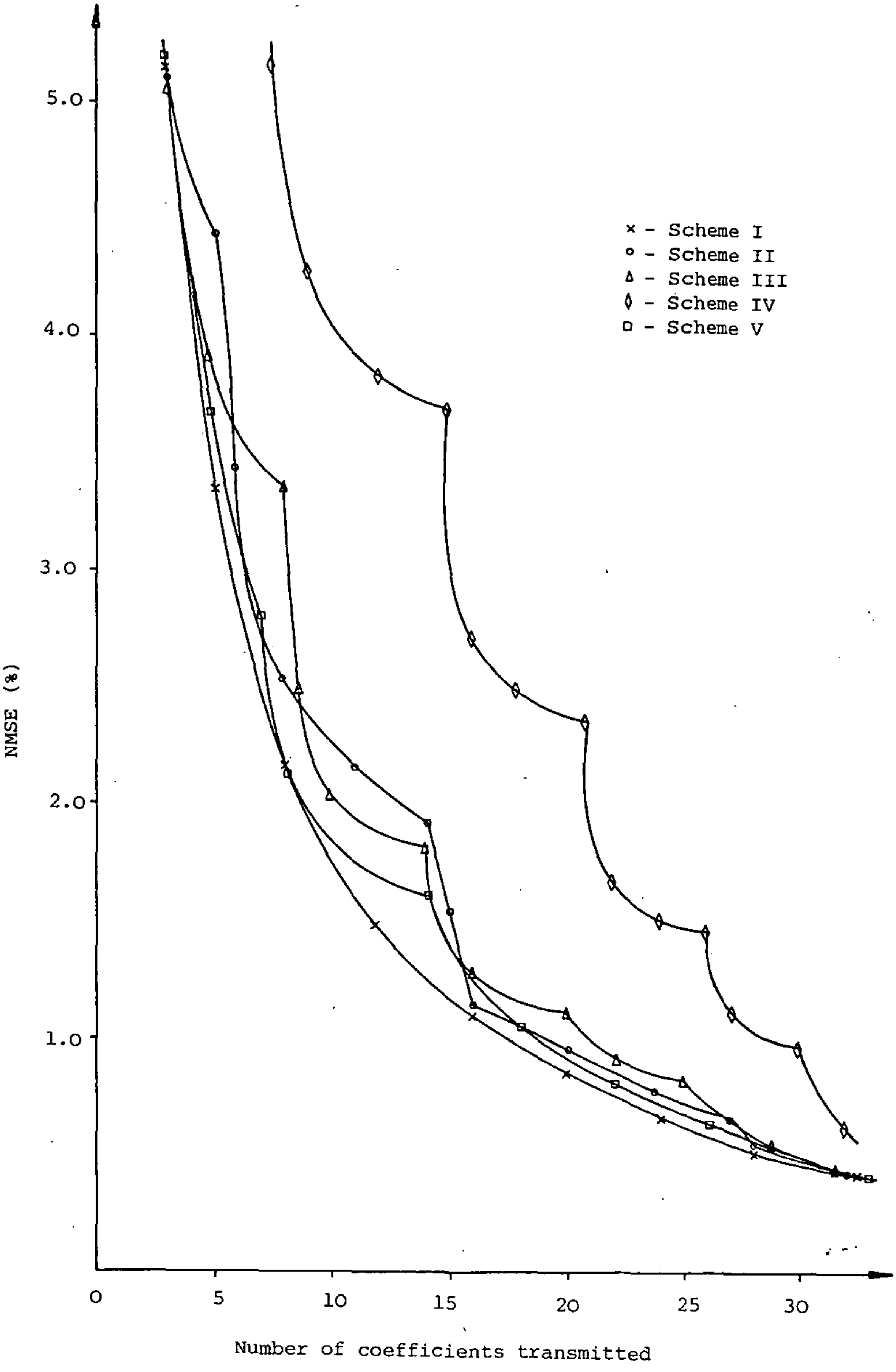

Figure 5.4 Results for the 'FLAT' picture

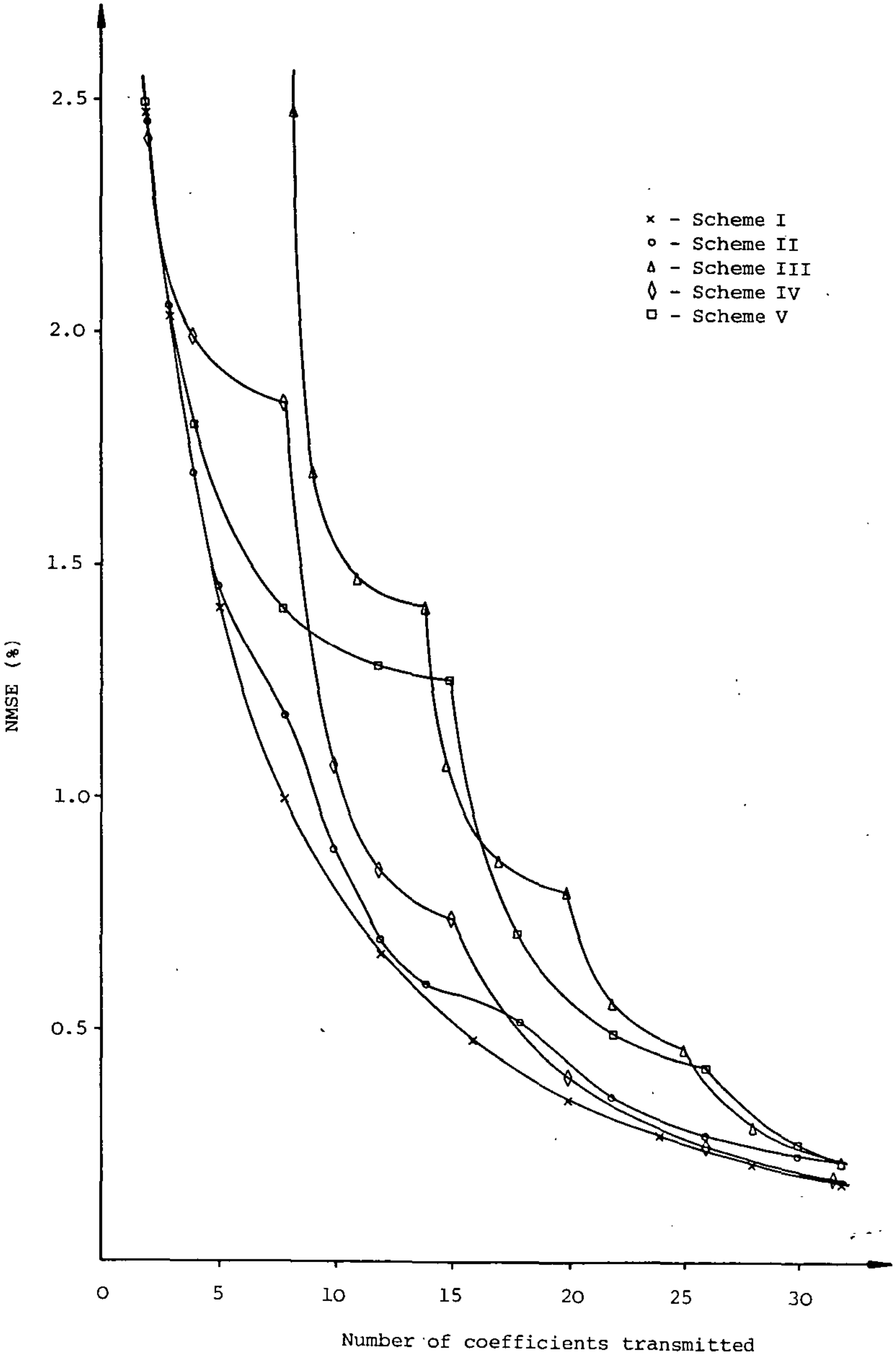

Figure 5.5 Results for the 'SCENE' picture

(i) Scheme I

(ii) Scheme II

Figure 5.6

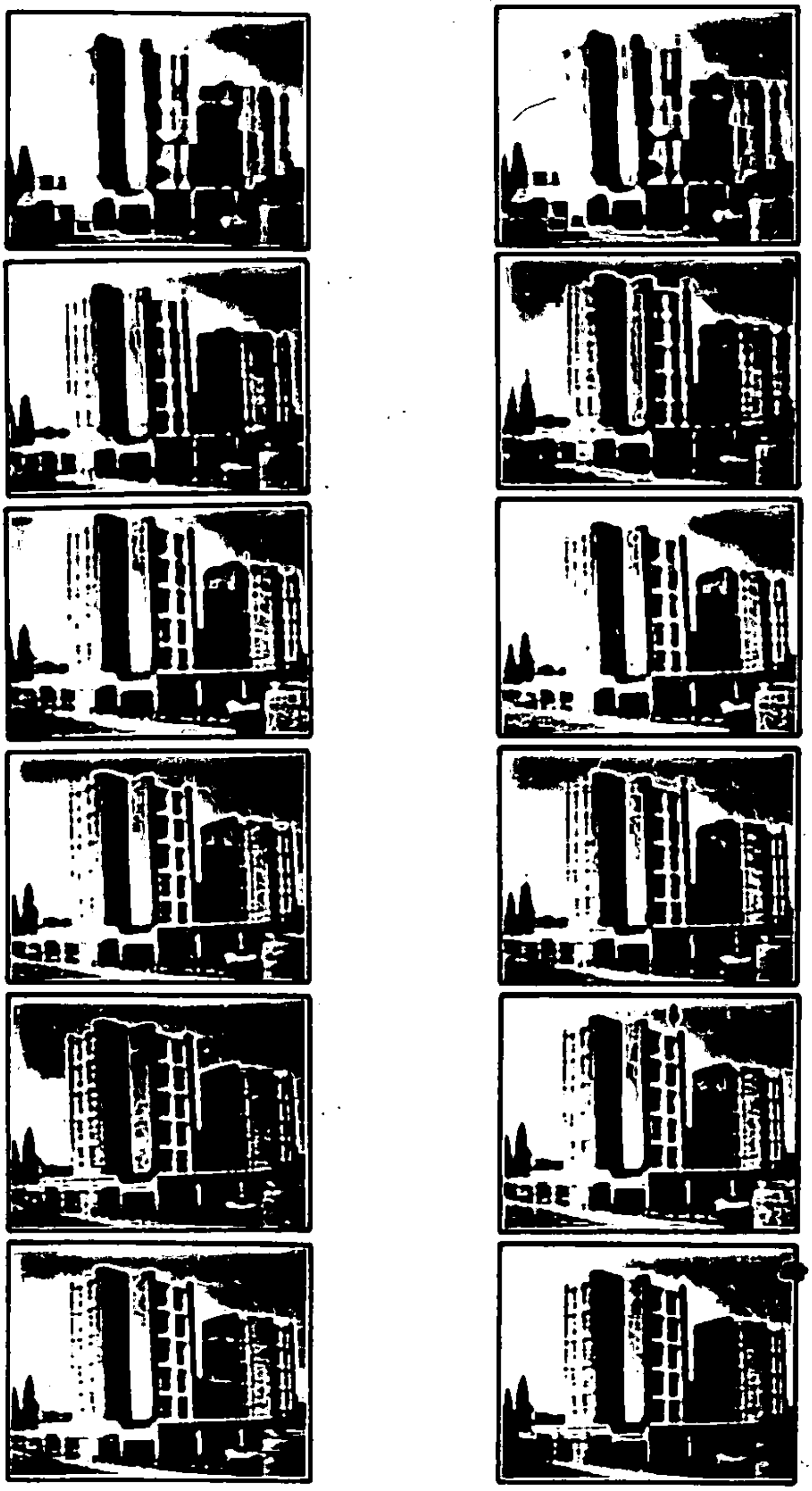

(i) Scheme I

(ii) Scheme V

Figure 5.7

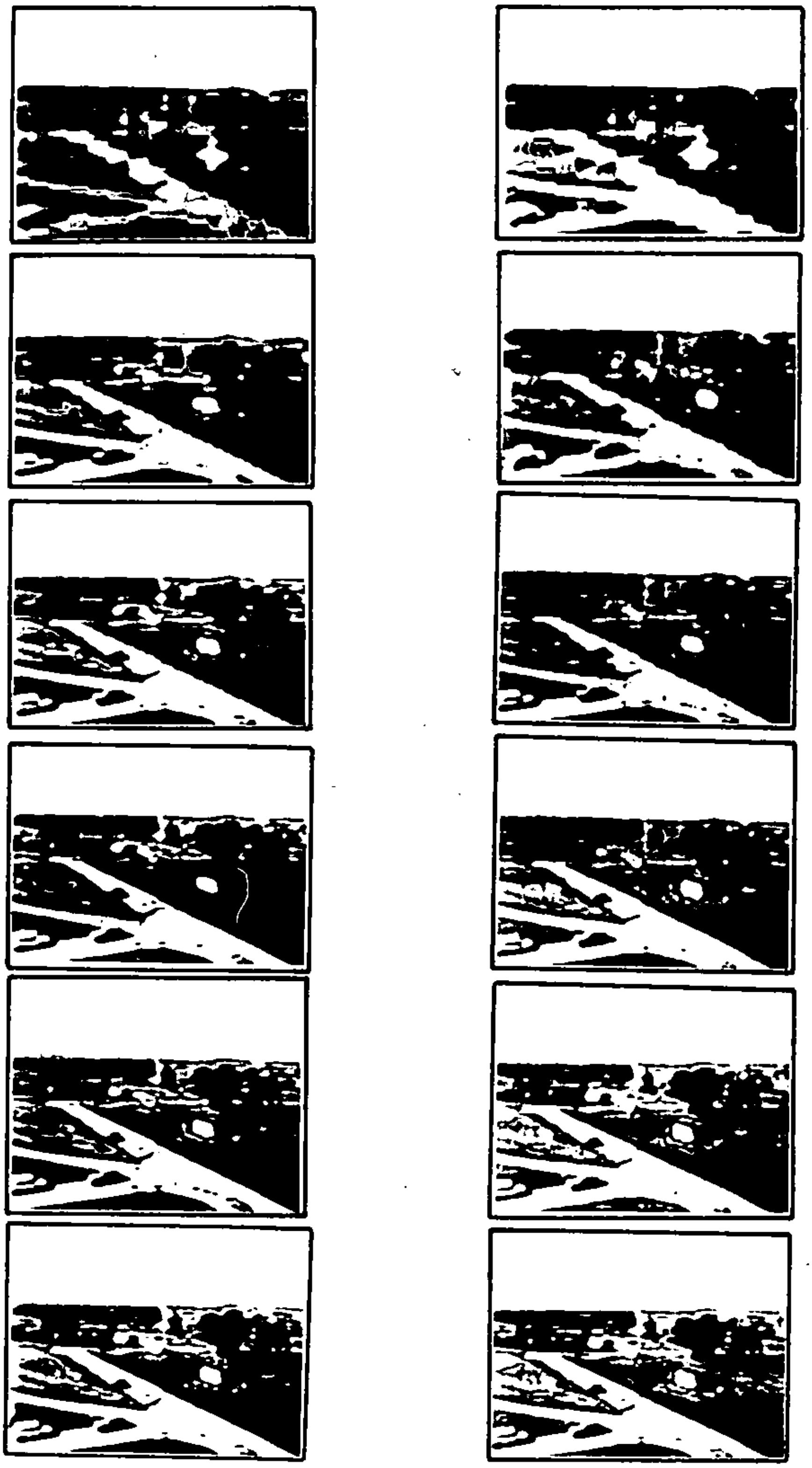

(i) Scheme I

(ii) Scheme II

Figure 5.8

Scheme II for the 'GIRL' and 'SCENE' images, and that used in Scheme V for the 'FLAT' image, because their performances are very close to that of Scheme I.

The results give credence to Tescher and Cox's view(116) that for a normal image, the logarithm of the variance or energy of the transform coefficients decreases along the diagonal scan path shown in Figure 4.7 except in images where there are a lot of horizontal and vertical edges. Therefore for display purposes, images can be classified into two categories : one with smooth features and the other with significant edge detail. For the former category, Scheme II would provide the best transmission sequence without incurring the extra overhead information required if Scheme I is used. On the other hand, Scheme V would be appropriate for images of the latter category.

The other two Schemes (III and IV) perform less satisfactorily because they only take into consideration one-dimensional correlation in the image. Since most of images encountered in everyday life contain high correlation in both horizontal and vertical directions, these two schemes will not be suitable for the transmission of coefficients except in cases where the image statistics are highly directional in nature.

5.5 CONCLUSIONS

The scheme that provides the optimum transmission sequence is undoubtedly Scheme I for all the three source images used in the investigation. However, it suffers from the disadvantage that it needs a hierarchy map for its implementation. Schemes II and V give comparable performances without requiring any overhead information, and are amenable to different source statistics. In this case, Scheme II performs well with the 'GIRL' and 'SCENE' images which contain smooth features whereas Scheme V produces results very close to Scheme I with the 'FLAT' image which contains many sharp horizontal and vertical transitions.

F4·54

Stanly Chroma

3stage MSMSVQ

1 Adap.

$Y \sim 1.25$ b/p

$U,V \sim 1.38/10$ b/p

CHAPTER VI - RECAPITULATION AND SUGGESTIONS FOR FUTURE WORK

6.1 INTRODUCTION

The insertion of true video images instead of graphics in a viewdata page represents a major improvement in the viewdata service. The problem with the present system which employs DPCM encoding, is the slow build-up of the video images on the screen. To provide a possible alternative encoding technique for the picture viewdata systems, transform coding is investigated.

Initially, in order to become familiarised with picture viewdata systems, error detection and correction of DPCM-coded picture viewdata signals was carried out. Then an image reduction system was successfully designed employing three unitary transforms, the DFT, DCT, and HT. Image size reduction is necessary both to reduce the update time for the image and to save space so that alphanumeric text can be inserted alongside the reduced image.

Reduction of image size reduces the amount of information needed for transmission. However, redundancy exists in the smaller image and can be reduced by adaptive transform coding techniques. Five adaptive schemes, two involving the human visual system were implemented. The final stage in the research programme was devoted to a search for a transmission sequence which gives good visual effect and needs little or no overhead information.

6.2 ERROR DETECTION AND CORRECTION

The error detection algorithm is a variant of the Difference Detection and Correction Scheme(65) employed in detecting errors in speech, and works by forming an adaptive detection threshold from the statistics of the received signal. An error is said to have occurred if the difference between adjacent pels is greater than the threshold. Correction is then carried out by simple interpolation of the adjacent pels. Error propagation inherent in DPCM coding is prevented by transmitting a PCM update at the end of each line. In cases where the scheme fails, line replacement is employed instead.

The detection and correction algorithm was first investigated using a PCM system, and then further extended to a DPCM system. For PCM systems, the improvement in SNR is approximately 10dB for BER between 0.1 and 2.0%. Virtually all the errors were removed when BER < 0.6%. In the case of DPCM images, the improvement in SNR is 18dB over a range of BER from 0.1 to 1.0%, representing a substantial improvement in picture quality.

System complexity can be traded against performance depending on the application. For example, line replacement is effective at low error rates but at high error rates, produces a mosaic structure in the enhanced image. In this instance, the statistical detection and correction method may be preferred even though its SNR values are lower than those of the line replacement method, because the enhanced picture does not contain the mosaic structure and is thus more pleasing to the eye.

6.3 IMAGE SIZE REDUCTION

Image size reduction is basically a two-dimensional decimation process. Prior to decimation, two-dimensional lowpass filtering is carried out to bandlimit the baseband signal so that aliasing is avoided. Lowpass filtering is usually achieved by convolution in the time domain or conversely, multiplication in the Fourier or frequency domain. It is also possible to carry out the filtering process in domains other than Fourier e.g. cosine(100), sine and Hadamard. Three different approaches to achieve image reduction were investigated.

Initially, lowpass filtering and decimation in the time domain is examined. Lowpass filters used are the FIR and the 4th order Butterworth filter. Decimation takes place by selecting every Mth sample in the filtered sequence for a reduction factor of M. For image reduction by a rational factor $\frac{M}{L}$, the original sequence is interpolated by adding (L-1) zeroes between each pair of the original samples. It is then lowpass filtered and decimated as before. It is important that in this case, interpolation precedes decimation so that the baseband width of the intermediate signal i.e. the interpolated signal after filtering, is greater than or equal to that of the original and of the decimated signal. From the results of the simulations, the 4th order Butterworth filter is shown to give a better subjective performance than the FIR filter.

With the ultimate objective of designing an image reduction system for transform coding, a scheme in which lowpass filtering is carried out in the cosine trasform domain but with decimation in the time domain was implemented. Lowpass filtering is achieved by multiplying together the transforms of the original signal and the filter impulse response. Inverse transformation of the resulting product gives the filtered signal. Decimation is then carried out on the filtered signal as described above.

Finally, a transform image reduction system was designed and implemented. It combines the lowpass filtering and decimation process in one operation, thus reducing processing time and system complexity. Lowpass filtering and decimation is achieved in the transform domain by discarding (as distinct from setting to zero) the coefficients outside a zone determined by the original transform block size and the reduction factor. Inverse transformation of the decimated transform block with an inverse transformation matrix of appropriate size produces the decimated image block.

Transforms used in the simulations include the DFT, DCT and HT. The performance of the transforms is based on their ease of implementation; their ability to provide a wide range of block sizes and last but not least, their subjective performance. Based on the criteria mentioned above, it is found that the DCT has the best performance of the three transforms used.

6.4 DATA COMPRESSION

Further to reduce the bit rate after the reduction of image size, adaptive transform coding techniques were employed. Five schemes were examined, including two which incorporate the human visual model in the formulation of their adaptive algorithms. Scheme I makes use of the high correlation that exists between the logarithms of the variances of the transform coefficients in a zig-zag scan path as shown in Figure 4.7. The variance map from which the bit allocation map is derived is estimated instead of transmitted, thus effecting a saving in overhead information. In Scheme II,the local activity of the transform block is exploited to divide the blocks into four classes in which a lower activity block is allocated a lower bit rate and vice versa. Bit allocation for both schemes is proportional to the logarithm of the variances of the coefficients. Unlike the previous two schemes, Scheme III seeks to equalise the quantization distortions of the coefficients by assigning more bits to those coefficients with higher distortions. To take into account the unequal visibility of the quantization distortions, they are weighted by the human visual characteristic given by Equation 4.15 so that the distortions which are most sensitive to the eye are quantized with the most number of bits.

So far, in all the previous schemes, overhead information is necessary to implement the adaptive algorithms at the receiver. In a departure from the previous approach, the variances of the coefficients are estimated solely from a knowledge of the received coefficients (Equation 4.33) in Scheme IV. Two coefficients are first transmitted with a fixed number of bits to start the estimation process. Lastly, in Scheme V, instead of using estimated variances for bit allocation, they are derived from the power spectrum of the image (Equation 4.35). Quantization employs the Max quantizer(126) with minimum mean square error criterion. The probability density function is assumed to be Rayleigh for the DC coefficients and Laplacian for the AC coefficients.

The performance of the schemes depends on two important factors : the source image and the transform used. Two transforms (the DCT and HT) were used on three different source images (Figures 4.12 to 4.14). It is found that the DCT achieves a higher data compression ratio than the HT for the same picture quality for all schemes. Also, Scheme V produces results with the best overall subjective quality for both transforms and all three images.

6.5 IMAGE DISPLAY

Transform coding has the virtue of providing a blurred impression of the image quickly by inverse transforming only the first few coefficients. As more and more of the coefficients are included, the image is gradually restored to its original definition. A different sequence of transmission of the coefficients produces different visual effects as the image is built up. Obviously the optimum sequence of transmission is one which transmits the coefficients according to their hierarchy which is formed by ranking the NMSEs of the reconstructed images obtained as a result of transmitting each coefficient separately with the DC coefficient. Needless to say, this sequence of transmission requires the computation of the hierarchy map and this must be made known to the receiver. This overhead information can be excessive if the block size is large.

Therefore, other sequences of transmission which are independent of the source images were examined. Two of them produced results close to those obtained with the hierarchical transmission of coefficients for different source images. One, which transmits the coefficients according to the diagonal scan path shown in Figure 4.7, is comparable in performance to hierarchical transmission for the 'GIRL' and 'SCENE' images. For the 'FLAT' image, the transmission sequence is shown in Figure 5.2. This illustrates the effect of source statistics on the energy distribution in the transform domain. Transformation of images with smooth features such as the 'GIRL' image, produces coefficients with magnitudes which decrease with increasing distance from the DC coefficient. On the other hand, images with many horizontal and vertical edges, e.g. the 'FLAT' image, produce coefficients with large magnitudes along the horizontal and vertical edges of the transform block.

6.6 SUGGESTIONS FOR FUTURE WORK

Owing to the constraints of facilities and time available, work was carried out on monochrome images only, and could be extended to code colour images with slight modifications, especially if they are available in component form. The research carried out on data compression indicates the potential of adaptive transform coding. Here only two-dimensional transformation is investigated. It is possible to include one more dimension, i.e. the temporal dimension, as in moving pictures, in order to exploit the redundancy that exists there.

So far in most of the adaptive transform coding work available in the literature, the quantization strategy employs the Max quantizer with minimum mean square error criterion. Since the human observer is the end user of an image processing system, a quantizer design based on subjective criteria would increase the observed fidelity of the processed image. Thus, a possible area of research would be to improve the modelling of human visual system and the design of the quantizers based on such models.

REFERENCES

1. C.E. Shannon and W. Weaver, "The mathematical theory of communication", Univ. of Illinois Press, Urbana, 1949.

2. T. Berger, "Rate distortion theory : a mathematical basis for data compression", Prentice-Hall, Englewood Cliffs, New Jersey, 1971.

3. L. D. Davisson, "Rate distortion theory and applications", Proc. IEEE, vol.60, No.7, July 1972, pp.800-8.

4. L. G. Roberts, "Picture coding using pseudo-random noise", IRE Trans. Inf. Theory, vol.8, pp.145-54.

5. A. H. Reeves, French Pat. 852183(1938), British Pat. 535860(1939), U.S.A. Pat. 2270070 (1942).

6. K. W. Cattermole, "Principles of pulse code modulation", Iliffe, London, 1969.

7. W. M. Goodall, "Television transmission by pulse code modulation", BSTJ, vol.30, Jan. 1951, pp.33-49.

8. R. L. Cabrey, "Video transmission over telephone cable pairs by pulse code modulation", Proc. IRE, vol.48, No.9, Sept.1960, pp.1546-61.

9. L. H. Harper, "PCM picture transmission", IEEE Spectrum, vol.3, June 1966, pp.146.

10. C. C. Cutler, "Differential quantization of communication systems", U.S. Pat.2605361, July 1952.

11. R. E. Graham, "Predictive quantization of television signals", IRE Wescon Conv. Rec., Part 4, Aug.1958, pp.147-56.

12. J. B. O'Neal Jnr., "Predictive quantizing systems (differential pulse code modulation) for the transmission of television signals", BSTJ, Vol.45, May 1966, pp.689-721.

13. D. J. Connors, R.F.W. Pease and W. G. Scholes, "Television coding using two-dimensional spatial prediction", BSTJ, vol.50, Mar. 1971, pp.1049-61.

14. I. Dukhovich and J. B. O'Neal, "A three-dimensional spatial non-linear predictor for television", IEEE Trans. Commun., vol.27, Apr. 1979, pp.703-10.

15. J. C. Candy and R. H. Bosworth, "Methods for designing differential quantizers based on subjective evaluations of edge busyness", BSTJ, vol.51, No. 7, 1972, pp.1495-516.

16. B. G. Haskell and R. L. Schmidt, "A low bit-rate interframe coder for videophone", BSTJ, vol.54, Oct. 1975, pp.1475-95.

17. D. K. Sharma and A. N. Netravali, "Design of quantizers for DPCM coding of picture signals", IEEE Trans. Commun. vol.25, Nov. 1977, pp.1267-74.

18. D. E. Pearson, "Quantization of composite colour television signals", Proc. of Conf. on Digital Process. of Signals in Commun., Loughborough, vol.49, 1981, pp.413-26.

19. H. Enomoto and K. Shibata, "Features of Hadamard transformed television signals", 1965 Nat. Conf. IECE, Japan, paper No.881.

20. W. K. Pratt and H. C. Andrews, "Fourier transform coding of signals", Proc. of Int. Conf. on Syst. Sciences, Hawaii, Jan. 1968.

21. A. Habibi and P. A. Wintz, "Optimum linear transformation for encoding two-dimensional data", Symposium of Picture Bandwidth compression, M.I.T., Cambridge, MA, 1969.

22. H. J. Landau and D. Slepian, "Some computer experiments in picture processing for bandwidth compression", BSTJ, vol.50, May 1977, pp.1525-40.

23. P. A. Wintz, "Transform picture coding", Proc. IEEE, vol.60, No.7, July 1972, pp.809-20.

24. H. Hotelling, "Analysis of a complex of statistical variables into principal components", J. Educ. Psychol., vol.24, 1933, pp.417-41.

25. H. Karhunen, "Uber Lineare Methoden in der Wahrscheinlichkeitsrechnung", Ann. Acad. Sci. Fenn., Ser. A.I.37, Helsinki, Finland 1947.

26. M. Loeve, "Fonctions aleatoires de seconde ordre", in P. Levy, Processus Stochastiques et Mouvement Brownien, Paris, France, Hermann, 1948.

27. A. K. Jain, "A fast Karhunen-Loeve transform for a class of stochastic processes", IEEE Trans. Commun., vol.24, Sept. 1976, pp.1023-9.

28. A. K. Jain, S. H. Wang and Y. Z. Liao, "Fast KL transform data compression studies", Proc. NTC '76 Dallas, Texas, Nov. 1976.

29. N. Ahmed, T. Natarajan and K. Rao, "On image processing and a discrete cosine transform", IEEE Trans. Comput., vol.23, Jan. 1974, pp.90-3.

30. H. C. Andrews, J. Kane and W. K. Pratt, "Hadamard transform image coding", Proc. IEEE, vol.57, Jan. 1969, pp.58-68.

31. W. K. Pratt, W. H. Chen and L. R. Welch, "Slant transform image coding", IEEE Trans. Commun., vol.22, Aug. 1974, pp.1075-93.

32. A. Haar, "Zur Theorie der Orthogonalen Funktionen-System", Inaugural Dissertation, Math. Annalen, vol.5, 1955, pp.17-31.

33. M. Ghanbari and D. E. Pearson, "Probability density functions for Hadamard coefficients in transformed television pictures", Electronics Lett., vol.14, No.8, Apr. 1978, pp.252-4.

34. T. N. Cornsweet, "Visual perception", Academic Press, New York, 1970.

35. G. Wald, "The receptors for human colour vision", Science, vol.45, 3636, Sept. 4, 1964, pp.1007-17.

36. M. H. Pirenne, "Vision and the eye", 2nd. ed., Associated Book Publishers, London, 1967.

37. P. K. Brown and G. Wald, "Visual pigment in single rods and cones of the human retina", Science, vol. 144, 3614, Apr. 3, 1964, pp.45-52.

38. R. L. Gregory, "Eye and brain, the psychology of seeing", Wiedenfeld and Nicolson, 1966.

39. S. S. Stevens, "On the psychophysical law", Psychol. Rev., vol.64, 1957, pp.153-81.

40. C. F. Hall and E. L. Hall, "A non-linear model for the spatial characteristics of the human visual system", IEEE Trans. Syst. Man and Cybern., vol.7, No.3, 1977, pp.161-70.

41. G. Westheimer and F. W. Campell, "Light distribution in the image formed by the living human eye", J. Opt. Soc. Amer., vol.52, 1962, pp.1040-5.

42. J. L. Mannos and D. J. Sakrison, "The effects of a visual fidelity criterion on the encoding of images", IEEE Trans. Inf. Th., vol.20, 1974, pp.525-36.

43. D. E. Pearson, "Methods for scaling television picture quality", in Picture Bandwidth compression, ed. by T. S. Huang and O. J. Tretiak, Gordon and Breach, New York, 1972, pp.47-95.

44. P. Mertz, D. Fowler and H. N. Christopher, "Quality rating of television images", Proc. IRE, vol.38, No.11, 1950, pp.1269-83.

45. G. L. Fredenhall and W. L. Behrend, "Picture quality - procedures for evaluating subjective effects of interference", Proc. IRE, vol.48, No.6, 1960, pp.1030-4.

46. R. D. Prosser, J. W. Allnatt and N. W. Lewis, "Quality grading of impaired television pictures", Proc. IEE, vol. 111, No.3, 1964, pp.491-502.

47. S. A. Money, "Teletext and viewdata", Newnes Technical Books, Butterworth & Co. Ltd., 1979.

48. S. Fedida, "Viewdata - development of computer-based information services for the general public", Proc. of 2nd. Int. Symp. on Subscriber Loops and Services, London, England, 1976, pp.127-32.

49. S. Fedida and R. Malik, "Viewdata revolution", Associated Business Press, 1979.

50. R. C. Nicol, B. Fenn and R. D. Turkington, "Transmission techniques for picture viewdata", IBC '80 Conf. Rec., IEE Conf. Pub. No.191, pp.109-13.

51. W. K. Pratt, "Digital image processing", John Wiley & Sons, 1978.

52. R. Lippmann, "Influence of channel errors on DPCM picture coding", ACTA Electronica, vol.19, No.4, 1976, pp.289-94.

53. P. Stammnitz, "Error protection of 34 M bit/sec DPCM encoded TV signals with multiple error correcting BCH codes", 1980 Zurich Seminar on Digital Commun., March 4-6, 1980, pp.G4/1-6.

54. M. F. Maxemchuk and J. A. Stuller, "Reduction of transmission error propagation in adaptively predicted DPCM encoded pictures", BSTJ, vol.58, No.6, July 1979, pp.1413-23.

55. P. Jung and R. Lippmann, "Error response of DPCM decoders", NTZ Commun. J., vol.28, No.12, 1975, pp.431-8.

56. J. A. Kitchen, R. C. Nicol and J. M. Corbett, "Subjective effects of DPCM errors and predictor leak on visual telephone pictures", Proc. IEEE, vol.124, No.9, 1977, pp.737-42.

57. R. J. Arguello, H. R. Sellner and J. A. Stuller, "The effect of channel errors in the differential pulse code modulation transmission of sampled imagery", IEEE Trans. Commun. Tech., vol.19, No.6, 1971, pp.926-33.

58. K. Y. Chen and R. W. Donaldson, "Non-adaptive DPCM transmission of monochrome pictures over noisy communication channels", IEEE Trans. Commun., vol.24, No.2, 1976, pp.173-83.

59. J. O. Limb and F. W. Mounts, "Digital differential quantizer for television", BSTJ, vol.48, 1969, pp.2583-99.

60. D. J. Connors, "Techniques for reducing the visibility of transmission errors in digitally encoded video signals", IEEE Trans. Commun., vol.21, No.6, 1973, pp.695-706.

61. M. C. W. van Buul, "Hybrid D-PCM, a combination of PCM and DPCM", IEEE Trans. Commun., vol.26, No3, 1978, pp.362-8.

62. D. M. Fenwick, R. Steele and N. Vasanji, "Partial correction of DPCM video signals using a Walsh corrector", The Radio and Electronic Engineer, vol.48, No.6, 1978, pp.271-6.

63. R. Lippmann, "A technique for channel error correction in differential PCM picture transmission", Proc. of ICC '73, Seattle, Wash., June 11-13, 1973, pp.48.12-18.

64. R. Steele and D. J. Goodman, "Detection and selective smoothing of transmission errors in linear PCM", BSTJ, vol.56, No.3, 1977, pp.399-409.

65. R. Steele, K. N. Ngan and D. J. Goodman, "Adaptive Difference Detection and Correction system for partial correction of transmission errors in linear PCM", Electronics Lett., vol.14, No.12, 1978, pp.381-2.

66. R. Steele, "Partial removal of transmission errors in digitally encoded speech", Electronics and Power, vol.24, No.6, 1978, pp.451-4.

67. R. Steele, D. J. Goodman and C. A. McGonegal, "A Difference Detection and Correction scheme for combatting DPCM transmission errors", IEEE Trans. Commun. vol.27, No.1, 1979, pp.252-5.

68. R. Steele, D. J. Goodman and C. A. McGonegal, "DPCM with forced updating and partial correction of transmission errors", BSTJ, vol.58, No.3, 1979, pp.721-8.

69. W. C. Wong, R. Steele and D. J. Goodman, "Hardware for detection and partial correction of PCM transmission errors", IEEE Trans. Commun., vol.27, No.9, 1979, pp.1310-5.

70. R. Steele, N. S. Jayant and C. E. Schmidt, "Statistical block protection coding", BSTJ, vol.58, No.7, 1979, pp.1647-57.

71. E. G. Bowen and J. O. Limb, "Subjective effect of substituting lines in videophone signals", IEEE Trans. Commun., Oct. 1976, pp.1208-13.

72. A. W. Crooke and J. W. Craig, "Digital filters for sample rate reduction", IEEE Trans. Audio Electroacoustics, vol.20, 1972, pp.308-15.

73. R. W. Schafer and L. R. Rabiner, "A digital signal processing approach to interpolation", Proc. IEEE, vol.61, June 1973, pp.692-702.

74. M. G. Bellanger, J. L. Dagnet and G. P. Lepagnol, "Interpolation, extrapolation and reduction of computation speed in digital filters", IEEE Trans. Acoust., Speech and Signal Process., vol.22, Aug. 1974, pp.231-5.

75. R. R. Shively, "On multistage FIR filters with decimation", IEEE Trans. Acoust., Speech and Signal Process., vol.23, Aug. 1975, pp.353-7.

76. R. E. Crochiere and L. R. Rabiner, "Optimum FIR digital filter implementation for decimation, interpolation and narrow-band filtering", IEEE Trans. Acoust., Speech and Signal Process., vol.23, Oct. 1975, pp.444-56.

77. R. E. Crochiere and L. R. Rabiner, "Further considerations in the design of decimators and interpolators", IEEE Trans. Acoust., Speech and Signal Process., vol.24, Aug. 1976, pp.296-311.

78. D. J. Goodman and M. J. Carey, "Nine digital filters for decimation and interpolation", IEEE Acoust., Speech and Signal Process., vol.25, Apr. 1977.

79. R. A. Meyer and C. S. Burrus, "Design and implementation of multirate digital filters", IEEE Trans. Acoust., Speech and Signal Process., vol.24, Feb. 1976, pp.53-8.

80. E. O. Brigham and R. E. Morrow, "The fast Fourier transform", IEEE Spectrum, vol.4, No.12, 1967, pp.63-70.

81. H. C. Andrews, "A high speed algorithm for the computer generation of Fourier transforms", IEEE Trans. Computers, vol.17, No.4, 1968, pp.373.

82. H. C. Andrews, "Fourier coding of images", USCEE Rep. No. 271, Univ. of Southern California, Electronic Sciences Lab., June 1968.

83. H. C. Andrews and W. K. Pratt, "Fourier transform coding of images", Int. Conf. on Syst., Sc., Hawaii, 1968, pp.677-9.

84. H. C. Andrews and W. K. Pratt, "Television bandwidth reduction of Fourier image coding", Soc. of Motion Picture and Television Engrs., vol.77, Dec. 1968, pp.1279-81.

85. H. C. Andrews, "Multidimensional rotation and feature selection", IEEE Trans. Computers, vol. 20, July 1972, pp.636-41.

86. J. Pearl, "Walsh processing of random signals", IEEE Trans. Electromag. Compat., vol.13, Aug. 1971, pp.137-41.

87. J. Pearl, H. C. Andrews and W. K. Pratt, "Performance measures for transform data coding", IEEE Trans. Commun. Tech., vol.20, June 1972, pp.411-5.

88. E. O. Brigham, "The fast Fourier transform", Prentice-Hall, Englewood Cliffs, New Jersey, 1974.

89. W. Chen, C. H. Smith and S. C. Fralick, "A fast computational algorithm for the discrete cosine transform", IEEE Trans. Commun. vol.25, No.9, 1977, pp.1004-9.

90. J. Makhoul, "A fast cosine transform in one and two dimensions", IEEE Trans. Acoust., Speech and Signal Process., vol.28, No.1, 1980, pp.27-34.

91. R. E. Crochiere and L. R. Rabiner, "Interpolation and decimation of digital signals - a tutorial review", Proc. IEEE, vol.69, Mar. 1981, pp.300-31.

92. M. H. Ackroyd, "Digital filters", Butterworth Press, 1973.

93. B. Gold and K. L. Jordon, "A direct search procedure for designing finite duration impulse response filters", IEEE Trans. Audio Electroacoustics, vol.17, No.1, 1969, pp.33-6.

94. L. R. Rabiner, B. Gold and C. A. McGonegal, "An approach to the approximation problem for non-recursive digital filters", IEEE Trans. Audio Electroacoustics, vol.18, No.2, 1970, pp.83-106.

95. W. H. Chen and S. C. Fralick, "Image enhancement using cosine transform filtering", Proc. of Symp. on Current Math. Problems in Image Sc., Monterey, Ca., Nov. 1976, pp.186-92.

96. N. Ahmed and K. Rao, "Orthogonal transforms for digital signal processing", Springer-Verlag, 1975.

97. R. E. A. C. Paley, "On orthogonal matrices", Jour. of Math. and Physics, ML7, vol.12, 1933, pp.311-20.

98. J. Williamson, "Hadamard determinant theorem and sum of four squares", Duke Math. Jour., vol.11, 1944, pp.65-81.

99. R. J. Clarke, Private communication.

100. K. N. Ngan and R. J. Clarke, "Lowpass filtering in the cosine transform domain", Proc. of ICC'80, Seattle, Wash., June 1980, pp.31.7.1-5.

101. G. A. Reitmeier, "Spatial compression and expansion in digital television images", RCA Review, vol.42, No.1, Mar. 1981, pp.3-59.

102. F. deJager, "Delta modulation, a method of PCM transmission using a 7-unit code", Philips Research Rep., Dec. 1952, pp.442-66.

103. G. M. Dillard, "Application of ranking techniques to data compression for image transmission", NTC '75 Conf. Rec., vol.1, 1975, pp.22.18-22.

104. G. B. Anderson and T. S. Huang, "Piecewise Fourier transformation for picture bandwidth compression", IEEE Trans. Commun. Tech., vol.19, Apr. 1971, pp.133-40.

105. J. J. Y. Huang and P. M. Schultheiss,"Block quantization of correlated Gaussian random variable", IEEE Trans. Commun. Syst., vol.11, No.3, Sept. 1963, pp.289-96.

106. P. A. Wintz and A. J. Kurtenbach, "Waveform error control in PCM telemetry", IEEE Trans. Inf. Th., vol.14, No.5, Sept. 1968, pp.650-61.

107. A. Habibi and P. A. Wintz, "Image coding by linear transformation and block quantization", IEEE Trans. Commun. Tech., vol.19, No.1, Feb. 1971, pp.50-62.

108. E. T. Claire, "Bandwidth compression in image transmission", Proc. of ICC '72, pp.39.2-13.

109. T. I. Gimlett, "Use of activity classes in adaptive transform image coding", IEEE Trans. Commun., vol.23, July 1975, pp.785-6.

110. A. N. Netravali, B. Prasada and F. W. Mounts, "Some experiments in adaptive and predictive Hadamard transform coding of pictures", BSTJ, vol.56, Oct.1977, pp.1531-47.

111. W. H. Chen and C. H. Smith, "Adaptive coding of monochrome and colour images", IEEE Trans. Commun., vol.25, Nov. 1977, pp.1285-92.

112. M. Tasto and P.A. Wintz, "Image coding of adaptive block quantization", IEEE Trans. Commun. Tech., vol.19, No.6, Dec. 1971, pp.957-71.

113. A. G. Tescher, "The role of phase in adaptive image coding" Ph.D. Thesis, Univ. of S. California, E. E. Dept., Jan. 1974.

114. A. G. Tescher, H. C. Andrews and A. Habibi, "Adaptive phase coding in two and three-dimensional Fourier and Walsh image compression", Picture Coding Symp., Goslar, Germany, Aug. 1974.

115. R. V. Cox and A. G. Tescher, "Generalised adaptive transform coding", Picture Coding Symp., Asilomar, CA, Jan. 1976.

116. A. G. Tescher and R. V. Cox, "An adaptive transform coding algorithm", Proc. of ICC '76, pp.47.20-25.

117. W. C. Wong and R. Steele, "Adaptive coding of discrete cosine transform video telephone pictures", Picture Coding Symp., Ipswich, England, July 1979.

118. W. C. Wong and R. Steele, "Adaptive discrete cosine transformation of pictures using a logarithmic energy distribution model", Proc. of Digital Process. of Signals in Commun. Conf., Loughborough, England, April 1981, pp.427-34.

119. T. Ohira, M. Hayakawa and K. Matsumoto, "Adaptive orthogonal transform coding system for NTSC colour television signals", NTC '78, Birmingham, AL, Dec. 1978, pp.10.6.1-5.

120. T. Ohira, M. Hayakawa and K. Matsumoto, "Orthogonal transform coding system for NTSC colour television signals", IEEE Trans. Commun., vol.26, No.10, 1978, pp.1454-63.

121. W. Mauersberger, "An adaptive transform coding system based on two-dimensional classification", Picture Coding Symp., Ipswich, England, July 1979.

122. E. L. Hall, "Computer image processing and recognition", Academic Press, New York, 1979.

123. R. V. Cox and A. G. Tescher, "Channel rate equalization techniques for adaptive transform coders", Proc. SPIE, vol.87, 1976, pp.239-46.

124. W. K. Pratt, "Image transmission techniques", Academic Press, New York, 1979.

125. A. Habibi, "Survey of adaptive transform coding techniques", IEEE Trans. Commun., vol.25, No.11, 1977, pp.1275-84.

126. J. Max, "Quantization for minimum distortion", IRE Trans. Inf. Th., vol.6, 1960, pp.7-12.

127. P. F. Panter and W. Dite, "Quantizing distortion in pulse code modulation with non-uniform spacing levels", Proc. IRE, vol.39, 1951, pp.44-8.

128. V. R. Algazi, "Useful approximations to optimum quantization", IEEE Trans. Commun. Tech., vol.14, No.3, June 1966, pp.297-301.

129. B. Smith, "Instantaneous companding of quantized signals", BSTJ, vol.36, May 1957, pp.653-709.

130. M. Ghanbari, "Real-time transform coding of broadcast-standard TV pictures", Ph.D. Thesis, Univ. of Essex, 1979.

131. W. C. Wong, "Adaptive transform coding of viewphone signals", Ph.D. Thesis, Univ. of Technology, Loughborough, 1980.

132. A. N. Netravali and J. O. Limb, "Picture coding - a review", Proc. IEEE, vol.68, No.3, 1980, pp.366-406.

133. R. C. Gonzalez and P.A.Wintz, "Digital image processing", Addison-Wesley, 1977.

134. H. Gharavi, "Differential pulse code modulation of colour television signals using various prediction methods", Ph.D. Thesis, University of Technology, Loughborough, 1980.

135. R. Steele, "Delta modulation systems", Pentech Press, London, 1975.

APPENDIX I

From Equation (3.58),

$$H(z) = \sum_{n=0}^{N-1} h(n)\ z^{-n} \qquad (I.1)$$

Substituting Equation (3.59) in Equation (3.58), we have

$$H(z) = \frac{1}{N} \sum_{k=0}^{N-1} \sum_{n=0}^{N-1} H(k)\ e^{\frac{j2\pi kn}{N}}\ z^{-n} \qquad (I.2)$$

To show that Equation(I.2) is reducible to Equation (3.61), we evaluate the following expression:

$$\frac{1-z^{-N}}{1-z^{-1}\ e^{\frac{j2\pi k}{N}}} = (1-z^{-N})\left[1-z^{-1}\ e^{\frac{j2\pi k}{N}}\right]^{-1}$$

$$= (1-z^{-N})\left[1+z^{-1}\ e^{\frac{j2\pi k}{N}} + z^{-2}\ e^{\frac{j4\pi k}{N}} + ----\right]$$

$$= (1+z^{-1}\ e^{\frac{j2\pi k}{N}} + z^{-2}\ e^{\frac{j4\pi k}{N}} + ---- + z^{-(N-1)}\ e^{\frac{j2\pi k}{N}(N-1)}$$

$$+ z^{-N}\ e^{j2\pi k} + z^{-(N+1)}\ e^{\frac{j2\pi k}{N}(N+1)} + ----) - (z^{-N} + z^{-(N+1)}\ e^{\frac{j2\pi k}{N}}$$

$$+ ----)$$

$$= 1+z^{-1}\ e^{\frac{j2\pi k}{N}} + z^{-2}\ e^{\frac{j4\pi k}{N}} + --- + z^{-(N-1)}\ e^{\frac{j2\pi k}{N}(N-1)}$$

$$= \sum_{n=0}^{N-1} z^{-n}\ e^{\frac{j2\pi kn}{N}} \qquad (I.3)$$

Hence

$$H(z) = \frac{1-z^{-N}}{N} \sum_{k=0}^{N-1} \frac{H(k)}{1-z^{-1}\, e^{\frac{j2\pi k}{N}}} \tag{I.4}$$

Evaluating Equation (I.4) on the unit circle where $z=e^{jw}$, we have

$$H(jw) = \frac{1-e^{-jwN}}{N} \sum_{k=0}^{N-1} \frac{H(k)}{1-e^{-j(w-\frac{2\pi k}{N})}} \tag{I.5}$$

Now

$$1-e^{-jwN} = e^{\frac{-jwN}{2}}\left(e^{\frac{jwN}{2}} - e^{\frac{-jwN}{2}}\right)$$

$$= 2j\, e^{\frac{-jwN}{2}} \sin\left(\frac{wN}{2}\right) \tag{I.6}$$

Similarly,

$$1-e^{-j(w-\frac{2\pi k}{N})} = 2j\, e^{-j(\frac{w}{2}-\frac{\pi k}{N})} \sin\left(\frac{w}{2}-\frac{\pi k}{N}\right) \tag{I.7}$$

Substituting Equations (I.6) and (I.7) into Equation (I.5) and rearranging,

$$H(jw) = \frac{1}{N}\, \frac{e^{\frac{-jwN}{2}}}{e^{-j(\frac{w}{2}-\frac{\pi k}{N})}} \sum_{k=0}^{N-1} H(k)\, \frac{\sin(\frac{wN}{2})}{\sin(\frac{w}{2}-\frac{\pi k}{N})}$$

$$= \frac{\exp\left[-jw\frac{(N-1)}{2}\right]}{N} \sum_{k=0}^{N-1} \frac{H(k)\, e^{\frac{-j\pi k}{N}} \sin(\frac{wN}{2})}{\sin(\frac{w}{2}-\frac{\pi k}{N})} \tag{I.8}$$

APPENDIX II

From Equation (3.70),

$$W_c(k) = X_c(k)\ H_c(k) \tag{II.1}$$

The inverse cosine transform of $W_c(k)$ is

$$w(n) = \sum_{k=0}^{N-1} C(k)\ W_c(k)\ \cos\left[\frac{(2n+1)k\pi}{2N}\right] \tag{II.2}$$

Since $C(k) = 0$ for $k > N$, this can be written as

$$w(n) = \mathrm{Re}\left\{\sum_{k=0}^{2N-1} C(k)\ W_c(k)\ e^{\frac{j2\pi nk}{2N}}\ e^{\frac{j\pi k}{2N}}\right\} \tag{II.3}$$

Substituting Equations (II.1) and (3.65) in Equation (II.3), we have

$$\begin{aligned} w(n) &= \mathrm{Re}\left\{\sum_{k=0}^{2N-1} 4\ C^3(k)\ \hat{X}_F(k)\ \hat{H}_F(k)\ e^{\frac{-jk\pi}{2N}}\ e^{\frac{j\pi nk}{N}}\right\} \\ &= \mathrm{Re}\left\{F^{-1}\left[4\ C^3(k)\ \hat{X}_F(k)\ \hat{H}_F(k)\ e^{\frac{-jk\pi}{2N}}\right]\right\} \end{aligned} \tag{II.4}$$

where $F^{-1}[\ ]$ indicates inverse DFT.

Note that in Equation (II.4), the inverse DFT, $F^{-1}[\ ]$ is summed over 2N points. But since $C(k) = 0$ for $k > N$, it is valid to sum over N points. Thus(99)

$$F^{-1}\left[4\ C^3(k)\ e^{\frac{-jk\pi}{2N}}\right] = \sum_{k=0}^{N-1} 4\ C^3(k)\ e^{\frac{-jk\pi}{2N}}\ e^{\frac{jkn\pi}{N}}$$

$$= 4\left[\left(\frac{1}{\sqrt{2}}\right)^3 + \sum_{k=1}^{N-1} e^{\frac{jk\pi}{2N}(2n-1)}\right] \qquad \text{(II.5)}$$

Let $z = e^{\frac{j\pi}{2N}(2n-1)}$, therefore

$$\sum_{k=1}^{N-1} e^{\frac{jk\pi}{2N}(2N-1)} = \sum_{k=1}^{N-1} z^k$$

$$= z + z^2 + ---- + z^{(N-1)} \qquad \text{(II.6)}$$

Now consider the expression

$$\frac{1-z^N}{1-z} = (1-z^N)\ (1-z)^{-1}$$

$$= (1-z^N)(1+z+z^2+ ----)$$

$$= (1+z+z^2+ ----) - (z^N+z^{(N+1)} + ----)$$

$$= 1+z+z^2+ ---- + z^{(N-1)} \qquad \text{(II.7)}$$

i.e.
$$\sum_{k=1}^{N-1} z^k = \frac{1-z^N}{1-z} - 1 \qquad \text{(II.8)}$$

Hence

$$\sum_{k=1}^{N-1} e^{\frac{jk\pi}{2N}(2n-1)} = \frac{1 - e^{j\frac{\pi}{2}(2n-1)}}{1 - e^{j\frac{\pi}{2N}(2n-1)}} - 1 \qquad \text{(II.9)}$$

From Equation (II.9) above,

$$1 - e^{j\frac{\pi}{2}(2n-1)} = -2j\, e^{j\frac{\pi}{4}(2n-1)} \sin\left[\frac{\pi}{4}(2n-1)\right] \qquad (II.10)$$

Similarly,

$$1 - e^{j\frac{\pi}{2N}(2n-1)} = -2j\, e^{j\frac{\pi}{4N}(2n-1)} \sin\left[\frac{\pi}{4N}(2n-1)\right] \qquad (II.11)$$

Equation (II.9) then becomes

$$\sum_{k=1}^{N-1} e^{j\frac{k\pi}{2N}(2n-1)} = \frac{e^{j\frac{\pi}{4}(2n-1)} \sin\left[\frac{\pi}{4}(2n-1)\right]}{e^{j\frac{\pi}{4N}(2n-1)} \sin\left[\frac{\pi}{4N}(2n-1)\right]} - 1$$

$$= e^{j\frac{\pi}{4N}(2n-1)(N-1)} \frac{\sin\left[\frac{\pi}{4}(2n-1)\right]}{\sin\left[\frac{\pi}{4N}(2n-1)\right]} - 1 \qquad (II.12)$$

Taking only the real parts,

$$\sum_{k=1}^{N-1} e^{j\frac{k\pi}{2N}(2n-1)} = \cos\left[\frac{\pi}{4N}(2n-1)(N-1)\right] \frac{\sin\left[\frac{\pi}{4}(2n-1)\right]}{\sin\left[\frac{\pi}{4N}(2n-1)\right]} - 1 \qquad (II.13)$$

Substituting Equation (II.13) in Equation (II.5)

$$F^{-1}\left[4\, C^3(k) \cdot e^{j\frac{k\pi}{2N}}\right] = 4 \left\{ \frac{1}{2\sqrt{2}} - 1 \right.$$

$$\left. + \cos\left[\frac{\pi}{4N}(2n-1)(N-1)\right] \frac{\sin\left[\frac{\pi}{4}(2n-1)\right]}{\sin\left[\frac{\pi}{4N}(2n-1)\right]} \right\} \qquad (II.14)$$

Therefore,

$$w(n) = \hat{x}(n) * \hat{h}(n) * 4\left\{\frac{1}{2\sqrt{2}} - 1 + \cos\left[\frac{\pi}{4N}(2n-1)(N-1)\right] \frac{\sin\left[\frac{\pi}{4}(2n-1)\right]}{\sin\left[\frac{\pi}{4N}(2n-1)\right]}\right\} \qquad (II.15)$$

where $\hat{x}(n)$ and $\hat{h}(n)$ are the IDFT of $\hat{X}_F(k)$ and $\hat{H}_F(k)$ respectively.

APPENDIX III

Let $\{y_i\}$ be a sequence of J sample values, $\{x_i\}$ the sample numbers and $\{\hat{y}_i\}$, the estimated values of $\{y_i\}$ as given by

$$\hat{y}_i = mx_i + c \qquad (III.1)$$

where m and c are constants.

The mean square error between y_i and $\hat{y}_i$ is defined by

$$\overline{e_i^2} = \frac{1}{J} \sum_{i=1}^{J} (y_i - m\,x_i - c)^2 \qquad (III.2)$$

Minimising $\overline{e_1^2}$, we have

$$\frac{\partial \overline{e_i^2}}{\partial m} = -\frac{2}{J} \sum_{i=1}^{J} x_i\,(y_i - m\,x_i - c) = 0 \qquad (III.3)$$

$$\frac{\partial \overline{e_i^2}}{\partial c} = -\frac{2}{J} \sum_{i=1}^{J} (y_i - m\,x_i - c) = 0 \qquad (III.4)$$

From Equation (III.3),

$$\sum_{i=1}^{J} x_i y_i - m \sum_{i=1}^{J} x_i^2 = c \sum_{i=1}^{J} x_i \qquad \text{(III.5)}$$

which gives

$$c = \frac{\frac{1}{J} \sum_{i=1}^{J} x_i y_i - m \overline{x_i^2}}{\bar{x}} \qquad \text{(III.6)}$$

where $$\bar{x} = \frac{1}{J} \sum_{i=1}^{J} x_i \qquad \text{(III.7)}$$

$$\overline{x^2} = \frac{1}{J} \sum_{i=1}^{J} x_i^2 \qquad \text{(III.8)}$$

From Equation (III.4),

$$\sum_{i=1}^{J} y_i - m \sum_{i=1}^{J} x_i = \sum_{i=1}^{J} c = Jc \qquad \text{(III.9)}$$

which gives

$$m = \frac{\bar{y} - c}{\bar{x}} \qquad \text{(III.10)}$$

where $$\bar{y} = \frac{1}{J} \sum_{i=1}^{J} y_i \qquad \text{(III.11)}$$

Substituting Equation (III.6) into Equation (III.10)

$$m = \left[\bar{y} - \frac{\frac{1}{J} \sum_{i=1}^{J} x_i \, y_i - m \, \overline{x^2}}{\bar{x}} \right] / \bar{x} \qquad \text{(III.12)}$$

which on simplification gives

$$m = \frac{\frac{1}{J} \sum_{i=1}^{J} x_i \, y_i - \bar{x} \, \bar{y}}{\sigma_x^2} \qquad \text{(III.13)}$$

where $\sigma_x^2 = \overline{x^2} - (\bar{x})^2$ (III.14)

Also from Equation (III.10),

$$c = \bar{y} - m \, \bar{x} \qquad \text{(III.15)}$$

The correlation coefficient r is defined as

$$r = \frac{\frac{1}{J} \sum_{i=1}^{J} x_i \, y_i - \bar{x} \, \bar{y}}{\sigma_x \, \sigma_y} \qquad \text{(III.16)}$$

From Equations (III.13) and (III.16),

$$r = \frac{m \, \sigma_x}{\sigma_y} \qquad \text{(III.17)}$$